Responses of boreal vegetation to recent climate change

by

Jonathan Barichivich

Thesis
Submitted to the University of East Anglia
for the degree of
Doctor of Philosophy

Supervisors: Prof. Keith Briffa, Dr Timothy Osborn, Dr Tom Melvin and Dr. Kevin Anchukaitis

Climatic Research Unit
School of Environmental Sciences
May 2014

I dedicate this intellectual journey to my dear supervisor,
Keith Briffa.

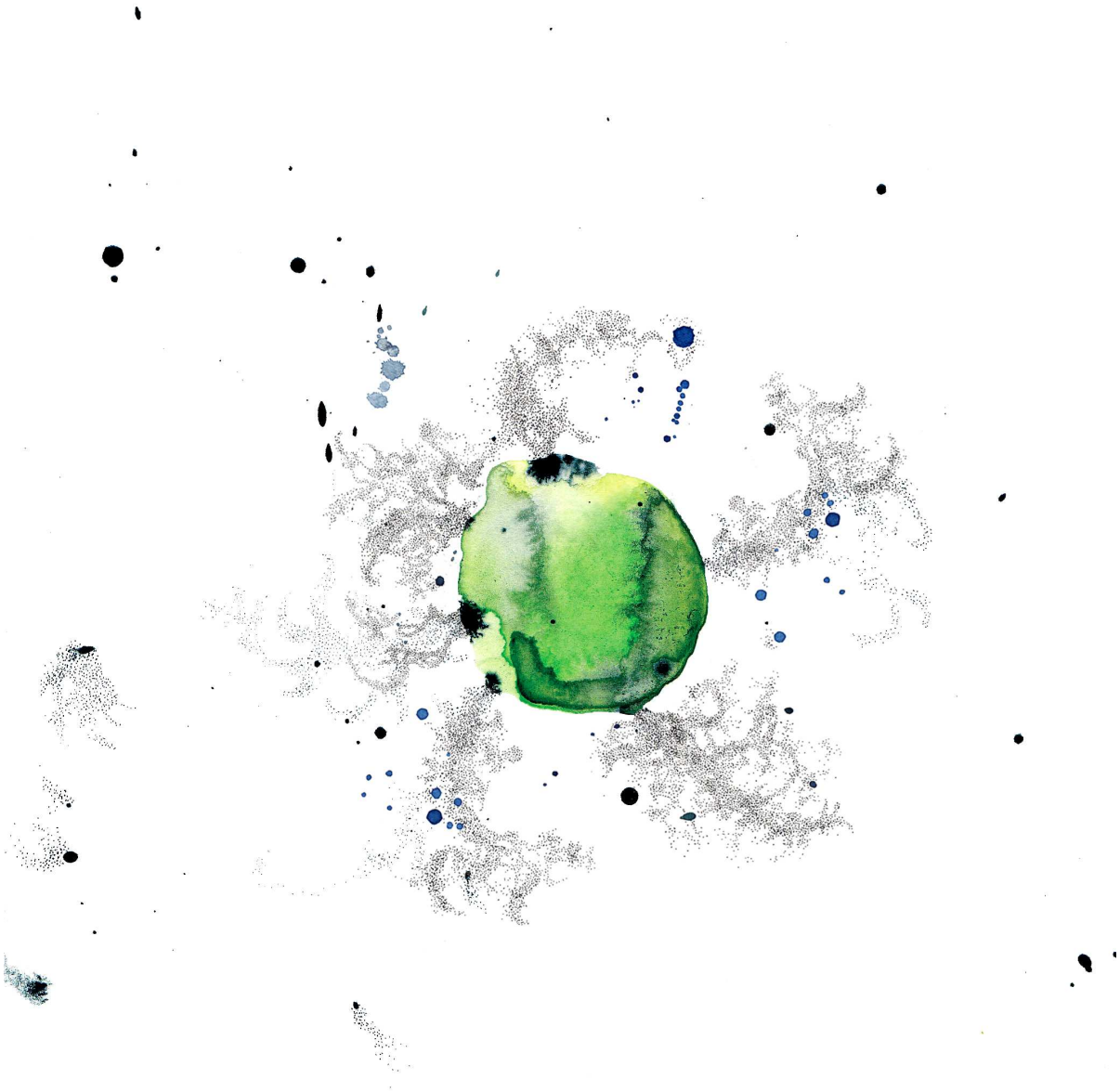

Etoile de terre, aquarelle et encre de Chine. Dessin de Sidonie Rocher, Juin 2014, Paris.

Abstract

The high northern latitudes have warmed faster than anywhere else in the globe during the past few decades. Boreal ecosystems are responding to this rapid climatic change in complex ways and some times contrary to expectations, with large implications for the global climate system. This thesis investigates how boreal vegetation has responded to recent climate change, particularly to the lengthening of the growing season and changes in drought severity with warming. The links between the timing of the growing season and the seasonal cycle of atmospheric CO_2 are evaluated in detail to infer large-scale ecosystem responses to changing seasonality and extended period of plant growth. The influence of warming on summer drought severity is estimated at a regional scale for the first time using improved data. The results show that ecosystem responses to warming and lengthening of the growing season in autumn are opposite to those in spring. Earlier springs are associated with earlier onset of photosynthetic uptake of atmospheric CO_2 by northern vegetation, whereas a delayed autumn, rather than being associated with prolonged photosynthetic uptake, is associated with earlier ecosystem carbon release to the atmosphere. Moreover, the photosynthetic growing season has closely tracked the pace of warming and extension of the potential growing season in spring, but not in autumn. Rapid warming since the late 1980s has increased evapotranspiration demand and consequently summer and autumn drought severity, offsetting the effect of increasing cold-season precipitation. This is consistent with ongoing amplification of the hydrological cycle and with model projections of summer drying at northern latitudes in response to anthropogenic warming. However, changes in snow dynamics (accumulation and melting) appear to be more important than increased evaporative demand in controlling changes in summer soil moisture availability and vegetation photosynthesis across extensive regions of the boreal zone, where vegetation growth is often assumed to be dominantly temperature-limited. Snow-mediated moisture controls of vegetation growth are particularly significant in northwestern North America. In this region, a non-linear growth response of white spruce growth to recent warming at high elevations was observed. Taken together, these results indicate that net observed responses of northern ecosystems to warming involve significant seasonal contrasts, can be non-linear and are mediated by moisture availability in about a third of the boreal zone.

Contents

List of Figures

List of Tables

I acknowledge the support from a doctoral scholarship from the Chilean Government under the program Formación de Capital Humano Avanzado of CONICYT. I thank the government for this great initiative to help young Chilean scientists entering the international scientific community from the best institutions in the world.

I thank Keith Briffa for being a great supervisor and friend during the past few years. I will always appreciate all his encouragement during difficult times and also those lovely family Christmas times. My thanks also go to Tom Melvin, Tim Osborn, Kevin Anchukaitis and Ed Cook for their supervision, computer code and help during the different stages of this research. Eugene Vanganov kindly provided access to his VS model.

Ranga Myneni, Jim Tucker and Dave Sauchyn provided inspiration, data and help from the other side of the Atlantic. From the continent, it was fantastic to have had the chance to work with Gerard van der Schrier and Wouter Dorigo. Thanks for having contributed to my research.

Stephen Sitch and Guillermo Murray from Exeter kindly shared some TRENDY data and hosted me during my visit. The detailed comments of Peter Cox and Phil Jones helped to improve the final version of the thesis.

I thank my mums Nena and Nancy and all my aunties for being patient all this time I have been away from home. I also thank you Kim Nommesch for being with me for a while during the difficult times and to you Cliodhna Donnan for being with me in the very difficult times. Cliodhna, thank you so much for those positive texts to wake me up when I most needed support.

I am grateful to all my dear friends I made in Norwich and more recently in Paris, some of which I shared beers with, wine and tons of good moments or PhDs. This includes a bunch more or less in order as I met them along the way: Jeppe Graugaard, Felipe Colon, Piotrek Bentkowski, Mario Gomez, Jorge Luis Vasquez, Jessica Vial, Carlos Rengifo, Alex Kemp, Charlotte Seifert, Helen Adams, Marisa Goulden, Chris May, Nessa Buth, Isabel Taylor, Lolita Moreno, Rocio Hiraldo, and now Paris; Luis Molina, Lisbeth Ron, Monsieur Johannes Stauffer and the rest of the LSCE foreign gang. I also wish to thank here to Philip (Chris) Reid and Renata Hari for their encouragement during the later phase of my writing and during the day of my viva!

My thanks also go to Philippe Peylin and Emanuel Gloor for being great persons to work with and for letting me complete the last stage of my writing whilst working on my postdoc. I thank Richard Cornes for sharing his pretty Latex code with me. It saved me a great deal of time.

I am grateful to Sidonie Rocher for making a beautiful artistic impression of the thesis: *Etoile de terre*.

Finally, thanks to all in CRU for all the good moments shared during my stay. I will miss you!

Chapter 1

Introduction

The circumpolar boreal forest biome represents about 14% of the vegetated cover of the Earth's surface and is the second most extensive terrestrial biome on Earth, after tropical forests (Roy *et al.*, 2001). Changes in the structure and functioning of this forested biome exert a significant influence on the global climate system through the exchange of huge amounts of water, energy and carbon with the atmosphere (Bonan *et al.*, 1995; Chapin *et al.*, 2000). Boreal soils account for about a third of the readily decomposable soil organic matter on Earth (McGuire *et al.*, 1995). This represents a quantity of stored carbon similar to that in the atmosphere. Release of this large carbon stores could affect the rate at which climate warms globally. The boreal forest is also the coldest forested biome in the planet and thus it is highly vulnerable to warming.

High-latitude amplification of 20th century anthropogenic warming has caused boreal forest and tundra biomes to warm twice as faster as the global average (Solomon *et al.*, 2007; Serreze & Barry, 2011). Mean annual air temperature has increased by 2–3^{o}C during the past 60 years and is projected to increase by an additional 3–6 ^{o}C by the end of the 21st century (Solomon *et al.*, 2007). The rapid climatic warming during the past few decades has provided an unprecedented opportunity to examine how a large biome adjusts to change and test ecological hypotheses. This has been aided by the increasing availability of Earth Observing data from a variety of satellite platforms since the late 1970s and early 1980s, monitoring a myriad of aspects of the atmosphere, the ocean and the land surface at the scale of meters and from a few hours to days. This technological advance has revolutionised our understanding on how the boreal forest is responding to climate change. However, the longest satellite records are only now reaching a sufficient length to discern decadal and longer-term trends in environmental change from natural variability. Moreover, long-term satellite monitoring records have typically been assembled from multiple sensors and this has introduced additional uncertainties in the identification of long-term ecological changes.

Multiple, complementary data streams and products should be used to overcome the limitations of the individual data streams and reduce uncertainties. This approach is adopted in this thesis to study the responses of boreal vegetation to recent climate change, with a focus on responses to the extension of the growing season and changes in summer drought severity accompanying recent warming. Quantifying the magnitude of these changes and inferring how northern terrestrial ecosystems are responding is necessary to test the ecological hypotheses and models that underlie our expectations for future ecosystem responses and feedbacks to the climate system.

1.1 Growing season and carbon cycle

In a seminal study, Keeling *et al.* (1996) showed that since the early 1960s the annual amplitude of the seasonal cycle of atmospheric CO_2 increased by 40% in the Arctic and 20% in Hawaii. This was accompanied by an advance of 7 days in the timing of the seasonal drawdown of CO_2 in spring. They attributed these changes in atmospheric CO_2 concentrations to increased CO_2 assimilation by northern terrestrial vegetation in response to a lengthening of the growing season due to rapid warming during that period. Using satellite observations, Myneni *et al.* (1997) confirmed that large increases in photosynthetic activity have occurred in the boreal forests between 1981 and 1991 in connection with significant spring warming and earlier snowmelt.

These two pioneer studies demonstrated for the first time how the northern biosphere was greening in response to surface warming and affecting the global carbon cycle. Subsequently, a large number of studies have analysed the linkages between spring warming and the carbon cycle (Randerson *et al.*, 1999; Piao *et al.*, 2007). Empirical and modelling studies have shown that warmer and earlier springs stimulate early-season ecosystem productivity more than ecosystem respiration, leading to earlier onset of net ecosystem carbon uptake and enhanced net ecosystem productivity (Goulden *et al.*, 1998; Randerson *et al.*, 1999).

Ecosystem responses during autumn have received less attention than during spring. However, recent studies have shown that warmer autumns tend to stimulate ecosystem respiration more than gross productivity (Piao *et al.*, 2008; Vesala *et al.*, 2010). This occurs in part because autumn carbon assimilation in northern terrestrial ecosystems tends to be light-limited (Suni *et al.*, 2003) and ecosystem respiration in permafrost regions is stimulated by warmer soils and deeper thawing depths (Randerson *et al.*, 1999). Yet, some stand-level studies have found that autumn respiratory losses are insufficient to offset concurrent productivity gains in some temperate and boreal ecosystems (Richardson *et al.*, 2010; Dragoni *et al.*, 2011). This indicates that ecosystem responses in autumn are more complex than in spring.

Piao *et al.* (2008) showed that ecosystem carbon losses associated with warmer autumns in recent decades have accelerated autumn CO_2 build-up in the atmosphere, reducing the length of the period of net biospheric carbon uptake as measured from the annual cycle of atmospheric CO_2. This implies that longer growing seasons may not always be associated with extended biospheric carbon sequestration, since respiratory losses resulting from prolonged autumn warmth can overwhelm concurrent productivity gains (Piao *et al.*, 2007, 2008). Further warming and extension of the potential growing season in autumn may offset the increases in carbon uptake associated with an earlier growing season and reduce the ability of northern ecosystems to capture carbon dioxide from the atmosphere.

Changes in the timing and length of the growing season at high northern latitudes have been extensively investigated during the past three decades of continuous satellite observation using a range of land surface phenological metrics (Cleland *et al.*, 2007). However, there is still a lack of Hemispheric assessments that put the short satellite records in a longer term context. Moreover, combined analyses of long-term climate and vegetation parameters of seasonality are required to assess whether vegetation and northern terrestrial ecosystems are tracking the pace of the rapid climatic warming in recent decades.

1.2 Warming and increasing drought severity

The hydrological cycle is expected to intensify in response to global warming due to increases in evaporation rates, higher atmospheric water vapour content, and changes in moisture transport (Allen & Ingram, 2002; Held & Soden, 2006; Seager *et al.*, 2010). Wet regions are projected to become wetter, and dry regions drier (Meehl *et al.*, 2007). A similar intensification of the existing patterns may also apply to the seasonal cycle of precipitation, with wet seasons getting wetter and dry seasons drier (Chou & Lan, 2012). As a result, global warming is expected to increase drought severity over many land areas (Dai, 2011b, 2012; Trenberth *et al.*, 2014). However, to date observational evidence of increased drought severity with recent warming is inconsistent among global studies (Dai, 2012; Sheffield *et al.*, 2012; van der Schrier *et al.*, 2013) despite increasing evidence indicating that the intensification of the water cycle is already underway in some regions (Huntington, 2006; Miralles *et al.*, 2013).

A regional synthesis of the observational record over the Arctic basin suggests that upward trends in annual precipitation, evapotranspiration, and river discharge to the Arctic Ocean could indicate that the expected intensification of the hydrological cycle is already taking place (Rawlins *et al.*, 2010). Recent estimates of continental evapotranspiration based on satellite observations show an increasing trend in northern latitudes at a rate consistent with expectations based on temperature trends (Miralles *et al.*, 2013). Increased evapotranspiration at high latitudes is also consistent with the trend toward earlier and longer growing seasons. Earlier spring thaw generally enhances annual evapotranspiration in colder areas. However, it can also suppress summer evapotranspiration by increasing drought stress in areas where moisture limits evapotranspiration, such as in the southern boreal region (Zhang *et al.*, 2011). The timing of the autumn freeze does not exert a strong influence on evapotranspiration as with the spring thaw.

A number of studies have suggested that northern terrestrial ecosystems are responding to changes in the regional hydrological cycle induced by surface warming. In particular, it is thought that 'temperature-induced drought stress' associated with increasing evaporative demand may be offsetting the positive benefits of warmer and longer growing seasons (Barber *et al.*, 2000; Goetz *et al.*, 2005; Bunn & Goetz, 2006; Zhang *et al.*, 2008). Enhanced evaporative demand could have intensified the severity of exceptional regional droughts observed during the late 1990s and 2000s (Zhang *et al.*, 2008; Dai, 2012). These droughts have increased fire disturbance (Kasischke & Turetsky, 2006) and resulted in regional decreases in vegetation productivity in the boreal forest as indicated by atmospheric CO_2 anomalies (Angert *et al.*, 2005), satellite vegetation indices (Goetz *et al.*, 2005; Bunn & Goetz, 2006), modelled vegetation productivity (Zhang *et al.*, 2008), forest inventory data (Hogg *et al.*, 2008; Ma *et al.*, 2012) and tree rings (Barber *et al.*, 2000; Hogg & Wein, 2005). These ecological responses have led to the perception that summer drought severity in the northern latitudes is increasing along with recent warming because of greater evaporative demand (Barber *et al.*, 2000; Angert *et al.*, 2005). Yet, the links between warming, summer drought severity, and observed vegetation dynamics at northern latitudes are still uncertain.

The lack of long-term soil moisture observations in the pan-Arctic region precludes a direct analysis of decadal changes in soil moisture. However, model-based estimates broadly

support the notion of increased drought severity with recent warming in the boreal zone (Sheffield & Wood, 2007; Dai, 2011a).

Understanding the drivers of summer drought severity in the northern latitudes requires realistic estimates of soil moisture variability and quantification of the relative contributions of changes in moisture supply (precipitation and snow) and evaporative demand (potential evapotranspiration), which depends not only on temperature but also on radiation, humidity and winds (Wang & Dickinson, 2012). Quantifying the role of increased evaporative demand on high-latitude droughts remains a challenge.

1.3 Aim and outline of the research

The main goal of this thesis is to investigate the responses of boreal vegetation to the lengthening of the growing season and changes in drought severity with recent warming using multiple observational data streams. The thesis is organised in seven sequential chapters and is divided into two parts: Part I has two chapters and investigates the linkages between recent changes in the growing season and the carbon cycle, and Part II has three chapters and provides an analysis of changes in drought severity in the boreal region and associated vegetation responses. An outline of each chapter is presented below.

Chapter 2. Thermal growing season and biospheric carbon uptake
This chapter investigates the relationship between the timing and duration of the thermal potential growing season and the period of biospheric carbon uptake in the extra-tropical Northern Hemisphere. Gridded daily mean temperature data over the period 1950–2011 are used to characterise the spatiotemporal variability of the thermal growing season. The analysis highlights a strong autumn warming during the 2000s and a contrasting response of northern ecosystems to the seasonal timing of temperatures in spring and autumn, supporting earlier findings by Piao *et al.* (2008).

The findings of this chapter were published in *Global Biochemical Cycles* as:

> Barichivich, J., K. R. Briffa, T. J. Osborn, T. Melvin, and J. Caesar (2012), Thermal growing season and timing of biospheric carbon uptake across the Northern Hemisphere, *Global Biogeochem. Cycles*, 26, GB4015, doi:10.1029/2012GB004312.

Chapter 3. Changes in growing season and the seasonal cycle of atmospheric CO_2
The analysis presented in this chapter provides an update to the work of Keeling *et al.* (1996) and Myneni *et al.* (1997). The simple thermal indices developed in Chapter 2 are combined with satellite and other ground observations to investigate the long-term links between multiple climate (air temperature and cryospheric dynamics) and vegetation (greenness and atmospheric CO_2 concentrations) indicators of the growing season of northern ecosystems and their connection with the carbon cycle during 1950–2011. One of the main findings of this study is that the photosynthetic growing season based on satellite-observed greenness has closely tracked the pace of warming and extension of the potential growing season in spring, but not in autumn, when factors other than temperature seem to constrain photosynthesis.

The findings of this chapter were published in *Global Change Biology* as:

> Barichivich, J., K. R. Briffa, R. Myneni, T. J. Osborn, T. Melvin, P. Ciais, S. Piao and C. Tucker (2013), Large-scale variations in the vegetation growing season and annual cycle

of atmospheric CO_2 at high northern latitudes from 1950 to 2011, *Global Change Biology*, doi: 10.1111/gcb.12283.

Chapter 4. Changes in summer drought severity using the scPDSI
In this Chapter, an improved version of a recently published dataset of the self-calibrating Palmer Drought Severity Index (scPDSI) is evaluated and analysed to infer changes in drought severity across the high northern latitudes since 1950. Multiple comparisons with soil moisture observations and simulations from two modern land surface models show that the index is a good indicator of summer and autumn soil moisture variability, with a skill similar to complex land surface models. The analysis of this new dataset shows that rapid warming since the late 1980s has increased evaporative demand and drought severity during summer and autumn, offsetting the effect of increasing cold-season precipitation. This validated dataset is used as the basis for the analyses presented in Chapter 5.

Some of the analyses presented in this Chapter contributed to the following publications:

– van der Schrier, G., J. Barichivich, K.R. Briffa, P.D. Jones (2013), A scPDSI-based global dataset of dry and wet spells for 1901-2009, *J. Geophys. Res. Atmos.*, 118, doi:10.1002/jgrd.50355.

– Trenberth, K.E., A. Dai, G. van der Schrier, P.D. Jones, J. Barichivich, K.R. Briffa, and J. Sheffield (2014), Global warming and changes in drought, *Nature Climate Change,* 4, doi:10.1038/nclimate2067.

Chapter 5. Temperature and moisture controls on summer vegetation greenness
This chapter presents a comprehensive analysis of moisture and temperature controls on summer vegetation greenness in the northern latitudes during the period 1982–2011. The results highlight a significant snow-mediated moisture control of summer vegetation photosynthetic activity in northwestern North America. It is found that in this region, declining trends in vegetation greenness reported in earlier studies are consistent with declining snowpack rather than with changes in evapotranspiration demand.

The main findings of this chapter were published in *Remote Sensing* in the special issue "Monitoring Global Vegetation with AVHRR NDVI3g Data (1981-2011)" as:

Barichivich, J., K. R. Briffa, R. Myneni, G. van der Schrier, W. Dorigo, J. Tucker, T. J. Osborn and T. Melvin (2014), Temperature and snow-mediated moisture controls of summer vegetation photosynthetic activity in northern terrestrial ecosystems between 1982 and 2011, *Remote Sens.*, 6(2), 1390–1431.

Chapter 6. Moisture and tree-ring growth in northwestern North America
This last analysis chapter re-evaluates the roles of soil moisture and non-linear responses on the observed growth patterns of white spruce in northwestern North America. The process-based Vaganov-Shashkin (VS) model of tree-ring formation is used to evaluate growth responses in three well-know cases of 'tree-ring divergence'. The results of this chapter highlight the significant influence of moisture limitation on boreal vegetation in northwestern North America and provide evidence for an apparent non-linear growth response of white spruce growth to recent warming at high elevations. The calibrated VS model identifies a non-linear growth response to

temperature in sites showing divergence and suggests that tree growth at these locations starts to decline when daily temperatures exceed a threshold of about 17^{o}C.

Chapter 7. Conclusions and further research

A summary of the main results obtained in the previous chapters is presented and discussed, highlighting avenues for future research.

Part I

Boreal growing season and carbon cycle

Chapter 2

Thermal potential growing season and timing of biospheric carbon uptake across the Northern Hemisphere

Abstract

Gridded daily temperature from 1950 to 2011 and atmospheric CO_2 concentration data from high-latitude observing stations and the CarbonTracker assimilation system are used to examine recent spatiotemporal variability of the thermal growing season and its relationship with seasonal biospheric carbon uptake and release in the Northern Hemisphere. The results indicate that the thermal growing season has lengthened substantially since 1950 but most of the lengthening has occurred during the last three decades (2.9 days decade^{-1}, $p < 0.01$ for 1980-2011), with stronger rates of extension in Eurasia (4.0 days decade^{-1}, $p < 0.01$) than in North America (1.2 days decade^{-1}, $p > 0.05$). Unlike most previous studies, which had more limited data coverage over the past decade, this study shows that strong autumn warming of about 1^{o}C during the second half of the 2000s has led to a significant shift toward later termination of the thermal growing season, resulting in the longest potential growing seasons since 1950. On average, the thermal growing season has extended symmetrically by about a week during this period, starting some 4.0 days earlier and ending about 4.3 days later. The earlier start of the thermal growing season is associated with earlier onset of the biospheric carbon uptake period at high northern latitudes. In contrast, later termination of the growing season is associated with earlier termination of biospheric carbon uptake, but this relationship appears to have decoupled since the beginning of the period of strong autumn warming during the second half of the 2000s. Therefore, owing to these contrasting biospheric responses at the margins of the growing season, the current extension in the thermal growing season length has not led to a concomitant extension of the period of biospheric carbon uptake.

Published as: Barichivich, J., K. R. Briffa, T. J. Osborn, T. Melvin, and J. Caesar (2012), Thermal growing season and timing of biospheric carbon uptake across the Northern Hemisphere, *Global Biogeochem. Cycles*, 26, GB4015, doi:10.1029/2012GB004312

2.1 Introduction

The plant growing season is the period of the year when plants are able to grow and assimilate carbon from the atmosphere. In northern temperate and boreal regions, it begins in spring with increasing temperatures and solar radiation, the melting of snow, eventual thawing of the soil organic horizons, and the start of photosynthesis. It terminates in autumn as temperatures and day length decrease, soils refreeze, and photosynthesis ceases (Jarvis & Linder, 2000; Kimball *et al.*, 2004; Euskirchen *et al.*, 2006). The rapid winter/spring warming observed at northern latitudes during recent decades has resulted in earlier melting of snow and soil thawing, stimulating an earlier start and sustained lengthening of the growing season of northern vegetation (Keeling *et al.*, 1996; Myneni *et al.*, 1997; Menzel & Fabian, 1999; Zhou *et al.*, 2001; Smith *et al.*, 2004; Linderholm, 2006; Piao *et al.*, 2006a; Christidis *et al.*, 2007; Piao *et al.*, 2007). Lower rates of autumn warming (Christidis *et al.*, 2007) and the influence of other environmental effects on autumn phenology and growth cessation (Suni *et al.*, 2003; Kimball *et al.*, 2004; Hänninen & Tanino, 2011) have contributed to a weaker rate of concurrent extension in autumn.

Changes in timing and length of the growing season affect the timing and magnitude of carbon assimilation from local to hemispheric scale (e.g., Goulden *et al.*, 1998; Keeling *et al.*, 1996; Baldocchi & Wilson, 2001; Churkina *et al.*, 2005; Barr *et al.*, 2009). Empirical and modelling studies have shown that warmer and earlier springs stimulate early-season gross ecosystem productivity (GEP) more than ecosystem respiration (ER), leading to earlier onset of net ecosystem carbon uptake and enhanced net ecosystem productivity (NEP = GEP–ER) (Goulden *et al.*, 1998; Keeling *et al.*, 1996; Randerson *et al.*, 1999). Increased early-season ecosystem carbon uptake driven by recent spring warming has led to enhanced amplitude and advanced timing of the seasonal cycle of atmospheric CO_2 concentration at northern latitudes since the 1960s (Keeling *et al.*, 1996; Randerson *et al.*, 1999; Nemani *et al.*, 2003).

Recent studies have found that unlike in spring, warmer autumns tend to stimulate more ER than GEP (Piao *et al.*, 2008; Vesala *et al.*, 2010), since autumnal carbon assimilation of northern terrestrial ecosystems tends to be light-limited (Suni *et al.*, 2003) and ecosystem respiration is enhanced by warmer soil temperatures and deeper thawing depths in permafrost regions (Randerson *et al.*, 1999). Autumnal ecosystem carbon losses associated with warmer autumns have accelerated autumn CO_2 build-up in the atmosphere during recent decades, reducing the length of the period of net biospheric carbon uptake based on the annual cycle of atmospheric CO_2 (Piao *et al.*, 2008). This has shown that longer growing seasons are not always associated with extended biospheric carbon sequestration, since respiratory losses resulting from prolonged autumn warmth can be larger than concurrent GEP gains (Piao *et al.*, 2007, 2008). Further warming and extension of the potential growing season in autumn may offset the increases in carbon uptake associated with an earlier growing season and reduce the ability of northern ecosystems to capture carbon dioxide from the atmosphere.

A recent study based on satellite-derived Normalized Difference Vegetation Index (NDVI) data since 1982 found that the hemispheric extension of the photosynthetic growing season between 2000 and 2008 was dominated by delayed termination, rather than earlier onset (Jeong *et al.*, 2011). During this period, autumn senescence was further delayed by 2.3 days

presumably due to a recent amplification of late-season warming, whereas spring green-up further advanced at a lower rate of 1.8 days due to a reduction of spring warming rates compared with previous decades. Zhu *et al.* (2012) used a shorter version of the same satellite dataset and a network of phenological observations through the period 1982-2006 to investigate changes in the growing season in North America, where the lengthening has been driven almost exclusively by a trend toward delayed termination since the 1980s (Piao *et al.*, 2007). They found that the strongest delay in senescence occurred during the last four years (2003-2006) of their study period. The overall trends toward delayed senescence and extended growing season since 1982 were not statistically significant if these four years were excluded from trend analysis, indicating a large contribution of the anomalies during this period to the long-term trend. However, a comparison between the NDVI dataset used in these studies (GIMMS NDVIg) and a newer, improved version (GIMMS NDVI3g) indicates that the strong autumn delay reported in these studies appears to be in large part related to a calibration issue in the earlier NDVIg dataset since around 2003 (see Chapter 3). Therefore, the magnitude of recent autumn delay based on long-term satellite data remains uncertain.

The amplification of autumn warming and delayed termination of the growing season during recent years may have important implications for the carbon balance of northern ecosystems. Furthermore, in comparison with the 1980s and 1990s, temporal and spatial changes in the growing season during the 2000s are still very uncertain because few studies span the complete decade. This chapter examines recent spatial and temporal variation of the thermal growing season in a longer-term context and its correlation with the timing of biospheric carbon uptake across the Northern Hemisphere (north of 30^{o}N). The specific aims are *(i)* to characterize the spatio-temporal variability of the duration and the timing of the start and end of the thermal growing season over the period 1950–2011 using an updated dataset of gridded daily temperature and *(ii)* to investigate the relationship between these parameters and the timing and duration of the period of biospheric carbon uptake based on in-situ measurements of atmospheric CO_2 concentration at four high-latitude observing stations and simulated CO_2 concentrations from the CarbonTracker assimilation system (Peters *et al.*, 2007). This work complements earlier large-scale studies of the growing season as it spans some recent years not previously analyzed, thus helping to reduce current uncertainties in growing season changes over the past decade and their potential impact on the carbon balance of northern terrestrial ecosystems.

2.2 Data and Methods

2.2.1 Temperature data and thermal growing season

The HadGHCND gridded dataset (2.75^ox3.75^o) of maximum and minimum daily temperatures (Caesar *et al.*, 2006) was used to derive daily mean temperature data over the period 1950-2011 at valid grid points on land areas north of 30^oN, excluding Greenland. Missing values in the mean temperature field, located principally after the year 2007 and at grid points in Siberia, Japan and Scandinavia (Supplementary Figure A1), were imputed using the regularized expectation maximization algorithm with truncated total least squares (Schneider, 2001). Given the large size of the data matrix, this regularization scheme (RegEM-TTLS) was preferred because it is computationally faster than the alternative scheme based on ridge regression (RegEM-Ridge). Grid points with more than three years of missing data were discarded from analysis. For convenience, data for February 29th in leap years were excluded, leaving 365 daily values for each year. Earlier versions of this dataset have been used in previous studies of the climatological growing season (Christidis *et al.*, 2007) and extreme events (Caesar *et al.*, 2006; Hamilton *et al.*, 2012).

The TIMESAT package (Jönsson & Eklundh, 2004) was used to compute the date of the start (STS) and end (ETS) of the growing season for each grid point and year. First, each seasonal cycle was smoothed using a double logistic fit to reduce noise associated with high day-to-day variability. Then, the dates for STS and ETS were obtained from the points where the smoothed cycle intersected a fixed temperature threshold of 5^oC, which is a widely used value for determining the boundaries of the thermal growing season at mid and high latitudes (Frich *et al.*, 2002). The length of the thermal growing season (LTS) was calculated as the difference between ETS and STS. Warmer regions like western Europe and the Middle East were masked out from further statistical analysis because the temperature threshold was too low to derive continuous yearly time series of thermal growing season parameters in these areas.

Linear trends in the STS, ETS and LTS parameters were estimated over the period 1980–2011 using the non-parametric Mann-Kendall trend test based on the Sen slope and a trend free pre-whitening procedure (Yue *et al.*, 2002) as implemented in the *zyp* R package (Bronaugh, 2009). This 32–year period was chosen to make the results of this study more comparable with studies based on satellite data. The non-linear trend of the circumpolar averages of these parameters between 1950 and 2011 was estimated using a generalized additive mixed model (GAMM) approach that allows modelling slowly varying trends by fitting a thin-plate spline to the time series with a first-order autoregressive term for the residuals (Wood, 2006; Curtis & Simpson, 2014). Models were fitted with the *mgcv* R package (Wood, 2011) using restricted maximum likelihood (REML: Wood, 2006) for smoothing parameter selection. Unlike simple linear trends, this statistical technique fits a local rather than a global time series model that better describes temporally varying trends in a time series.

In order to aid the visualisation of the spatial patterns of temperature and thermal growing season linear trends over the forested regions of the study domain, the outline of the boreal forests was computed using the latest version (Collection 5) of the MODIS IGBP land cover classification map (Friedl *et al.*, 2010) and woody fraction from MODIS Vegetation Continuous Fields product (Townshend, 2011). All evergreen needleleaf, deciduous needleleaf and mixed

forests north of 45^{o}N with woody fraction greater than 30% were considered as boreal forest (Xu *et al.*, 2013).

2.2.2 Biospheric carbon uptake period

The seasonal cycle of atmospheric CO_2 concentrations can be used as an integrated measure of the net carbon exchange between the terrestrial biosphere and the atmosphere (Keeling *et al.*, 1996; Heimann *et al.*, 1998). The annual cycle of the atmospheric CO_2 concentration was used to estimate the timing and duration of the biospheric carbon uptake period at Alert (82^{o}N), Point Barrow (71^{o}N), Ocean Station M (66^{o}N) and Shemya Island (53^{o}N) observing stations (GLOBALVIEW-CO_2, 2011). Three of these stations are located in the Arctic and one in the north Pacific so their seasonal cycles primarily reflect changes in carbon exchange (NEP) across northern terrestrial ecosystems with little influence of ocean exchange, fossil fuel emissions and tropical biomass burning (Randerson *et al.*, 1997; Piao *et al.*, 2008).

The curve-fitting procedures developed by Thoning *et al.* (1989) and implemented in the CCGVU routine (available at: *ftp://ftp.cmdl.noaa.gov/ccg/software/*) were used to extract the seasonal cycle from the monthly records. This algorithm decomposes the CO_2 time series into a long-term trend and seasonal and interannual components using a polynomial function and a series of annual harmonics combined with a digital filtering technique based on Fast Fourier Transform (FFT) and low-pass filters. The routine was run using a quadratic polynomial to fit the trend, four annual harmonics for the seasonal component, and short and long frequency cutoff parameters of 100 and 650 days in the FFT low-pass filtering in order to remove high-frequency noise and isolate the trend component. These settings have been commonly used in previous studies of long-term changes in the CO_2 seasonal cycle (e.g., Thoning *et al.*, 1989; Buermann *et al.*, 2007).

The output of this procedure is a time series of smoothed and detrended annual cycles of the original data. The downward (upward) zero-crossing date of CO_2 was determined as the day when the atmospheric CO_2 annual cycle crosses the zero line from positive (negative) to negative (positive) values during spring (autumn). A sensitivity test showed that the relative temporal variations in these parameters of the CO_2 annual cycle are not affected by the choice of the parameter values used in the curve-fitting and filtering procedure (Supplementary Figure A2).

The downward (spring: SZC) and upward (autumn: AZC) zero-crossing dates have often been used to derive the timing and duration of the net carbon uptake period (CUP = AZC – SZC) for each year (e.g., Piao *et al.*, 2008), though this is not strictly correct. If the annual cycle of CO_2 concentration at a high-latitude measuring station were controlled only by biospheric fluxes, then the net CUP would run from the spring maximum in concentration to the late summer minimum, rather than from the downward to upward zero-crossing times. Nevertheless, the zero-crossing times and their difference were used here as surrogates for the onset, termination and duration of the net CUP for two reasons. First, to allow easier comparisons with earlier work. Second, because the timing of a zero-crossing can be determined more accurately than the timing of a maximum or minimum, especially if they are broad and superimposed with shorter-term variability. Because of this issue, the term biospheric carbon uptake rather than *net* biospheric carbon uptake is used, though one might expect that an earlier maximum in

CO_2 concentration (e.g. due to the earlier onset of the net CUP) should be associated with an earlier spring downward zero-crossing (and similarly for autumn). In other words, if the shape of the seasonal cycle does not change significantly, then a relative change in the phase of the cycle identified at one point (e.g. the maximum) will be matched by relative phase changes at all other points (e.g. zero-crossings).

In order to examine the reliability of the four CO_2 observing stations, column-averaged CO_2 mole fractions from the latest release of CarbonTracker (CT2010) were used to derive spatial fields of zero-crossing dates for the period 2000–2009. CarbonTracker is a reanalysis of the recent global surface land and ocean fluxes and the corresponding atmospheric CO_2 mole fractions estimated by assimilating surface flask measurements from the NOAA/ESRL network and tall tower measurements using an Ensemble Kalman Filter technique (Peters *et al.*, 2007, 2010). The underlying atmospheric transport model TM5 (Krol *et al.*, 2005) with 25 vertical layers is driven by meteorological data from the European Centre for Medium Range Weather Forecasts (ECMWF). The global data of carbon dioxide mole fraction are available at 3-hour time steps with 3^ox2^o horizontal resolution and 25 vertical levels. Daily column-averaged mole fraction data for the free-troposphere (850–500 hPa or 1.2–5 km) were used. This corresponds to levels 5 through 10 of the TM5 model before 2005 and levels 6 through 10 since 2006 due to an improvement in the vertical resolution. CO_2 concentration gradients in this layer result from the exchange between the atmosphere and the land surface before subsequent transport and atmospheric mixing by weather systems. The same procedure explained above was applied to daily CO_2 fields in order to extract the timing and length of the biospheric CUP for every grid box.

Quantitative comparisons between the corresponding parameters of the thermal growing season and biospheric carbon uptake were made using linear correlation analysis. The statistical significance of correlations was estimated using a non-parametric random phase test with 1000 Monte-Carlo simulations (Ebisuzaki, 1997). This method ensures that the significances are appropriate given the degrees of freedom associated with each of the time series being correlated.

Table 2.1: Mann-Kendall linear trends (Sen slope ± 1 s.e.) in the circumpolar and continental area-averaged series of STS, ETS, LTS and spring (March-April) and autumn (September-October) temperatures between 1980-2011. Trends in bold are significantly different from zero at $p < 0.05$ and an asterisk indicates that the coefficient is also significant at $p < 0.01$.

	Growing season (days · decade^{-1})			Temperature (^{o}C · decade^{-1})	
Region	STS	ETS	LTS	Spring	Autumn
Circumpolar	**-1.42 ± 0.62***	**1.50 ± 0.77***	**2.86 ± 1.31***	**0.43 ± 0.24***	**0.46 ± 0.17***
North America	0.53 ± 1.20	**1.39 ± 1.21**	1.15 ± 2.11	0.03 ± 0.48	**0.42 ± 0.26***
Eurasia	**-2.25 ± 0.93***	**1.59 ± 0.63***	**4.00 ± 1.14***	**0.50 ± 0.41***	**0.41 ± 0.18***

2.3 Results

2.3.1 Spring and autumn temperatures

Spring and autumn land temperatures have risen by about 1^{o}C during the study period (Figure 2.1a–b). Spring temperatures have increased linearly since 1950 whilst autumn temperatures have risen only since the late 1980s, with the strongest increase during the 2000s. On a mean circumpolar scale, temperatures in spring and autumn have warmed at a similar rate of around 0.40^{o}C per decade over the period 1980-2009 (Table 2.1). However, there is considerable spatial variability in the temperature trends. Eurasia has warmed significantly in both spring (0.50±0.41^{o}C decade^{-1}) and autumn (0.41±0.18^{o}C decade^{-1}), whereas in North America the warming has been significant only during autumn (0.42±0.26^{o}C decade^{-1}).

In general, since 1980 spring surface warming has been significant across Europe, northern Canada and most of the mid and high latitudes of Eurasia, while spring temperatures have either cooled or not warmed significantly in the region located between 30^{o}N and 70^{o}N in central and western North America (Figure 2.1c). Autumn has also warmed significantly across mid and high latitudes of Eurasia and most of the boreal regions in North America but not in Europe (Figure 2.1d). At the biome level, spring warming has not been significant over the circumpolar boreal forests, although the Eurasian boreal forest has experienced more spring warming than its counterpart in North America, which has cooled in the western part of the continent (Figure 2.1c). The boreal forest and tundra of eastern North America, Alaska and western Russia have experienced strong and significant autumnal warming (Figure 2.1d). The only northern region that has warmed significantly during spring and autumn is the coastal tundra in eastern Siberia.

2.3.2 Variability of the thermal growing season

During the study period there is a general long term trend toward earlier and longer-lasting growing seasons until the first half of the 2000s, when an unprecedented period of delayed termination began and further extended the growing season by an amount similar to the advance in the beginning (Figure 2.2a–c). This recent shift in termination of about 4 days resulted from a sustained increase in autumn temperatures of around 1^{o}C during the second half of the 2000s (Figure 2.1b). The combination of earlier STS with the recent shift toward delayed ETS has resulted in the longest thermal growing seasons during the study period, particularly in Eurasia (Figure 2.2c). At the circumpolar scale, the thermal growing season has extended by a week since 2005, following an initial extension of about 5 days during the 1990s. It has lengthened at a rate of 2.86±1.31 days per decade since 1980, as a result of significant trends toward advanced STS (-1.42±0.62 days decade^{-1}, $p < 0.01$) and delayed ETS (1.5±0.77 days decade^{-1}, $p < 0.01$) during the same period (Table 2.1). The overall lengthening has been larger in Eurasia (4.0±1.14 days decade^{-1}, $p < 0.01$) associated with significant changes in both STS and ETS, but the lengthening in North America (1.15±2.11 days decade^{-1}, $p > 0.05$) has not been statistically significant (Table 2.1).

The spatial pattern of trends in LTS over the period 1980-2011 shows that the extension of the thermal growing season has been significant across most of Asia, eastern Europe, Alaska and the far north of Canada, including most of the boreal forest and tundra occurring in these regions

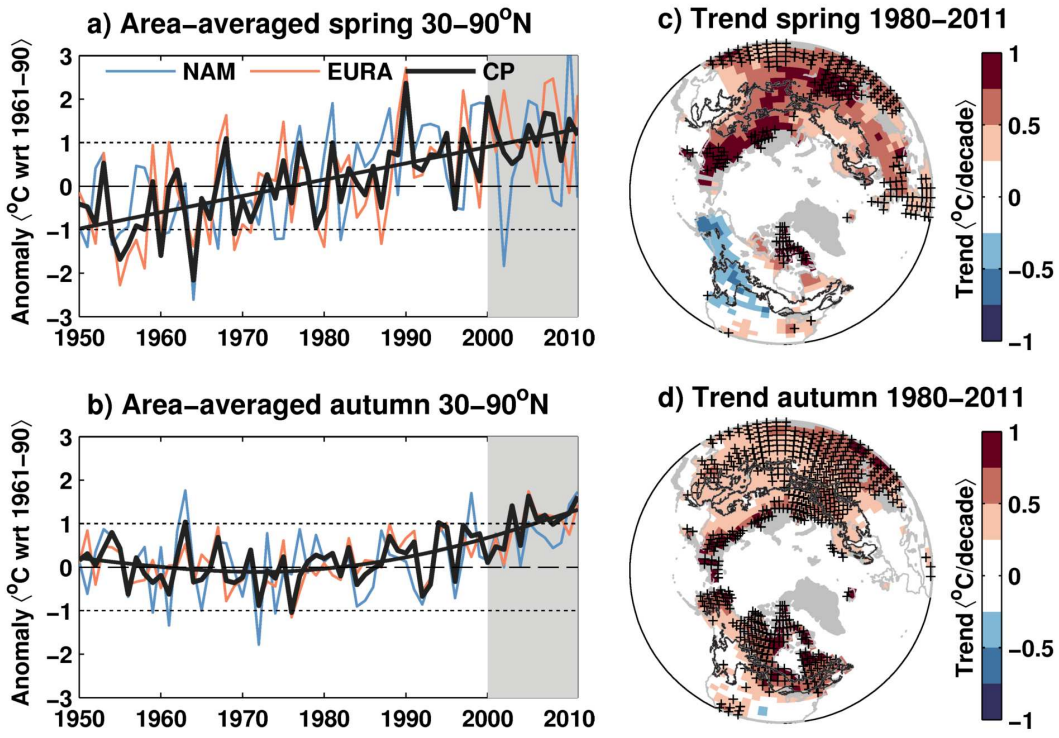

Figure 2.1: Temporal variability (a-b) and Mann-Kendall linear trends (c-d) of spring (March-April) and autumn (September-October) mean surface air temperature from the HadGHCND dataset. Area-averaged time series north of 30°N are shown for North America (NAM, red), Eurasia (EURA, blue) and the entire circumpolar region (CP, black). In the left panels, the smoothed black lines denote the non-linear trend of the circumpolar averages and the period 2000–2011 is highlighted with gray shading. Linear trends shown in the maps correspond to the Sen slope computed over the period 1980–2011. Grid boxes with significant trends ($p < 0.05$) are indicated by black crosses, whilst areas excluded from analysis due to permanent ice cover and missing data are shown in gray. The spatial extent of the boreal forest is indicated by the black polygons.

(Figure 2.2f). Significant advance in STS has driven the extension across most of Asia and Europe (Figure 2.2d), whereas in Alaska and northern Canada the extension has been dominated by significant trends toward delayed ETS (Figure 2.2e). Although not statistically significant, in the region of the boreal forest in central and western North America the thermal growing season length has decreased because spring and autumn cooling has produced a moderate delay in STS and no change in ETS. The continental average in ETS (Figure 2.2b) is dominated by trends in Alaska and northern Canada.

2.3.3 Carbon uptake period and thermal growing season

2.3.3.1 Observing stations

Most CO_2 observing stations began recording during the second half of the 1980s and all of them have data spanning the period 1987 to 2009 (Table 2.2), which was chosen as the common period of analysis. The timing of CO_2 zero-crossing dates and the resulting length of the biospheric CUP vary considerably from year to year (Figure 2.3b–d), but there are no significant trends during the period 1987-2009 (Table 2.2). In a longer term context, Point Barrow shows a clear trend toward advanced SZC (-1.5±0.84 days decade^{-1}, $p < 0.001$) and AZC (-1.6±1.53

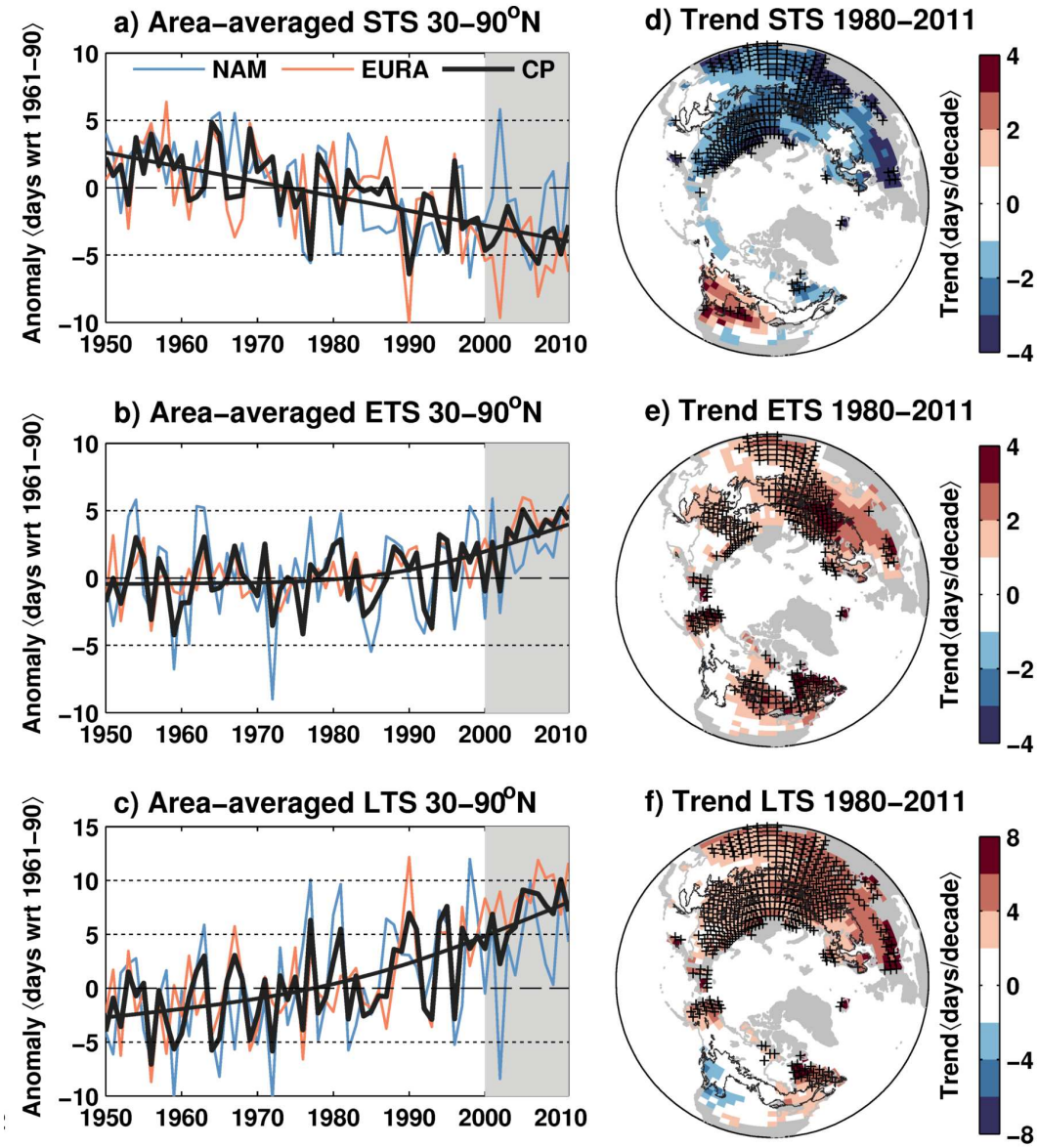

Figure 2.2: Temporal variability (a-c) and Mann-Kendall linear trends (d-f) of the start (STS), end (ETS) and length (LTS) of the thermal growing season. Area-averaged time series north of 30°N are shown for North America (NAM, red), Eurasia (EURA, blue) and the circumpolar region (CP, black). In the left panels, the smoothed black lines denote the non-linear trend of the circumpolar averages and the period 2000–2011 is highlighted with gray shading. Linear trends shown in the maps correspond to the Sen slope computed over the period 1980–2011. Grid boxes with significant trends ($p < 0.05$) are indicated by black crosses, whilst areas excluded from analysis due to permanent ice cover and missing data or discontinuous time series of thermal growing season parameters are shown in gray. The spatial extent of the boreal forest is indicated by the black polygons.

days decade^{-1}, $p < 0.05$) since 1972 but the length of the CUP does not show any significant concurrent long-term trend as a result of relatively parallel advances in the zero-crossing dates.

The interannual variability of zero-crossing dates is more coherent between stations in spring than in autumn (Figure 2.3), indicating a larger and more consistent spatial footprint of variations in biospheric carbon exchange during spring. Over the period 1987-2009, variations in the timing of SZC at the four stations are strongly and positively correlated with circumpolar anomalies in STS (r = 0.66 to 0.70, $p < 0.05$), despite a strong continental contrast in the magnitude of the correlations (Table 2.3). This indicates that earlier STS is associated with

Table 2.2: Mann-Kendall linear trends (Sen slope ± 1 s.e.) of zero-crossing dates and length of CUP between 1987–2009 at four monitoring stations from the global NOAA-ERSL air-sampling network (Alert, Point Barrow, Station M and Shemya Island). None of the trends is significantly different from zero at $p < 0.05$.

			Zero-crossing dates (days · decade^{-1})		CUP
Station	Location	Period	Spring (SZC)	Autumn (AZC)	(days · decade^{-1})
ALT	82.5°N – 62.5°W	1986-2009	-0.50 ± 1.60	-0.03 ± 2.68	0.38 ± 2.50
BRW	71.3°N – 156.6°W	1972-2009	-0.82 ± 1.88	0.68 ± 3.36	0.66 ± 3.97
STM	66.0°N – 2.0°E	1983-2009	-1.14 ± 1.36	-3.11 ± 3.40	-1.63 ± 3.43
SHM	52.7°N – 174.1°E	1987-2009	-1.79 ± 2.12	-0.87 ± 2.89	-0.01 ± 2.72

earlier biospheric carbon uptake. Figure 2.4a–d illustrates the good agreement between time series of SZC and circumpolar STS over the full length of the individual station records. Note that the agreement is strong not only for interannual anomalies but also for longer-term decadal features, especially in the longer station records. For instance, it is clear that the circumpolar trend toward earlier STS is consistent with the long-term variability of SZC at Point Barrow since 1972 (r = 0.64, $p < 0.05$; Figure 2.4b). The continental contrast in the associations was further examined using a spatial correlation analysis (Figure 2.1a–d), which reveals that the stations share a very similar STS spatial footprint with significant correlations across most of Eurasia and poor correlations over North America. This suggests that the springtime biospheric signal in the atmosphere at high northern latitudes is dominated by temperature-induced variations in the timing of biospheric uptake over Eurasia. Regression analysis between SZC for the four station records combined and STS averaged over Eurasia during 1987-2009 indicates that the timing of net spring carbon uptake at high-northern latitudes advanced by 0.61±0.09 days for each day of advance in STS over Eurasia. The slope of the relationship is practically zero when using STS averaged over North America, consistent with the poor correlations observed in Table 2.3. Point Barrow, in Alaska, is the only station where SZC is moderately correlated with STS in North America (r = 0.30, $p > 0.05$), although over a small region near the station (Figure 2.5b).

Table 2.3: Correlations between the timing and duration of the biospheric carbon uptake period at each CO_2 monitoring station and the timing and duration of the thermal growing season averaged over North America (NAM), Eurasia (EURA) and the the circumpolar region (CP) between 1987–2009. Correlations in bold are significant at $p < 0.05$ and the asterisk indicates that the coefficient is also significant at $p < 0.01$. The significance of the correlations was estimated using a non-parametric random phase test with 1000 Monte-Carlo simulations.

	STS vs SZC			ETS vs AZC			LTS vs CUP		
Station	NH	NAM	EURA	NH	NAM	EURA	NH	NAM	EURA
ALT	**0.66**	0.01	**0.74**	**-0.61***	**-0.59***	**-0.36**	**-0.28**	**-0.51***	0.08
BRW	**0.65**	0.30	**0.52**	**-0.41**	**-0.43***	-0.23	-0.24	-0.32	0.02
STM	**0.70**	-0.03	**0.71**	-0.12	0.12	-0.21	0.18	0.35	0.07
SHM	**0.61**	-0.20	**0.82**	-0.26	-0.25	-0.23	0.01	**-0.42**	0.32

In contrast to spring, variations of zero-crossing date in autumn are negatively correlated with circumpolar and continental anomalies in ETS (Table 2.3). Correlations are slightly stronger and more significant in North America than in Eurasia, but the continental contrast in the magnitude of correlations is not as strong as in spring. Practically all stations show a negative correlation, with two out of four stations displaying statistically significant correlations with ETS averaged over North America and the hemisphere (r = -0.41 to -0.61, $p < 0.05$). This implies that delayed ETS or prolonged thermal growing season is associated with earlier termination of

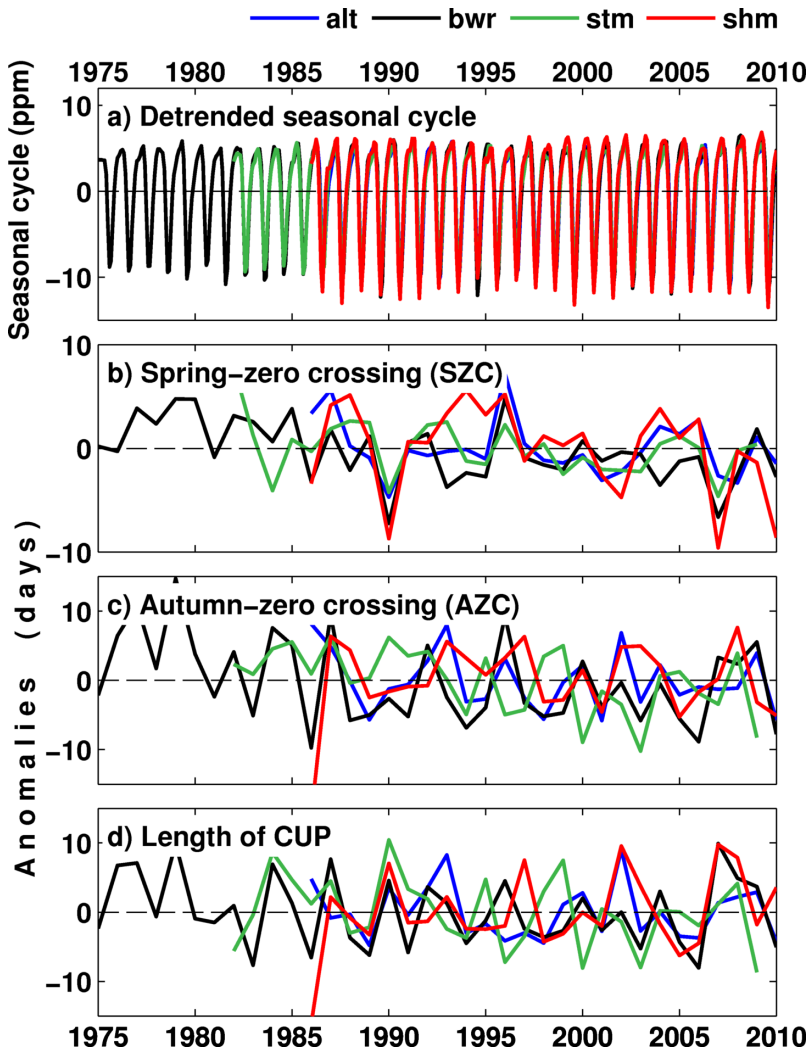

Figure 2.3: Interannually detrended seasonal cycle of atmospheric CO_2 (a) and time series of spring zero-crossing dates (b), autumn zero-crossing dates (c), and length of the carbon uptake period (d) at high-latitude monitoring stations (ALT, BRW, STM and SHM) of the global NOAA-ERSL air-sampling network.

biospheric carbon uptake at high northern latitudes.

A comparison between the time series of AZC and circumpolar ETS shown in Figure 2.4e–h, however, indicates that the shift toward delayed ETS during the second half of the 2000s is not associated with an increased advance in AZC as might be expected. Indeed, it appears that during this recent period there is a decoupling in the relationship between AZC and ETS. Before 2005, the interannual and longer-term variability of ETS and AZC agree relatively well. The circumpolar trend toward delayed ETS is consistent with a long-term advance in AZC at Point Barrow since 1972 (r = -0.39, $p < 0.05$ for 1972-2009; Figure 2.1f). Spatial correlations show predominantly negative correlations over large regions of Eurasia and North America but, unlike spring, the spatial footprints of the station records are quite variable and display fewer common regional features (Figure 2.5e–h).

As a result of the opposite biospheric responses to variations at the margins of the thermal growing season, the length of the biospheric CUP is not consistently correlated with LTS (Table 2.3, Figure 2.4i–l). However, LTS averaged over North America is negatively and significantly correlated with CUP at Alert, in the eastern Arctic (r = -0.51, $p < 0.01$), and Shemya Island, in the North Pacific (r = -0.42, $p < 0.05$). The spatial correlation maps for these stations show

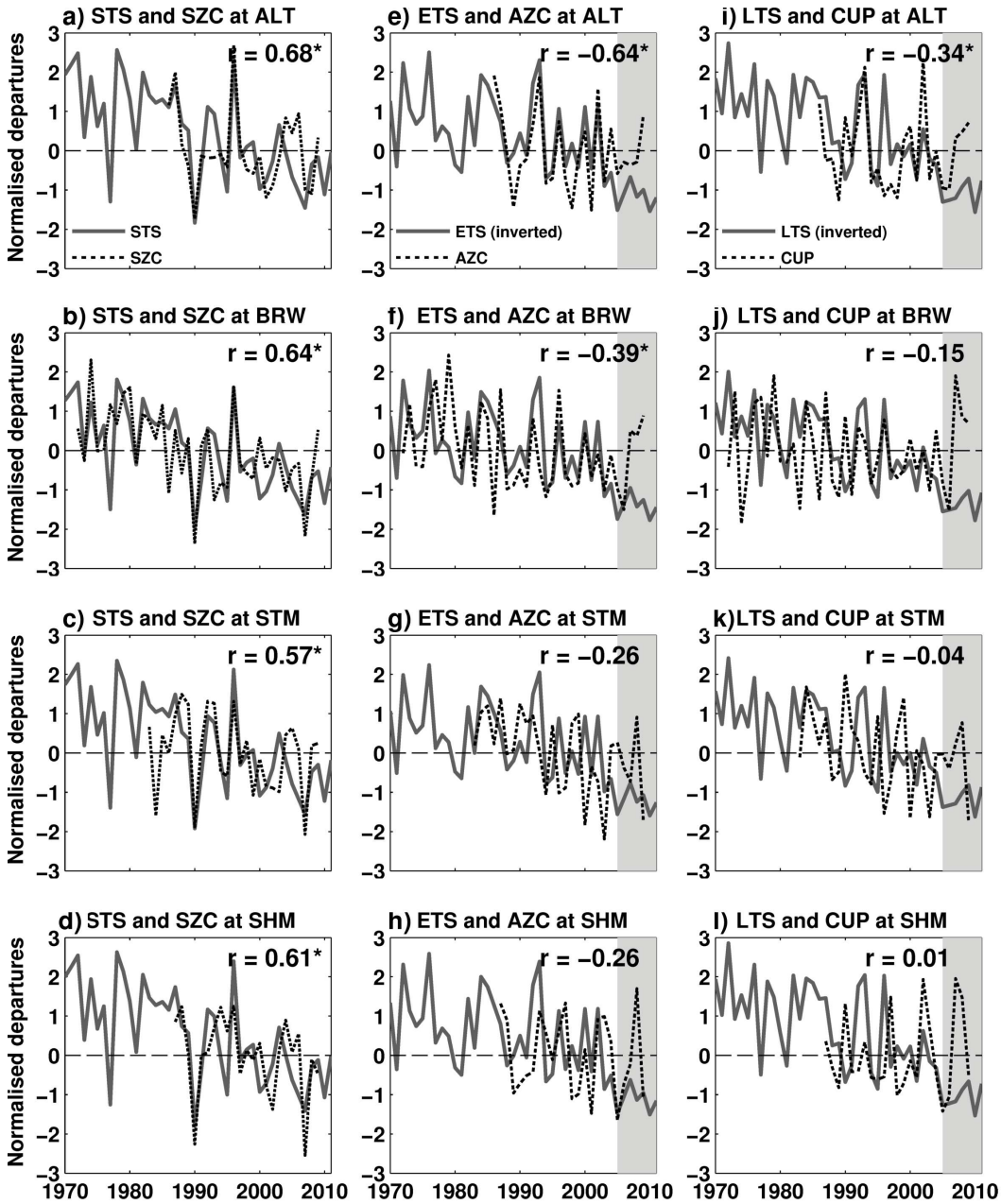

Figure 2.4: Comparison of circumpolar time series of STS (a-d), ETS (e-h) and LTS (i-l) with SZC, AZC and length of the biospheric CUP at each monitoring station. ETS (e-h) and LTS (i-l) time series are plotted inverted to aid visual comparison with AZC and CUP. The correlation between the series over their common period is indicated in each plot and significant correlations ($p < 0.05$) are indicated by an asterisk. The vertical gray shading in the middle and right panels highlights the period of strong autumn warming and delay in ETS between 2005–2011.

that this is due to a relatively large area of significant association centred on the north-eastern part of the continent (Figure 2.5i,l). Overall, the results show that LTS does not equate with biospheric CUP because of the contrasting biospheric responses at the margins of the thermal growing season.

2.3.3.2 CarbonTracker

The spatial footprints of the relationships found between the timing of the thermal growing season and biospheric CUP at the four CO_2 observing stations were examined using the CO_2

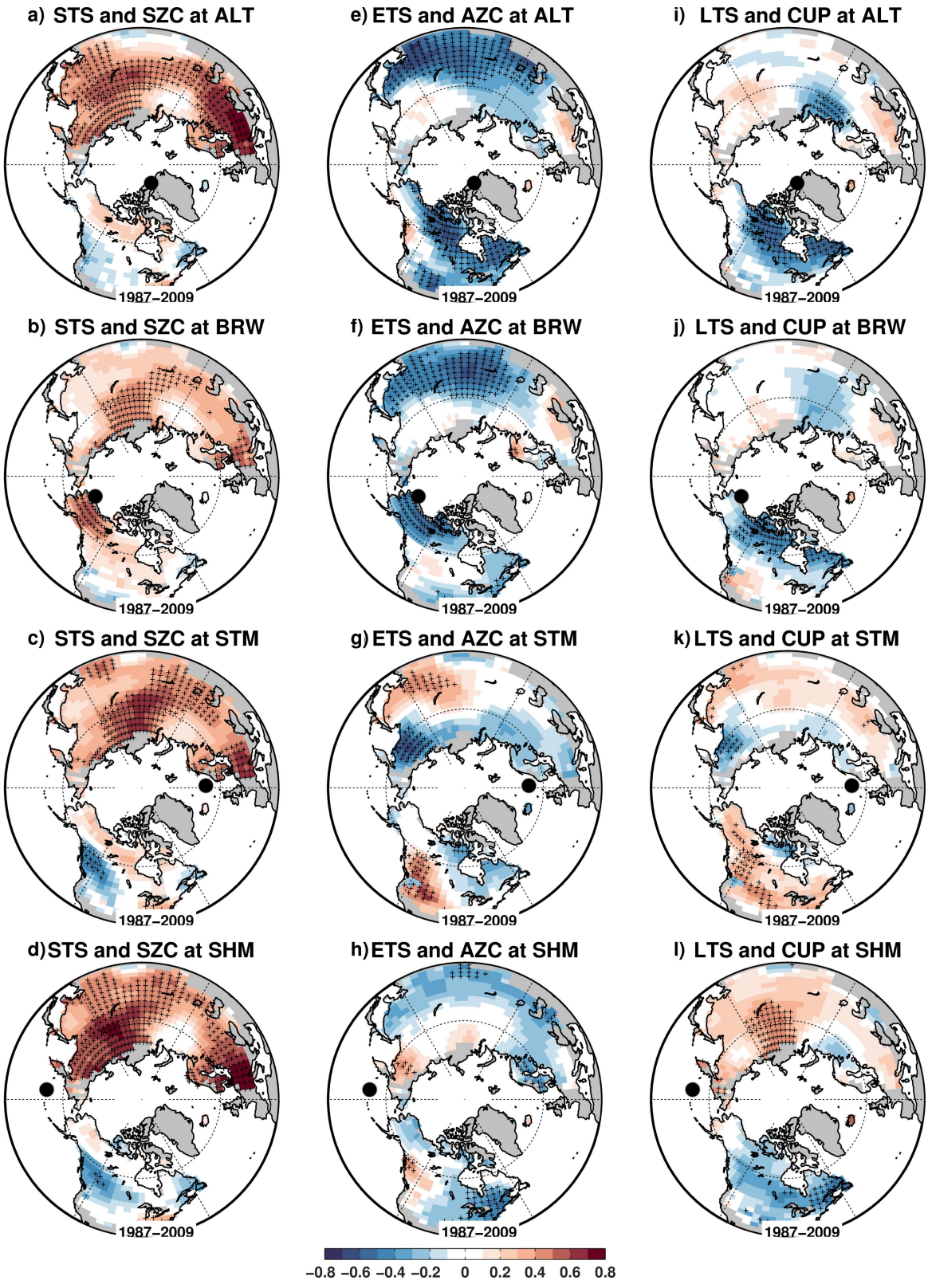

Figure 2.5: Correlation of the time series of timing (a-d and e-h) and duration (i-l) of the biospheric carbon uptake period at each monitoring station (black dot) with gridded fields of timing and duration of the thermal growing season for the period 1987-2009. The significance of the correlations at each grid box was estimated using a non-parametric random phase test with 1000 Monte-Carlo simulations and grid boxes with significant correlations ($p < 0.05$) are indicated by black crosses. Grid boxes excluded from analysis due to permanent ice cover, missing data or discontinuous time series of growing season parameters are shown in gray.

zero-crossing fields based on free-tropospheric CO_2 concentrations as represented by CarbonTracker between 2009 and 2010. The interannual variability of zero-crossing dates at the observing stations and co-located grid boxes of CarbonTracker agree better in spring than in autumn (Supplementary Figure A4). This suggests that, at least at the location of the observing stations, the seasonal cycle simulated by CarbonTracker tends to better capture the greening signal in spring and the concurrent onset of biospheric carbon uptake than it does the process of senescence and carbon release in autumn. However, a comparison of variations in the timing of the thermal growing season at continental and circumpolar scales with zero-crossing dates averaged over high northern latitudes shown in Figure 2.6, confirms most of the features seen in the correlations based on data from observing stations. The timing of high-latitude SZC from CarbonTracker is positively correlated with anomalies in STS averaged over Eurasia and the circumpolar region but poorly correlated with STS over North America. This is consistent with the results based on the observed station records shown in Table 2.3, and reinforces the finding that temperature-driven variations in biospheric activity over Eurasia dominate the biospheric signal in the atmosphere at high northern latitudes during spring.

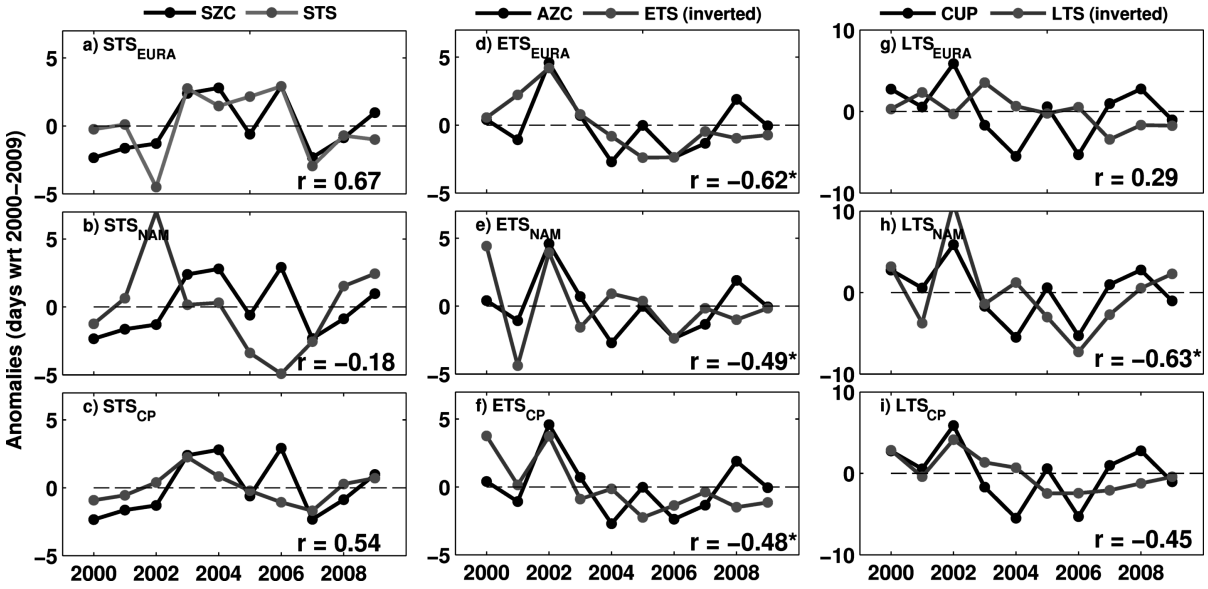

Figure 2.6: Comparison of continental and circumpolar time series of STS (a-c), ETS (d-f) and LTS (g-i) with zero-crossing dates and length of biospheric CUP derived from CT2010 and averaged over latitudes north of 55°N. Time series of ETS and LTS are plotted inverted to aid visual comparison with AZC and biospheric CUP. Correlations are indicated in each plot and significant coefficients ($p < 0.05$) are indicated by an asterisk.

Also in agreement with the station records, Figure 2.6 shows that variations in high-latitude AZC from CarbonTracker are negatively correlated with circumpolar and continentally averaged ETS. However, correlations are clearly stronger with ETS averaged over Eurasia. This autumnal continental contrast is not as clear at the observing stations (Table 2.3). On the other hand, some degree of disagreement between the anomalies of AZC and ETS during recent years (Figure 2.6d–f) appears to be consistent with the apparent decoupling in the relationship between AZC and ETS observed at the stations during the second half of the 2000s (Figure 2.4e–h), although this could also be due to the change in vertical resolution of the TM5 transport model in 2006. Thus, CarbonTracker zero-crossing data confirm the relationships found at the observing stations

and suggest a dominant role of Eurasian biospheric activity on variations in CO_2 concentration in the atmosphere not only during spring but also during autumn.

Figure 2.6 also shows a continental contrast in the the relationship between the length of the biospheric CUP and LTS. The correlation is negative and stronger with LTS averaged over North America and positive but weak with LTS averaged over Eurasia. Although the relationship between LTS and length of the biospheric CUP was not consistent for all the stations, this negative correlation over North America is consistent with the significant negative correlations seen in the Alert and Shemya Island station records (Table 2.2).

2.4 Discussion

2.4.1 Recent changes in temperature and thermal growing season

Northern Hemisphere land surface temperature has increased by 0.32±0.08^{o}C per decade over the period 1979–2005, with the largest increases during winter and spring (Trenberth *et al.*, 2007). Rising temperatures during this period have resulted in a large-scale pattern of earlier and longer-lasting growing seasons seen in many vegetational and biophysical indicators (Keeling *et al.*, 1996; Myneni *et al.*, 1997; Menzel & Fabian, 1999; Zhou *et al.*, 2001; Linderholm, 2006; Piao *et al.*, 2006a; Christidis *et al.*, 2007; Piao *et al.*, 2007). Recent updates of the instrumental temperature record show that the rate of warming slowed between 2005 and 2008, where global surface temperatures declined by around 0.2^{o}C, but increased again during 2009 and 2010 (Kaufmann *et al.*, 2011). This resulted in little overall warming during the past decade.

The results of this study indicate that during this recent period the warming signal has weakened in spring but strengthened in autumn (Figure 2.1). On a circumpolar scale, autumn temperatures during the past decade have been the warmest since 1950 and have increased by up to about 1^{o}C above the mean from 2005 until the end of the record in 2011. This change in the pattern of seasonal warming has resulted in a symmetrical extension of the thermal growing season during the second half of the 2000s, in contrast to previous decades where the extension was dominated by earlier springs (e.g., Linderholm, 2006; Christidis *et al.*, 2007). On average, circumpolar STS has advanced by 4.0 days since 2005 while ETS has shifted later by 4.3 days, resulting in an unprecedented extension of the thermal growing season by 8.4 days (Figure 2.2). This result is in line with recent findings of phenological studies based on long-term satellite NDVI data showing reduced rates of advance in spring greening, but increased delay in vegetation senescence and extended growing season during the past decade (Jeong *et al.*, 2011; Piao *et al.*, 2011; Zhu *et al.*, 2012; Zeng *et al.*, 2011).

Previous studies have reported that the rate of extension of the nominal growing season between the 1980s and early 2000s has been more pronounced in Eurasia than North America (Piao *et al.*, 2007), mirroring differences in magnitude and timing of seasonal warming. Earlier beginning due to greater warming in spring has driven the extension in Eurasia, whereas in North America the extension has been dominated by delayed senescence associated with greater autumn warming (Piao *et al.*, 2007). However, during recent years the extension of the thermal growing season in Eurasia has been caused by a combination of significantly advanced STS and delayed ETS, resulting from significant spring and autumn warming trends (Table 2.1). An earlier modelling study by Piao *et al.* (2007), found that during the period 1980-2002 autumn delay did not contribute to the extension of the growing season in Eurasia as a result of insignificant autumn warming. The contrast with the results presented here shows the importance of recent autumn warming in the overall trend. In North America, the rate of extension of the thermal growing season has been significant only at high-northern latitudes and driven exclusively by delayed ETS, resulting from significant autumn warming in this region. Unlike Eurasia, most of North America has experienced a slight spring cooling during recent decades, precluding any advance in STS. This climate feature has been associated with reduced photosynthetic activity and reversal of a former spring greening trend in the region (Wang *et al.*, 2011), which coincides

with some degree of delay in spring green-up (Zhu *et al.*, 2012) and timing of STS (Figure 2.2d).

Regionally, recent autumn warming and the associated delay in ETS have been stronger in central Asia, Alaska and eastern North America (Figures 2.1 and 2.2). A similar spatial pattern of seasonal warming was found by Jeong *et al.* (2011) using NCEP/NCAR reanalysis temperature and satellite NDVI data (GIMMS NDVIg) through 2008. Furthermore, they found that increased late-season temperatures in these regions have been associated with a concurrent shift toward delayed timing of vegetation senescence. In the North American tundra, Zhu *et al.* (2012) found that the extension of the growing season based on NDVI data has been driven exclusively by delayed vegetation senescence, particularly from 2003 until the end of their dataset in 2006. Although they did not discuss the role of temperature changes in their results, the results presented here indicate that this is the only region of North America that has undergone significant autumn warming (Figure 2.1d) and extension of the thermal growing season during recent decades (Figure 2.2f). However, as discussed earlier in this chapter, the magnitude of the autumnal NDVI change reported in these two earlier studies is uncertain due to an apparent quality issue recently detected in the GIMMS NDVIg dataset since 2003 (see Chapter 3 for details).

In northwest China, significant delay in ETS since 1980 (Figure 2.2e) is consistent with the findings of a recent study based on daily temperature from local meteorological stations, showing a significant contribution of autumn delay to the extension of the thermal growing season across the region (Jiang *et al.*, 2011).

2.4.2 Biospheric response

Interannual variations in the timing of the seasonal cycle of atmospheric CO_2 at high northern latitudes integrate large-scale changes in boreal growing season and associated impacts on the balance between photosynthetic drawdown and respiratory release of CO_2 by northern terrestrial ecosystems (Keeling *et al.*, 1996; Randerson *et al.*, 1997; Heimann *et al.*, 1998). The downward spring zero-crossing point of the detrended annual cycle of CO_2 is used as a surrogate (see discussion in Section 2.2.2) for the timing of the seasonal switch of the biosphere from a net carbon source to a sink, while the upward autumn zero-crossing point is used similarly for the return to a net carbon source (e.g. Piao *et al.*, 2008). Thus, zero-crossing dates are indicative of variations in the period when the biosphere acts as a net carbon sink during the boreal growing season.

Variations in the simple indices of thermal growing season (STS and ETS) correlate significantly with variations in zero-crossing dates at high northern latitudes, but the sign of the relationship is opposite at the two margins of the growing season (Table 2.3). Earlier thermal growing seasons (warm springs) are consistently associated with earlier biospheric carbon uptake while, in contrast, delayed termination of the thermal growing season (warm autumns) is generally associated with earlier net biospheric carbon release. This means that the length of the thermal growing season is not equivalent to the period of biospheric carbon uptake. These large-scale relationships between the temperature-defined growing season and the biospheric carbon uptake period are consistent among stations (Figure 2.4), and are confirmed by high-latitude (north of 55^{o}N) daily fields of CO_2 concentration in the free-troposphere as simulated by the CarbonTracker assimilation system (Figure 2.6).

A similar seasonal contrast between spring (March-May) and autumn (September-November) temperatures and the timing of CO_2 zero-crossing dates was found recently by Piao *et al.* (2008) in a set of ten observing stations with long and continuous CO_2 records between 20^oN and 82^oN, including Alert and Point Barrow. They mechanistically attributed the negative correlation between temperature and CO_2 zero-crossing in autumn to a larger stimulation of ecosystem respiratory release than photosynthetic drawdown of CO_2 by warmer temperatures and delayed vegetation senescence. This mechanism requires a higher temperature sensitivity of respiration than photosynthesis in autumn. They estimated a regional temperature sensitivity of 5 gC m^{-2} $^oC^{-1}$ and 2.5 gC m^{-2} $^oC^{-1}$ for ecosystem respiration and photosynthesis, respectively. On the other hand, they attributed the positive correlation between temperature and CO_2 zero-crossing in spring to a larger stimulation of photosynthesis than ecosystem respiration by warmer temperatures, in agreement with earlier studies (Keeling *et al.*, 1996; Myneni *et al.*, 1997; Randerson *et al.*, 1997, 1999; Piao *et al.*, 2007). These contrasting ecosystem responses to temperature are the most likely cause of the correlations observed between the thermal indices and the timing of biospheric carbon uptake, as the threshold-based thermal growing season depends completely on spring and autumn temperatures.

Several studies have reported significant trends toward earlier spring and autumn CO_2 zero-crossing dates during recent decades, with changes of around 2 to 4 days per decade and larger changes in autumn (Keeling *et al.*, 1996; Randerson *et al.*, 1997; Piao *et al.*, 2008; Thompson, 2011). The study by Piao *et al.* (2008) also highlighted a trend toward shorter net carbon uptake period from 1980 to 2002 owing to a larger advance in autumn zero-crossing as a result of rising autumn temperatures. In contrast to these earlier studies, the present study found that variations in zero-crossing dates and biospheric carbon uptake period at the high-latitude observing stations are characterized by the absence of significant long-term trends during the last two decades (Table 2.2). This is likely due to differences in the time-frame of this study, as zero-crossing dates at the observing stations closely follow large-scale variations in the timing of the thermal growing season (Figure 2.4) and trend coefficients, even when not significant, are nearly all negative. Considering a longer time-frame between 1972 and 2009, Point Barrow shows significant long-term trends toward earlier zero-crossing in spring and autumn. Furthermore, results from Piao *et al.* (2008) indicate that the magnitude of the trends in zero-crossing dates and carbon uptake period from 1980 to 2002 are stronger at mid latitudes and relatively weak at high latitudes. This may also explain in part the lack of significant trends found in this study between 1987 and 2009.

An examination of the temporal variability of zero-crossing dates and timing of the thermal growing season suggests that the relationship between the timing of autumn zero-crossing and the termination of the thermal growing season may have decoupled during the second half of the 2000s, with a shift toward later termination of the thermal growing season. This apparent change in the relationship might be caused by some bias in the HadGHCND temperature dataset during recent years due to the imputation of missing temperature data in a fraction of grid boxes (Supplementary Figure A1). However, if this were true a similar bias in spring would be expected, and clearly this is not the case. Also, the magnitude of circumpolar temperature anomalies in spring and autumn are highly consistent with the CRUTS3.1 dataset (Mitchell & Jones, 2005, Supplementary Figure A3). Comparisons of HadGHCND with two other datasets representing

changes in cold and warm days and nights also show good agreement on the global scale (Lisa Alexander, pers. comm.). Therefore, it seems unlikely that this apparent change in the relationship is associated with biases in the temperature data. It may be related to the influence of other natural or anthropogenic factors on summer or late growing season carbon fluxes that may have modulated the overall biospheric response to recent autumn warming. The role of the ocean and other factors (e.g., soil moisture, CO_2 and nitrogen fertilization, ecosystem disturbances) that could critically influence the autumn zero-crossing time during recent years warrants further research but is beyond the scope of this study.

Correlation analysis indicates that biospheric activity over Eurasia dominates variations in CO_2 concentration in the atmosphere at high northern latitudes during spring and apparently also during autumn. In part, this is due to the larger size of Eurasia but also may reflect continental differences in the strength of the carbon sink. During recent decades, the carbon sink has been stronger in Eurasia than in North America (Denman *et al.*, 2007). This has been associated with stronger vegetation greening trends and lengthening of the growing season in Eurasia because of larger rates of warming, particularly in spring (Zhou *et al.*, 2001; Piao *et al.*, 2007, 2011; Jeong *et al.*, 2011).

Further warming due to ongoing climate change is expected to result in longer growing seasons until internal physiological factors and other environmental cues (e.g., photoperiod or reduced soil water availability) limit photosynthesis. Climate model projections indicate that on a hemispheric scale the length of the thermal potential growing season will increase by more than a month by the end of the twenty-first century, due to a major shift of the annual cycle toward higher temperatures (Tebaldi *et al.*, 2006; Christidis *et al.*, 2007; Meehl *et al.*, 2007; Ruosteenoja *et al.*, 2011). In addition, delayed termination (i.e., autumnal extension) will become increasingly important in the lengthening of the thermal growing season during the course of this century (Christidis *et al.*, 2007). This may result in increased rates of soil respiration in autumn and further decrease the length of the net carbon uptake period in northern ecosystems. However, the results of this study suggest that the overall response of the biosphere to autumnal temperature changes is more complex compared with spring and appears to be strongly modulated by other environmental factors not investigated here.

2.5 Conclusions and outlook

An updated dataset of gridded daily temperature and atmospheric CO_2 concentration data from high-latitude observing stations and CarbonTracker were used to characterize recent spatiotemporal variability of the thermal growing season across the Northern Hemisphere in a long-term context from 1950 to 2011 and to examine its correlation with the period of biospheric carbon uptake. The main conclusions of this Chapter are summarised as follows:

- The length of the thermal potential growing season has increased significantly since 1950, but most of the increase has taken place during the last three decades (1980-2011) and across Eurasia.
- Unprecedented autumn warming during the second half of the 2000s has resulted in a change from asymmetrical to symmetrical extension of the thermal growing season due to a shift toward later termination. This is broadly consistent with the findings of recent studies based on long-term NDVI data showing a shift toward delayed growing season in the Northern Hemisphere during the past decade. The analyses here have also shown that earlier start together with further delay in termination during the second half of the 2000s have resulted in the longest thermal growing seasons since 1950.
- Earlier thermal growing season is associated with earlier onset of biospheric carbon uptake, whereas delayed termination of the thermal growing season, rather than being associated with prolonged biospheric carbon uptake, is associated with earlier termination of biospheric carbon uptake. Thus the length of the thermal growing season is not equivalent to the length of the biospheric carbon uptake period and the current extension in potential growing season length has not led to an extended period of biospheric carbon uptake. This result is consistent with the findings of Piao *et al.* (2008) showing increased ecosystem carbon losses during warm autumns over the period 1980–2002. However, in contrast to this earlier study there were no statistically significant trends toward shorter carbon uptake period over the period of analysis 1987–2009.
- Unlike earlier decades, the strong delay in termination of the thermal growing season owing to unprecedented autumn warming during the second half of the 2000s was not associated with a concurrent increase in the advance of the termination of biospheric carbon uptake. This has led to an apparent decoupling in the negative relationship between autumn zero-crossing dates and the timing of the termination of the thermal growing season during the later part of the past decade. The underlying cause of this change in ecosystem response warrants investigation using a modelling approach to attempt to disentangle the relative influence of different possible causal factors.

The results of this study raise new research questions regarding the response of northern ecosystems to warming in spring and autumn. First, further investigation of how thermal growing season changes relate to interannual and longer-term changes in the timing of spring thaw, snow melt and autumn freeze is required for a more mechanistic interpretation of how these simple thermal indices are associated with physical controls on ecosystem function and phenology. Second, in order to better understand the contrasting biospheric response to the extension of

the thermal potential growing season in spring and autumn it is necessary to establish to what extent vegetation photosynthetic activity (i.e., actual growing season) across the major northern biomes is tracking the ongoing spring and autumn warming. Lastly, the biospheric response integrated over the whole growing season should be investigated to assess the net impact of spring and autumnal ecosystem responses identified in this study. These research questions are addressed in the study presented in the following chapter by exploring the associations between the thermal indices described here and the variability in multiple cryospheric, biospheric and vegetation parameters.

Chapter 3

Changes in the vegetation growing season and the annual cycle of atmospheric CO_2 at high northern latitudes from 1950 to 2011

Abstract

The thermal indices developed in the previous chapter are combined with satellite and other ground observations to study the long-term links between multiple climate (air temperature and cryospheric dynamics) and vegetation (greenness and atmospheric CO_2 concentrations) indicators of the growing season of northern ecosystems (>45^{o}N) and their connection with the carbon cycle during 1950–2011. During the last three decades, the thermal potential growing season has lengthened by about 10.5 days ($p < 0.01$, 1982–2011), which is unprecedented in the context of the past 60 years. The overall lengthening has been stronger and more significant in Eurasia (12.6 days, $p < 0.01$) than North America (6.2 days, $p > 0.05$). The photosynthetic growing season, based on the seasonal cycle of vegetation greenness, has closely tracked the pace of warming and extension of the potential growing season in spring, but not in autumn when other factors such as light and moisture may constrain photosynthesis. The autumnal extension of the photosynthetic growing season since 1982 appears to be only about half that of the thermal potential growing season, yielding a smaller lengthening of the photosynthetic growing season (6.7 days at hemispheric scale, $p < 0.01$). Nevertheless, when integrated over the growing season, photosynthetic activity has closely followed the interannual variations and warming trend of cumulative growing season temperatures. This lengthening and intensification of the photosynthetic growing season, principally over Eurasia rather than North America, is associated with a long-term increase (22.2% since 1972, $p < 0.01$) in the amplitude of the CO_2 annual cycle at northern latitudes. The springtime extension of the photosynthetic and potential growing seasons has apparently stimulated earlier and stronger net CO_2 uptake by northern ecosystems, while the autumnal extension is associated with an earlier net release of CO_2 to the atmosphere. These contrasting responses may be critical in determining the impact of continued warming on northern terrestrial ecosystems and the carbon cycle.

Manuscript published as: Barichivich, J., K. R. Briffa, R. Myneni, T. J. Osborn, T. Melvin, P. Ciais, S. Piao and C. Tucker (2013), Large-scale variations in the vegetation growing season and annual cycle of atmospheric CO_2 at high northern latitudes from 1950 to 2011, *Global Change Biology*, doi: 10.1111/gcb.12283.

3.1 Introduction

The seasonal photosynthetic dynamics of northern vegetation are tightly coupled to the timing and duration of the warm season and associated snow-free and non-frozen ground conditions (Goulden *et al.*, 1998; Nemani *et al.*, 2003). The instrumental temperature record shows convincingly that northern terrestrial ecosystems have experienced the largest warming rates on the globe during recent decades, particularly in winter and spring (Trenberth *et al.*, 2007). Warming has shifted the timing of the seasonal warmth earlier in spring and later in autumn (Burrows *et al.*, 2011; Barichivich *et al.*, 2012), reducing snow cover duration and extending the length of the vegetation growing season (Keeling *et al.*, 1996; Myneni *et al.*, 1997). In these regions, phenology controls the seasonal onset and ending of the carbon uptake period, thereby directly affecting net ecosystem carbon balance (Goulden *et al.*, 1998; Barr *et al.*, 2009; Richardson *et al.*, 2010) and the exchange of water and energy with the atmosphere (Peñuelas *et al.*, 2009).

Earlier and longer growing seasons are generally associated with increased ecosystem carbon sequestration because more days are available for carbon uptake and biomass growth (Richardson *et al.*, 2010). In some instances, however, earlier spring growth advances soil water depletion, which counteracts higher early spring carbon assimilation through the enhancement of mid-summer drought conditions (White & Nemani, 2003; Angert *et al.*, 2005; Hu *et al.*, 2010; Buermann *et al.*, 2013). While the extension of the growing season in autumn prolongs photosynthesis in some vegetation types despite decreasing radiation levels, the net impact on seasonal ecosystem carbon balance is not always positive as soil respiration tends to increase more than photosynthesis (Piao *et al.*, 2008).

The warming-driven lengthening of the vegetation growing season by about 7 to 12 days during the 1980s and 1990s has produced a strong seasonal advance and increase in terrestrial photosynthetic activity at northern latitudes (Myneni *et al.*, 1997; Zhou *et al.*, 2001). This has led to a substantial phase advance and magnification of the peak-to-trough amplitude of the atmospheric CO_2 annual cycle during this period (Keeling *et al.*, 1996). Together, these observations suggest a significant influence of large-scale vegetation phenology on the terrestrial carbon sink that has also been indicated in modelling studies (Randerson *et al.*, 1999; Lucht *et al.*, 2002; Piao *et al.*, 2007).

Large-scale variations in the duration and intensity of the vegetation growing season across the extratropical Northern Hemisphere have been widely studied using a range of approaches (Linderholm, 2006; Cleland *et al.*, 2007), but estimates are typically restricted to the satellite period over the last three decades. Most assessments of long-term changes in the seasonal photosynthetic dynamics at these large spatial scales have relied on the satellite record of Normalized Difference Vegetation Index (NDVI) derived from Advanced Very High Resolution Radiometer (AVHRR) observations from 1981 to the present (e.g., James & Kalluri, 1994; Los *et al.*, 1994; Tucker *et al.*, 2005). Since the study by Myneni *et al.* (1997), the continuous analysis of this satellite record has shown a picture of progressively earlier, longer and more productive growing seasons throughout most of the northern vegetated lands during the 1980s and 1990s (e.g., Zhou *et al.*, 2001; Tucker *et al.*, 2001; Dye & Tucker, 2003; Nemani *et al.*, 2003; Piao *et al.*, 2006a; Julien & Sobrino, 2009; White *et al.*, 2009; Bhatt *et al.*, 2010; Jeong *et al.*,

2011; Xu *et al.*, 2013), followed by a weakening or reversal of some of these trends during the 2000s (Angert *et al.*, 2005; Goetz *et al.*, 2005). Independent studies based on satellite observations of snow cover (Dye & Tucker, 2003; Grippa *et al.*, 2005) and freeze-thaw dynamics extending back to 1979 (Smith *et al.*, 2004; Kimball *et al.*, 2004; Zhang *et al.*, 2011; Kim *et al.*, 2012) have confirmed the general advance and extension of the vegetation growing season at northern latitudes.

The satellite observed changes in the duration and intensity of the vegetation growing season are broadly consistent with ground-based observations of local phenology and surface air temperature (e.g., Jones & Briffa, 1995; Parmesan & Yohe, 2003; Menzel *et al.*, 2003, 2006; Schwartz *et al.*, 2006), atmospheric CO_2 concentrations (Keeling *et al.*, 1996; Piao *et al.*, 2008), and spatially continuous gridded fields of daily surface air temperatures (Christidis *et al.*, 2007; Barichivich *et al.*, 2012) extending back to the mid-20th century. However, only limited analyses of multiple long-term climate and vegetation variables exist at continental or hemispheric scales (e.g., Dye & Tucker, 2003; Bunn *et al.*, 2005; White *et al.*, 2009; Wu *et al.*, 2012). Studies comparing changes in vegetation and climate seasonality at these large spatial scales are needed to assess the extent to which vegetation and terrestrial ecosystems are tracking the pace of the rapid climatic warming and concomitant changes in seasonality (Burrows *et al.*, 2011; Xu *et al.*, 2013), particularly in spring and autumn. The relative responses of vegetation and ecosystem phenology in these transitional seasons have significant and often opposite impacts on the carbon cycle as shown in the previous chapter and the earlier work by Piao *et al.* (2008).

In this chapter, the analysis presented in the previous chapter is extended by comparing the thermal growing season indices with independent streams of satellite and ground observations of NDVI, snow cover, freeze-thaw dynamics and atmospheric CO_2 concentration covering different periods between 1950 and 2011. The aim is to conduct an integrated assessment of long-term continental and circumpolar changes in the vegetation growing season and evaluate their impact on the net carbon uptake by terrestrial ecosystems north of 45^oN. The specific aims are: *(i)* to assess interannual and longer term temporal variations in the timing, length and intensity of the NDVI-based photosynthetic growing season in the context of the climatically-defined potential vegetation growing season; and *(ii)* to examine the influence of these variations on the annual cycle of atmospheric CO_2 concentration at high northern latitudes.

This combined assessment of multiple inter-related variables of the climate system and the biosphere should provide a better overall understanding of the nature of the responses of terrestrial ecosystems to the rapid climate change ongoing at northern latitudes. Furthermore, it provides a robust observational benchmark for validating the large-scale variability and trends in the growing season simulated by ecosystem models (e.g., Sitch *et al.*, 2013).

3.2 Data and Methods

3.2.1 Photosynthetic growing season

The latest version of the biweekly 8 km NDVI data set (NDVI3g) produced from AVHRR level 1b observations by the Global Inventory Modeling and Mapping Studies (GIMMS) group at NASA Goddard Space Flight Center is used to characterize changes in the photosynthetic growing season of the vegetated land north of 45^oN between 1982 and 2011 (see Table 3.1). This new, third generation GIMMS NDVI(3g) dataset extends the record from December 2006 in the previous GIMMS NDVIg dataset (Tucker *et al.*, 2005) to December 2011. Like GIMMS NDVIg, it has been processed to account for orbital drift, sensor degradation, cloud cover and aerosols. Some important issues affecting the GIMMS NDVIg dataset at northern latitudes have been corrected, such as a calibration-related lack of data north of 72^oN that was rectified in GIMMS NDVI3g by using SeaWiFS (Sea-viewing Wide Field-of-view sensor) instead of SPOT (Système Probatoire d'Observation de la Terre) Vegetation NDVI data for cross-sensor intercalibration (i.e., SPOT Vegetation data end at 72^oN while SeaWiFS data do not). The use of SeaWiFS data for cross-calibration with the NDVI3g data also resulted in improved calibration of the data from NOAA-16, -17, and -18 due to the bilinear gains in the AVHRR instruments' channel one on these satellites. These improvements resulted in a higher correlation and closer correspondence of the NDVI3g data with MODIS Aqua and Terra NDVI coincident data. These and other methodological refinements, such as an improved coastal land-water mask and pixel quality flags, have considerably improved data quality for northern vegetated lands, making NDVI3g better suited to studies of northern ecosystems as well as elsewhere.

The methodology used to develop and validate the dataset has yet to be published (Pinzon and Tucker, *A non-stationary 1981–2012 AVHRR NDVI3g time series.*. Remote Sensing, In review, 2013). However, the dataset has already been used in several studies analyzing vegetation dynamics in northern ecosystems (e.g., Bhatt *et al.*, 2010; Epstein *et al.*, 2012; Fensholt & Proud, 2012; Raynolds *et al.*, 2012; Xu *et al.*, 2013). It has been shown that the dataset compares well with NDVI from Moderate Resolution Imaging Spectroradiometer (MODIS) sensors since the early 2000s (Fensholt & Proud, 2012).

Prior to data processing, the Collection 5 MODIS land cover product (MCD12C1) with International Geosphere Biosphere Programme (IGBP) classes for the year 2007 (Friedl *et al.*, 2010) was used to exclude from analysis grid points corresponding to croplands, cropland/natural vegetation mosaics, urban and built-up, and barren or sparsely vegetated land cover classes. Here, the land cover product at 0.05^o resolution was spatially resampled to match the resolution of the NDVI3g dataset ($1/12^o$) using the nearest neighbour algorithm. Then, the TIMESAT software for time-series analysis of satellite data (Jönsson & Eklundh, 2004) was used to smooth the bi-weekly NDVI time series at each grid point with a double logistic fit to describe the yearly trajectory of the NDVI and reduce high-frequency noise. The curve fitting procedure included adaptation to the upper envelope of the NDVI time series in order to minimize the influence of factors not related to vegetation dynamics, such as snow and cloud cover that generally decrease the NDVI values (Reed *et al.*, 1994; Stockli & Vidale, 2004). A double logistic function was chosen for data smoothing because it has been shown to perform better than the other approaches for modelling NDVI data from high latitudes (Beck *et al.*, 2006; Gao *et al.*, 2008).

After smoothing, the biweekly NDVI data were linearly interpolated to daily resolution. Then, for each grid point the NDVI values corresponding to the inflection points for the maximum rate of green-up and senescence were determined from the first derivative of the long-term mean seasonal curve of smoothed NDVI data (i.e. 30-year NDVI climatology) interpolated to daily resolution. These NDVI thresholds were then used to compute the day the of year corresponding to the start (SOS) and end (EOS) of the photosynthetic growing season for each year and grid box (Table 3.1). The length of the photosynthetic growing season (LOS) was estimated as the difference between EOS and SOS. The 'intensity' of the photosynthetic growing season in terms of greenness or photosynthetic potential (see Section 5.2.2 on page 91), defined here as the time-integrated NDVI (TI-NDVI) over the growing season, was computed by integrating daily interpolated smoothed NDVI values from SOS to EOS.

The threshold approach based on the local rate of change in NDVI has a better biophysical basis than using an arbitrary NDVI threshold value to estimate SOS and EOS across a wide range of vegetation types (Piao *et al.*, 2006a; Jeong *et al.*, 2011; Tan *et al.*, 2011). Two other threshold-based approaches for estimating the start, end and length of the photosynthetic growing season from the smoothed NDVI data were also assessed. One was based on the NDVI thresholds corresponding to the beginning of the green-up and the senescence periods estimated from the second derivative of the NDVI climatology. The other used an arbitrary threshold of 25% of the yearly amplitude of the annual cycle of NDVI. It was found that the three methods produce very similar results (Supplementary Figure B1), but the approach based on the first derivative was chosen for consistency with earlier studies and because of its better biophysical basis (e.g., Piao *et al.*, 2006a; Jeong *et al.*, 2011), though it should be noted that it had a slightly higher correlation with the climatically-defined potential growing season.

It has been shown that northern latitude phenological patterns retrieved from AVHRR GIMMS NDVI data can differ significantly from patterns derived from other satellite sensors (Zhang *et al.*, 2013). In order to assess the sensitivity of the results to dataset version and satellite sensor, the suite of phenological parameters was also computed using the previous version of the 15-day GIMMS NDVI dataset (NDVIg) over the period 1982–2006 (available at http://glcf.umd.edu/data/gimms/) and 16-day Terra MODIS NDVI from the MOD13C1 product (0.05^o) during the overlapping period 2001–2011 (available at https://lpdaac.usgs.gov/products/modis). Terra MODIS NDVI data are of higher radiometric and geometric quality than AVHRR data and have been atmospherically corrected and masked for water, clouds and shadows. The datasets were first remapped to match the $1/12^o$ GIMMS NDVI3g grid using bilinear interpolation and then processed following the same procedure used for GIMMS NDVI3g.

The Collection 5 MODIS IGBP land cover classification map (Friedl *et al.*, 2010) and woody fraction from the MODIS Vegetation Continuous Fields product (Townshend, 2011) were used to examine changes in photosynthetic activity for each of the major biogeographic regions (biomes) in the study domain (Archibold, 1995). Continental and circumpolar spatial averages for the suite of phenological parameters were computed for the northern temperate region, boreal forest region, and Arctic region. The boreal forest region was defined as all evergreen needleleaf, deciduous needleleaf and mixed forests north of 45^oN with woody fraction greater than 30% (Xu *et al.*, 2013). Natural grasslands and temperate forests north of 45^oN and south of the

boreal forest were considered as the northern temperate region. Open woodlands (forests with woody fraction less than 30%), open/closed shrublands and grasslands north of the boreal forests were combined into a mixed biogeographic unit termed here Arctic region, since the NDVI signal in these land cover classes is dominated by shrubby and herbaceous vegetation.

3.2.2 Potential growing season: thermal and non-frozen seasons

Low temperatures and frozen ground conditions strongly limit the metabolic activity of northern vegetation (Jarvis & Linder, 2000; Nemani *et al.*, 2003). Therefore, the potential vegetation growing season can be conceptually defined as the period of the year when air temperatures remain above a certain threshold that allows vegetation growth (thermal growing season) or alternatively when the ground surface is not frozen (non-frozen season).

Gridded daily mean air temperatures from the HadGHCND dataset (Caesar *et al.*, 2006) were used to characterize the thermal growing season for northern vegetation on a regular 2.75^ox3.75^o grid from 1950 to 2011, following the same procedure described in Chapter 2. Missing values were imputed using the RegEM algorithm (Schneider, 2001), but grid points with more than three years of missing data were discarded. The thermal growing season was quantitatively defined as the period of the year with daily mean temperatures greater than 5^oC (Table 3.1), which is a common threshold value for determining the boundaries of the thermal potential growing season at mid and high latitudes (Jones & Briffa, 1995; Frich *et al.*, 2002; Barichivich *et al.*, 2012). The curve-fitting procedure of TIMESAT was applied to smooth the daily mean temperature data and to estimate the start (STS), end (ETS) and length (LTS) of this seasonal period using the geographically constant 5^oC threshold (Table 3.1). The 'intensity' of the thermal growing season, defined here as the time-integrated temperature (TI-TEM) over the growing season, was computed as the sum of smoothed daily mean temperatures between STS and ETS.

A satellite dataset of daily landscape (soil, snow and vegetation) freeze-thaw dynamics on a 25x25 km resolution (Kim *et al.*, 2011) was used to estimate the timing and length of the non-frozen season between 1988 and 2007 (Table 3.1). This dataset is based on global microwave observations from morning (a.m.) and afternoon (p.m.) equatorial crossings of the Special Sensor Microwave Imager (SSM/I). The timing (day of year) of the primary spring thaw (STH) for each 25 km grid box and year was estimated from the daily combined parameter as the first day when at least 12 out of 15 consecutive days were classified as non-frozen (a.m. and p.m. thawed) between January and June (Kim *et al.*, 2012), whereas the timing of the autumn freeze (AFZ) was estimated following the same procedure for frozen days (a.m. and p.m. frozen) between September and December. The length of the non-frozen season (LNF) was then defined as the number of days between STH and AFZ.

In addition, a daily freeze-thaw classification between 1950 and 2011 was derived based on gridded minimum and maximum air temperatures from the HadGHCND dataset in order to investigate the large-scale consistency of the satellite observations and long-term trends in freeze-thaw dynamics. Thawed and frozen days were defined as days with minimum air temperatures above and below 0^oC, respectively.

Finally, in order to assess the relationship between snow cover and the timing of spring thawing and start of the thermal growing season, the timing of spring snowmelt (SMT) over

the continuous period 1972–2011 was estimated from the satellite-based weekly gridded snow cover dataset maintained by the Rutgers University Global Snow Lab (Robinson *et al.*, 1993). The date of snowmelt was defined as the first week of a continuous run of 5 weeks without snow between January and June.

3.2.3 Atmospheric CO_2

The seasonal signature in the atmospheric concentration of CO_2, which reflects the changing balance between photosynthesis and respiration of ecosystems through the year, has commonly been used to infer the seasonal course of the net carbon exchange between the terrestrial biosphere and the atmosphere (i.e., net ecosystem productivity – NEP; Houghton, 1987; Keeling *et al.*, 1996; Piao *et al.*, 2008). Previous studies have shown that the annual cycle of atmospheric CO_2 at high northern latitudes is dominated by the metabolism of northern terrestrial ecosystems, with minimal impacts from ocean exchange, fossil fuel emissions, and tropical biomass burning (Randerson *et al.*, 1997; Wittenberg *et al.*, 1998; Piao *et al.*, 2008). Hence, long-term monthly observations of atmospheric CO_2 concentration at Point Barrow (71^oN), Alaska, over the period 1972–2010 (GLOBALVIEW-CO_2, 2011) were used to assess the influence of changes in the growing season on the land-atmosphere net carbon exchange. Point Barrow is the longest continuous record of background CO_2 concentrations at northern latitudes and integrates the net seasonal flux of carbon from all land regions north of 40^oN, though with a larger regional contribution from fluxes near the station in Alaska (Kaminski *et al.*, 1996).

As in some earlier studies (e.g., Buermann *et al.*, 2007; Barichivich *et al.*, 2012), the data filtering technique of Thoning *et al.* (1989) was applied to the monthly time series of flask CO_2 observations to isolate the detrended, smoothed annual cycle and extract metrics for the peak-to-trough amplitude and phasing (zero-crossing dates in spring and autumn) of the annual cycle of CO_2 (Table 3.1). The peak-to-trough amplitude provides a measure of the relative magnitude of net photosynthetic carbon uptake by terrestrial ecosystems (photosynthesis CO_2 uptake minus CO_2 release from ecosystem respiration and disturbance) over the period when photosynthesis exceeds ecosystem respiration, running from the start of the growing season until the day when minimum CO_2 is reached (Keeling *et al.*, 1996; Buermann *et al.*, 2007). Thus, variations in CO_2 amplitude largely reflect changes in photosynthesis (net CO_2 uptake) over the course of the growing season in the north. The spring (SZC) and autumn (AZC) zero-crossing dates are surrogates for the respective onset and termination of the net carbon uptake period (Keeling *et al.*, 1996; Piao *et al.*, 2008; Barichivich *et al.*, 2012), which is affected by changes in the seasonal timing of the growing season.

In order to verify the large-scale validity of the CO_2 observations at Point Barrow, time series of zero-crossing dates and annual amplitude were also derived from monthly zonal-mean CO_2 concentrations north of 60^oN from the reference marine boundary layer matrix of GLOBALVIEW-CO_2 (2011) over the period 1979–2010.

3.2.4 Intercomparison and statistical analysis

A summary of the parameters used to characterize the potential and photosynthetic growing season is given in Table 3.1. All the parameters were converted to anomalies with respect to

Table 3.1: Summary of parameters used in this study to characterize the growing season and the annual cycle of atmospheric CO_2 at northern latitudes. See text for a detailed definition and description of the datasets used to derive each parameter.

Parameter	Resolution	Period	Short definition
Start of season			
STH – Spring thaw	0.25^ox0.25^o	1988–2007	First day of a 15-day running window with at least 12 non-frozen days during Jan–Jun
SMT – Spring snowmelt	190x190 km	1972–2011	First week of continuous run of at least 5 snow-free weeks during Jan–June
STS – Start of thermal growing season	2.75^ox3.75^o	1950–2011	Day when temperature rises to 5^oC in spring
SOS – Start of photosynthetic growing season	8x8 km	1982–2011	Day when NDVI reaches a local threshold for maximum green-up rate
End of season			
AFZ – Autumn Freeze	0.25^ox0.25^o	1988–2007	First day of a 15-day running window with at least 12 days with frozen status during Sept–Dec
ETS – End of thermal growing season	2.75^ox3.75^o	1950–2011	Day when temperature decreases to 5^oC in autumn
EOS – End of photosynthetic growing season	8x8 km	1982–2011	Day when NDVI decreases to a local threshold for maximum browning rate
Length of season			
LNF – Length of non-frozen period	0.25^ox0.25^o	1988–2007	Days between STH and AFZ
LTS – Length of thermal growing season	2.75^ox3.75^o	1950–2011	Days between STS and ETS
LOS – Length of photosynthetic growing season	8x8 km	1982–2011	Days between SOS and EOS
Intensity of season			
TI-NDVI – Seasonally integrated NDVI	8x8 km	1982–2011	Time integrated NDVI over LOS
TI-TEM – Seasonally integrated temperature	2.75^ox3.75^o	1950–2011	Time integrated temperature over LTS
CO_2 annual cycle			
SZC – Spring zero-crossing	station	1972–2010	Day when the detrended CO_2 annual cycle exceeds 0 ppm in spring
AZC – Autumn zero-crossing	station	1972–2010	Day when the detrended CO_2 annual cycle falls below 0 ppm in autumn
AMP – Amplitude CO_2 annual cycle	station	1972–2010	Maximum minus minimum detrended seasonal CO_2 concentration

their common period 1988–2007 and then spatially averaged over North America, Eurasia and the entire circumpolar region north of 45^oN.

The temporal agreement among the continental and circumpolar estimates of timing and length of the non-frozen season and the photosynthetic and thermal growing seasons was examined using the Kendall coefficient of concordance (W; Legendre, 2010) and linear correlation analysis over the common period 1988–2007. W is a non-parametric measure of correlation among three or more variables and varies between 0 (no association) and 1 (perfect association). The statistical significance of W was estimated using a permutation test with 10000 simulations (Oksanen *et al.*, 2011). The significance of correlations was estimated using a non-parametric random phase test with 1000 Monte-Carlo simulations (Ebisuzaki, 1997), which is robust to autocorrelation in the series. Trend analysis was carried out using the non-parametric Mann-Kendall trend test implemented in the *zyp* package in R statistics (Bronaugh, 2009).

The response of growing season photosynthetic activity to temperature changes was examined by comparing the seasonal integrals of NDVI (TI-NDVI) and temperature (TI-TEM) over the period 1982–2011. The influence of changes in the timing of the growing season on the timing of net carbon uptake by northern ecosystems was assessed by comparing the zero-crossing dates (SZC, AZC) at Point Barrow with the timing of the non-frozen season and the thermal and photosynthetic growing seasons over the common period 1988–2007. The seasonal NDVI integral was also compared with the amplitude of the annual cycle of CO_2 (AMP) at Point Barrow to assess the linkages between variations in gross photosynthesis and changes in the magnitude of net carbon uptake by northern ecosystems.

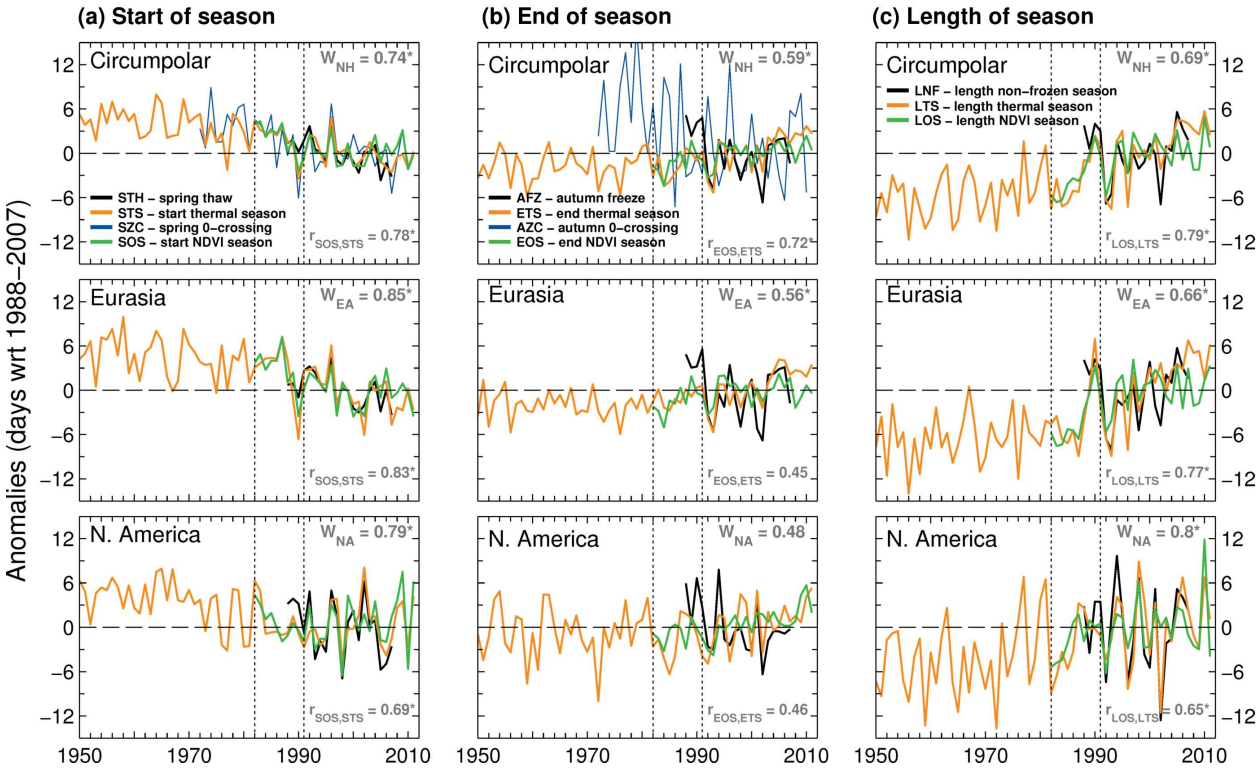

Figure 3.1: Hemispheric and continental variations of timing (a, b) and length (c) of the growing season at latitudes north of 45°N and CO_2 zero-crossing dates at Point Barrow. The W statistic for each parameter and spatial domain is given in the upper-right corner of each panel as a measure of the temporal consistency among variations in non-frozen season and thermal and photosynthetic growing seasons over the period 1988–2007. The correlation between the corresponding series of photosynthetic and thermal growing season over the period 1982–2011 is shown in the lower-right corner of each panel. An asterisk denotes significance at $p < 0.05$. The vertical dotted lines indicate the dates of the volcanic eruptions of El Chichón in 1982 and Mount Pinatubo in 1991.

3.3 Results

3.3.1 Timing

Figure 3.1 compares continental and circumpolar time series of anomalies in the timing and length of the non-frozen season and the photosynthetic and thermal growing seasons covering different periods between 1950 and 2011. The spatially averaged anomalies agree very well in spring on a continental ($W_{EA} = 0.85$, $W_{NA} = 0.79$, $p < 0.05$) and circumpolar ($W_{NH} = 0.74$, $p < 0.05$) scale (Figure 3.1a), indicating a strong synchrony between variations in the timing of the spring thaw (STH) and the start of the thermal (STS) and photosynthetic (SOS) growing seasons. Continental and circumpolar anomalies in spring thaw are highly correlated with anomalies in the start of the photosynthetic and thermal growing seasons, particularly over Eurasia (Table 3.2). This indicates a strong springtime coupling between the start of the potential (STH and STS) and the photosynthetic growing season at northern latitudes.

The timing of the start of the photosynthetic growing season based on GIMMS NDVI3g is highly consistent with estimates based on the previous NDVIg dataset (r = 0.95 to 0.98 for 1982–2006; Supplementary Figure B2) and on higher quality MODIS NDVI data (r = 0.50 to 0.88 for 2001–2011; Supplementary Figure B3), so the estimates of variations in spring canopy

green-up in this study are robust to uncertainties due to differences in satellite sensors and data processing. However, in spite of efforts to minimize the influence of snow dynamics on the phenological retrievals, snowmelt variations may still affect the green-up signal retrieved from NDVI, though snowmelt and the onset of photosynthetic activity would be expected to covary significantly at northern latitudes because of their strong common temperature control (Supplementary Figure B4).

Table 3.2: Correlation matrix of timing and length of the non-frozen season (STH, AFZ, LNF), thermal growing season (STS, ETS, LTS), photosynthetic growing season (SOS, EOS, LOS) and CO_2 zero-crossing dates (SZC, AZC) at Point Barrow over the period 1988–2007. Values in bold are significant at $p < 0.05$ and an asterisk indicates those that are also significant at $p < 0.01$.

	Start				End				Length	
Variable	STH	STS	SZC		AFZ	ETS	AZC		LNF	LTS
Circumpolar										
STH	·			AFZ	·					
STS	**0.73**	·		ETS	0.44	·		LNF	·	
SZC	**0.53**	**0.65**	·	AZC	-0.24	**-0.58***	·	LTS	**0.74**	·
SOS	**0.66**	**0.67**	0.43	EOS	0.16	**0.74**	**-0.26**	LOS	0.46	**0.74**
Eurasia										
STH	·			AFZ	·					
STS	**0.75***	·		ETS	**0.57**	·		LNF	·	
SZC	**0.45**	**0.55**	·	AZC	-0.14	**-0.35**	·	LTS	**0.56**	·
SOS	**0.78**	**0.77**	0.34	EOS	0.21	**0.57**	**-0.31**	LOS	0.40	**0.78**
North America										
STH	·			AFZ	·					
STS	**0.71**	·		ETS	0.33	·		LNF	·	
SZC	0.38	0.30	·	AZC	**-0.40**	**-0.68***	·	LTS	**0.82**	
SOS	**0.71**	**0.58**	0.23	EOS	-0.10	0.33	-0.11	LOS	**0.63**	**0.58**

The phenological series shown in Figure 3.1a (STH, SOS, STS) depict a consistent circumpolar trend toward earlier growing seasons. Trend analysis indicates that the circumpolar start of the thermal growing season has shifted earlier by 6.8 days since 1950 at a rate of -1.10±0.28 days per decade^{-1} (Table 3.3). This long-term advance has been stronger and more sustained in Eurasia (-1.28±0.39 days decade^{-1}, $p < 0.01$) than in North America (-0.93±0.47 days decade^{-1}, $p < 0.01$), where the spring advance halted in the early 1990s (Figure 3.1a). The weaker rate of change over North America has resulted in contrasting continental trends during the satellite period between 1982 and 2011. In North America, neither the start of the thermal nor the photosynthetic growing seasons has changed significantly since 1982 (Table 3.3). In contrast, over Eurasia both the thermal and photosynthetic growing seasons have begun significantly earlier since 1982 by 6.9 days (-2.3±0.97, days decade^{-1}, $p < 0.01$) and 5.3 days (-1.78±1.06, days decade^{-1}, $p < 0.01$), respectively. However, there is some indication that these advancing trends have weakened during the 2000s (Figure 3.1a).

Long-term trends in the timing of the start of the photosynthetic growing season are highly heterogeneous within the continents and differ substantially between biomes (Figure 3.2a), but are always consistent with changes in the timing of spring thaw (Supplementary Figure B5). The strongest (>15 days since 1982) and more extensive spring extension of the photosynthetic growing season has occurred in the boreal forests and the temperate region of Eurasia, particularly in western Russia and Scandinavia. On a biome scale, the photosynthetic growing seasons of the Eurasian boreal forests and temperate region have extended significantly ($p < 0.05$) in spring by 7.4 and 8.6 days, respectively (Supplementary Figure B5). Surprisingly, the spring

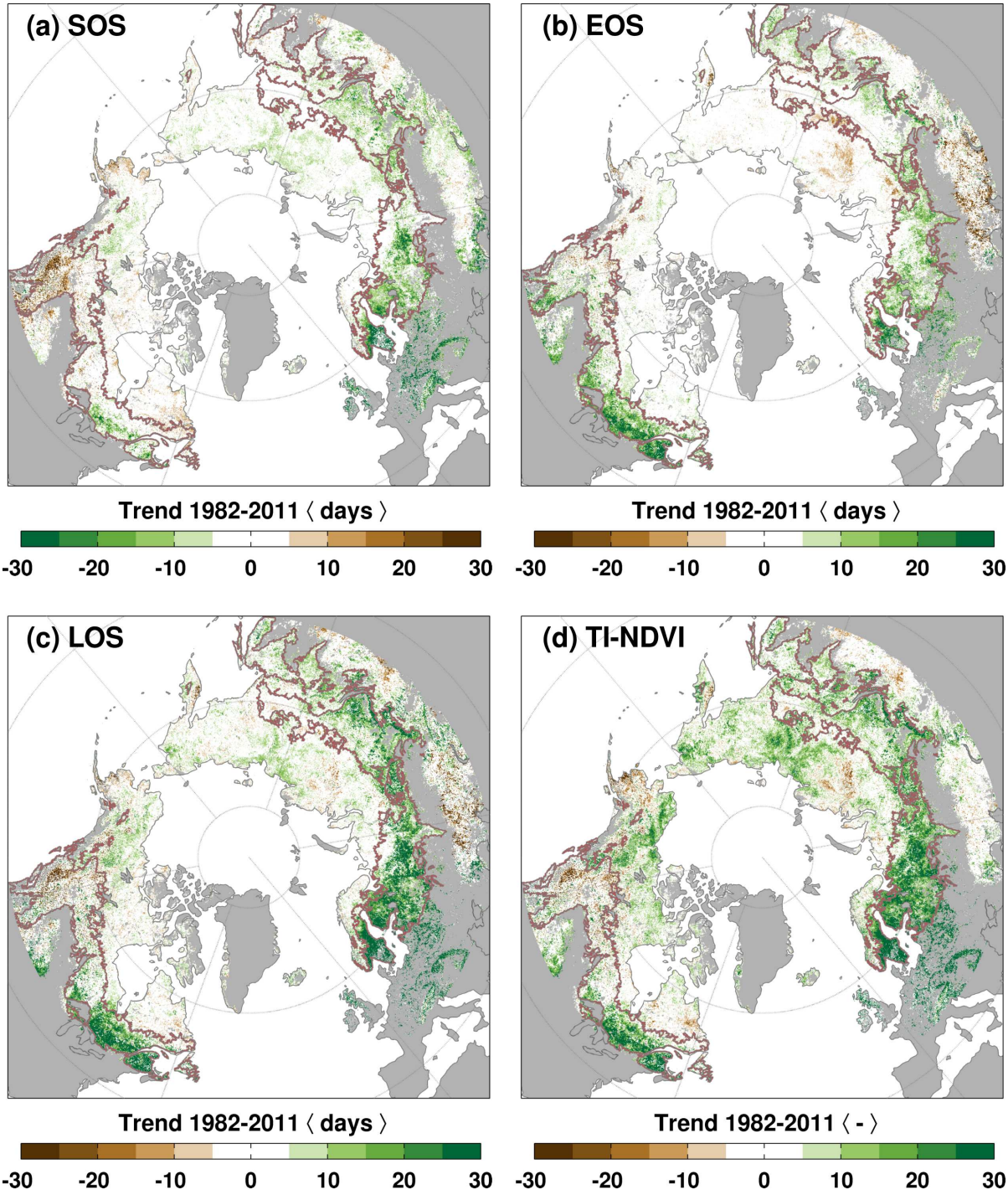

Figure 3.2: Spatial pattern of linear trends in timing (a,b), length (c) and intensity (d) of the photosynthetic growing season from 1982 to 2011. Inland water bodies, croplands, urban and barren or sparsely vegetated regions north of 45°N are shaded gray. The brown polygons represent the extent of the boreal forests (evergreen needleleaf, deciduous needleleaf and mixed forests with woody fraction greater than 30%). Non significant trends ($p > 0.1$) over this period are masked out as white.

extension of the photosynthetic growing season has not been significant in the colder regions north of the boreal forest in the Arctic region (-2.4 days since 1982, $p > 0.05$; see Supplementary Figure B5), where the greenness signal is dominated by shrubs. In North America, a relatively weak spring extension has occurred along the southern edge of the boreal forest in southeastern Canada and in western Alaska, while localised spring delays of up to a month have taken place

in the boreal and montane forests of the western part of the continent (Figure 3.2a). However, on a biome level, there are no significant trends in North America (Supplementary Figure B5).

In contrast to spring, Figure 3.1b shows that the overall agreement between anomalies in the timing of the autumn freeze (AFZ) and the end of the photosynthetic (EOS) and thermal (ETS) growing seasons is weaker on both circumpolar ($W_{NH} = 0.59$, $p < 0.05$) and continental ($W_{EA} = 0.56$, $p < 0.05$; $W_{NA} = 0.48$, $p > 0.05$) scales. The agreement is particularly low in North America, where none of the variables (AFZ, EOS and ETS) is significantly correlated with any other (Table 3.2). The lack of relationship between the timing of the termination of the photosynthetic growing season and the autumn freeze is particularly clear in the Arctic region (Supplementary Figure B6). This generally poor agreement suggests a lack of coupling between the termination of the potential (AFZ, ETS) and the photosynthetic (EOS) growing season.

The two GIMMS NDVI datasets produce very similar variability in the timing of the termination of the photosynthetic growing season (r = 0.85 to 0.91 for 1982–2011) but the earlier dataset (NDVIg) tends to produce stronger autumn delay since around 2003, likely due to calibration issues (Supplementary Figure B2). During the past decade, estimates based on GIMMS NDVI3g are relatively less consistent with MODIS NDVI data (r = 0.25 to 0.51 for 2001–2011) than for the start of the growing season, although the overall difference between the datasets is related to disagreements only during 2001 and 2011 (Supplementary Figure B3).

Table 3.3: Mann-Kendall linear trends (± 1 s.e.) in timing and length of the thermal and photosynthetic growing season for the period 1982–2011. Trends in the thermal growing season over the longer 1950–2011 period are given in brackets. Values in bold are significantly different from zero at $p < 0.05$ while an asterisk indicates additional significance at $p < 0.01$.

	Start (days decade^{-1})		End (days decade^{-1})		Length (days decade^{-1})	
Station	STS	SOS	ETS	EOS	LTS	LOS
Circumpolar	**-1.64 ± 0.71*** (**-1.10 ± 0.28***)	**-1.11 ± 0.88**	**1.87 ± 0.76*** (**0.74 ± 0.29***)	**0.97 ± 0.61**	**3.50 ± 1.33*** (**1.72 ± 0.48***)	**2.24 ± 1.24***
Eurasia	**-2.30 ± 0.97*** (**-1.28 ± 0.39***)	**-1.78 ± 1.06***	**1.65 ± 0.67*** (**0.72 ± 0.31***)	0.78 ± 0.77	**4.21 ± 1.33*** (**2.06 ± 0.55***)	**2.47 ± 1.21***
N. America	0.16 ± 1.26 (**-0.93 ± 0.47***)	0.14 ± 1.53	**1.99 ± 1.29*** (0.42 ± 0.49)	**1.32 ± 0.75***	2.08 ± 2.18 (**1.33 ± 0.71***)	0.96 ± 1.42

There is a general trend towards more delayed timing of the end of the thermal and photosynthetic growing seasons during the study period (Table 3.3). Most of the shift toward later cessation occurred during the second half of the 2000s, when a rapid change took place in Eurasia and to a lesser extent in North America (Figure 3.1b). This represents a significant trend towards delayed termination of the thermal growing season in Eurasia by about 4.9 days (1.65±0.67 days decade^{-1}, $p < 0.01$) over the period 1982–2011 (Table 3.3). The change was smaller for the termination of the photosynthetic growing season and the trend since 1982 is not significant. In North America, the terminations of the thermal and photosynthetic growing seasons have both been delayed significantly since 1982 by 6 and 4 days at linear rates of 1.99±1.29 and 1.32±0.75 days decade^{-1}, respectively. These continental-scale changes have resulted in a circumpolar delay in the termination of the thermal growing season of 5.6 days (1.87±0.76 days decade^{-1}, $p < 0.01$) but only 2.9 days in the termination of the photosynthetic growing season since 1982 (0.97±0.61 days decade^{-1}, $p < 0.05$). Thus, these results indicate that the autumnal extension of the thermal potential growing season since 1982 has been nearly twice that of the photosynthetic growing season.

On a biome scale, the autumn extension of the photosynthetic growing season since 1982

has been significant across most of the circumpolar boreal forests and also in some temperate regions dominated by grasslands (Figure 3.2b). Notably, the magnitude of the extension has been similar in the Eurasian (7.5 days, $p < 0.01$) and North American (7.7 days, $p < 0.01$) boreal forests (Supplementary Figure B6). For the temperate region, the autumn extension has been significant only in North America (10.9 days, $p < 0.01$; see Supplementary Figure B6). Unlike in the boreal forests and the temperate region, the timing of the autumn senescence in the colder Arctic region has not changed much from year to year (Supplementary Figure B6). This exacerbates the disagreement with the anomaly series of the timing of the autumn freeze, indicating a weaker sensitivity of vegetation phenology to late growing season temperature variability in these northern latitudes.

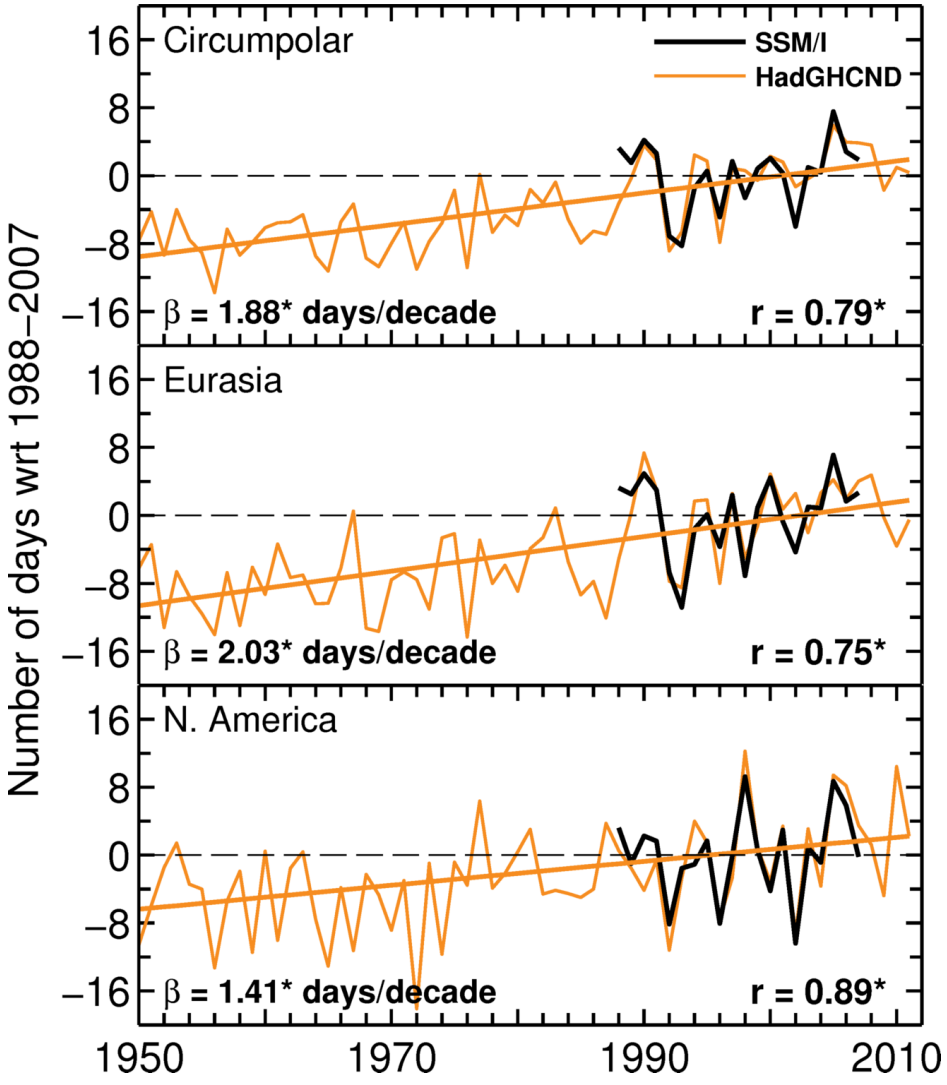

Figure 3.3: Changes in annual number of non-frozen days estimated from satellite microwave (SSM/I) and from gridded surface air temperature observations (HadGHCND) north of 45°N. Correlations between the satellite and temperature-based series for the period 1988–2007 and trends (β) for HadGHCND series over the 1950–2011 period are given in each panel. An asterisk denotes significance at the $p < 0.05$ level.

3.3.2 Length

Figure 3.1c shows that the lengths of the non-frozen season (LNF) and the thermal (LTS) and photosynthetic (LOS) growing seasons have increased steadily since the early 1980s in Eurasia, while in North America there has been no overall increase during this period. The overall agreement in the temporal anomalies of the three variables is significant and stronger in North America ($W_{NH} = 0.69$, $W_{EA} = 0.66$, $W_{NA} = 0.80$, $p < 0.05$), where all three variables are significantly correlated with each other (Table 3.2). There is also a consistent pattern of temporal variability in the length of the photosynthetic growing season between the GIMMS NDVI datasets and MODIS NDVI data (Supplementary Figures B2 and B3).

Trend analysis indicates that in Eurasia the thermal and photosynthetic growing seasons have lengthened by 12.6 and 7.4 days since 1982, with respective linear rates of 4.21±1.33 and 2.47±1.21 days decade^{-1} (Table 3.3). Thus, the lengthening of the thermal growing season has been almost twice that of the photosynthetic growing season. Clearly, this pattern of lengthening has been dominated by spring advance (Figure 3.1a) and the large difference in trends occurs because of a smaller rate of delay in the termination of the photosynthetic growing season.

In North America, there has been no overall lengthening in either the thermal or photosynthetic growing seasons during the satellite period, largely because of the pause in the spring advance in the early 1990s. Yet, the thermal growing season has lengthened significantly since 1950, but primarily because of the spring advance prior to the 1990s (Table 3.3). On a circumpolar scale, the lengthening of the thermal growing season since 1982 has been substantially larger than that of the photosynthetic growing season, with respective changes of 10.5 and 6.7 days and linear rates of 3.50±1.33 and 2.24±1.24 days decade^{-1} (Table 3.3).

The different magnitudes of change in the timing of the photosynthetic growing season between the Arctic region, boreal forests, and northern temperate region have resulted in contrasting long-term trends in the duration of the photosynthetic growing season between these biomes (Figure 3.2c). In Eurasia, most of the lengthening of the photosynthetic growing season has occurred in the boreal forests (16.6 days, $p < 0.01$; Supplementary Figure B7), though the overall trend is largely dominated by a rapid lengthening in the earlier part of the record between 1982 and 1990. Unlike the boreal forests, the Eurasian temperate region has not experienced a significant lengthening of the photosynthetic growing season (9.9 days, $p > 0.05$). The period of lengthening at the beginning of the record was followed by a slight shortening (Supplementary Figure B7). Also, the notorious lack of any extension of the photosynthetic growing season in either the spring or autumn across the vast shrub-dominated Arctic region has precluded any long-term lengthening of the photosynthetic season on a biome scale (2.8 days, $p > 0.05$). Despite of a lack of significant lengthening trends in North America, there has been a strong autumn-driven lengthening of the photosynthetic growing season over most of the boreal forests in the east (Figure 3.2b–c). Nevertheless, large regions with no change in the western part of the continent have obscured this regional lengthening in the biome average (Supplementary Figure B7).

The boreal forest is the only biome that has undergone a significant lengthening of the photosynthetic growing season on a circumpolar scale (10.3 days, $p < 0.01$). This lengthening is generally consistent with a concurrent lengthening in the non-frozen season between 1988 and 2007 (Supplementary Figure B7), in spite of the observed autumnal decoupling (Supplementary

Figure B6). The cold Arctic region is the biome with the weakest change in the duration of the photosynthetic season at this large spatial scale (1.7 days, $p > 0.05$), whilst in the temperate region the photosynthetic season lengthened only between 1982 and 1990 but shortened thereafter (Supplementary Figure B7).

The continental and circumpolar rates of lengthening of the thermal growing season over the full record from 1950 to 2011 shown in Table 3.3 (1.33 to 2.06 days decade^{-1}) agree closely with the rates of increase (1.41 to 2.03 days decade^{-1}) in the annual number of non-frozen days derived from minimum surface air temperatures from the same dataset shown in Figure 3.3. This indicator of non-frozen days is roughly equivalent to the length of the continuous non-frozen season (LNF) and is strongly correlated with SSM/I satellite microwave observations of landscape freeze-thaw dynamics between 1988 and 2007. As shown in Figure 3.3, the strength of the correlation varies from 0.75 ($p < 0.05$) over Eurasia to 0.89 ($p < 0.05$) in North America and 0.79 ($p < 0.05$) on a circumpolar scale. The correlations are also high for the number of non-frozen days during spring and autumn (Supplementary Figure B8).

This strong agreement validates the satellite landscape freeze-thaw record, and the close relationship with the indicator of non-frozen days based on minimum temperatures enables us to estimate long-term changes in the non-frozen season from 1950 to the present. During this 62-year period, the annual number of non-frozen days has increased significantly by 12.6 days in Eurasia and 8.7 days in North America (Figure 3.3). This compares well with a concurrent lengthening of the thermal growing season by 12.7 days (2.06±0.55 days decade^{-1}, $p < 0.01$) in Eurasia and 8.2 days (1.33±0.71 days decade^{-1}, $p < 0.01$) in North America (Table 3.3). On a circumpolar scale, the increase in the annual number of non-frozen days has been 11.7 days during the same period, which is similar to a lengthening of the thermal growing season of 10.7 days (1.72±0.48 days decade^{-1}, $p < 0.01$). Seasonally, the increase in non-frozen days is significant in both spring (0.77 to 1.07 days decade^{-1}) and autumn (0.62 to 0.66 days decade^{-1}), but the greater increase has occurred in spring (Supplementary Figure B8).

3.3.3 Intensity

Figure 3.4a compares the spatially averaged time series of cumulative growing season NDVI (TI-NDVI) and temperature (TI-TEM). The agreement between these two variables is very good, with correlation values ranging from 0.68 ($p < 0.05$) in North America to 0.81 ($p < 0.05$) in Eurasia and 0.80 ($p < 0.05$) on a circumpolar scale. The correlations remain statistically significant even after removing the trend from the series by applying a high-pass filter (Supplementary Figure B9). Thus, there is a strong indication that cumulative thermal growing season temperature drives most of the interannual and long-term variations in growing season photosynthetic activity over the study domain (r^2 up to 66%).

The large-scale patterns of cumulative growing season NDVI are consistent between the two GIMMS NDVI datasets, but NDVIg shows a more negative trend than NDVI3g over the period 1982–2006 (Supplementary Figure B2). In the most recent decade, GIMMS NDVI3g agrees reasonably well with MODIS NDVI data (Supplementary Figure B3), indicating a common large-scale vegetation signal shown by the AVHRR and MODIS sensors during recent years.

Neither the continental nor the circumpolar series of cumulative thermal growing season temperatures (TI-TEM) show any significant warming during the three decades prior to the

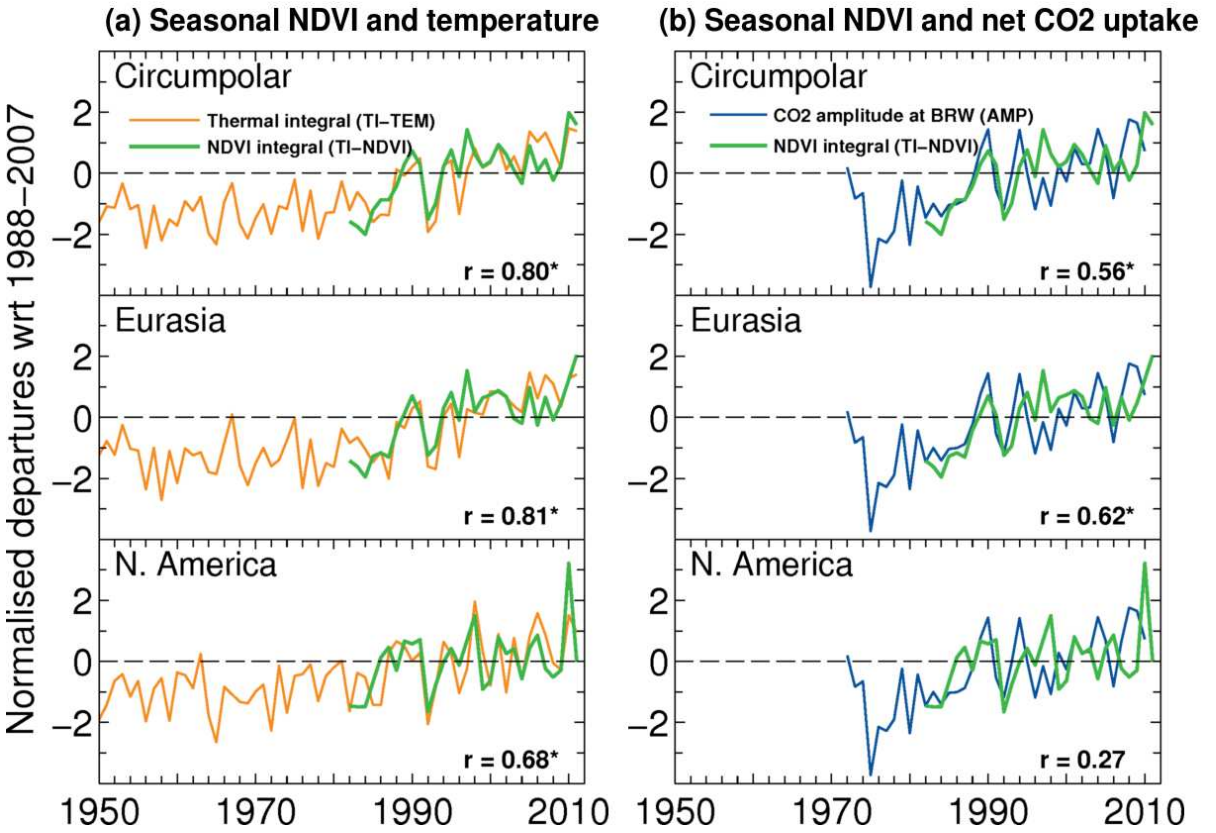

Figure 3.4: Comparison of variations in seasonally integrated NDVI with seasonally integrated temperature (a), and peak-to-trough amplitude of the annual cycle of atmospheric CO_2 at Point Barrow (b). The correlation between the series over their common period is shown in each panel. An asterisk denotes significance at the $p < 0.05$ level.

start of the satellite NDVI record in 1982 (Figure 3.4a). Shortly after this date, thermal growing season temperatures and photosynthetic intensity (TI-NDVI) increased, especially after around 1988, then decreased temporarily during 1992 and 1993 because of the transient spring and summer cooling induced by the eruption of Mount Pinatubo in 1991, and continued to rise until about 1997. Thereafter, the rate of growing season warming and photosynthetic greening trends weakened until the increases that occurred in the final two years of the record (2010 and 2011).

The year 2010 is characterised by a very intense photosynthetic growing season in North America, with an anomaly about 3 standard deviations above the mean (Figure 3.4a). This continental anomaly is also shown by MODIS NDVI (Supplementary Figure B3) and was dominated by a strong seasonal greening in eastern North America, in connection with a concurrent pattern of strong seasonal warming (Figure 3.5). These anomalies are also consistent with an abrupt advance of about 6 days in the start of the thermal and photosynthetic seasons over North America in 2010 (Figure 3.1a).

The continental scale warming and greening trends are stronger in Eurasia than in North America and the circumpolar average is dominated by changes over Eurasia. The spatial distribution of trends in growing season photosynthetic intensity reveals that the boreal forests in Eurasia and eastern North America have experienced the strongest greening since 1982 (Figure 3.2d). However, as seen at the continental scale, the biome averages for Eurasia and the circumpolar region indicate that this greening was sustained only between 1982 and 1997 (Sup-

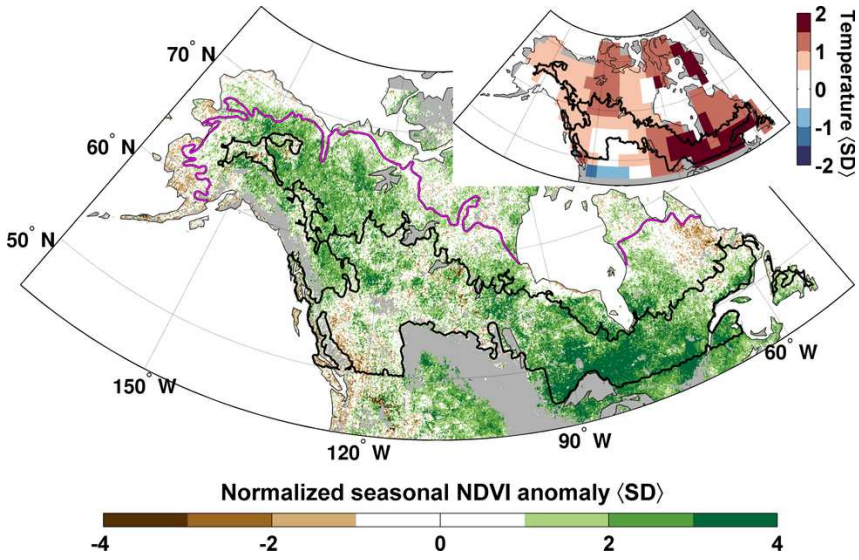

Figure 3.5: Spatial pattern of normalized anomalies of seasonally integrated NDVI (TI-NDVI) and temperature (TI-TEM) in North America during 2010. Inland water bodies, croplands, urban and barren or sparsely vegetated regions are shaded grey. The black polygon represents the extent of the continuous needleleaf boreal forest and the purple line indicates the position of the Artic treeline (Brown *et al.*, 1998).

plementary Figure B10). The same temporal pattern of greening is evident in the Eurasian temperate region, but the reduction in photosynthetic activity after 1997 is stronger than in the boreal forests.

In the colder Arctic region, the growing season greening has been significant and more spatially consistent in eastern Siberia and northern Alaska (Figure 3.2d). Since the length of the photosynthetic growing season has not changed significantly in this biome, most of this greening has been driven by a widespread increase in peak summer greenness (Supplementary Figure B11). This is an important difference with the boreal forests and the temperate region, where the overall greening has been primarily associated with extended growing seasons rather than with increased peak summer greenness. Indeed, peak greenness has decreased in large regions of the North American boreal forests (Supplementary Figure B11). However, the summer browning in the boreal forests of eastern North America has been offset by strong autumn greening and delayed senescence (Figure 3.2b).

3.3.4 Correlation with atmospheric CO_2 annual cycle

Temporal variations in the amplitude and phase (zero-crossing dates) of the annual cycle of atmospheric CO_2 based on flask observations at Point Barrow are strongly correlated ($r > 0.71$, $p < 0.05$, 1979–2010) with those based on zonal-mean CO_2 concentrations in the marine boundary layer north of 60^oN (Supplementary Figure B12), indicating that this station record is representative of the northern latitudes. However, note that these two CO_2 records are not completely independent as the observations at Point Barrow are also included in the zonal averages.

Variations in the timing of the spring thaw (STH) and the start of the thermal (STS) and photosynthetic (SOS) growing seasons are positively correlated with anomalies in spring CO_2

zero-crossing date (SZC) at Point Barrow (Table 3.2). Though the correlations with the start of the photosynthetic growing season are not significant ($p > 0.05$) over the period 1988–2007, the circumpolar trend towards earlier growing seasons is consistent with an advance of 5.7 days (-1.45±0.84 days decade^{-1}, $p < 0.01$) in the timing of spring CO_2 zero-crossing date since 1972 (Figure 3.1a).

In contrast, variations in the timing of the autumn freeze (AFZ) and end of the photosynthetic (EOS) and thermal (ETS) growing seasons are all negatively correlated with the timing of the autumn CO_2 zero-crossing date (AZC) at Point Barrow (Figure 3.1b and Table 3.2). However, the significance of the correlations varies substantially and the magnitudes are weaker than for those for spring. The timing of the autumn zero-crossing date at Point Barrow shows very large year-to-year variability and the date has advanced by about 6.3 days (-1.61±1.53 days decade^{-1}, $p < 0.05$) since 1972, offsetting the concurrent advance in the spring zero-crossing date (5.7 days). This coincides with a general delay in the termination of the thermal and photosynthetic growing seasons (Table 3.3).

These inverse relationships indicate that unlike in spring, an extension of the potential and photosynthetic growing season in autumn tends to be associated with earlier rather than delayed termination of the period of net ecosystem carbon uptake at northern latitudes. Nevertheless, contrary to the negative relationship observed over the entire period, the autumnal extensions of the thermal and photosynthetic growing seasons in the mid-2000s have been mostly associated with a delayed termination of the period of net ecosystem carbon uptake (Figure 3.1b).

Figure 3.4b shows that the intensity of the photosynthetic growing season (TI-NDVI) is positively correlated with the peak-to-trough amplitude (AMP) of the annual cycle of atmospheric CO_2 at Point Barrow. The correlations over the period 1982–2010 range from 0.27 ($p > 0.05$) in North America to 0.62 ($p < 0.05$) in Eurasia and 0.56 ($p < 0.05$) on a circumpolar scale. However, after removing the trend in the series, only the correlation coefficient for Eurasia (r = 0.45, $p < 0.05$) is significant (Supplementary Figure B9). The continental contrast in the magnitude and significance of the correlations indicates that changes in CO_2 amplitude at this station are dominated by photosynthetic activity in Eurasia. Spatial correlations indicate that photosynthetic activity over most of Alaska is also significantly correlated with variations in CO_2 amplitude at Point Barrow (Supplementary Figure B13). Interestingly, the overall spatial distribution of significant correlations closely follows the spatial pattern of growing season greening shown in Figure 3.2d.

The temperature-driven greening trend in Eurasia is consistent with a long-term increase in peak-to-trough CO_2 amplitude of 22.2% ($p < 0.01$, 1972–2010) relative to the mean of the period 1972–1980. This increase in amplitude has been dominated by a concurrent trend towards lower summer minimum CO_2 concentrations of 24.9% ($p < 0.01$, 1972–2010) due to enhanced net growing season CO_2 uptake, while the seasonal maximum CO_2 concentrations show no long-term changes (Supplementary Figure B12). However, variations in seasonal maximum CO_2 concentrations, and hence presumably variations in wintertime ecosystem respiration, have increasingly influenced the amplitude of the CO_2 annual cycle during most of the 2000s, reducing the correlation with interannual variations in seasonally integrated NDVI (Figure 3.4b, Supplementary Figure B9).

3.4 Discussion

3.4.1 Synchronycity of climate and phenological changes during spring and autumn

This chapter presents a combined assessment of continental and circumpolar changes in potential and photosynthetic growing seasons, inferred from multiple ground and satellite observations of vegetation greenness, surface air temperature, snowcover and freeze-thaw dynamics covering different periods from 1950 to 2011. The results show that variations in the timing of the remotely sensed photosynthetic growing season are tightly coupled with the timing of the climatically-defined potential growing season in spring but not in autumn (Figure 3.1), suggesting a seasonal asymmetry in the phenological response to climate variability at these large spatial scales.

The winter-to-spring transition at northern latitudes is both rapid and dramatic. Typically, before the seasonal thaw, daily solar radiation is already abundant but vegetation metabolism is limited by frozen soils. Thus, rising temperatures strongly stimulate and synchronize the landscape thaw and the onset of vegetation photosynthetic activity (Goulden *et al.*, 1998; Jarvis & Linder, 2000), which in turn trigger the greening of the landscape observed by satellites (Myneni *et al.*, 1997). The pivotal role played by temperature in these inter-related processes explains the remarkable agreement observed in the vegetation, cryospheric and thermal phenological parameters in spring. Nevertheless, spring snowmelt produces a similar satellite signal to that induced by vegetation greening as represented by NDVI data (Dye & Tucker, 2003; Delbart *et al.*, 2006) and despite efforts to minimize the influence of snow dynamics on phenological retrievals, the potential remaining influence of the snowmelt signal on NDVI data may also contribute to this agreement.

The weak autumnal synchrony between thermal, cryospheric and vegetation transitions indicates that autumn senescence, as measured by canopy greenness, is less sensitive to temperature variability than is spring green-up. Autumn senescence is a complex biophysical process triggered by leaf-specific maturation processes and cumulative environmental constraints such as photoperiod, temperature and soil moisture (Kozlowski & Pallardy, 1997; Rosenthal & Camm, 1997; Vitasse *et al.*, 2009; Warren *et al.*, 2011; Dragoni & Rahman, 2012). Although the relative importance of these factors is still not well understood (Richardson *et al.*, 2013), it has been shown that late-season photosythetic activity and growth cessation in temperate and boreal regions can be strongly constrained by photoperiod (Suni *et al.*, 2003; Kimball *et al.*, 2004; Barr *et al.*, 2009; Bauerle *et al.*, 2012). This sensitivity of autumn phenology to photoperiod is consistent with the evidence for autumnal decoupling shown here between continental and biome-scale variations in the timing of canopy senescence and thermal and cryospheric transitions.

To some extent, the use of a fixed 5^{o}C threshold to define the end of the thermal growing season might also contribute to this autumnal mismatch, as temperature thresholds for late-season vegetation growth may vary considerably with vegetation type and latitude (Piao *et al.*, 2006a). Nevertheless, the lack of correlation between variations in the timing of vegetation senescence and the autumn freeze (Table 3.2 and Supplementary Figure B6) provides independent evidence for a decoupling between autumn phenology and thermal conditions, particularly in the northern biomes dominated by shrubs. As the influence of photoperiod does not change from year

to year, interannual and longer term variability of late-season canopy greenness and the timing of autumn senescence at northern latitudes is still correlated with temperature but less so than during spring (Estrella & Menzel, 2006; Piao *et al.*, 2011; Jeong *et al.*, 2011; Zeng *et al.*, 2011; Dragoni & Rahman, 2012; Zhu *et al.*, 2012).

3.4.2 Changes in potential and photosynthetic growing seasons

An examination of variations in the thermal growing season (Figure 3.1) and the frequency of temperature-based non-frozen days back to 1950 (Figure 3.3b) indicates that neither the length nor the timing of the termination of the potential growing season have changed significantly in the period prior to the satellite era (1950–1981). Nevertheless, there is evidence for a nearly hemispheric-wide advance in the start of the potential growing season since the early 1970s. This is characterized by advanced thermal growing seasons (Figure 3.1a), earlier snowmelt (Supplementary Figure B4) and increased frequency of non-frozen days in spring (Supplementary Figure B8). The spring advance and the associated trend towards earlier snowmelt have continued until the present in Eurasia but halted in North America in the early 1990s. These changes have resulted in a circumpolar advance of the thermal growing season of about 6.8 days since 1950 and a similar increase in non-frozen days in spring of 6 days. This finding is consistent with previous studies showing a shift by 7.3 days in the timing of spring land surface temperatures north of 20^{o}N from 1960 to 2009 (Burrows *et al.*, 2011), advanced timing of the last day below 5^{o}C by 6.7 days from 1955 to 2002 (Schwartz *et al.*, 2006) and a general advance in the timing of spring phenological events of animal and plant species over the last half-century (Parmesan & Yohe, 2003).

The extended historical context provided by the current multiple-parameter assessment shows that the potential growing season has undergone unprecedented changes during the satellite era (1982–2011) as a result of the rapid warming observed throughout most of the northern latitudes (Figures 3.1 and 3.4a). Nearly all of the circumpolar lengthening of the thermal growing season since 1950 (10.7 days) has occurred during the satellite period (10.5 days), with a similar extension in spring (4.9 days) and autumn (5.6 days). This finding is in close agreement with the widespread reduction of low temperature constraints on plant growth (Bunn *et al.*, 2007; Zhang *et al.*, 2008) and lengthening of the potential growing season observed at high latitudes during the past 30 years of continuous satellite observation of the cryosphere (Smith *et al.*, 2004; McDonald *et al.*, 2004; Zhang *et al.*, 2011; Kim *et al.*, 2012).

The NDVI-based photosynthetic growing season of northern vegetation has responded significantly to the rapid lengthening and warming of the potential growing season during the satellite period (Figures 3.1c and 3.4a). This conclusion is consistent with the results of earlier remote sensing and modelling studies showing a progressive lengthening of the photosynthetic growing season and large-scale greening trends across most of the northern latitudes (e.g., Myneni *et al.*, 1997; Zhou *et al.*, 2001; Tucker *et al.*, 2001; Lucht *et al.*, 2002; Euskirchen *et al.*, 2006; Piao *et al.*, 2007; Bhatt *et al.*, 2010; Beck & Goetz, 2011; Jeong *et al.*, 2011). However, a new finding of this study is that the circumpolar lengthening of the photosynthetic growing season over the satellite period has been substantially smaller than the lengthening of the thermal potential growing season, owing to a twofold autumnal extension of the latter (Table 3.3). During the period 1982–2011, the thermal growing season lengthened by 10.5 days (with an

extension of 4.9 days in spring and 5.6 days in autumn), whereas the photosynthetic growing season lengthened by 6.7 days in the same period (with an extension of 3.3 days in spring and 2.9 days in autumn). Admitting data and methodological uncertainties, these trends suggest that, unlike in spring, the photosynthetic growing season has not tracked the extension in the thermal potential growing season in autumn, when photosynthesis and canopy greenness become more limited by factors other than temperature (Kozlowski & Pallardy, 1997; Rosenthal & Camm, 1997; Dye & Tucker, 2003; Piao *et al.*, 2011; Warren *et al.*, 2011). This is particularly clear in the Arctic region where the timing of autumn senescence is almost invariant from year to year (Supplementary Figure B6).

A recent study based on a slightly extended version of the GIMMS NDVIg dataset from 1982 to 2008 (Jeong *et al.*, 2011) highlighted a hemispheric-scale lengthening of the NDVI-based growing season (10.5 days) driven primarily by an autumnal (7.6 days) rather than a spring extension (3.5 days). So, even though these authors found a spring extension similar to the present study (3.3 days), they estimated a more than twofold extension in autumn (2.9 vs 7.6 days). The present study has shown that phenological variations based on GIMMS NDVIg and the newer NDVI3g dataset are highly consistent, except for a substantially stronger autumn delay in the NDVIg dataset since around 2003 (Supplementary Figure B2). The general agreement between the phenological parameters based on the NDVI3g dataset and Terra MODIS NDVI data during the past decade (Supplementary Figure B3) suggests that the discrepancy between the results presented here and those of Jeong *et al.* (2011) could be related to calibration issues in the later part of the GIMMS NDVIg dataset that may have led to an overestimation of autumnal trends in the Jeong *et al.* (2011) study. Differences in the methodologies employed to compute phenology may further contribute to the different inferences between these studies. The analysis of other NDVI datasets and alternative vegetation indices (Huete *et al.*, 2002; Jones *et al.*, 2011; Liu *et al.*, 2011) should shed more light on the significance of this apparent autumnal decoupling between northern vegetation activity and climate variability.

Large-scale phenological trends during the satellite period (1982–2011) are characterized by a marked continental contrast. Trends in thermal and photosynthetic growing season length and intensity are stronger in Eurasia than in North America (Figures 3.1 and 3.4a), consistent with findings of earlier studies (Piao *et al.*, 2007; Jeong *et al.*, 2011; Barichivich *et al.*, 2012). The springtime extension has been greater in Eurasia, whereas the autumnal extension has been larger in North America. As in the circumpolar average, the lengthening of the thermal growing season in Eurasia (12.6 days) has been substantially larger than that of the photosynthetic growing season (7.4 days) because of a smaller autumnal extension of the latter (Table 3.3). The same pattern of greater lengthening of the thermal growing season occurs in North America. However, unlike in Eurasia, neither the thermal nor the photosynthetic growing seasons have lengthened significantly, despite significant autumnal extensions (Table 3.3).

Earlier phenological studies have shown that these contrasting continental trends are consistent with differences in the magnitude and timing of the seasonal warming over the two continents, most apparent as a rapid rise of spring temperatures in Eurasia and of autumn temperatures in North America (Piao *et al.*, 2007, 2008; Wang *et al.*, 2011; Barichivich *et al.*, 2012). Large-scale oscillatory modes of decadal climate variability (Buermann *et al.*, 2003; Zhang *et al.*, 2007; de Beurs & Henebry, 2008) and increases in the frequency and severity of droughts (Dai,

2011a), fire and insect disturbances (Westerling *et al.*, 2006; Kurz *et al.*, 2008), feedbacks from declining snow-cover extent and melting permafrost (Callaghan *et al.*, 2011), and compositional and structural vegetation changes (Elmendorf *et al.*, 2012) have also been important influences on the spatiotemporal variability of these long-term phenological patterns. Thus these factors might drive some of the contrast in phenological trends observed within continents (Figure 3.2) and between biomes (Supplementary Figures B5–B7), consistent with findings of earlier studies (Goetz *et al.*, 2005; Jeong *et al.*, 2011).

Recent remote sensing studies based on GIMMS NDVIg data have documented seasonal greenness changes that are suggestive of a weakening of the springtime extension and a magnification of the autumnal extension of the photosynthetic growing season at northern latitudes since the early 2000s (Jeong *et al.*, 2011; Piao *et al.*, 2011; Zhu *et al.*, 2012). Similar decadal changes are apparent in the thermal and NDVI phenological parameters during the past decade (Figure 3.1a–b). In particular, the year 2005 saw a rapid change towards a further extension of the thermal and, to a lesser extent, the photosynthetic growing season in Eurasia (Figure 3.1b). Although in North America this change is less obvious, there has also been a conspicuous autumnal extension in the photosynthetic growing season since around 2009.

These decadal phenological changes are consistent with a recent weakening of the long-term warming in winter/spring and a rapid increase in autumn temperatures (Jeong *et al.*, 2011; Barichivich *et al.*, 2012; Cohen *et al.*, 2012). In Chapter 2 (see also Barichivich *et al.*, 2012), it was shown that the recent autumnal shift in the thermal growing season was associated with an abrupt autumn warming of about 1^oC at northern latitudes since 2005. This rapid warming has resulted in the longest thermal growing seasons since 1950 over Eurasia and on a circumpolar scale (Figure 3.1c). Nevertheless, the magnitude of the concurrent autumnal extension of the photosynthetic growing season has been substantially smaller (Figure 3.1b), consistent with the weaker temperature sensitivity of autumn phenology discussed above. However, recent warming-induced increases in fire disturbance and insect defoliation in northern forests (Westerling *et al.*, 2006; Soja *et al.*, 2007; Kurz *et al.*, 2008) may have also influenced the seasonal patterns of vegetation greenness during the past decade (Beck & Goetz, 2011). Also, the magnitude and even the sign of these short-term trends in seasonal greenness have been found to differ substantially between NDVI datasets from different satellite sensors (Zeng *et al.*, 2011; Zhang *et al.*, 2013).

Unlike studies based on GIMMS NDVIg data (Jeong *et al.*, 2011; Piao *et al.*, 2011; Zhu *et al.*, 2012), a recent study based on Terra MODIS NDVI for the period 2000–2010 (Zeng *et al.*, 2011) reported a continuous extension of the photosynthetic growing season in spring but no clear extension in autumn over the circumpolar region north of 60^oN. This earlier study also found a stronger spring extension (11.5 days/decade) in North America than in Eurasia (2.7 days/decade). Such a strong spring extension in North America is inconsistent with the results of the present study based on temperature and NDVI3g data through 2011 (Figure 3.1). Since it was shown above that phenological variations based on GIMMS NDVI3g and Terra MODIS NDVI agree well over the period 2001–2011, particularly in spring (Supplementary Figure B3), it can be concluded that this apparent discrepancy must be related to differences in data processing, spatial domain or the period used for analysis, rather than to any difference in NDVI datasets. This highlights the difficulty of extracting and interpreting meaningful phenological trends from short satellite records.

The variability of seasonally integrated NDVI presents a very consistent picture of vegetation productivity tightly coupled to continental and circumpolar variations in seasonally integrated temperatures during the entire satellite period (Figure 3.4a). This is illustrated by the unprecedented increase in seasonally integrated NDVI across the east of North America during the anomalously warm growing season in 2010 (Figure 3.5), despite severe canopy damage by a late spring frost event following the exceptionally early leaf-out across the region (Hufkens *et al.*, 2012). A similar correspondence in temperature and NDVI integrals has been reported for the circumpolar tundra region (Bhatt *et al.*, 2010), in agreement with the strong temperature limitation of vegetation productivity at high northern latitudes (Nemani *et al.*, 2003).

Continentally averaged series of NDVI and temperature integrals indicate that the large-scale greening trend observed over northern latitudes during recent decades (Myneni *et al.*, 1997; Zhou *et al.*, 2001) was associated with an abrupt warming of the growing season since the late 1980s, particularly in Eurasia (Figure 3.4a). The seasonal warming and associated greening trend paused during the second half of the 1990s and 2000s. Earlier studies based on AVHRR NDVI data have attributed this decadal change in the magnitude of growing season greening to regional cooling, increased summer drought stress and divergent climate responses of tundra and boreal forests (Angert *et al.*, 2005; Goetz *et al.*, 2005; Zhang *et al.*, 2008; Beck & Goetz, 2011; Piao *et al.*, 2011; Wang *et al.*, 2011). However, the results of this study suggest that changes in growing season temperature alone explain most of this decadal weakening of the greening trend on continental and circumpolar scales (Figure 3.4a). This suggests that other factors such as drought, fire, insect outbreaks, land use change, and nitrogen and CO_2 fertilization have individually played a smaller role than temperature in driving large-scale vegetation productivity integrated over the entire growing season.

The analysis of the growing season NDVI integral stratified by biome revealed that the overall greening in the Arctic region has been driven by increasing summer greenness while, in contrast, the greening across the boreal forests and temperate grasslands has been driven by the lengthening of the growing season (Figure 3.2). This result is consistent with a contrast between summer (June-August) greening in tundra regions and little change or even summer browning in the boreal forests reported in earlier studies (Angert *et al.*, 2005; Goetz *et al.*, 2005; Bunn & Goetz, 2006). However, the contrast between multi-decadal patterns of greenness in tundra and forests is relatively small when NDVI changes are integrated over the whole growing season (Supplementary Figure B10).

3.4.3 Growing season and atmospheric CO_2 annual cycle

It has previously been shown that the extensions of the growing season in spring and autumn have contrasting effects on the net carbon balance of northern ecosystems due to a greater increase in ecosystem respiration over photosynthesis during autumn (Randerson *et al.*, 1999; Piao *et al.*, 2008; Vesala *et al.*, 2010; Barichivich *et al.*, 2012). Nevertheless, net ecosystem responses in autumn are generally less consistent than in spring and increased rather than decreased autumnal net carbon uptake has been observed in some stand-level studies (Richardson *et al.*, 2010; Dragoni *et al.*, 2011). Yet, these opposite net ecosystem responses to changes in the beginning and end of the growing season are a clear large-scale feature of this analysis of the annual cycle of atmospheric CO_2 at Point Barrow. While extensions of the potential and photosynthetic

growing seasons in spring are consistently associated with earlier net ecosystem uptake of atmospheric CO_2 (earlier spring CO_2 zero-crossing), an extension in autumn tends to be associated with an earlier rather than a delayed net ecosystem release of CO_2 to the atmosphere (earlier autumn CO_2 zero-crossing).

An important finding of this study is that in Eurasia and North America the autumnal extension of the thermal potential growing season during the satellite period has been substantially larger than that of the photosynthetic growing season. The extended warmth might be expected to have resulted in a substantial stimulation of autumnal ecosystem carbon release and earlier termination of the period of net carbon uptake (i.e., earlier autumn CO_2 zero-crossing), potentially offsetting the spring advance in net carbon uptake period. Indeed, the overall advance in spring CO_2 zero-crossing date at Point Barrow since 1972 (5.7 days) has been offset by a concurrent advance in the autumn zero-crossing date (6.3 days). Yet, the abrupt autumn warming and associated autumnal extension of the potential and photosynthetic growing seasons after 2005 have not been associated with an advance in autumn CO_2 zero-crossing date at Point Barrow as might be expected (Figure 3.1b). Instead the autumn CO_2 zero-crossing has been delayed during this period, suggesting an autumnal extension rather than a shortening of the period of net carbon uptake in recent years.

A similar delay in autumn CO_2 zero-crossing during this recent period was found at several other high-latitude observing stations in the analysis presented in Chapter 2 (see also Barichivich *et al.*, 2012) and is also apparent in the marine boundary layer CO_2 concentrations (Supplementary Figure B12). This anomaly could be in part related to a decrease in ecosystem respiration and to large-scale processes other than the metabolism of terrestrial ecosystems, such as temporal changes in atmospheric transport, ocean uptake and fossil fuel emissions. It has been shown that atmospheric transport changes can account for up to about 15% of the interannual variability in autumn CO_2 zero-crossing at Point Barrow (Piao *et al.*, 2008). Modelling studies are needed to investigate the relative contribution made by changes in atmospheric transport dynamics and other factors that produced this recent change in autumn CO_2 zero-crossing at northern latitudes after 2005.

Earlier analyses of the annual cycle of atmospheric CO_2 at Point Barrow have shown a consistent increase in the peak-to-trough amplitude (Keeling *et al.*, 1996), associated with the increase in growing season photosynthetic activity, particularly in spring, observed at northern latitudes during the 1980s and 1990s (Myneni *et al.*, 1997; Randerson *et al.*, 1999). The updated analysis presented in this study indicates that this increase in amplitude has continued until the present, following the temperature-driven growing season greening over Eurasia (Figure 3.4b). Except for Alaska, photosynthetic activity over most of North America seems to have little influence on the amplitude of the annual cycle of atmospheric CO_2 at this station (Supplementary Figure B13), consistent with the spatial footprint of the station described by earlier studies (Kaminski *et al.*, 1996; Barichivich *et al.*, 2012).

Overall, since 1972, the peak-to-trough CO_2 amplitude has increased significantly by 22.2% with respect to the 1970s as a result of a decreasing trend (24.9%) in summer minimum CO_2 concentrations associated primarily with a shift towards warmer, longer and more productive growing seasons in Eurasia during the late 1980s. This concurrent large-scale shift in temperature and vegetation greenness at northern latitudes is strongly consistent with earlier evidence for

an abrupt increase in the mean of the net land carbon sink of about 1 Pg C/yr in 1988/1989 (Sarmiento *et al.*, 2010; Beaulieu *et al.*, 2012). More recently, the greater influence of wintertime ecosystem respiration on the seasonal amplitude of the CO_2 annual cycle during most of the 2000s has reduced the correspondence in year-to-year variations in the amplitude of the annual CO_2 cycle and growing season NDVI over Eurasia (Figure 3.4b).

A number of studies have shown that summer warming and longer growing seasons are associated with reduced rather than increased plant productivity during recent years at mid to high northern latitudes because of increased drought stress on vegetation growth (Angert *et al.*, 2005; Buermann *et al.*, 2007; Zhang *et al.*, 2008; Peng *et al.*, 2011; Piao *et al.*, 2011; Ma *et al.*, 2012; Buermann *et al.*, 2013). On a biome scale, only in the temperate region of Eurasia is there a clear reduction in growing season NDVI since around 1997. In the other northern biomes and in North America the NDVI varied around the mean during this recent period (Supplementary Figure B10). There is no clear evidence for widespread reductions in NDVI-based photosynthetic activity integrated over the entire growing season or for net carbon uptake from atmospheric CO_2 records with recent warming.

3.5 Conclusions

Independent streams of satellite and ground-based observations of NDVI, surface air temperature, snow cover, freeze-thaw dynamics and atmospheric CO_2 concentrations from 1950 to 2011 were used to investigate temporal variations in the photosynthetic and potential (thermal) vegetation growing seasons and evaluate their connection with the carbon cycle at northern latitudes ($>45^oN$). The combined analysis of these multiple climate and vegetation indicators of growing season changes has revealed a picture of complex and highly dynamical responses of terrestrial ecosystems to the rapid warming over the past three decades at these latitudes. The main findings are summarised as follows:

- The thermal potential growing season has lengthened substantially since 1950, but most of the change has occurred during the last three decades and over Eurasia. The warmest and longest thermal seasons occurred during the 2000s because of a recent acceleration of the autumnal extension.

- The photosynthetic growing season has closely tracked long-term changes in the potential growing season in spring, but not during autumn when light and other factors increasingly constrain photosynthesis and growth. While the extensions of the photosynthetic and thermal potential growing seasons have been similar since 1982 in spring, the autumnal extension of the photosynthetic growing season has been only about half that of the thermal growing season, yielding a smaller overall lengthening of the photosynthetic growing season. Nevertheless, the photosynthetic activity integrated over the whole growing season has closely tracked interannual variations and the general warming trend apparent in seasonally integrated temperatures throughout the entire satellite period.

- The long-term increase in the peak-to-trough amplitude of the CO_2 annual cycle at northern latitudes since 1972 indicates that the net effect of the observed warming and intensification of the growing season has been an increase in the uptake of atmospheric CO_2 by cool northern terrestrial ecosystems, particularly the boreal forests of Eurasia.

- The synchronised spring extensions of the potential and photosynthetic growing seasons have stimulated earlier and stronger net CO_2 uptake by northern ecosystems, but the autumnal extension appears to have been associated predominantly with earlier rather than delayed net ecosystem release of CO_2 to the atmosphere. These different ecosystem responses at the opposite ends of the growing season, together with the autumnal decoupling between the potential (thermal) and photosynthetic growing seasons have had contrasting effects on the net flux of CO_2 between the terrestrial biosphere and the atmosphere.

Determining the impact of continuing twenty-first century warming on the carbon balance of northern terrestrial ecosystems requires that these complex responses be taken into consideration, including the possibility that the autumn respiration response may become dominant. In addition, an emerging consequence of the earlier start of the growing season in the boreal forests is the potential increase in moisture constraints and reduction in peak vegetation productivity during the following summer as a result of earlier snowmelt. This negative effect of earlier springs on summer soil water balance and peak of vegetation growth is of special concern, as it may

offset productivity gains due to warmer springs and longer growing seasons (e.g., Angert *et al.*, 2005; Trujillo *et al.*, 2012; Buermann *et al.*, 2013). However, the lack of soil moisture observations and suitable moisture indices that take into account snow dynamics has precluded a robust analysis of this apparent link between the timing of spring and summer soil moisture status in the boreal region.

The potential influence of summer soil moisture on the functioning of northern ecosystems with longer and hotter growing seasons is currently the subject of intense research as new datasets of soil moisture are becoming available to the scientific community. This emerging issue is addressed in Part II of this dissertation, where a detailed analysis of changes in summer drought and their influence on northern vegetation during recent decades is presented.

Part II

Drought and northern vegetation

Chapter 4

Recent changes in summer drought severity in the northern latitudes based on the scPDSI

Abstract

The rapid warming of the northern latitudes during recent decades has been accompanied by increasing precipitation and longer active seasons. In spite of increased moisture inputs, it has been hypothesised that warming may have increased summer drought severity because of enhanced atmospheric moisture demand and longer evaporation periods. The lack of long-term soil moisture observations in the northern latitudes has precluded a direct evaluation of the impact of warming on drought severity. In this chapter, an enhanced version of a recently released dataset of the self-calibrating Palmer Drought Severity Index (scPDSI) is evaluated and analysed to infer changes in drought severity across the circumpolar northern latitudes (>45^{o}N) since 1950. Comparisons with field measurements of soil moisture, satellite observations and simulations from two modern land surface models show that the scPDSI is a good indicator of summer and autumn soil moisture variability in the top meter of the soil profile, with a skill similar to complex land surface models. Although uncertainties in the in situ and satellite observations during the spring hamper a conclusive evaluation of the ability of the scPDSI and the models to represent snow hydrology, variations in maximum snow accumulation are consistent with moisture anomalies inferred during the melting period. The scPDSI suggests that rapid warming since the late 1980s has increased evapotranspiration demand and consequently summer and autumn drought severity in the northern latitudes, offsetting the effect of increasing cold-season precipitation. This result is consistent with ongoing amplification of the hydrological cycle and with model projections of summer drying at northern latitudes in response to anthropogenic warming. The warming-driven increase in moisture demand has attenuated recent wetting trends in most of Siberia and intensified episodic droughts and regional drying trends in Alaska, northern Canada and central Asia. However, changes in permafrost and snowpack dynamics with recent warming might have had a stronger effect on drought severity in these snow-dominated regions than increased evaporative moisture demand.

4.1 Introduction

Low temperatures and frozen ground strongly constrain ecosystem metabolism and the exchange of water and energy in the northern latitudes (Zhang *et al.*, 2011). As a result, ecosystem and hydrological processes in these regions are strongly sensitive to temperature variability and changes in the cryosphere (Jarvis & Linder, 2000; Barnett *et al.*, 2005). The rapid warming of the high latitudes during recent decades has stimulated higher evapotranspiration rates (Zhang *et al.*, 2009; Miralles *et al.*, 2013) and longer evaporative periods (Zhang *et al.*, 2011). This increase in evapotranspiration coincides with a general increase in precipitation (Trenberth *et al.*, 2007), which is consistent with the expected intensification of the hydrological cycle with global warming (Allen & Ingram, 2002; Held & Soden, 2006; Seager *et al.*, 2010; Polson *et al.*, 2013). A recent synthesis of the observational record over the vast Arctic region suggests that positive trends in annual precipitation, evapotranspiration, and river discharge to the Arctic Ocean could indicate that the anticipated intensification of the hydrological cycle is already underway (Rawlins *et al.*, 2010). However, the relative magnitudes and spatial heterogeneity of these trends are highly uncertain due to sparse measurement networks and large natural variability in the climate of the region.

A growing body of evidence indicates that changes in the regional water cycle are impacting ecosystem processes in northern biomes. During the late 1990s and 2000s, several widespread and persistent droughts have occurred across the boreal high latitudes (Zhang *et al.*, 2008; Dai, 2012). These droughts have increased fire disturbance (Kasischke & Turetsky, 2006) and resulted in regional decreases in vegetation productivity in the boreal forest as indicated by atmospheric CO_2 anomalies (Angert *et al.*, 2005), satellite vegetation indices (Goetz *et al.*, 2005), modelled vegetation productivity (Zhang *et al.*, 2008), forest inventory data (Hogg *et al.*, 2008; Ma *et al.*, 2012) and tree rings (Barber *et al.*, 2000). These ecological responses have led to the perception that summer drought severity in the northern latitudes is increasing along with recent warming because of greater evaporative demand (Barber *et al.*, 2000; Angert *et al.*, 2005). Although the lack of long-term soil moisture observations in the pan-Arctic region (Dorigo *et al.*, 2011) precludes a direct analysis of decadal changes in soil moisture, model-based estimates broadly support the notion of increased drought severity with recent warming in the boreal zone (Sheffield & Wood, 2007; Dai, 2011a). Nevertheless, the magnitude and regional variation of such an increase is uncertain.

Better understanding of recent changes in drought severity across the northern latitudes requires realistic estimates of soil moisture variability and quantification of the relative contributions of changes in moisture supply (precipitation and snow) and evaporative demand (potential evapotranspiration; PET), which depends not only on temperature but also on radiation, humidity and winds (Wang & Dickinson, 2012). Due to the general scarcity of soil moisture measurements, meteorological drought indices and model-based estimates are commonly used as a substitute for observations to quantify changes in drought and their impact on terrestrial ecosystems (Sheffield & Wood, 2007; Zhao & Running, 2010; Dai, 2012; Vicente-Serrano *et al.*, 2013). The ability of drought indices and land surface models to represent changes in moisture availability accurately depends on the realism of their physical formulation and the quality of the meteorological data used to drive them. Oversimplification in some drought indices and un-

certainties in the meteorological drivers of more realistic, but necessarily complex, land surface models result in large uncertainties in the estimates of global and regional changes in drought severity associated with recent warming (Seneviratne *et al.*, 2012; Trenberth *et al.*, 2014). These uncertainties are particularly large in remote regions with sparse meteorological observations and snow-dominated hydrology, such as the high northern latitudes.

Although simpler than land surface models, the most popular index currently used to quantify drought severity is the Palmer Drought Severity Index (PDSI; Palmer, 1965). The PDSI was originally developed to monitor agricultural drought in the United States. In recent years it has been refined to study the influence of climate change on global trends in drought using readily available monthly historical meteorological observations or output from climate models (Dai, 2012; Sheffield *et al.*, 2012; van der Schrier *et al.*, 2013; Trenberth *et al.*, 2014).

Several aspects of the formulation and assumptions underlying the PDSI have been criticised over the years as the index came to be applied outside the regional context for which it was created. However, the popularity of the index and its advantage over other drought indices relate to the use of monthly input data that are readily available in most parts of the world, the use of a soil water balance model at its core, and the flexibility to incorporate more comprehensive formulations for critical components of the algorithm. The latter flexibility has resulted in several improved variants of the index (Dai, 2011a). A 'self calibrating' version, called scPDSI (Wells *et al.*, 2004), is perhaps the most important. The scPDSI solves an issue of lack of spatial comparability of the original PDSI by using a local climatology to better characterise the results in the intended Palmer categories of drought across different climate regimes.

In this study, an enhanced version of a recently released global gridded dataset of monthly scPDSI for the period 1901–2009 (van der Schrier *et al.*, 2013) is used as the basis for investigating long-term changes in drought severity in the northern latitudes ($>45^{o}$N). This dataset was jointly developed by the Climatic Research Unit (CRU) and the Royal Netherlands Meteorological Institute (KNMI) and is the first global dataset of the scPDSI that includes a representation of snow dynamics in the underlying water balance estimates. This and other methodological improvements in the dataset allow a better quantification of drought changes in the northern latitudes than was previously possible with the available gridded scPDSI datasets (e.g., Dai, 2011a; Sheffield *et al.*, 2012). The PDSI and its newer variants have been widely validated in the mid-latitudes against runoff, in situ soil moisture measurements, satellite observations and modern land surface models (Dai *et al.*, 2004; Dai, 2011a; van der Schrier *et al.*, 2013). In contrast, little is known about the ability of the index to represent changes in moisture availability in the northern latitudes, because earlier datasets did not consider snow dynamics in the soil water balance.

The aims of this study are to validate the scPDSI dataset in the northern latitudes and assess the evidence for changes in drought severity with recent warming in the region. Significant correlations between the scPDSI and other moisture measures should provide empirical evidence of the usefulness of this improved scPDSI dataset to investigate drought changes at high northern latitudes. The seasonal performance of the scPDSI to represent variations in available moisture is evaluated against in situ soil moisture measurements in 82 sites across northern Eurasia and Alaska, gridded soil moisture estimates from two state-of-the-art land surface models and two simple multi-scale drought indices. The results of this evaluation provide independent support

for the inferences based on this dataset.

4.2 Data and methods

4.2.1 The scPDSI data

The PDSI and its variants are based on a set of empirical parameterisations of soil moisture anomalies in the rooting zone. Soil moisture is simulated by a simple two-layer water balance model. The bucket-type model is driven only by monthly precipitation (water supply) and potential evapotranspiration (water demand). In the model, precipitation is partitioned into soil water recharge and runoff. The surface soil layer is assumed to have a fixed water holding capacity of 25 mm and is recharged first. Then, the bottom layer is recharged until it saturates. Runoff occurs when both layers (the entire soil column) reach the field capacity and potential evapotranspiration demand has been met. When precipitation and soil moisture in the surface layer can not meet the water demand from potential evapotranspiration, soil moisture in this layer is completely evapotranspirated at the potential rate, then moisture in the bottom layer is evapotranspirated at a rate that depends on its moisture content and unmet potential evapotranspiration (i.e., actual evapotranspiration).

The CRU-scPDSI dataset incorporates several methodological improvements that make it more suitable for analysing drought severity at northern latitudes (van der Schrier *et al.*, 2013). First, the more physically-based Penman-Monteith (PM) parameterization for potential evapotranspiration is used instead of the simple temperature-dependent Thornthwaite (TH) approach. Second, the actual vegetation cover rather than a fixed simple reference crop is used for computing potential evapotranspiration. Third, seasonal snowpack dynamics are considered in the water balance model for the first time. The effect of snow is simulated by a simple degree-day algorithm calibrated at each grid box using satellite observations of snow water equivalent (see Appendix B in van der Schrier *et al.*, 2013). Below 0^oC, precipitation falls as snow and is added to snow storage. Above 0^oC, snow melts at a locally-calibrated potential rate and melt water is added to the liquid precipitation fraction that enters into the soil moisture model.

The consideration of snow is essential for achieving a more realistic estimate of seasonal soil moisture variability in the snow-dominated northern latitudes. van der Schrier *et al.* (2013) showed that the dataset compares well with satellite-based surface soil moisture observations and soil moisture estimates from the GLDAS-2 Noah land surface model. In addition, the inclusion of the snow parametrisation resulted in significant correlations between monthly anomalies in terrestrial water storage from GRACE satellites and the sum of monthly estimates of snow water equivalent (SWE) and soil moisture storage in the scPDSI. Other factors that could also affect soil moisture availability in the northern latitudes, such as permafrost dynamics (Sugimoto *et al.*, 2002), vegetation phenology (Bonan, 2002) and the influence of increasing atmospheric concentration of carbon dioxide on plant transpiration (Gedney *et al.*, 2006) are not accounted for in the water balance of the scPDSI. In permafrost soils, the scPDSI should be interpreted only as an index of meteorological drought since the actual water content of these soils is strongly regulated by seasonal and long-term permafrost dynamics.

The original version of the CRU-scPDSI dataset is based on the CRUTS 3.10.01 meteorological fields (precipitation for water supply; temperature, cloud cover, vapour pressure and

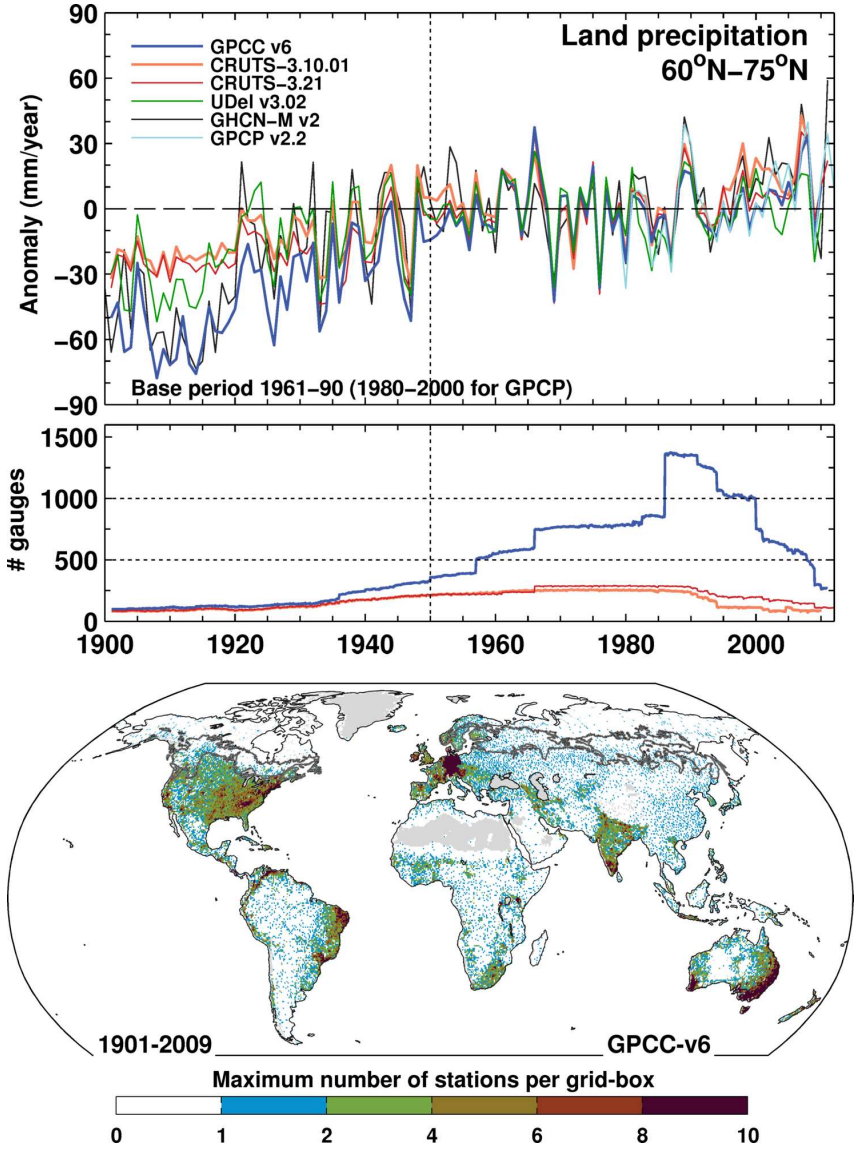

Figure 4.1: Annual land precipitation anomalies in the Arctic region as represented by different datasets along with their associated temporal and spatial gauge coverage since 1900. The datasets used are: Global Precipitation Climatology Centre (GPCC v6), Climatic Research Unit (CRU TS–3.10.01 and CRU TS–3.21), University of Delaware (UDel v3.02), Global Historical Climatology Network-Monthly (GHCN–M v2) and Global Precipitation Climatology Project (GPCP v2.2). The vertical dotted lines indicate the start of the period of analysis used in this study. The grey lines in the map denote the extent of the boreal forests.

wind speed for PM PET) produced by the Climatic Research Unit at 0.5^o spatial resolution (Harris *et al.*, 2014). Recently, Trenberth *et al.* (2014) observed that since around 1996 the CRUTS 3.10.01 precipitation data are slightly 'wetter' at northern latitudes than some other precipitation products based on many more rain gauge data (Figure 4.1). They showed that this results in a slight underestimation of recent drought trends in the CRU-scPDSI dataset and other datasets based on CRU precipitation data (e.g., Sheffield *et al.*, 2012). For this reason, the scPDSI was recomputed using precipitation data from the GPCC Full Data Reanalysis version 6 at 0.5^o resolution (Schneider *et al.*, 2013) instead of using the CRUTS 3.10.01 precipitation.

GPCC is the precipitation analysis with the greater number of rain gauges processed currently available. However, most of the gauge data incorporated in any global precipitation dataset represent the more populated regions south of the Arctic circle (Figure 4.1). North of

60^{o}N, the number of rain gauges in the GPCC product drops from a maximum of 1374 in the late 1980s to about 300 in 2010, whilst CRUTS 3.10.01 has a maximum of only 300 gauges, falling to less than 120 after 1995. Prior to 1936, the number of gauge records in both products is less than 180. Using the GPCC product to drive the scPDSI algorithm reduces uncertainties in regional precipitation estimates during recent decades, but not in the first half of the 20th century (Figure 4.1). Therefore, the analysis of the scPDSI was restricted to the period 1950–2009.

4.2.2 Evaluation of the scPDSI

The ability of the scPDSI to represent interannual moisture variability at different soil depths and time scales was assessed based on correlations with short-term field measurements, multi-decadal satellite observations, land surface model simulations and multi-scale drought indices (see Table 4.1). Correlations were computed separately for the spring melting period in the boreal region (April-May), summer (June-August) and autumn (September-October). This allows seasonal differences in performance to be identified and related to the decreasing influence of snow and frozen ground through the growing season. In the following subsections, the datasets and periods used for correlation analysis are briefly described.

Table 4.1: Characteristics of the datasets used to validate the scPDSI.

Dataset	Resolution	Time span	Reference
Soil moisture			
in situ soil moisture, LTER Bonanza Creek, Alaska	hourly	2002–2012	Hollingsworth (2005)
in situ soil moisture, ISMN networks over the fUSSR, Finland and Alaska	hourly	since 1978	Dorigo *et al.* (2011)
Satellite microwave soil moisture (MW–SMO)	0.25^{o}x0.25^o, daily	1979–2010	Liu *et al.* (2012)
GLDAS–2 Noah soil moisture	1^{o}x1^o, monthly	1948–2007	Rui (2011)
ERA-Land soil moisture	0.5^{o}x0.5^o, 6-hourly	1979–2010	Balsamo *et al.* (2013)
Drought indices			
Standardized Precipitation Index (SPI)	0.5^{o}x0.5^o, monthly	1901–2010	This study
Standardized Precipitation Evapotranspiration Index (SPEI)	0.5^{o}x0.5^o, monthly	1901–2011	Vicente-Serrano *et al.* (2010)
Snow			
Globsnow SWE version 1.3	25x25 km, monthly	1979–2011	Takala *et al.* (2011)

4.2.2.1 In situ and satellite observations

Historical and operational in situ soil moisture measurements north of 45^{o}N were obtained from the International Soil Moisture Network (ISMN, http://ismn.geo.tuwien.ac.at/). The ISMN is a data hosting centre where soil moisture measurements collected in monitoring networks and field validation campaigns around the world are archived, quality controlled and distributed to the scientific community (Dorigo *et al.*, 2011, 2013a). The database includes data from 1952 until the present. Most records are from the mid-latitudes of Eurasia and North America and have been originated from monitoring networks created during the last decade. Multi-year soil moisture records for the high northern latitudes are available from some historical networks in the in the former Soviet Union (fUSSR) and recent operational networks in Finland and Alaska.

Station records north of 45^{o}N with a length of at least 7 years were selected for analysis (Figure 4.2). A large number of stations covering the period 1978–1985 were extracted from the RUSWET-GRASS (67 stations) and RUSWET-VALDAI (3 stations) historical networks in

the fUSSR (Vinnikov & Yeserkepova, 1991; Robock *et al.*, 1995). These data represent total volumetric soil moisture measurements of plant available soil moisture integrated over the upper 10 cm and 1 m soil layers, made at 0.1-ha flat observational plots with natural grass vegetation. Each record is the average of measurements made at four points in the plot with a frequency of three times per month during the warm season and once a month during winter. These relatively dense historical networks have been widely used for evaluating the performance of land surface models (Robock *et al.*, 1995) and also the PDSI (Dai *et al.*, 2004).

For the most recent period, hourly records included in the ISMN archive covering most of the 2000s were extracted from high-latitude operational networks, such as SNOTEL (Snow

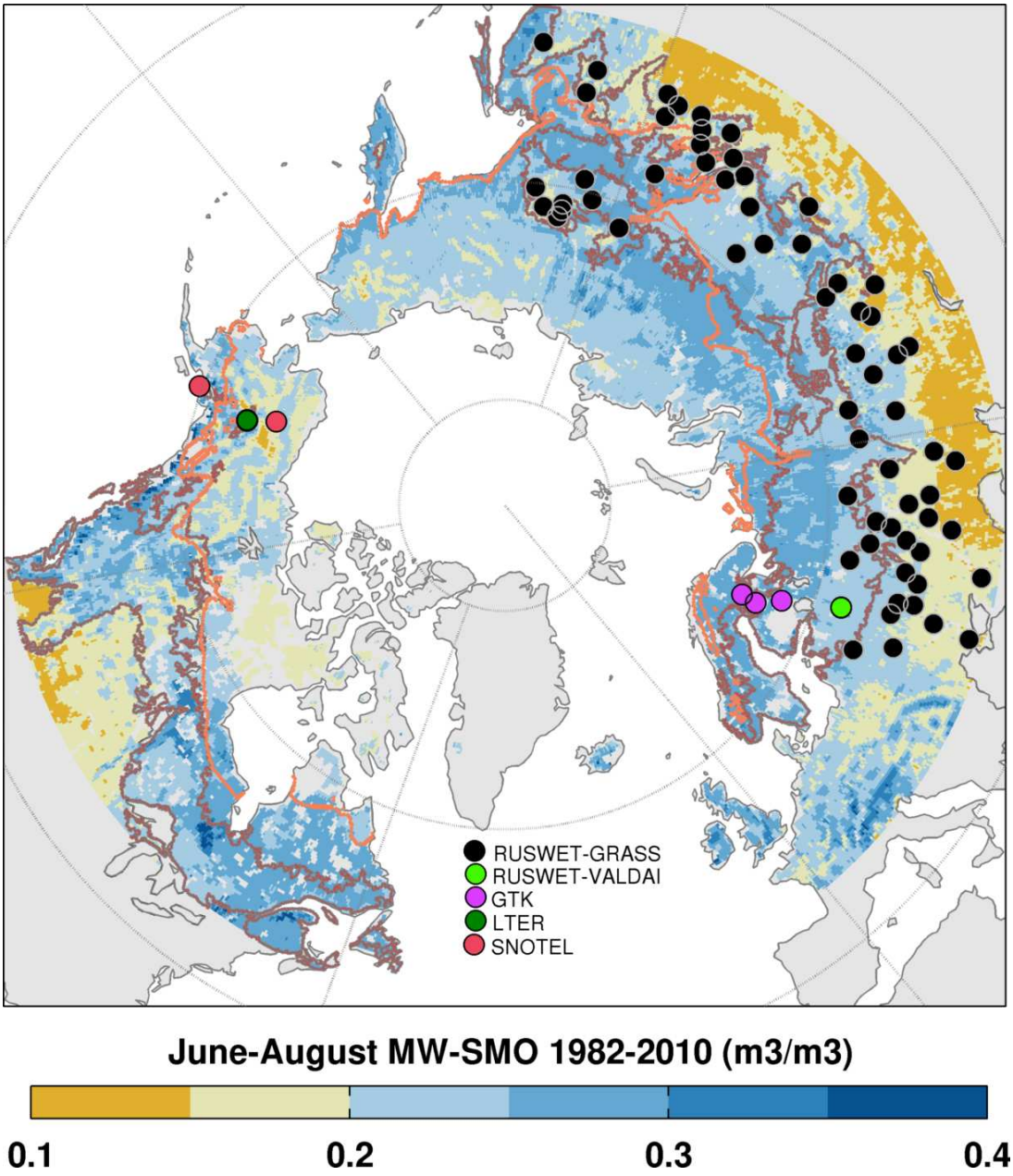

Figure 4.2: Map showing the locations of the 82 in situ soil moisture records used to evaluate the scPDSI. Mean summer surface soil moisture (MW-SMO) over 1982–2010 is shown in the background to illustrate the geographic patterns of moisture availability. Note that these patterns are imposed by the Noah land surface model. The boreal forests are outlined in gray and the the orange line indicates the southern edge of the discontinuous permafrost (Brown *et al.*, 1998). Areas without data or outside the study domain are indicated by gray shading.

Telemetry; 2 stations) in Alaska and GTK (Geological Survey of Finland; 3 stations) in Finland. In addition, 7 continuous hourly soil moisture records since 2002 were obtained from the LTER research program at Bonanza Creek Experimental Forest in Alaska (available at: http://www.lter.uaf.edu/data_detail.cfm?datafile_pkey=5, Hollingsworth, 2005; Yarie, 2008). The hourly or 3-hourly records from all these operational networks are generally available for the upper meter of the soil profile at every 5 or 10 cm near the surface and every 20 or 50 cm in the lower part.

Overall, a dataset of 82 soil moisture stations with at least 7 years of measurements made at several depths and temporal frequencies was compiled. Most of the stations are located in the northern temperate grasslands and croplands of Eurasia and only about a third are located in the boreal forest region (Figure 4.2). Several stations in the boreal region of eastern Siberia and Alaska are located in the zone of discontinuous permafrost. The hourly data at each depth were aggregated into daily averages and subsequently into monthly averages. Historical observations with a frequency of 10 days were also aggregated into monthly averages. When available, quality flags were used to exclude observations with poor quality or physically unrealistic values. Finally, only representative series for 'surface' and 'root zone' soil moisture dynamics at each station were retained for comparison with the scPDSI and other gridded estimates of moisture availability. These series were selected by taking the moisture record available at the nearest depth to 10 cm and 20 cm, respectively.

In addition to site-level moisture measurements, a recently released (June 2012) global dataset of soil moisture based on historical satellite microwave observations since 1978 (available at: http://www.esa-soilmoisture-cci.org/, Liu *et al.*, 2012) was used to evaluate the scPDSI. This observational dataset has provided a new avenue for studying large-scale changes in soil moisture dynamics (Dorigo *et al.*, 2012) and evaluating the performance of land surface models (Albergel *et al.*, 2012, 2013a,b; Szczypta *et al.*, 2013). The product has a spatial resolution of 0.25^o and is based on the statistical blending of daily passive and active microwave observations from multiple satellites between November 1978 and December 2010. The rescaling and merging is based on a reference surface soil moisture climatology provided by the GLDAS-Noah land surface model. The resulting product inherits the absolute values of GLDAS-Noah (Figure 4.2) but retains the long-term moisture signals (e.g., autocorrelation, trends) sensed by the satellites (Liu *et al.*, 2012; Dorigo *et al.*, 2012).

Despite some temporal and spatial inhomogeneities due to changes in satellite sensors, the merged dataset has been shown to be consistent with in situ observations and simulations from state-of-the-art land surface models in the mid and low latitudes (Albergel *et al.*, 2013a; Dorigo *et al.*, 2013b; Loew *et al.*, 2013). van der Schrier *et al.* (2013) found a good agreement between the interannual variability of this dataset and the CRU-scPDSI over most of the global land, though correlations in the northern latitudes were weaker and sometimes negative. Loew *et al.* (2013) also observed weak or negative correlations between soil moisture fields simulated by two land surface models and the satellite observations over the northern latitudes. Frozen ground and snow cover limit data availability in these regions and surface water, peat soils, rough topography and errors in determining the freeze/thaw and snowmelt transitions can reduce the quality of the available data. Prior to data processing, product quality flags were used to remove daily observations for most of these surface conditions. The remaining data were

aggregated into seasonal averages. Then, correlations between the scPDSI and MW–SMO were computed for each season over the period 1979–2009.

4.2.2.2 Soil moisture simulated by land surface models

ERA-Land (http://apps.ecmwf.int/datasets/data/interim_land/) and GLDAS-2 (Global Land Data Assimilation System Version 2.0; http://ldas.gsfc.nasa.gov/gldas/) soil moisture fields were used to asses the ability of the scPDSI to represent interannual soil moisture variability at different depths across the northern latitudes. ERA-Land is a global land surface dataset describing the dynamics of the soil (moisture and temperature) and snowpack at a spatial resolution of about 80 km every six hours during the period 1979–2010 (Balsamo *et al.*, 2013). This product is a revised version of the ERA-Interim land surface reanalysis and is based on a single 32-year offline (land-only) simulation with the latest ECMWF land surface model driven by meteorological forcing from the ERA-Interim atmospheric reanalysis and precipitation adjustments based on GPCP v2.1. A number of improvements in the parameterisations for the land surface scheme have been made compared with the original ERA-Interim dataset, which makes it more suitable for hydrological studies. In ERA-Land, six types of soil are used and moisture is simulated for four layers (0-7, 7-28,28-100 and 100-289 cm). The soil moisture data for 18:00 UTC of each day were extracted for the three upper layers and monthly averages were computed for each layer.

Monthly soil moisture data from GLDAS-2 simulated by the Noah land surface model at 1^o resolution (Rui, 2011) were extracted for the upper three layers (0-10,10-40 and 40-100 cm). The Noah model included an improved snow assimilation scheme and was driven with the Princeton global meteorological forcings of Sheffield *et al.* (2006) from January 1948 to December 2007. Since the product is provided at 1^o resolution, the data were regridded to the 0.5^o grid of the scPDSI using bilinear interpolation.

The ERA-Land and GLDAS-2 Noah soil moisture data at each layer were averaged for the spring, summer and autumn months. Then, for each season, correlations between the scPDSI and soil moisture at each depth were computed over the period 1979-2009 for ERA-Land and 1979–2008 for Noah.

4.2.2.3 Multi-scale drought indices

The PDSI has been criticised for having a relatively fixed temporal scale compared with other drought indices that can be computed to represent accumulated moisture anomalies at arbitrary time scales (Vicente-Serrano *et al.*, 2012). The most basic multi-scalar drought index is the Standardized Precipitation Index (SPI; McKee *et al.*, 1993), which represents only accumulated precipitation deficits or surpluses without accounting for water losses to runoff or evapotranspiration. To overcome this limitation in the SPI, Vicente-Serrano *et al.* (2010) proposed the Standardized Precipitation Evapotranspiration Index (SPEI). The SPEI represents accumulated anomalies of precipitation minus potential evapotranspiration and thus it can be thought as standardised anomalies of accumulated net precipitation.

In order to evaluate the ability of the scPDSI to represent short and long-term moisture variability through the growing season, simple correlations between the scPDSI and these two drought indices were computed for time scales of 3, 6, 9 and 12 months and for spring, summer and autumn. The seasonal correlations allow an assessment of the relative impact of the

snow parametrisation on the time scale of the scPDSI. The SPI was computed for the study domain from monthly GPCC precipitation data at a spatial resolution of 0.5^o from 1901 to 2010 (Schneider *et al.*, 2013). SPEI data for the period 1901–2011 were obtained from the Global SPEI database version 2.2 (https://digital.csic.es/handle/10261/72264). This database is based on monthly precipitation and Penmann-Monteith potential evapotranspiration from the CRU TS 3.20 dataset.

4.2.2.4 Snowpack

A positive correlation between winter snow accumulation and the scPDSI during the spring melting period would indicate a good performance of the index to simulate the effect of snow on seasonal soil moisture dynamics in the northern latitudes. Therefore, the realism of the snow hydrology of the scPDSI was tested by correlating peak spring snow water equivalent (SWE) with the scPDSI averaged during the spring melting period in the boreal (April–May) and Arctic (May–June) zones over the period 1979–2009. For comparison with the scPDSI, peak SWE was also correlated with the SPEI at a scale of 12 months (SPEI-12mo) and surface soil moisture simulated by ERA-Land (0–7 cm) and Noah (0–10 cm).

Peak SWE between January and July was computed from monthly gridded SWE data from the GlobSnow dataset (version 1.3) developed by the European Space Agency (Takala *et al.*, 2011). GlobSnow combines SWE retrieved from multi-satellite microwave observations with forward snow emission model simulations and ground-based weather station data for non-mountainous regions of the Northern Hemisphere. Because of the improved accuracy obtained by assimilating independent sources of information, this is the best SWE product currently available for climate analysis (Hancock *et al.*, 2013). The SWE data were remapped from their original 25-km spatial resolution to the 0.5^o grid of the scPDSI using bilinear interpolation.

4.2.3 Changes in drought severity and the influence of evapotranspiration demand

The scPDSI dataset contains two alternative runs computed using the same precipitation input but with different PET implementations. One run uses actual monthly PET and the other uses fixed climatological monthly PET based on the climatology for the period 1961–1990. In the latter setup, fixed climatological temperature data were also used to drive the snow model. The differences between the two analyses represent the influence of changes in atmospheric evapotranspiration demand and temperature-driven snow melt on drought severity.

To quantify the effect of evapotranspiration demand on summer drought severity over the entire study domain, percentages of dry (scPDSI $\leq$ -2) and wet (scPDSI $\geq$ 2) area computed with fixed and varying PET were compared. Trend analysis of summer scPDSI with actual PET and simulated soil moisture was carried out for the period since 1979 using the non-parametric Mann-Kendall trend test implemented in the *zyp* package (Bronaugh, 2009) in R statistics.

4.3 Results

4.3.1 Evaluation of the scPDSI in the northern latitudes

4.3.1.1 Comparison with in situ measurements

The scPDSI correlates positively with most (∼49-63%) in situ records of surface and root zone soil moisture, indicating a good ability of the index to represent interannual soil moisture variability (Figure 4.3). However, positive correlations are more common during summer and autumn than during spring (Figure 4.4). This suggests that the scPDSI performs better during the second half of the growing season when the influence of snow hydrology is smaller. Nevertheless, spurious soil moisture measurements in modern networks due to frozen soils during the early spring (Dorigo *et al.*, 2013a) could also account for the weaker correlations during this period.

Negative correlations occur in all seasons but are more prevalent during the spring melting period and over south-western Russia and Belarus. In general, negative correlations tend to be associated with unusual sites where field measurements are negatively correlated with precipitation and positively correlated with temperature (Supplementary Figure C1). Such locations are likely strongly influenced by local-scale processes (e.g., topography, water table, permafrost,

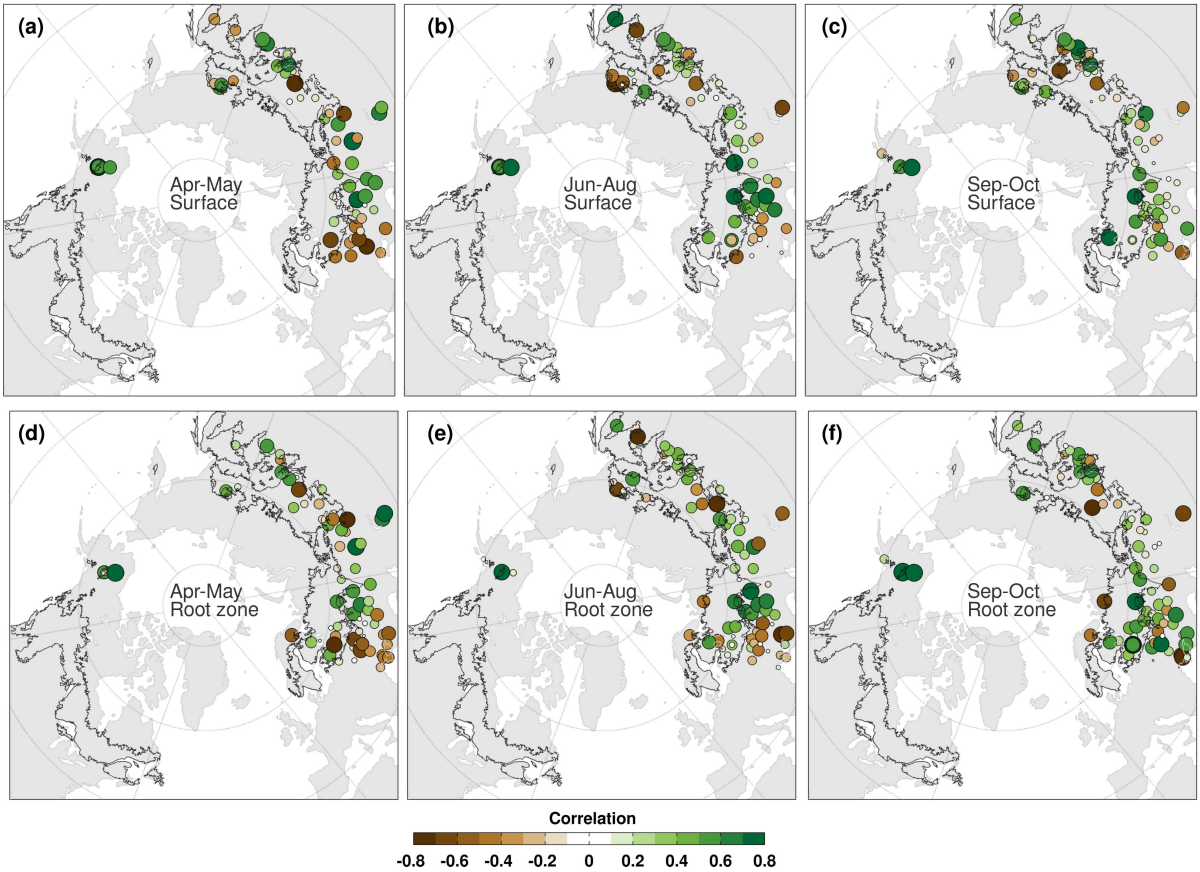

Figure 4.3: Correlation between the scPDSI and in situ measurements of (a–c) surface (< 10 cm) and (d–f) root zone (>10 cm) soil moisture during the spring, summer and autumn seasons. Correlations are shown only for sites with 7–9 years of overlap with the nearest scPDSI grid box. The overlapping period lies anywhere between 1978 and 1985 in the fUSSR (RUSWET-GRASS and RUSWET-VALDAI networks), and between 2002 and 2011 in Finland (GTK network) and Alaska (SNOTEL and LTER networks). The magnitude of the correlations is proportional to the symbol size, following the color bar. The boreal forests are outlined in black.

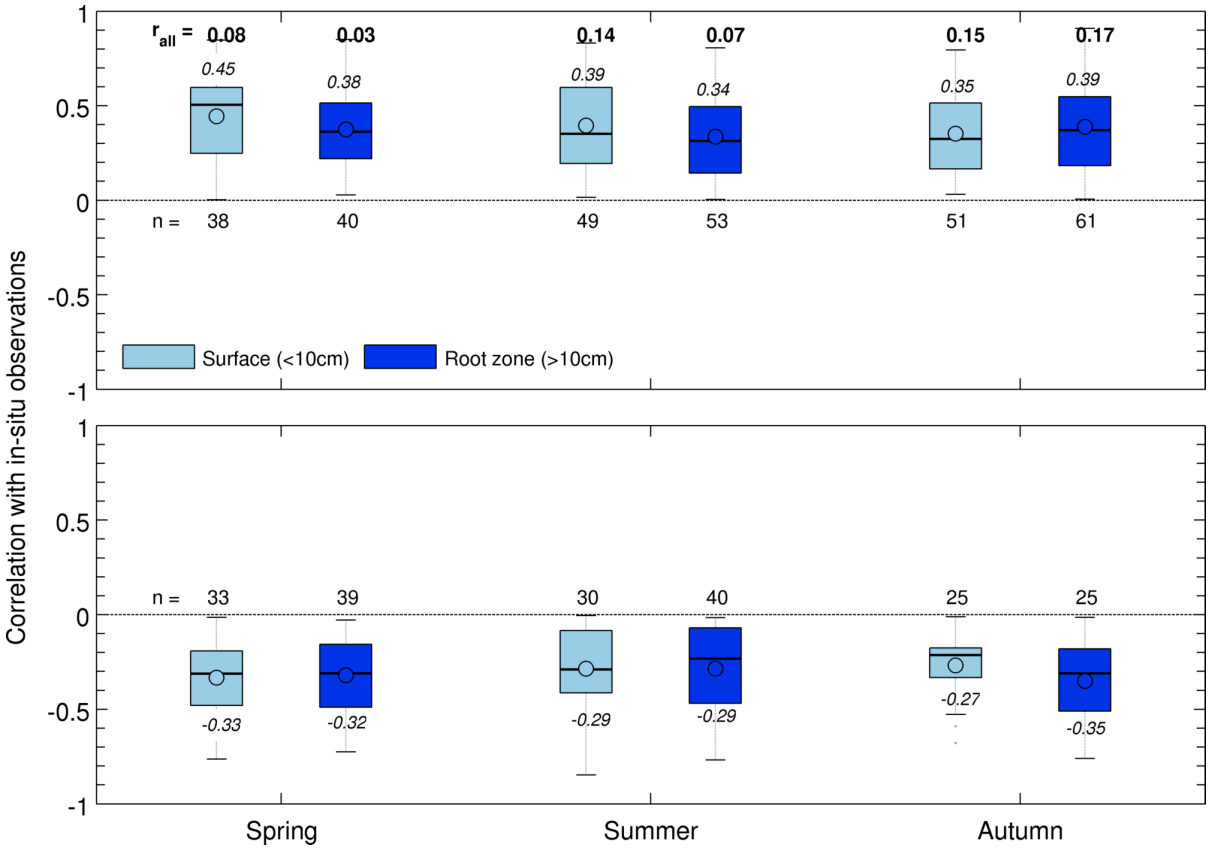

Figure 4.4: Box plots summarising the correlations between the scPDSI and in situ measurements of soil moisture in the surface and the root zone during spring (April-May), summer (June-August) and autumn (September-October). The mean is denoted by the circle inside the box, while the black horizontal line and the box edges denote the respective median and 25th and 50th quartiles. Whiskers denote 5th and 95th percentiles, and grey dots represent outliers. Box plots are shown separately for positive (top) and negative (bottom) correlations. The mean correlation values and the number of stations included in the average are indicated next to each bar. The overall mean correlation (r_{all}) is shown in the top panel.

delayed snowmelt) and thus are not representative of the regional moisture footprint associated with the gridded scPDSI estimates. Alternatively, interpolated precipitation anomalies might not represent well local variability at some of these stations.

Mean seasonal correlations indicate that the scPDSI is similarly correlated with surface and root zone soil moisture variability (Figure 4.4), though to some extent this is expected because root zone measurements in 70 stations obtained from historical networks (RUSWET-GRASS and RUSWET-VALDAI) also integrate surface soil moisture.

The seasonal performance of the scPDSI to represent surface soil moisture variability in the field relative to that of satellite observations (MW-SMO), land surface models (ERA-Land and Noah), drought indices (SPI-12mo and SPEI-12mo) and the earlier version of the dataset (CRU-scPDSI) is shown in Figure 4.5. In general, the consistency between the different products and field measurements is highly variable. There is no single product that is best correlated with field observations across all seasons. The scPDSI tends to perform similarly or slightly better than satellite observations and other drought indices, with similar mean correlations but a higher number of positive correlations with field measurements. The land surface models perform poorly in spring but perform better in summer and outperform all moisture metrics in autumn when the influence of snow is minimal. The two scPDSI datasets compare similarly to field measurements

in summer and autumn but the CRU–scPDSI version is slightly better correlated with field measurements in spring. This difference could be related to the influence of adjustments applied to cold season precipitation estimates in the GPCC dataset (Schneider *et al.*, 2013).

Most in situ moisture measurements are negatively correlated with temperature (Figure 4.5). The negative correlations are particularly strong in summer, suggesting an important influence of enhanced evapotranspiration rates with higher temperatures.

4.3.1.2 Comparison with gridded soil moisture estimates and multi-scale drought indices

A summary of grid-wise correlations between the scPDSI and soil moisture simulated by land surface models, satellite observations and multi-scalar drought indices is shown in Figure 4.6. The variability of the scPDSI is better correlated with satellite observations and model-based soil moisture fields during summer and autumn months than during the spring melting period, when simulated soil moisture was shown to be only weakly correlated with field measurements

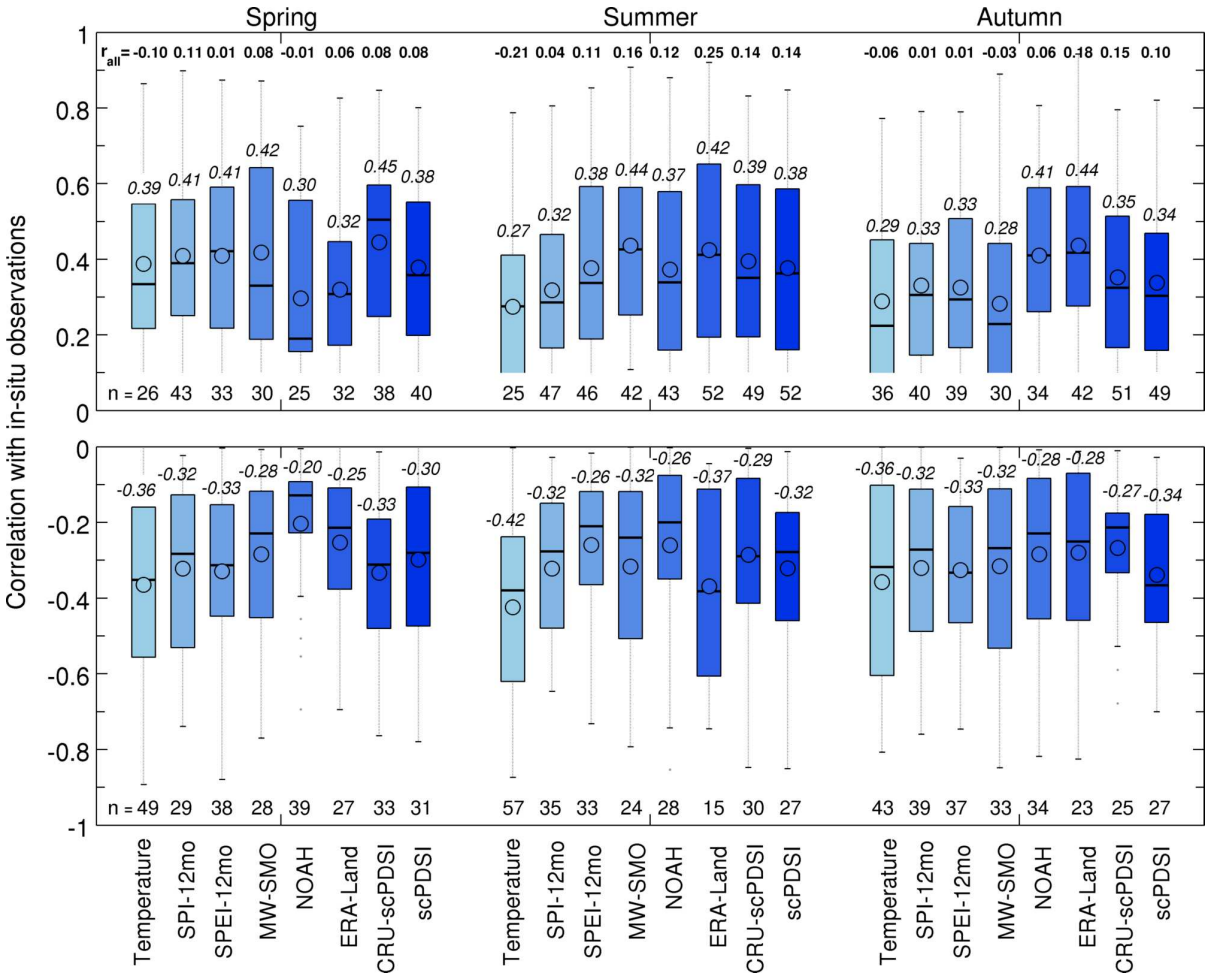

Figure 4.5: Box plots showing the relative performance of the scPDSI against in situ measurements of surface soil moisture through the growing season compared with satellite observations (MW–SMO), land surface models (ERA-Land and GLDAS-2 Noah) and other drought indices (SPI-12mo and SPEI-12mo). The original CRU-scPDSI version and temperature are also included for comparison. Box plots are shown separately for positive (top) and negative (bottom) correlations. The mean is denoted by the circle while the black horizontal line denotes the median. The mean correlation values and the number of stations included in the average are indicated next to each bar. The overall mean correlation (r_{all}) is shown in the top panel.

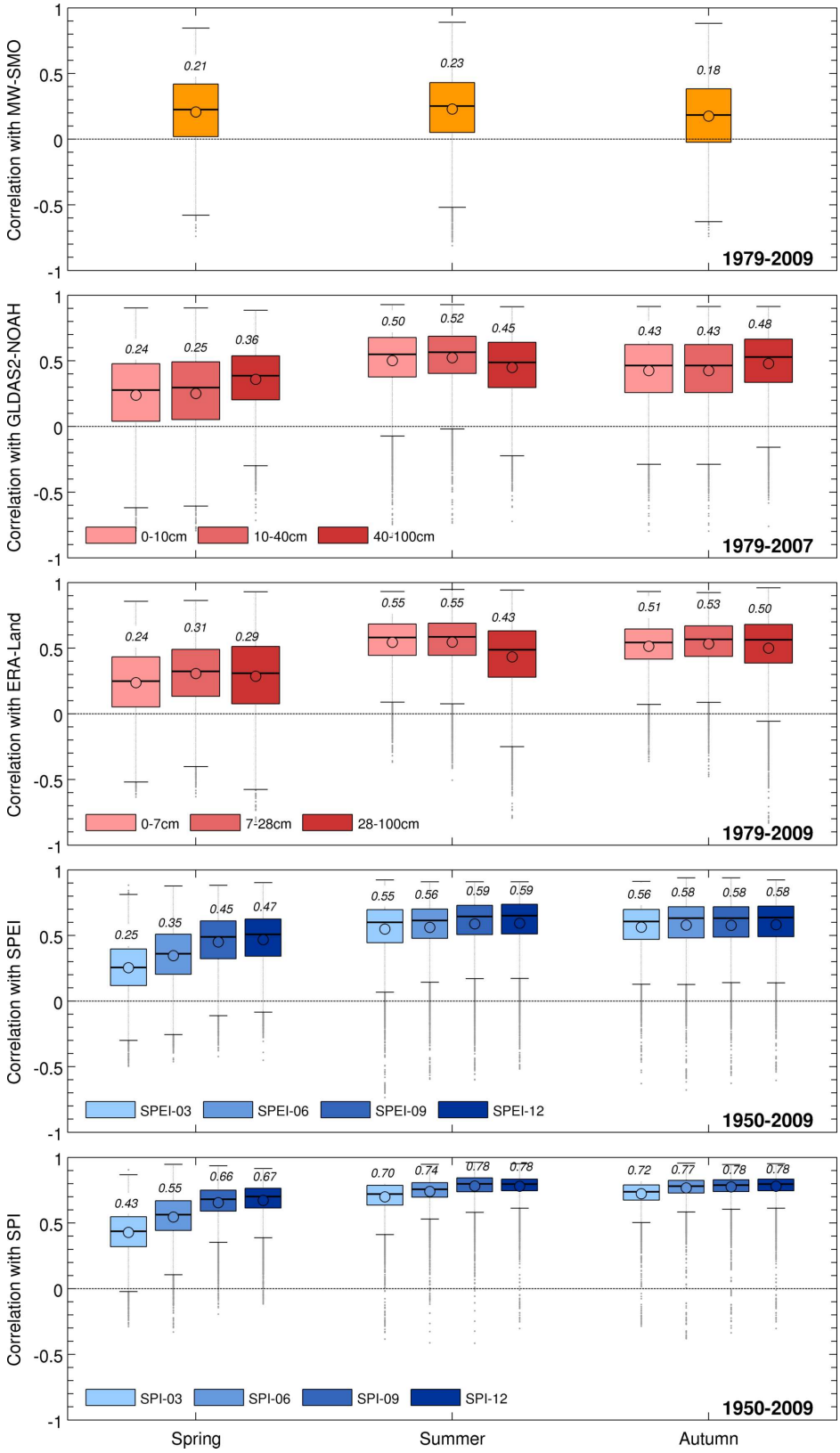

Figure 4.6: Box plots summarising the seasonal grid-wise correlations of the scPDSI with soil moisture simulated by land surface models (ERA-Land, Noah), satellite observations (MW–SMO) and multi-scalar drought indices (SPI and SPEI) during recent decades. The period used for correlation varies and is indicated in bottom-right corner of each panel. Note that during the spring, correlations with simulated soil moisture and drought indices are affected by snow cover in most of the subarctic region where snowmelt occurs in June.

in the boreal and northern temperate regions (Figure 4.5). However, it is important to note that during the spring (April-May) most of the subartic region north of the boreal forests is still covered by snow (see mask in Figure 4.10) and thus this may reduce correlations with model-based soil moisture. Compared with Noah, soil moisture variability simulated by ERA-Land agrees better with the scPDSI. Simulated moisture in the uppermost three soil layers is nearly equally correlated with the scPDSI. This indicates that the simple water balance of the scPDSI captures well warm-season moisture anomalies in the top meter of the soil profile.

Figure 4.6 shows that the SPI and SPEI are also more consistent with the scPDSI in summer and autumn, with little difference between time scales (3-12 months). In contrast, during the spring the consistency is substantially weaker but improves for longer time scales (9-12 months). This is because longer integration periods include cold-season precipitation, which in both reality and in the scPDSI is physically stored in the winter snowpack and released to the soil in spring. The scPDSI and SPI share the GPCC precipitation forcing and are thus more strongly correlated in comparison with the SPEI.

Correlation maps show that the consistency between the scPDSI and the different metrics of moisture availability varies considerably across the study domain (see Supplementary Figures C2–C5). In general, the scPDSI agrees better with model-based moisture estimates and multi-scalar drought indices in the northern temperate and southern boreal regions than in the remote subarctic region, where the influence of snow and permafrost on surface hydrology is stronger and the meteorological forcing data are more uncertain. Satellite-observed soil moisture variability is also better correlated with the scPDSI in the southern regions dominated by crops and grasslands than in the boreal and Arctic regions (Figure 4.7). In the high northern latitudes, satellite retrievals are fewer and less reliable as a result of longer snow cover, frozen ground, surface water and canopy interference in dense boreal forests. Larger uncertainties in satellite retrievals are likely the main cause of the weak and some times negative correlations observed in theses regions.

Biome and continental spatial averages of summer scPDSI are significantly correlated with the corresponding averages of summer surface soil moisture simulated by the GLDAS-2 Noah

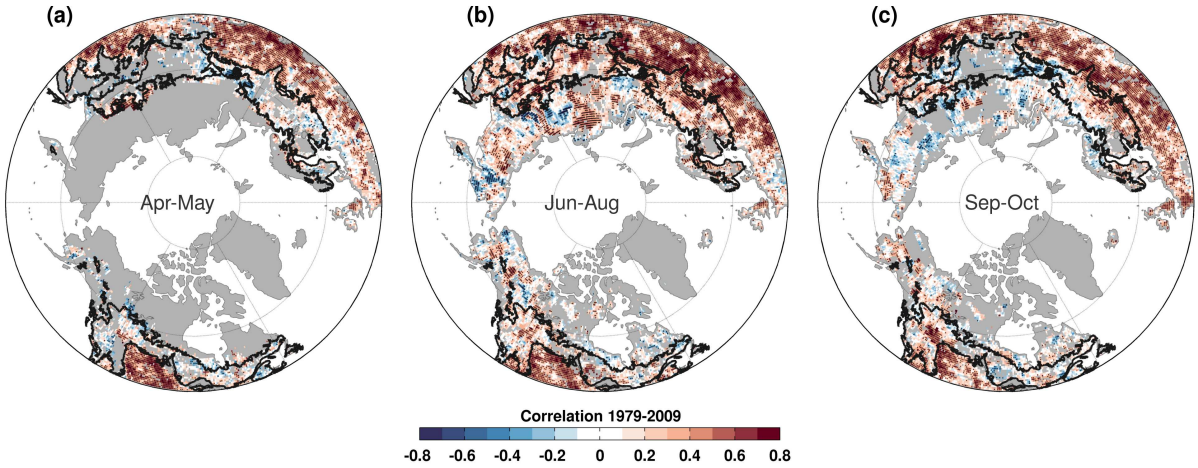

Figure 4.7: Correlation between the scPDSI and MW–SMO during (a) spring, (b) summer and (c) autumn. Correlations are shown for grid boxes with at least 15 years of MW–SMO estimates over the period 1979–2009. Areas with dense canopy, permanent ice cover, or with insufficient data for correlations are indicated by gray shading. The stippling denotes significant ($p < 0.1$) correlations.

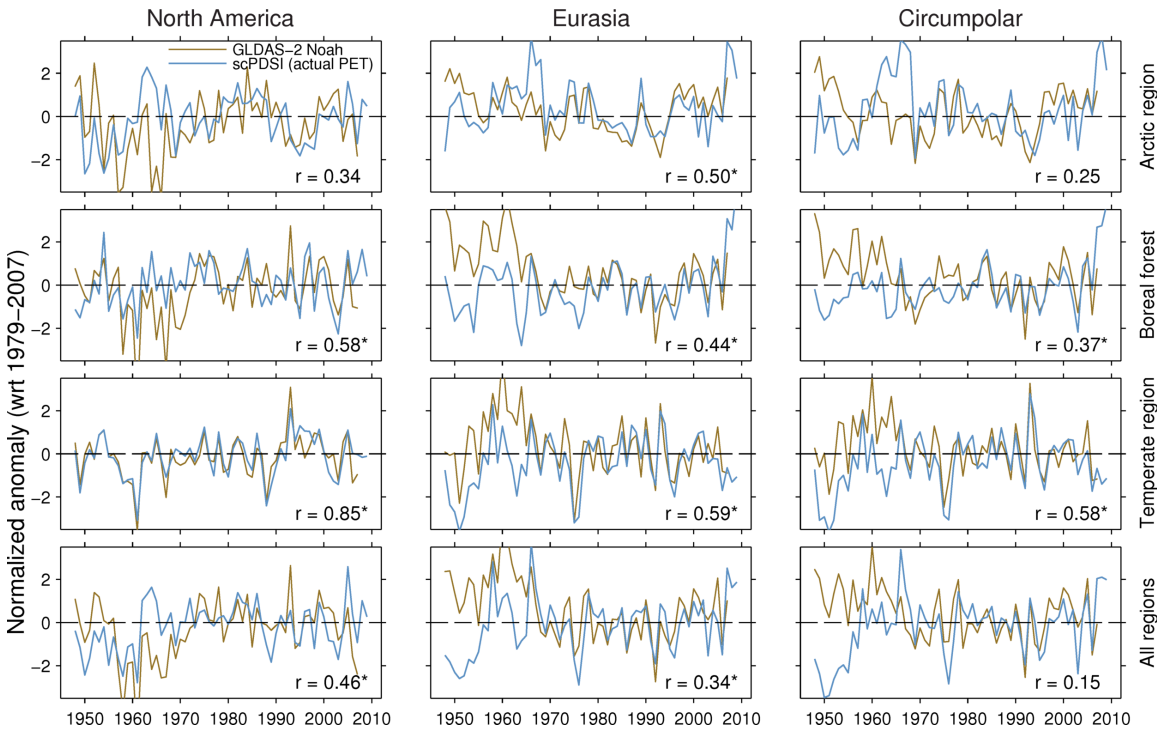

Figure 4.8: Comparison of average summer scPDSI (blue) and summer surface soil moisture (0–10 cm) simulated by GLDAS-2 Noah (brown) over the period 1948–2007 for each biogeographic region and continent. The Arctic and (northern) temperate regions correspond to the lands north and south of the boreal forests, respectively (see Figure 4.2 for a graphical reference). Correlations over the full overlapping period are indicated in each panel (*: $p < 0.1$).

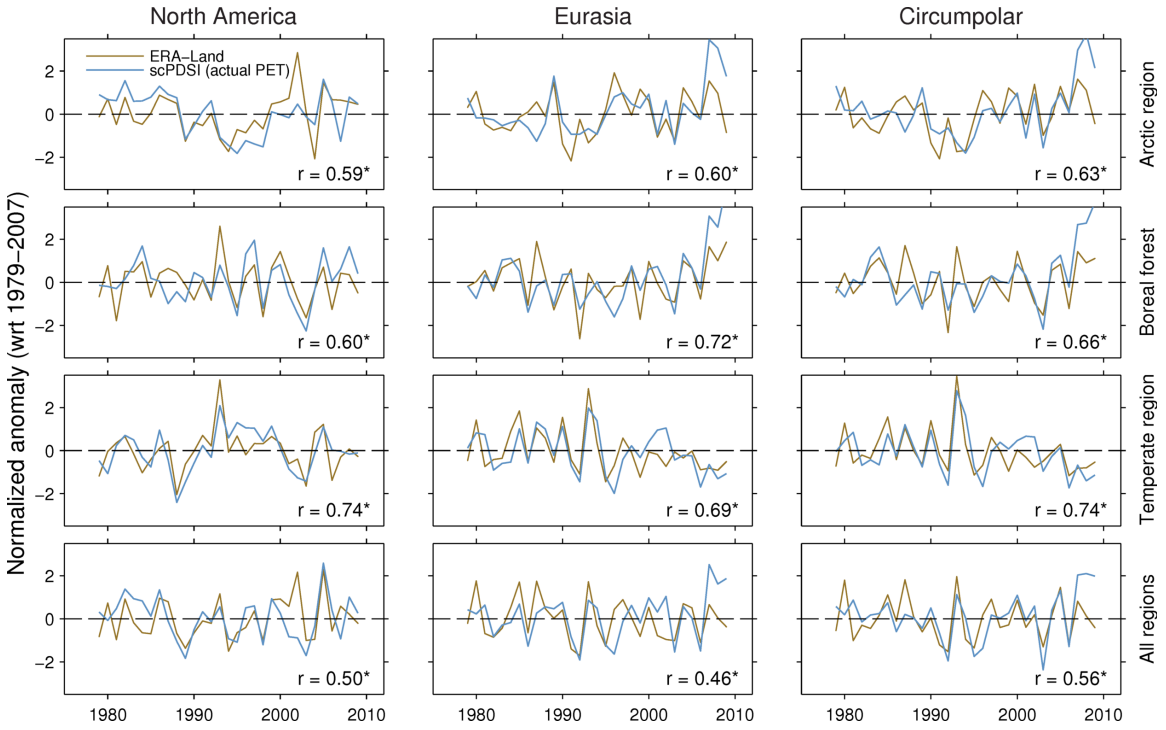

Figure 4.9: Comparison of average summer scPDSI (blue) and summer surface soil moisture (0–7 cm) simulated by ERA-Land (brown) over the period 1979–2009 for each major biogeographic region and continent. Correlations over the full period are indicated in each panel (*: $p < 0.1$).

land surface model and ERA-Land (Figures 4.8 and 4.9; for biome definitions see Section 3.2.1 on page 34). This illustrates the consistency between normalised moisture anomalies based on the scPDSI and simulations by more complex land surface models forced with different observations. The relationship between GLDAS-2 Noah and the scPDSI is generally poor in the earlier period before about 1970, but thereafter the datasets agree very well. The contrasting agreement between these two periods is consistent with larger uncertainties in the underlying meteorological forcings during the earlier period, particularly in the Princeton forcings used in GLDAS-2 Noah.

4.3.1.3 Comparison with snowpack accumulation

Similar patterns of positive correlations of winter snow accumulation with the scPDSI and soil moisture simulated by complex land surface models over extensive areas of the boreal region during the spring melting period (Figure 4.10; and also the subarctic during early-summer:

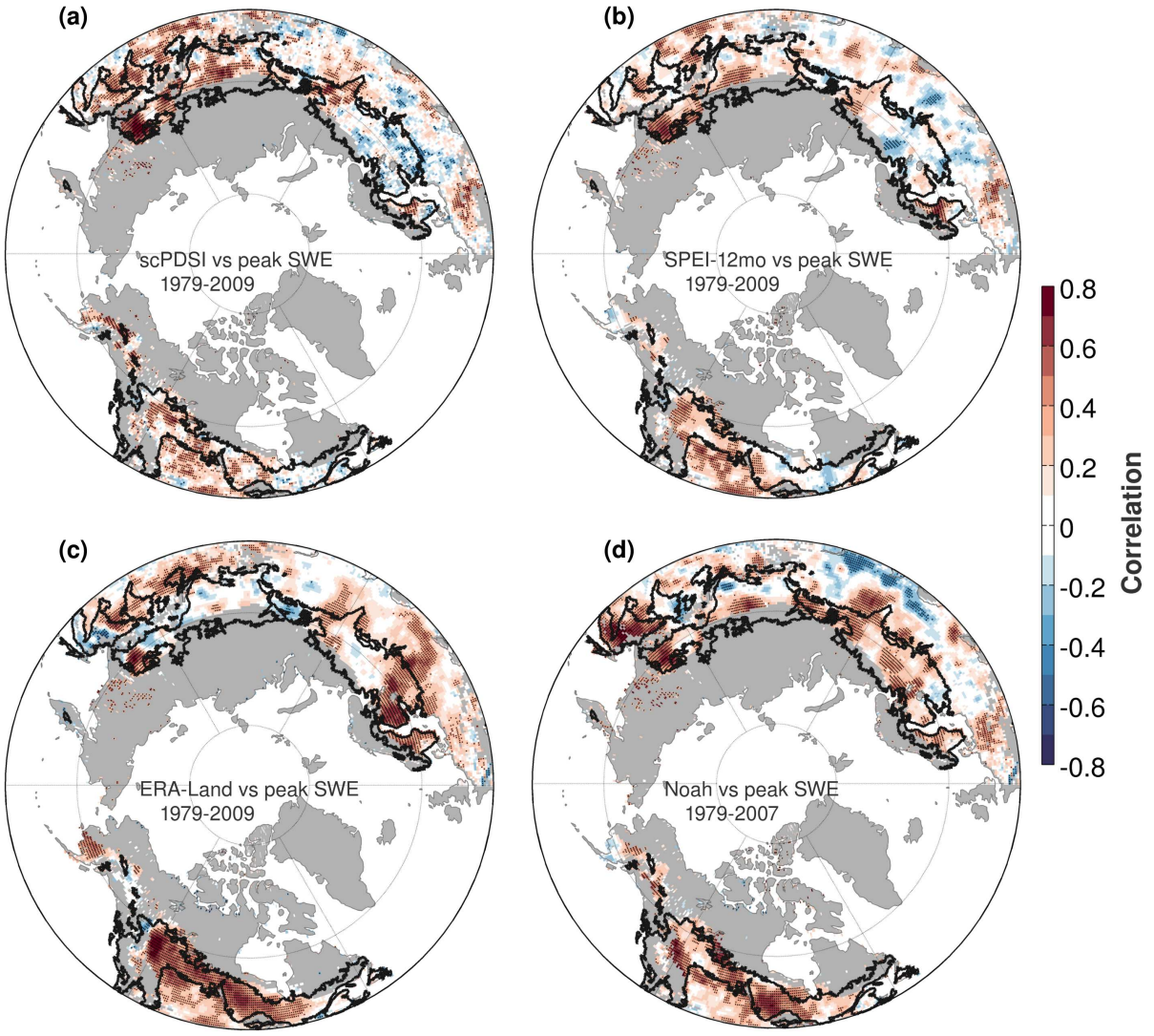

Figure 4.10: Correlations between variations in peak SWE and subsequent spring moisture anomalies produced by drought indices and land surface models. (a) scPDSI. (b) SPEI-12mo. (c) Soil moisture simulated by ERA-Land. (d) Soil moisture simulated by Noah. Correlations are shown only for non-mountainous areas without snow cover during May (SWE $<$ 10 mm).

Supplementary Figure C6) suggest that the index is able to represent soil moisture anomalies associated with snowmelt. Areas of particularly strong coupling between maximum snow accumulation and estimated moisture anomalies during the melting period occur in the western interior of Canada, Alaska, eastern Siberia and northern Scandinavia. The opposite occurs in parts of Eastern Europe, central Asia and eastern Canada.

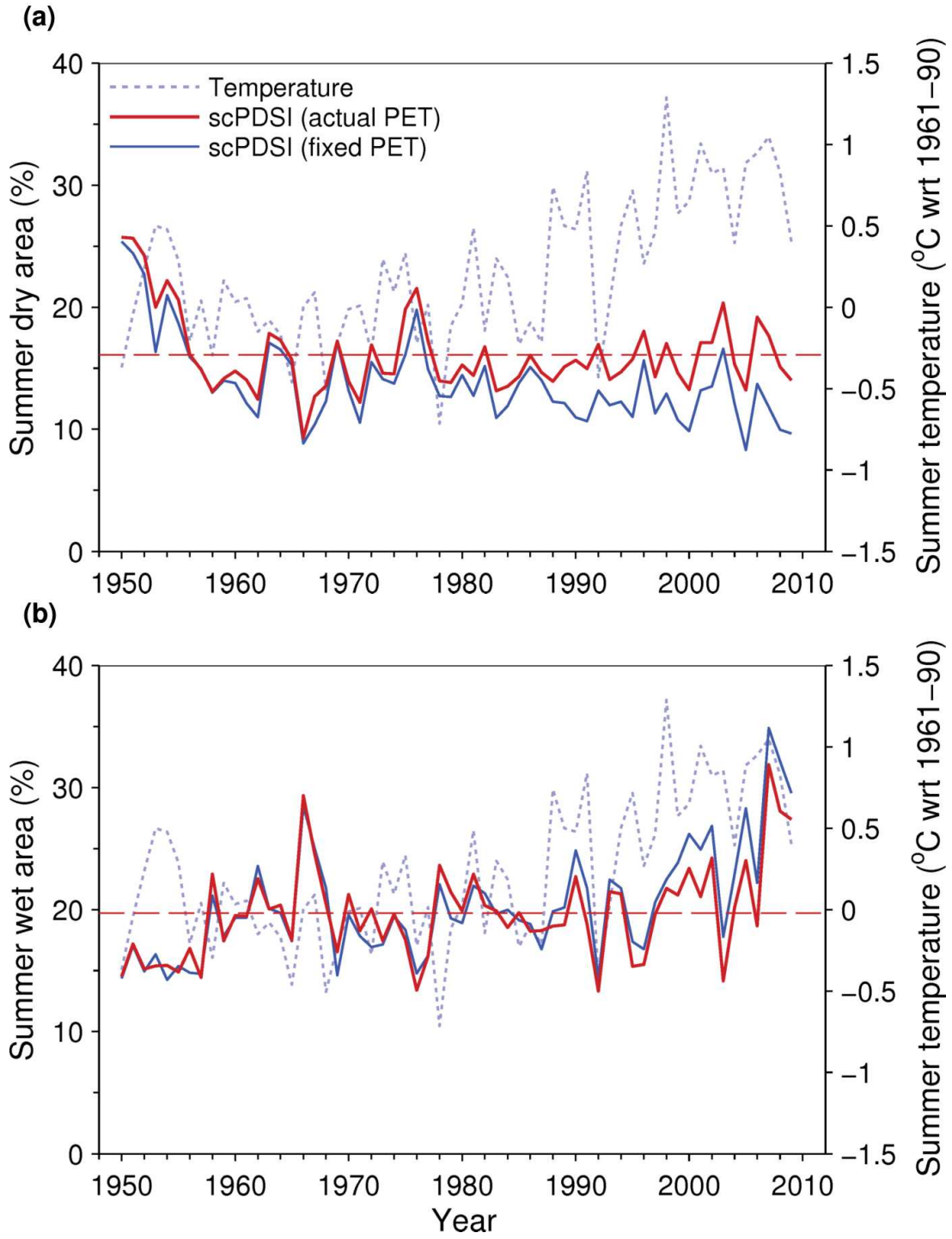

Figure 4.11: Temporal variability in percentages of summer dry and wet areas in the northern latitudes (>45°N) between 1950 and 2009 based on the scPDSI computed with (red) and without (blue) interannual changes in potential evapotranspiration (PET). (a) dry area (summer scPDSI $\leq$ -2). (b) wet area (summer scPDSI $\geq$ 2). Also shown are the mean summer temperature anomalies for the region (gray dotted line) and the long-term mean of the percentage area series based on actual PET (red dashed line).

Despite its simplicity, the SPEI-12mo shows a similar spatial pattern of correlations with snow accumulation as do the scPDSI and simulated soil moisture during the spring melting period in the boreal zone (Figure 4.10b). During early summer, when the snowpack melts in the subarctic region, the SPEI-12mo is more strongly correlated with snow accumulation than the scPDSI (Supplementary Figure C6a–b). This implies a larger impact of accumulated cold season precipitation on the SPEI anomalies compared with the scPDSI, likely because the more realistic accounting of water losses in the scPDSI soil water balance reduces the correlations with precipitation inputs.

4.3.2 Changes in drought severity

Figure 4.11a compares the yearly time series of the percentage of land area north of 45^{o}N that is dry in summer (scPDSI $\leq$ -2), based on the scPDSI with fixed and actual PET. The difference between the series reflects the influence of changing PET on summer drought severity. The series are very similar prior to the start of the surface warming trend around 1988. Both series show a strong decrease in dry area from about 25% to around 12% during the 1950s and values ranging between 9% and 22% thereafter. After 1988, the series consistently diverge along with the rapid surface warming, indicating an increasing influence of evaporative demand on summer drought severity during this period. Without the inferred increase in evaporative demand, the northern latitudes would have experienced a downward trend in drought severity. Although the general increase in PET since the 1980s has not resulted in a clear increasing trend in drought severity, it has offset the effect of the concurrent increase in precipitation at high latitudes (Supplementary Figure C7).

Greater evaporative demand since the 1980s has also consistently impacted the summer wet area (with scPDSI $\geq$ 2) in the northern latitudes (Figure 4.11b). Unlike the case for summer dry area, the effect appears to have been greater since around 1997, when summer temperatures further increased to a new level. The 2000s is the decade with the warmest and wettest summers since 1950. The wettest summer in the record is 2007, with nearly 32% of the area under moderately wet conditions when considering actual PET and about 35% when holding PET constant. This is more than 12% higher than the long-term average of summer wet area (about 20%).

The effect of recent increases in PET on the scPDSI over each biogeographic region and continent is illustrated in Figure 4.12. In general, the influence of PET on the scPDSI mirrors the magnitude of surface warming and has been larger in Eurasia than in North America. The circumpolar Arctic region (north of the boreal forests) has experienced the fastest warming rates and the greatest effect of increasing PET on summer drought severity since around 1988. Warming related increases in PET have also influenced drought severity in the boreal forests and temperate grasslands and croplands to the south, but only in Eurasia and since around 1997. In North America, these regions have experienced little or no warming, limiting the PET influence on summer drought severity in recent decades. Similar regional effects of increased evapotranspiration on drought severity occur during the autumn (Supplementary Figure C8) and the spring melting period (Supplementary C9). However, during the spring the influence of PET is not sufficiently strong as to offset the wetting trend.

A map of the difference in summer scPDSI averages over the period 2000–2009 using ac-

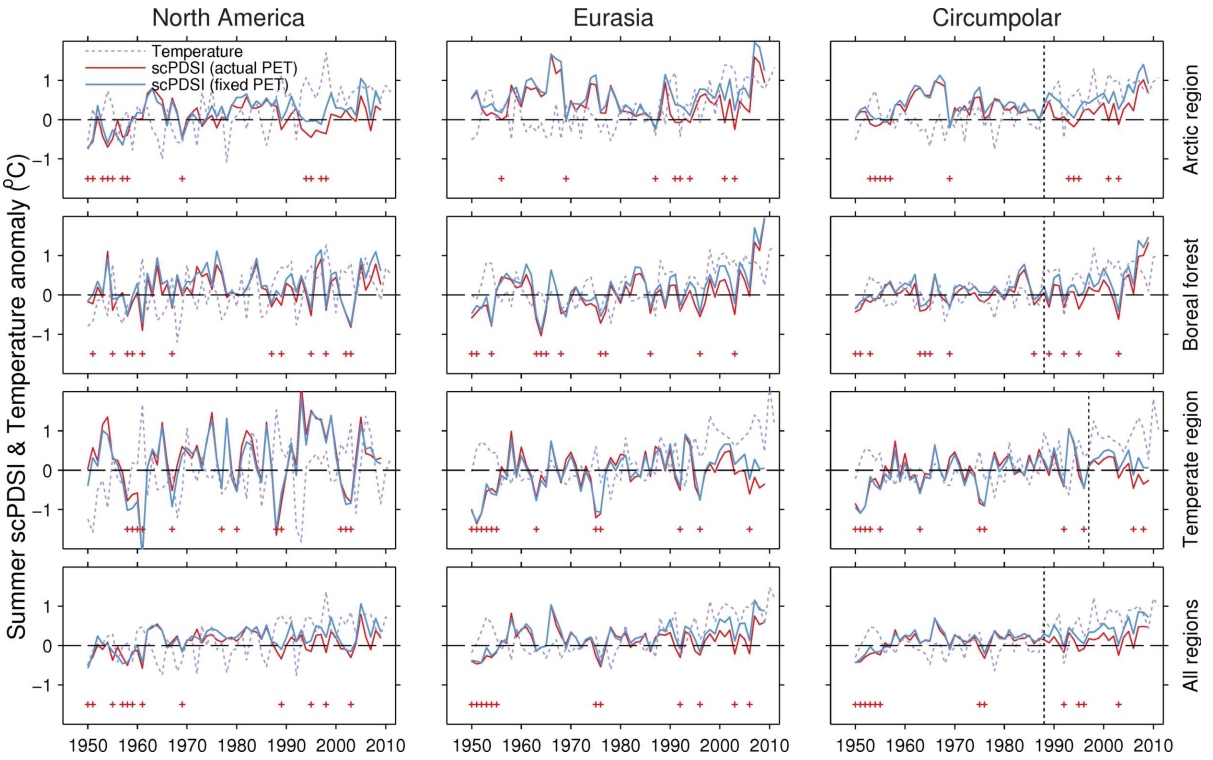

Figure 4.12: Comparison by region and continent between summer scPDSI averages with (red) and without (blue) interannual changes in potential evapotranspiration (PET). Mean summer temperature anomalies relative to the period 1961–1990 (dotted line) are shown for each biome. The red crosses in each panel indicate values of the average scPDSI series with actual PET within the bottom 20th percentile, which can be thought as regional summer droughts. Note that the severity of most of these drought events occurring during the warming period over the last two decades has been intensified by increasing evapotranspiration demand. The vertical dotted lines denote the years 1988 or 1997.

tual and fixed PET shows that the impact of increased evapotranspiration demand on summer scPDSI is widespread but its magnitude varies considerably (Figure 4.13a). A comparison of the difference between the scPDSI averages with the spatial patterns of linear trends in summer scPDSI since 1979 indicates that the recent increase in moisture demand may have intensified drying trends in northern Canada, Alaska, far east Siberia and most northern temperate Eurasia, whereas in most of Siberia it may have contributed to attenuate recent wetting trends (Figure 4.13b). Since moisture demand has not increased much in the Canadian Prairies, ongoing wetting trends centred in this region have not been attenuated.

The spatial patterns of trends in summer scPDSI are heterogeneous but still consistent with the corresponding patterns of trends in surface soil moisture simulated by ERA-Land and Noah (Figure 4.13b–d). Despite some regional differences, the three products show a very similar proportion of significant drying trends (about 9–10% of the total number of grid boxes). However, the proportion of significant wetting trends in the scPDSI (12.6%) is more consistent with Noah (15.6%) than with ERA-Land, which shows substantially less wetting (7.5%).

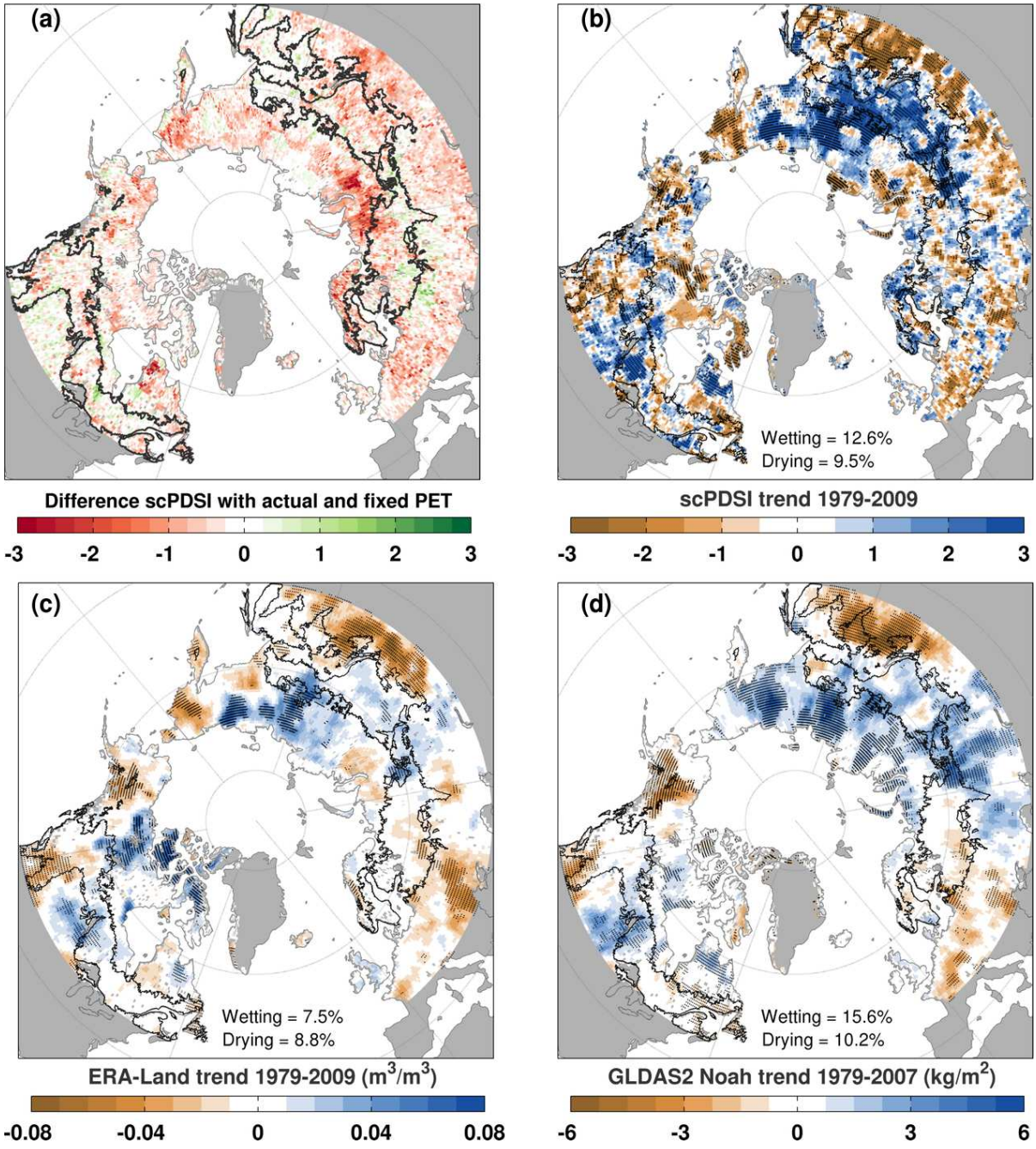

Figure 4.13: Influence of increased PET on summer scPDSI during the 2000s and moisture trends since 1979. (a) Summer scPDSI with actual PET averaged over 2000–2009 minus scPDSI with fixed PET averaged over the same period. (b) Trends in summer scPDSI during 1979–2009. (c) Trends in summer surface soil moisture (0–7 cm) simulated by ERA-Land during 1979–2009. (d) Trends in summer surface soil moisture (0–10 cm) simulated by Noah during 1979–2007. The stippling denotes significant ($p < 0.1$) trends. The percentages of grid boxes showing significant drying and wetting trends is indicated for comparison.

4.4 Discussion

Comparisons with field measurements and satellite observations suggest that the scPDSI is able to simulate moisture variability in the upper meter of the soil profile in the northern latitudes with comparable skill to offline land surface models. A similar result has been reported in earlier studies comparing the PDSI or its variants with field moisture measurements in the mid latitudes of Eurasia and North America (Dai *et al.*, 2004; Dai, 2011a). Like in these previous studies, correlations with field soil moisture measurements tend to be higher during summer and autumn than during the spring melting period (Figure 4.5). Yet, during the spring the scPDSI tends to be better correlated with field moisture measurements than moisture simulations of complex land surface models.

A definitive conclusion about the relative performance of the scPDSI and land surface models in spring can not be made based on comparisons with short and uncertain in situ soil moisture records, which tend to be strongly influenced by local conditions, snow and frozen soils (Dorigo *et al.*, 2013a). Moreover, a more extensive evaluation of the scPDSI with satellite observations during the spring is also limited by snow cover (Figure 4.7). Despite these limitations, positive associations between maximum snow accumulation and soil moisture anomalies during the melting period inferred from the scPDSI and land surface models suggest that these moisture estimates can represent well independently observed snowpack dynamics over most of the northern latitudes (Figure 4.10 and Supplementary Figure C6). Continued measurements of soil moisture in high-latitude observing networks (e.g., LTER, SNOTEL, SCAN, GTK) is required to produce high-quality records long enough for a better evaluation of soil moisture products.

The most consistent result of the evaluation presented in this study is that the scPDSI is a useful indicator of soil moisture variability in non-permafrost regions of the northern latitudes during summer and autumn, with a skill similar to complex land surface models (Figures 4.8 and 4.9). Therefore, the scPDSI can be used to make inferences about potential changes in summer drought severity. The analysis of the scPDSI dataset between 1950 and 2009 shows that increased evapotranspiration demand, driven mainly by surface warming, has significantly influenced summer drought severity in the northern latitudes since the late 1980s (Figure 4.11). The estimated enhancement of atmospheric moisture demand during this recent period has been balanced by the increase in precipitation in the northern latitudes (Supplementary Figure C7) and thus has not imposed an increasing trend in drought area (Figure 4.11a).

This finding is consistent with the ongoing intensification of the hydrological cycle observed at high latitudes characterised by increases in both precipitation and evapotranspiration (Rawlins *et al.*, 2010; Miralles *et al.*, 2013). A similar impact of surface warming on drought severity since the 1980s has been documented on a global scale by recent studies based on the scPDSI using a Penman-Monteith formulation for potential evapotranspiration, but forced with different meteorological datasets (Dai, 2011a, 2012; Sheffield *et al.*, 2012; van der Schrier *et al.*, 2013). As in these earlier scPDSI-based studies, the use of the more physically realistic Penman-Monteith, rather than the Thornthwaite, parametrisation for potential evapotranspiration improves the applicability of the index under global warming scenarios but it needs additional meteorological forcings (such as radiation, wind, humidity and vapour pressure) for which es-

timates are less reliable and have less spatial coverage than temperature. The magnitude of the influence of these uncertain forcings on soil moisture changes is likely to be underestimated in this study. In addition, the evapotranspiration estimates do not consider seasonal vegetation feedbacks and the potential influence of increasing atmospheric CO_2 on plant transpiration (Gedney *et al.*, 2006). However, a similar pattern of temperature-driven amplification of drought at northern latitudes was observed in an earlier study based on offline simulations of the terrestrial hydrological cycle using a land surface model driven by the Princeton forcing dataset between 1950 and 2000 (Sheffield & Wood, 2007).

The impact of increased evapotranspiration demand on the summer moisture balance has been stronger and more widespread in Eurasia than in North America, but the timing and magnitude were found to vary considerably within each continent following the spatiotemporal patterns of summer warming (Figure 4.12). Boreal and northern temperate North America are the only regions in the study domain where there has been no significant summer warming since the late 1980s and thus atmospheric moisture demand has not increased in recent decades (Figure 4.13a). These spatiotemporal patterns imply that the severe regional droughts observed in boreal and temperate North America during recent years (e.g., 1988, 2001–2003; Shabbar & Skinner, 2004; Bonsal & Regier, 2007; Zhang *et al.*, 2008) have been driven exclusively by precipitation deficits. In contrast, warming-driven evapotranspiration demand since the 1990s has been an additional factor driving the severity and extent of regional droughts documented in far northern North America (e.g., 1998, 2004; Hogg & Wein, 2005; Wendler *et al.*, 2011) and most of northern and inner Eurasia (e.g., 2001, 2010; Zhang *et al.*, 2008; Kogan *et al.*, 2013; Mohammat *et al.*, 2013).

Regional soil moisture variability during the spring snowmelt period, when soils are close to field capacity, appears to have also been influenced by warming and the associated increases in evapotranspiration demand (Supplementary Figure C9). However, the effect is only marginal when compared with summer (Figure 4.12) and autumn (Supplementary Figure C8) and thus moisture demand in spring has not counteracted the effect of increasing precipitation. This pattern of cold season wetting and summer drying with recent warming is consistent with some model projections of seasonal changes in soil moisture at high latitudes in response to anthropogenic warming (Sheffield & Wood, 2008), which were first made about 30 years ago (Manabe & Wetherald, 1987).

Regional trends in summer scPDSI over the past three decades are generally similar to trends in surface soil moisture simulated by land surface models, particularly GLDAS-2 Noah (Figure 4.13). Significant trends in the scPDSI and Noah soil moisture are similarly dominated by wetting trends. In contrast, ERA-Land soil moisture shows substantially less wetting. A recent study found a similar tendency for ERA-Land to show more drying trends than another modern reanalysis moisture product at the global scale (Albergel *et al.*, 2013a). This behaviour of ERA-Land was shown to be consistent with trends in satellite observed soil moisture in the temperate mid latitudes. Furthermore, in this study summer soil moisture variability simulated by ERA-Land has the strongest interannual correlations with field observations (Figure 4.5). Trenberth *et al.* (2014) found that most of the contradictory moisture trends described in earlier studies based on the PDSI were related to differences in the precipitation forcings, especially in the tropics and high northern latitudes (see Figure 4.1). This could also be the cause of the

disagreement in moisture trends found here between ERA-Land reanalysis and the estimates based on the scPDSI and Noah. Regional biases and temporal inhomogeneities in the merged gauge-satellite precipitation dataset (GPCP v2.1) underlying the ERA-Land moisture estimates are likely to occur in the northern latitudes and affect the derived long-term moisture trends. Moreover, adjustments to cold season precipitation amounts in the datasets could also contribute to these differences in trends.

The recent increase in PET appears to have intensified ongoing drying trends in northern Canada, Alaska, far east Siberia and most of the northern temperate region of Eurasia, whereas in most of Siberia it may have attenuated recent wetting trends (Figure 4.13). Ongoing trends toward thinner snowpacks and earlier snowmelt and growing seasons (Brown & Robinson, 2011; Barichivich *et al.*, 2013; Gan *et al.*, 2013) may be further enhancing summer drying in some regions by extending the period of evapotranspiration into the spring and thus accelerating seasonal soil moisture depletion (Zhang *et al.*, 2011; Buermann *et al.*, 2013). Indeed, pioneering modelling studies conducted in the 1980s using simple climate models suggested that, along with increasing evaporation demand, earlier snowmelt also contributed to projected summer drying at northern latitudes under scenarios of anthropogenic warming (Manabe & Wetherald, 1987). The snow model implemented in the formulation of the scPDSI used in this study may capture the influence of changes in snow accumulation on soil moisture dynamics more accurately than changes in the timing of the snowmelt. This is because the (monthly) resolution of the meteorological forcing data is quite coarse. However, the timing of snowmelt is closely associated with the amount of snow accumulated in the winter snowpack (Trujillo *et al.*, 2012) and thus the scPDSI estimates may still incorporate the effect of the widespread reduction in spring snow cover observed at northern latitudes (Brown & Robinson, 2011).

In permafrost soils, the simple scPDSI model provides only a limited indication of potential changes in regional soil water balance. Permafrost dynamics exert a strong control on the local water balance of the seasonally active soil layer. The active layer stores water surplus from late summer and autumn rainfalls during freezing and then gradually releases it over the course of the following warm season as the thawing depth increases (Ohta *et al.*, 2008). This interannual moisture transfer combined with water supply from the deeper thawing layer can sustain summer evapotranspiration and vegetation growth during periods of meteorological drought (Sugimoto *et al.*, 2002; Ohta *et al.*, 2008). In some cases, late summer droughts can be carried to the next spring if snowmelt does not replenish soil moisture (Forkel *et al.*, 2012). Permafrost water seems to be less important during rainy summers, when evapotranspiration is maintained mainly by rain water (Sugimoto *et al.*, 2002). Long-term changes in permafrost and active layer depth with ongoing warming can decrease or increase soil moisture availability depending on complex interactions between topography, permafrost characteristics, vegetation and snow cover (Jorgenson *et al.*, 2010; Park *et al.*, 2013). None of these these seasonal and long-term changes in permafrost dynamics are included in the water balance of the scPDSI and thus our moisture estimates in permafrost soils of the Arctic region might differ substantially from actual moisture anomalies.

The inferred enhancement of atmospheric moisture demand during recent decades might have impacted ecosystems processes in the northern latitudes. Changes such as the widespread disappearance of shallow Arctic ponds (Smol & Douglas, 2007) and the intensification of fire

regimes in the boreal zone (Kasischke & Turetsky, 2006; Forkel *et al.*, 2012) are consistent with greater evaporative demand.

4.5 Conclusions

The main conclusions of this Chapter are summarised as follows:

- The scPDSI dataset described in this study is a useful indicator of summer and autumn soil moisture variability in the top meter of the soil profile in the permafrost-free northern latitudes, with a skill similar to complex land surface models. However, it is necessary to bear in mind that historical changes in soil moisture simulated by this simple index neglect the important influence of seasonal and long-term changes in vegetation dynamics and the effect of increasing atmospheric CO_2 concentrations on plant transpiration.

- Limitations and uncertainties in the in situ and satellite observations of soil moisture during the spring preclude a robust evaluation of the skill of the scPDSI and the land surface models in simulating snow hydrology at high northern latitudes. However, the good agreement found between variations in maximum snow accumulation and the scPDSI and simulated moisture anomalies during the melting period provides evidence for a realistic estimation of snow dynamics.

- The scPDSI suggests that large-scale warming since the late 1980s has increased evapotranspiration demand and consequently summer and autumn drought severity in the northern latitudes, offsetting the effect of increasing cold-season precipitation. This result is consistent with ongoing amplification of the hydrological cycle and with model projections of summer drying at northern latitudes in response to anthropogenic warming.

- The estimated warming-driven increase in moisture demand has attenuated recent wetting trends and intensified episodic droughts and regional drying trends, as indicated by the scPDSI, in Eurasia and far northern North America. Enhanced drought severity in regions such as Alaska, northern Canada and central Asia is consistent with observed increases in fire activity, vegetation productivity losses and drying of shallow ponds during the late 1990s and 2000s. However, changes in winter snowpack accumulation and shifts to earlier spring snowmelt with recent warming might have had a stronger impact on drought severity in these snow-dominated regions than increased moisture demand.

The links between warming and changes in snowpack, drought severity and vegetation productivity across the northern latitudes is investigated in the next Chapter.

Chapter 5

Temperature and snow-mediated moisture controls of summer vegetation greenness in northern terrestrial ecosystems since 1982

Abstract

Rapid warming of boreal and Arctic regions since the late 1980s has stimulated the productivity of northern vegetation by reducing temperature limitations. However, warming has also increased evapotranspiration demand and consequently summer drought severity, but the impacts of these changes on northern vegetation are still uncertain. This chapter investigates the influence of summer warming and changes in snow and soil moisture availability on peak summer vegetation greenness at northern latitudes (>45^{o}N) based on satellite observations of the Normalized Difference Vegetation Index (NDVI) since 1982. Both moisture and temperature appear to exert control on the interannual variability of summer NDVI over about 29% (mean $r^2 = 0.29 \pm 0.16$) and 43% (mean $r^2 = 0.25 \pm 0.12$) of the northern vegetated land, respectively. For the remaining 28% of the vegetated land neither temperature nor moisture variability appear to influence NDVI anomalies significantly, yet most of this fraction of the vegetated land shows greening trends similar to those in temperature-limited regions. The environmental factors driving summer NDVI variability in these regions remain to be identified. Changes in snow dynamics (accumulation and melting) appear to be more important than increased evaporative demand in controlling changes in summer soil moisture availability and NDVI across extensive regions of the boreal zone, where vegetation growth is often assumed to be dominantly temperature-limited. In particular, NDVI declines in the boreal forest of North America are more consistent with reduced snowpack than with temperature-induced increases in evaporative demand as previously thought. Any further increase in evapotranspiration demand and reduction in snowpack accumulation with continued warming during the coming decades is likely to intensify summer drought severity and the emerging regional contrasts in summer NDVI trends.

Published as: Barichivich, J., K. R. Briffa, R. Myneni, G. van der Schrier, W. Dorigo, J. Tucker, T. J. Osborn and T. Melvin (2014), Temperature and snow-mediated moisture controls of summer vegetation photosynthetic activity in northern terrestrial ecosystems between 1982 and 2011, *Remote Sens.*, 6(2), 1390–1431.

5.1 Introduction

Vegetation gradients and productivity patterns across Arctic and boreal terrestrial ecosystems are interactively controlled by temperature, soil moisture, light and nutrient availability during the growing season (Jarvis & Linder, 2000; Roy *et al.*, 2001; Nemani *et al.*, 2003). Temperature is the main climate constraint on plant growth in the cooler northern regions, whilst soil moisture becomes more important toward the forest-grassland ecotone in the southern boreal region (Nemani *et al.*, 2003, see Figure 5.1). The rapid warming during recent decades has significantly ameliorated the limitations on plant production by frozen ground and low temperatures (Nemani *et al.*, 2003; Zhang *et al.*, 2008). This has resulted in widespread lengthening of the growing season, greater photosynthetic activity and enhanced ecosystem carbon sequestration across the northern latitudes (Myneni *et al.*, 1997; Keeling *et al.*, 1996; Nemani *et al.*, 2003; Piao *et al.*, 2007; Barichivich *et al.*, 2013). However, longer and warmer growing seasons have also promoted environmental conditions that favour surface drying (Zhang *et al.*, 2011; Dai, 2012). This is thought to have intensified summer droughts and forest disturbance by fire and insects (Zhang *et al.*, 2008; Mann *et al.*, 2012)

The analysis of the global satellite record of Normalized Difference Vegetation Index (NDVI) imagery since 1981 (e.g., Tucker *et al.*, 2005) has shown that increases in vegetation photosynthetic activity have been stronger in Eurasia than in North America and more sustained in the colder tundra biome than over the boreal forests (Goetz *et al.*, 2005; Bunn & Goetz, 2006; Piao *et al.*, 2011; Beck *et al.*, 2011; Xu *et al.*, 2013). The most recent studies have found that after the initial increasing trend in NDVI (i.e., greening) observed in the first decade of the record (Myneni *et al.*, 1997; Zhou *et al.*, 2001), longer and hotter growing seasons appear to have resulted in reductions of summer NDVI (i.e., browning) in the drier and more continental regions of the boreal forest since the 1990s (Angert *et al.*, 2005; Goetz *et al.*, 2005; Bunn & Goetz, 2006; Piao *et al.*, 2011). The most extensive vegetation browning has occurred in the North American boreal forests in Canada and Alaska (Beck & Goetz, 2011). Most of these regional reductions of summer NDVI have been attributed to increasing drought stress with hotter summers, an extended period of evaporation and enhanced atmospheric evapotranspiration demand asso-

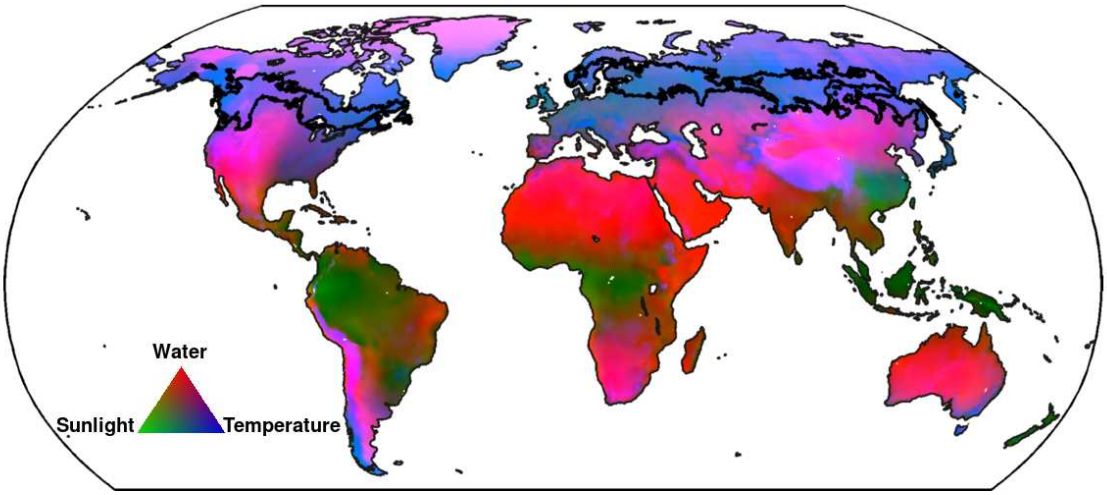

Figure 5.1: Map of relative climatic constraints on modelled vegetation net primary productivity (Nemani *et al.*, 2003). The black polygons represent the extent of the boreal forests as defined in this study (see Methods).

ciated with rising temperatures (Angert *et al.*, 2005; Goetz *et al.*, 2005; Bunn & Goetz, 2006; Beck & Goetz, 2011). This effect is commonly referred to as 'temperature-induced drought stress' (Barber *et al.*, 2000; Bunn & Goetz, 2006). Modelling studies that partially rely on remote sensing vegetation observations also show an increase in moisture limitation of vegetation growth in several regions of the boreal forest since the late 1990s, potentially offsetting the benefits of longer and warmer growing seasons (Zhang *et al.*, 2008).

Beyond the satellite period, tree ring studies have shown that the growth of boreal trees in some cool and relatively moist northern locations has not continued to track rising temperature trends since around the 1960s, whereas they had previously shown positive responses to summer warming, such as in the early part of the century (e.g., Jacoby & D'Arrigo, 1995; Briffa *et al.*, 1998; Jacoby *et al.*, 2000; Wilmking *et al.*, 2004; Lloyd & Fastie, 2002; Lloyd & Bunn, 2007; Pisaric *et al.*, 2007; Porter & Pisaric, 2011). This recent temporal change in the apparent positive response of tree growth to warming is known in the tree-ring community as the 'divergence' phenomenon (D'Arrigo *et al.*, 2008). A number of causal factors have been proposed and are still being debated though one suggestion is that the recent warming has invoked increasing drought stress (D'Arrigo *et al.*, 2008). A consistent long-term control of boreal forest growth by summer moisture availability has been observed in the drier continental interiors of Alaska and northwestern Canada where increased tree growth is stimulated by cooler and wetter growing seasons (e.g., Szeicz & MacDonald, 1996; Barber *et al.*, 2000; Wilmking & Juday, 2005; McGuire *et al.*, 2010; Juday & Alix, 2012; Lloyd *et al.*, 2013). Hence, warming in these boreal regions has often been associated with tree growth declines rather than with increases (Barber *et al.*, 2000). These growth declines are in some cases consistent with co-located NDVI browning trends (Beck *et al.*, 2011).

Landscape browning and declining tree-growth trends in the boreal zone have highlighted the potential role of summer drought in modulating regional responses of northern vegetation as climate warms. Yet, the emphasis of previous studies has been primarily on summer processes. The potential influence of changes in winter snowpack on summer soil moisture status and vegetation productivity has not received much attention, despite the well-known controls of snow dynamics on the hydrology and phenology of northern ecosystems (Vaganov *et al.*, 1999; Jarvis & Linder, 2000; Barnett *et al.*, 2005). Local studies have shown that reductions in winter snowpack and earlier spring snowmelt can lead to strong summer soil moisture deficits and productivity losses in boreal and alpine regions (Welp *et al.*, 2007; Hu *et al.*, 2010; Trujillo *et al.*, 2012), where snow is typically the main source of soil water recharge. A positive association has also been observed between deeper snowpack and summer NDVI in parts of North America and central Siberia (Grippa *et al.*, 2005; Buermann *et al.*, 2013), though it has also been suggested that deeper snowpacks can delay the start of the growing season and thus negatively affect tree growth (Vaganov *et al.*, 1999). Thus, recent declines in winter snowpack and snow cover duration documented in several regions of northern Eurasia and North America (Brown & Robinson, 2011; Park *et al.*, 2012; Gan *et al.*, 2013) are likely to have affected vegetation.

The lack of long-term soil moisture observations and uncertainties in model-based soil moisture estimates have hampered assessments of the links between trends in vegetation productivity and changes in soil moisture availability in the northern latitudes. Local and regional responses of boreal vegetation to moisture variability have typically been inferred indirectly from correla-

tions with soil moisture forcings, such as precipitation and temperature (e.g., Barber *et al.*, 2000; Wilmking *et al.*, 2004; Lloyd & Bunn, 2007). In other cases, comparisons have been made with simple meteorological drought indices that often neglect soil properties, snow dynamics and vegetation (e.g., Angert *et al.*, 2005; Lotsch *et al.*, 2005; Hogg *et al.*, 2008; Buermann *et al.*, 2013; Vicente-Serrano *et al.*, 2013).

The historical paucity of observational datasets of soil moisture dynamics has been notably improved by the recent release of a multi-satellite product of surface soil moisture with global coverage for the period 1979–2010 (Liu *et al.*, 2012) and an improved high-resolution global dataset of the self-calibrating Palmer Drought Severity Index (scPDSI) based on historical monthly meteorological observations since 1901 (van der Schrier *et al.*, 2013). Progress has also been made in producing improved estimates of seasonal snow mass dynamics by assimilating ground-based measurements with historical satellite observations within a consistent modelling framework (Takala *et al.*, 2011). Moreover, the reprocessing of the NDVI observations from Advanced Very High Resolution Radiometer (AVHRR) satellite sensors by the Global Inventory Modeling and Mapping Studies (GIMMS) group at NASA Goddard Space Flight Center has resulted in a 30-year NDVI product with improved data quality at northern latitudes (Pinzon & Tucker, 2013). These new datasets now enable a more direct and up-to-date assessment of the multi-decadal links between warming, snow, soil moisture variability and vegetation dynamics in the northern latitudes than was previously possible.

In this study, these newly released datasets are used to evaluate the influence of temperature, snowpack and soil moisture availability on peak summer NDVI in northern terrestrial ecosystems between 1982 and 2011. This empirical study is intended to provide a better understanding of the environmental drivers of interannual and longer term changes in vegetation productivity at northern latitudes.

5.2 Data and methods

5.2.1 Northern biomes

The study domain was divided into three major biogeographic regions: northern temperate, boreal and Arctic. The regions were defined from the Collection 5 MODIS International Geosphere-Biosphere Programme (IGBP) land cover classification map (Friedl *et al.*, 2010) and woody fraction from the MODIS Vegetation Continuous Fields product (Townshend, 2011). The first region includes the northern temperate grasslands, croplands and a small fraction of temperate forests. The second considers only the boreal forest, and the third includes the Arctic tundra and subarctic woodlands.

The boreal forest region was defined as all evergreen needleleaf, deciduous needleleaf and mixed forests north of 45^{o}N with woody fraction greater than 30% (Xu *et al.*, 2013). Natural grasslands, crops and relatively small areas of temperate forests north of 45^{o}N and south of the boreal forests were considered as the northern temperate grassland and cropland region. Open woodlands (forests with woody fraction less than 30%), open/closed shrublands and grasslands north of the boreal forests were combined into a large mixed region, here termed the Arctic region, since the NDVI signal in these land cover classes is dominated by shrubby and herbaceous vegetation. These major regions delineate circumpolar bands of relatively similar vegetation types and climate conditions (Supplementary Figure D1).

5.2.2 Vegetation greenness

The NDVI is a normalised spectral measure of vegetation canopy greenness (Tucker, 1979). It is based on the difference between radiation reflected in the near infra-red range (NIR; AVHRR Channel 1, 0.73–1.1 μm) and radiation absorbed by green leaves in the visible range (VIS; AVHRR Channel 2, 0.55–0.68 μm). Given NIR and VIS reflectances the index is defined as: $NDVI = (NIR - VIS)/(NIR + VIS)$. This simple ratio should be understood as a spectral measure of the photosynthetic potential of vegetation (Myneni *et al.*, 1995).

The GIMMS group at NASA Goddard Space Flight Center has produced a new version of their biweekly 8 km NDVI dataset from historical AVHRR level 1b observations covering the period from July 1981 to December 2011 (Pinzon & Tucker, 2013). This third generation dataset is termed GIMMS NDVI3g and supersedes the previous GIMMS NDVIg dataset, which had a calibration-related lack of data north of 72^{o}N (Tucker *et al.*, 2005). NDVI3g has an improved coastal land-water mask and better cross-sensor intercalibration, particularly of data from NOAA-16, -17, and -18 satellites that have bilinear gains in the channel one of their AVHRR instruments. The new calibration procedure has also rectified a previous data discontinuity at 72^{o}N. These and other methodological refinements have considerably improved data quality in the northern latitudes. The improvements are evident in higher correlation and closer correspondence of the NDVI3g data with NDVI data from Moderate Resolution Imaging Spectroradiometer (MODIS) Aqua and Terra sensors since the early 2000s (Fensholt & Proud, 2012; Barichivich *et al.*, 2013; Pinzon & Tucker, 2013).

Here, the NDVI3g dataset was used to characterise interannual variations in summer vegetation greenness across the region north of 45^{o}N between 1982 and 2011 (Table 5.1). The biweekly

NDVI data for each year and grid box were seasonally averaged over the summer months from June to August, when the peak in growing season photosynthetic activity occurs. Then, the summer NDVI data were regridded to a common 0.5^ox0.5^o regular grid using bilinear interpolation. This enables direct, grid-wise comparisons with temperature and moisture fields (Table 5.1).

NDVI data based on the 16-day Aqua MODIS MYD13C1 product (available at https://lpdaac.usgs.gov/products/modis) were used for independent validation of the peak growing season vegetation signals contained in the NDVI3g dataset during the overlapping period 2002–2011. The 16-day NDVI composites were averaged for summer months and regridded from their native 0.05^o resolution to 0.5^o. MODIS NDVI data are of higher radiometric and geometric quality than AVHRR data and have been atmospherically corrected and masked for water, clouds and shadows. Aqua MODIS NDVI was chosen instead of Terra NDVI because the latter product is affected by sensor degradation, which has imposed spurious negative trends in the dataset (Wang *et al.*, 2012a).

5.2.3 Influence of snow, moisture and temperature variability on summer NDVI

Temperature and moisture controls of interannual variability in summer vegetation greenness since 1982 were identified using correlation and stepwise multiple linear regression analyses involving summer NDVI and spring and summer averages of temperature and moisture variables at a 0.5^o grid box scale. The use of separate spring and summer averages shows the differences between antecedent and concurrent climate controls on summer NDVI. In order to examine the relationships on an interannual time scale, all time series at each grid box were linearly detrended prior to correlation and regression analysis. The statistical significance of correlations was estimated using a non-parametric random phase test with 1000 Monte-Carlo simulations (Ebisuzaki, 1997), which is robust to autocorrelation in the series. A 90% confidence level was used to report the statistical significance of the correlations. Also, only temperature and moisture predictors significant at the 90% confidence level were retained in the stepwise regression models.

Table 5.1 provides a summary of the datasets used for analysis. Mean air temperature data for the period 1982–2011 were obtained from the gridded CRUTS 3.20 dataset at a spatial resolution of 0.5^o (Harris *et al.*, 2014). Spring water supply to the soils was estimated using maximum

Table 5.1: Characteristics of the datasets used in this study.

Dataset	Resolution	Time span	Reference
Vegetation			
GIMMS NDVI3g	0.08^ox0.08^o, 15–day	1982–2011	Pinzon & Tucker (2013)
Aqua MODIS NDVI (MYD13C2)	0.05^ox0.05^o, 16–day	2002–2011	Huete *et al.* (2002)
Temperature			
CRUTS 3.20 mean air temperature	0.5^ox0.5^o, monthly	1901–2011	Harris *et al.* (2014)
Precipitation			
GPCC precipitation version 6	0.5^ox0.5^o, monthly	1901–2010	Schneider *et al.* (2013)
Globsnow SWE version 1.3	25x25 km, monthly	1980–2011	Takala *et al.* (2011)
Soil moisture			
Satellite microwave soil moisture (MW–SMO)	0.25^ox0.25^o, daily	1979–2010	Liu *et al.* (2012)
self-calibrating PDSI (scPDSI)	0.5^ox0.5^o, monthly	1901–2009	van der Schrier *et al.* (2013)
GLDAS–2 NOAH 10-cm soil moisture	1^ox1^o, monthly	1948–2007	Rui (2011)

monthly winter Snow Water Equivalent (SWE) during the period 1982–2011, computed from monthly gridded SWE data from the European Space Agency (ESA) GlobSnow dataset version 1.3 (Takala *et al.*, 2011). GlobSnow combines SWE retrieved from multi-satellite microwave observations with forward snow emission model simulations and ground-based weather station data for non-mountainous regions of the Northern Hemisphere. Because of the improved accuracy obtained by assimilating independent sources of information, this is arguably the best SWE product currently available for climate analysis (Hancock *et al.*, 2013). The SWE data were remapped from their original 25-km spatial resolution to a coarser 0.5^o grid using bilinear interpolation. Summer precipitation data during the period 1982–2010 were obtained from the gauge-based Global Precipitation Climatology Center (GPCC) dataset at a spatial resolution of 0.5^o (Schneider *et al.*, 2013).

Spring and summer averages of the enhanced snow-enabled CRU–scPDSI dataset (van der Schrier *et al.*, 2013) described in Chapter 4 were used to characterise soil moisture variability between 1982 and 2009. In addition, satellite microwave soil moisture observations (MW–SMO) from a newly developed global dataset (Liu *et al.*, 2012, available at: http://www.esa-soilmoisture-cci.org/) were also used to estimate summer surface soil moisture variability during the period 1982–2010. This soil moisture dataset is based on the statistical blending of daily passive (SMMR: November 1978-August 1987; SSM/I: July 1987-2007; TMI: 1998-2008 and AMSR-E: July 2002-2010) and active (ERS-1/2: July 1991-May 2006 and ASCAT: 2007-2010) satellite microwave observations between November 1978 and December 2010 on a 0.25^ox0.25^o regular grid. The scaling and merging is based on a reference surface soil moisture climatology provided by the GLDAS-Noah land surface model. This approach imposes the absolute values of GLDAS-Noah on the resulting product, but preserves the long-term moisture signals sensed by the satellites and minimises temporal inhomogeneities due to changing sensors (Liu *et al.*, 2012; Dorigo *et al.*, 2012). Although satellite sensors only measure moisture in the uppermost few centimetres of the soil profile, these observations generally correlate well with moisture variations measured at deeper layers (Albergel *et al.*, 2008). Soil moisture retrievals fail over very dense canopy and frozen ground while surface water and rough topography distort soil moisture signals and result in poor data quality. Product quality flags were used to filter daily observations for most of these surface conditions. Only grid boxes with at least 20 years of data over the period 1982–2010 were used for analysis.

Since earlier studies have reported apparent changes in the climate drivers of NDVI with recent climatic warming (Angert *et al.*, 2005; Zhang *et al.*, 2008), the association between interannual summer NDVI variability and each temperature and moisture variable at each grid box was empirically tested for temporal changes using a statistical approach based on time-varying regression with the Kalman Filter (Visser & Molenaar, 1988). This method allows for the estimation of simple linear regression models with time-varying coefficients that adapt to the changing relationship between the predictor (moisture or temperature) and the predictand (NDVI). A maximum likelihood estimation procedure is used to obtain the regression coefficients and associated standard errors to assess their significance over time. In order to restrict the analysis to interannual time scales, where the climate control on vegetation growth anomalies is stronger, all the variables were filtered with a 10-year high-pass filter prior to analysis.

After characterising the temperature and moisture controls of summer greenness on interan-

nual time scales, the consistency between temporal trends in summer NDVI and temperature and moisture controls was evaluated. In this context, warming trends are expected to correspond well with greening trends in temperature-limited regions whilst drying trends should correspond with browning trends in moisture-limited regions. Trend analysis was carried out using the non-parametric Mann-Kendall trend test implemented in the *zyp* package (Bronaugh, 2009) in R statistics. Maximum Covariance Analysis (MCA) (Bretherton *et al.*, 1992), also known as Singular Value Decomposition, was employed to describe the dominant patterns of coupled variability between climate constraints and summer NDVI. This is a statistical tool widely used in climate research to identify pairs of coupled modes in spatiotemporal geophysical fields (Wilks, 2011). MCA is good at separating dominant common signals from noise, and in this application it filters out the influence of fire and other local-scale disturbances on NDVI variability.

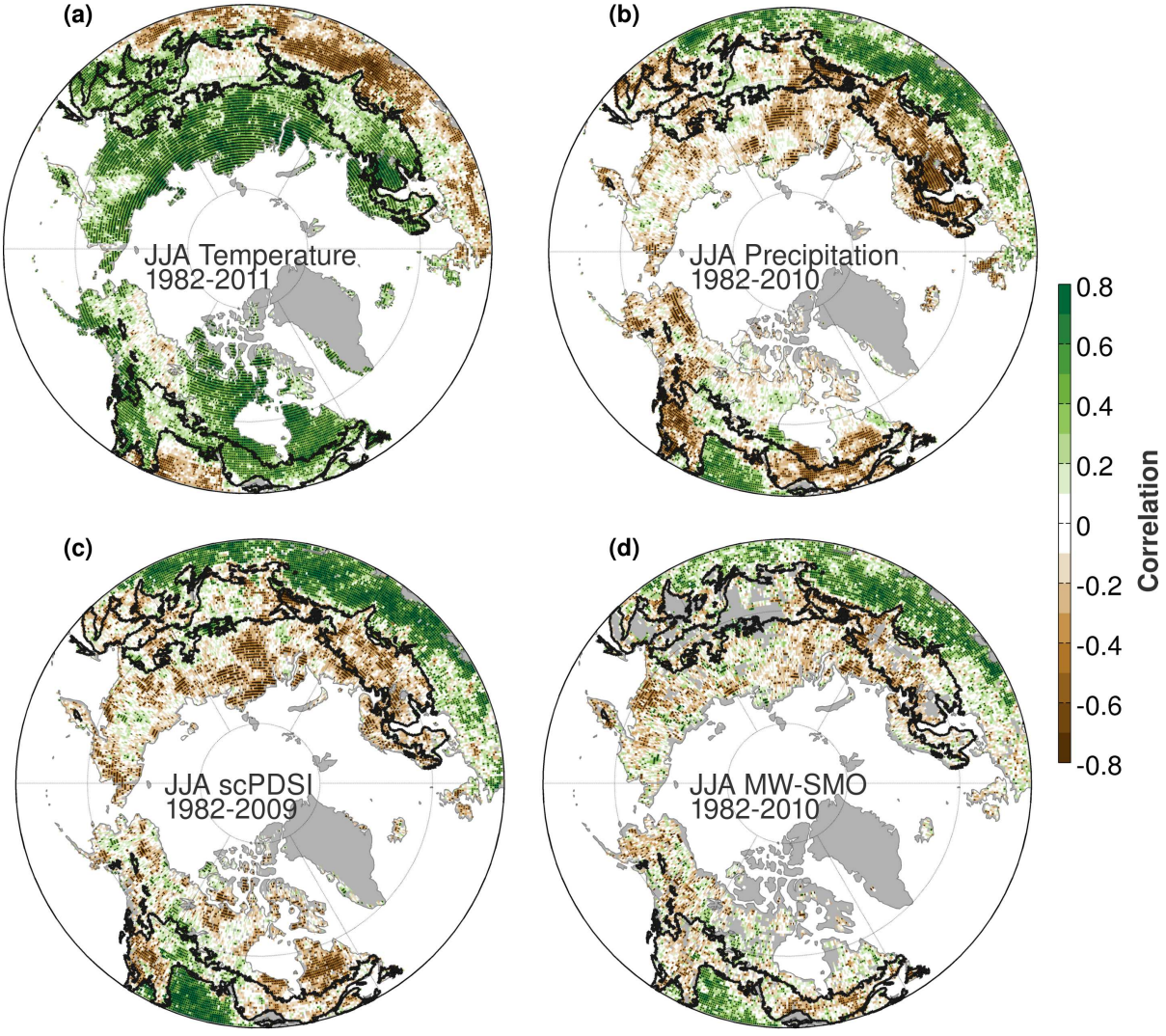

Figure 5.2: Correlation maps between summer NDVI and (a) summer temperature, (b) summer precipitation, (c) summer scPDSI, and (d) summer satellite microwave surface soil moisture (MW-SMO) variability since 1982. All correlations are based on linearly detrended data and the stippling indicates statistically significant ($p < 0.1$) values.

5.3 Results

5.3.1 Moisture and temperature controls on interannual summer NDVI variability

5.3.1.1 Correlations

Summer NDVI3g during the period 2003–2011 is consistent with Aqua-MODIS NDVI over most of the northern terrestrial ecosystems (Supplementary Figure D2). The agreement between the NDVI products is particularly strong in North America, with significant ($p < 0.1$) correlation values ranging from 0.80 in the boreal forests to 0.85 in the Arctic region and 0.94 in the temperate grasslands and croplands. The lowest agreement occurs over the vast Eurasian grasslands and croplands ($r = 0.38$, $p > 0.1$), but the products agree better in the boreal forests ($r = 0.63$, $p > 0.1$) and in the Arctic region of Eurasia ($r = 0.80$, $p < 0.1$). This demonstrates that both datasets capture similar vegetation signals at high latitudes.

It is expected that interannual variability in summer NDVI is associated with moisture variability in the northern temperate grasslands and croplands and with temperature variability in the cooler regions dominated by boreal forests and Arctic vegetation. This expectation is broadly consistent with the biome-scale spatial patterns of correlation between interannual anomalies of summer NDVI and concurrent variability in summer temperature, precipitation and available soil moisture shown in Figure 5.2. Summer NDVI across most of the Arctic and boreal regions is strongly positively correlated with summer temperature (Figure 5.2a), but it is generally negatively correlated with summer precipitation and soil moisture anomalies as indicated by the scPDSI and satellite-sensed MW-SMO (Figure 5.2b–d). This negative correlation of temperature-driven summer NDVI with summer precipitation and soil moisture anomalies largely reflects a strong negative association between summer temperature and precipitation in these regions (Supplementary Figure D3a). However, it might also indicate a degree of co-limitation by low radiation levels during rainy and cloudy summers. The opposite correlation patterns occur in the northern temperate grasslands and croplands, where summer NDVI is negatively correlated with temperature and strongly positively correlated with precipitation and soil moisture anomalies during summer. Overall, these broad-scale summer correlation patterns suggest a dominant temperature control on peak vegetation greenness in the boreal and Arctic regions and a moisture control in the temperate grasslands and to a lesser extent in croplands.

There are, however, large areas within the cool boreal and Arctic regions where correlation patterns suggest that moisture rather than temperature is the main control of summer NDVI anomalies, especially when considering the influence of snow water supply (Figures 5.2 and 5.3). This moisture control is apparent across most of the rainshadow area of the North American Cordillera along the western interior of Canada from the Prairies in the south to interior Alaska and the Arctic coast in the north, the basin of the Kolyma River in far-east Siberia and in some isolated areas north of Lake Baikal in south-central Siberia. Summer NDVI in these regions is not significantly correlated with temperature variability during summer (Figure 5.2a) or spring (Figure 5.3a), but it is generally significantly and positively correlated with summer precipitation, scPDSI and MW-SMO (Figure 5.2b–d). The influence of moisture on summer greenness in these cool regions is more spatially extensive when considering the effect of snow.

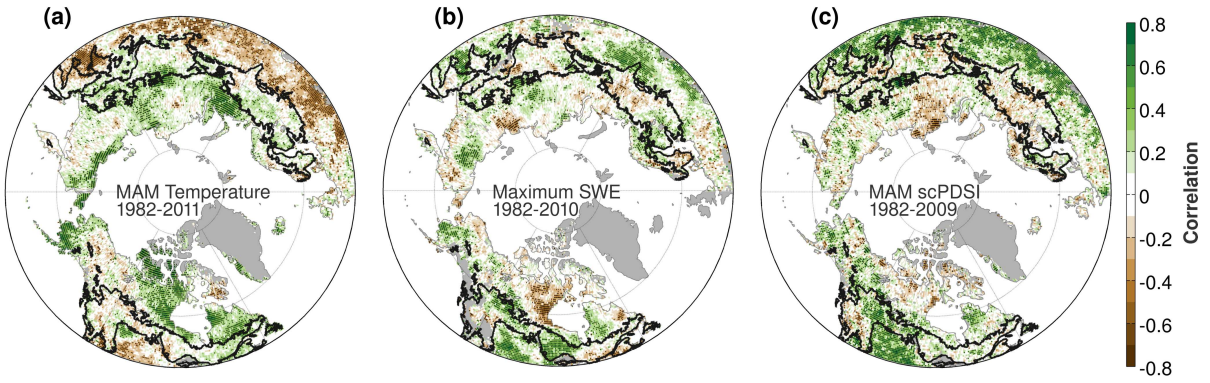

Figure 5.3: Correlation maps between summer NDVI and (a) spring (March–May) air temperature, (b) maximum winter Snow Water Equivalent (SWE), and (c) spring scPDSI variability since 1982. All correlations are based on linearly detrended data and the stippling indicates statistically significant ($p < 0.1$) values.

Maximum winter SWE and spring scPDSI are both strongly correlated with summer NDVI in the sense that deeper winter snowpacks and hence wetter spring soils enhance summer NDVI (Figure 5.3b–c). Therefore, the water supplied by the melting of the winter snowpack in spring appears to play the dominant role in modulating subsequent summer greenness of northern vegetation in these relatively cold but moisture-limited regions. Only few temperature-limited regions show negative associations between summer NDVI and maximum SWE, highlighting the beneficial effect of snow accumulation on peak summer vegetation growth.

Snow water supply and associated spring soil moisture anomalies (scPDSI) also significantly influence summer greenness in some typically moisture-limited regions, such as the Canadian Prairies and the vast steppes of central Asia (Figure 5.3b–c). Moreover, spring temperatures in these more southern regions are negatively correlated with summer NDVI (Figure 5.3a), implying that earlier and warmer springs favour surface drying and hence can reduce summer greenness when summer rainfall does not replenish moisture losses.

A more synthetic depiction of the geography of moisture and temperature limitations on peak summer greenness can be obtained by superposing the patterns of correlation of summer NDVI with summer temperature and scPDSI averaged over the spring-summer period from March to August. A bivariate map showing these associations together with their statistical significance and a detailed land cover classification map are illustrated in Figure 5.4. The composite map reveals a consistent pattern of long-term climate controls on peak summer greenness across northern biomes but it highlights important regional variations in the type and magnitude of climate limitation. The forest/grassland ecotone in central Asia and Canada marks a sharp transition between temperature limitation (i.e., strong and positive correlations with temperature and weak correlations with scPDSI) in the boreal forests and Arctic shrublands and tundra towards the north and moisture limitation (i.e., positive and strong correlations with scPDSI and negative correlations with temperature) in the temperate grasslands and croplands to the south (Figure 5.4a).

The composite map also highlights the extensive area of the boreal and Arctic regions with significant moisture sensitivity along the drier western interior of North America. Vegetation in this region varies from dense evergreen needleleaf forests in the central boreal region to sparsely forested woody savanna and open shublands toward the north (Figure 5.4b). Other

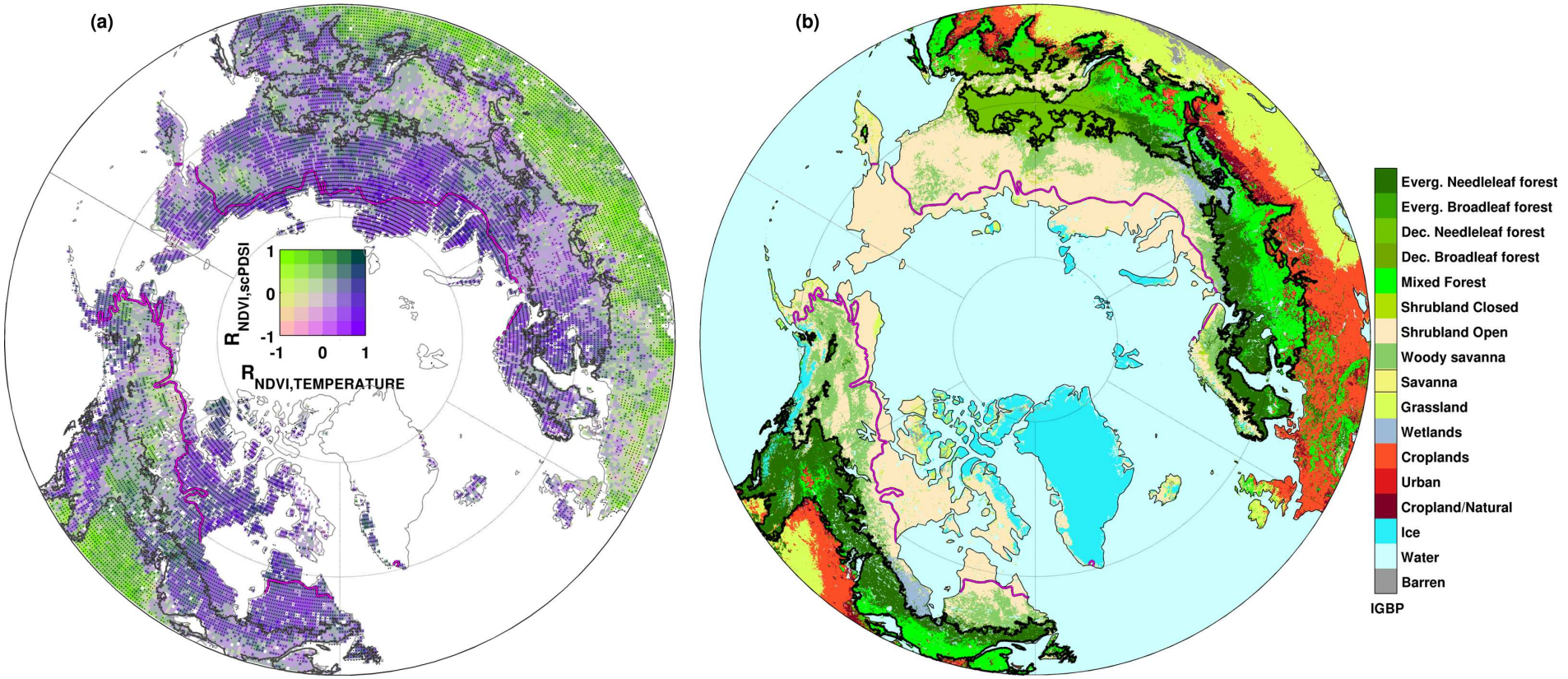

Figure 5.4: Geography of moisture and temperature controls on summer NDVI at northern latitudes during the past 30 years and relationship with major land cover types. (a) Bivariate correlation map between detrended summer (June–August) NDVI and detrended variations in spring-summer (March–August) scPDSI and summer temperature during the period 1982–2009. Light greens indicate a strong moisture limitation (i.e., strong positive correlation with precipitation and negative correlation with temperature), whilst purple shades indicate a dominant temperature limitation (i.e., strong positive correlation with temperature and weak correlation with precipitation). The stippling indicates grid boxes where either correlations with temperature or scPDSI are statistically significant ($p < 0.1$). (b) International Geosphere-Biosphere Programme (IGBP) land cover classification for the study domain. The black polygons in the maps denote the extent of the boreal forests as defined in this study. Also shown is the present position of the latitudinal treeline (purple line).

more localised high-latitude areas of moisture sensitivity, in sparsely forested areas near the treeline in the basin of the Kolyma River and in deciduous needleleaf forests north of Lake Baikal, are also evident. However, the magnitude of moisture limitation in all of these northern regions is typically smaller and less spatially coherent than that in the adjacent regions where growth is limited by temperature. There are also extensive parts of the mixed and evergreen needleleaf boreal forests in central Eurasia where neither temperature nor soil moisture appear to limit peak forest greenness significantly during the seasonal windows considered here. The same is true for the shrublands north of the treeline in the far east of Eurasia and northern Alaska, and most of the European croplands and mixed forests in eastern North America. It is interesting to note that a similar pattern of regional and broad-scale climate limitation of summer greenness is obtained from correlations computed over the past decade (instead of the entire period) and from Aqua-MODIS NDVI data between 2003 and 2009 (Supplementary Figure D4).

It is also noteworthy that summer scPDSI and MW-SMO are both similarly correlated with summer NDVI (Figure 5.2c–d), with a common spatial pattern that strongly resembles the pattern of correlations observed between NDVI and summer precipitation (Figure 5.2b). This high commonality between correlations with MW-SMO and scPDSI is linked to the common summer precipitation signal in these products. Summer MW-SMO variability is similarly correlated with summer precipitation and scPDSI anomalies, but the agreement is stronger in the northern temperate region than in the boreal and Arctic regions (Supplementary Figures D3b,d). Likewise, the influence of snowmelt water on spring scPDSI leads to similar correlation patterns between summer NDVI and maximum SWE and spring scPDSI over most of the snow-dominated regions (Figure 5.3b–c). The only exceptions are in western Russia and Scandinavia, where maximum SWE tends to be negatively correlated with spring scPDSI (Supplementary Figure D3c).

The correlation between vegetation and climate anomalies for a given region and year since 1982 can be also examined by comparing the annual maps of anomalies of summer NDVI, summer temperature, summer precipitation, summer MW-SMO, maximum annual SWE and spring-summer scPDSI presented in the Supplementary Figures D5–D10. An example is the Russian heat wave during the summer of 2010. In this extreme event, anomalously hot summer conditions ($>3^{o}$C above the mean for the period 1982–2010; Supplementary Figure D6) centred in western Russia were associated with a summer precipitation deficit of about 60% (Supplementary Figure D10) and a reduction in surface soil moisture of at least 30% (Supplementary Figure D8). The intense heat and drought led to an extensive browning of the water-limited grasslands and croplands across the region (Supplementary Figure D5).

5.3.1.2 Stepwise regression

The correlations show how changes in summer precipitation or summer soil moisture alone are not sufficient to fully capture the moisture signal in summer vegetation greenness in the boreal and Arctic regions. Snowmelt water and the associated spring soil moisture anomalies must also be taken into account. Stepwise multiple linear regression shows that the combined influence of either spring and summer water supply or soil moisture accounts for up to 20–30% of the total interannual variance in summer NDVI in the moisture-sensitive areas of the boreal forest and Arctic regions (Figure 5.5a–b). This amount of variance is small compared with the predominant influence of spring and summer temperature, which typically explains between 30%

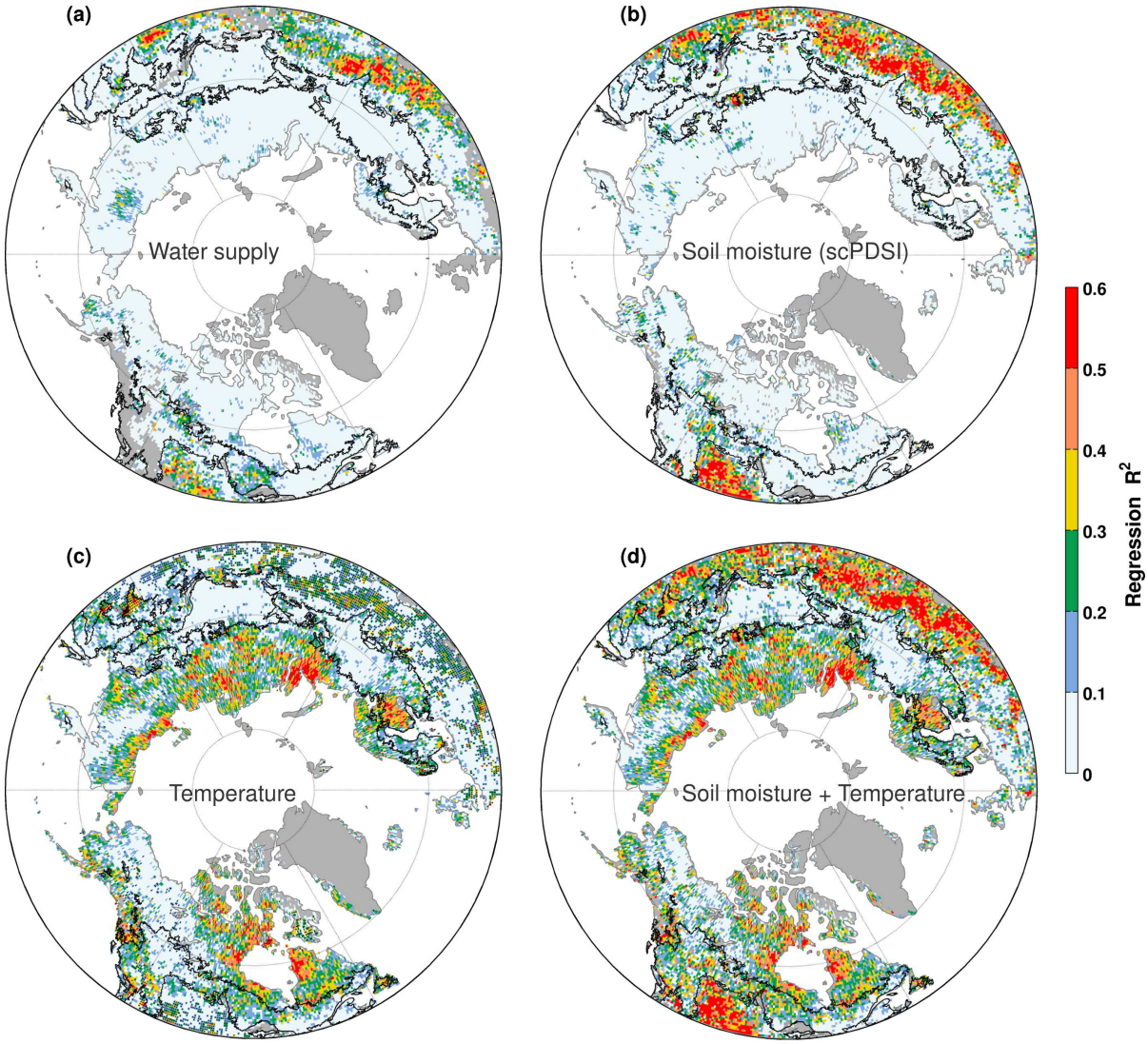

Figure 5.5: Fraction of interannual summer NDVI variance explained by spring (March-May) and summer water supply, soil moisture and temperature during the period 1982–2009. The maps show the R^2 for a stepwise multiple linear regression model predicting summer NDVI at each grid box based on: (a) water supply (x_1=peak SWE, x_2=summer precipitation), (b) soil moisture (x_1=spring scPDSI, x_2=summer scPDSI), (c) temperature (x_1=spring temperature, x_2=summer temperature), and (d) soil moisture and temperature (x_1=spring scPDSI, x_2=summer scPDSI, x_3=spring temperature, x_4=summer temperature). All the variables were linearly detrended prior to analysis and only predictors significant at the 90% confidence level were retained in the regression models. Only positive associations between summer NDVI and variables representing water supply and soil moisture were considered. The stippling in (c) indicates grid boxes where NDVI is inversely associated with temperature. Gray shading denotes non-vegetated areas or areas where climate data were not available.

and more than 50% of the total variance in summer NDVI in the coldest parts of these northern biomes, such as north-eastern Canada, Siberia and Scandinavia (Figure 5.5c). The largest area of the circumpolar boreal forests that exhibits a consistent moisture limitation occurs in the dense needleleaf forests of the continental interior of North America. As noted earlier, this region displays practically no temperature signal and extends northwards into the Arctic region through the rainshadow area of the North American Cordillera as far north as the interior of Alaska (Figure 5.5b–c).

In moisture limited regions where grasses are the dominant vegetation type, such as the steppes of central Asia and the Canadian prairies, precipitation and soil moisture typically

account for more than 50% of the interannual variance in NDVI (Figure 5.5a–b), though the influence of soil moisture is consistently stronger and more spatially extensive than that of precipitation. Locally negative associations between temperature and NDVI in these water-limited regions can account for up to about 30% of the total NDVI variance, indicating a moderate surface drying effect of spring and summer temperatures (Figure 5.5c).

The total amount of summer NDVI variance explained by the combined influence of temperature and moisture controls in spring and summer varies strongly along the major climate gradients and vegetation types (Figure 5.5d). However, this generally reflects the influence of a single limiting factor rather than a combination of both, since areas with strong moisture and temperature limitation rarely overlap. Individually, moisture and temperature significantly limit summer NDVI in about 29% (mean $r^2 = 0.29 \pm 0.16$) and 43% (mean $r^2 = 0.25 \pm 0.12$) of the northern vegetated land, respectively. In the remaining 28% of the vegetated land neither temperature nor moisture appear to influence greenness variability significantly. This is true for parts of the boreal forests in central Eurasia, shrublands north of the treeline in the far east of Eurasia and northern Alaska, and most of the European croplands and mixed forests in eastern North America.

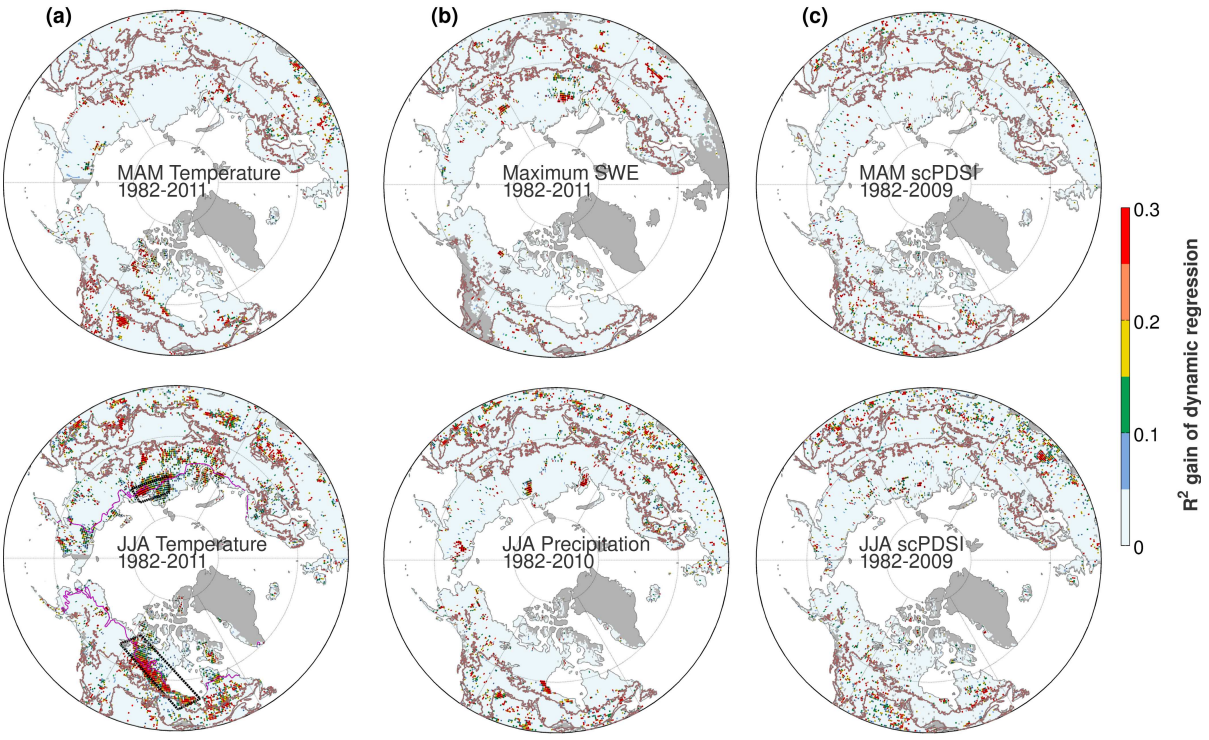

Figure 5.6: Maps of additional variance (R^2) explained by the univariate dynamic Kalman filter regression model between NDVI and potential climate drivers compared with a standard least squares linear regression model. R^2 gain for summer NDVI regressed onto: (a) spring and summer temperature, (b) spring and summer water supply, and (c) spring and summer soil moisture (scPDSI). A 10-year high-pass filter was applied to the data prior to analysis. R^2 values are shown for grid points where the dynamic regression model was selected over the standard fixed model based on the minimum Akaike Information Criteria (AIC). The rectangles show regions for which time-dependent associations are illustrated in Figure 5.7.

5.3.1.3 Kalman filter regression

The dynamic regression analysis with the Kalman filter shows little temporal dependence in the associations between interannual summer NDVI anomalies and spring and summer water supply, soil moisture and temperature variability across the study domain (Figure 5.6). There are no regions showing simultaneous time-dependent associations of NDVI with moisture and temperature that could indicate temporal shifts from temperature to moisture limitation. Time-dependent associations tend to occur in scattered grid boxes and in some small isolated regions, where local changes in NDVI linked to disturbances and land use change are more likely to produce temporal changes in the empirical associations. However, the analysis highlights some extensive temperature-limited regions in northern Canada and Siberia where the association between summer NDVI and summer temperature has changed substantially during the period 1982–2011 (Figure 5.6a). A visual comparison of NDVI and temperature series averaged over each of these regions shows that in the region located in northern Canada there was no significant association between summer NDVI and summer temperature during the 1980s, but thereafter the association became increasingly stronger and significant, particularly since the late 1990s (Figure 5.7a). The opposite occurs in the Siberian region, where summer NDVI was significantly associated with summer temperatures during the 1980s and 1990s, but the association became insignificant during the 2000s (Figure 5.7b).

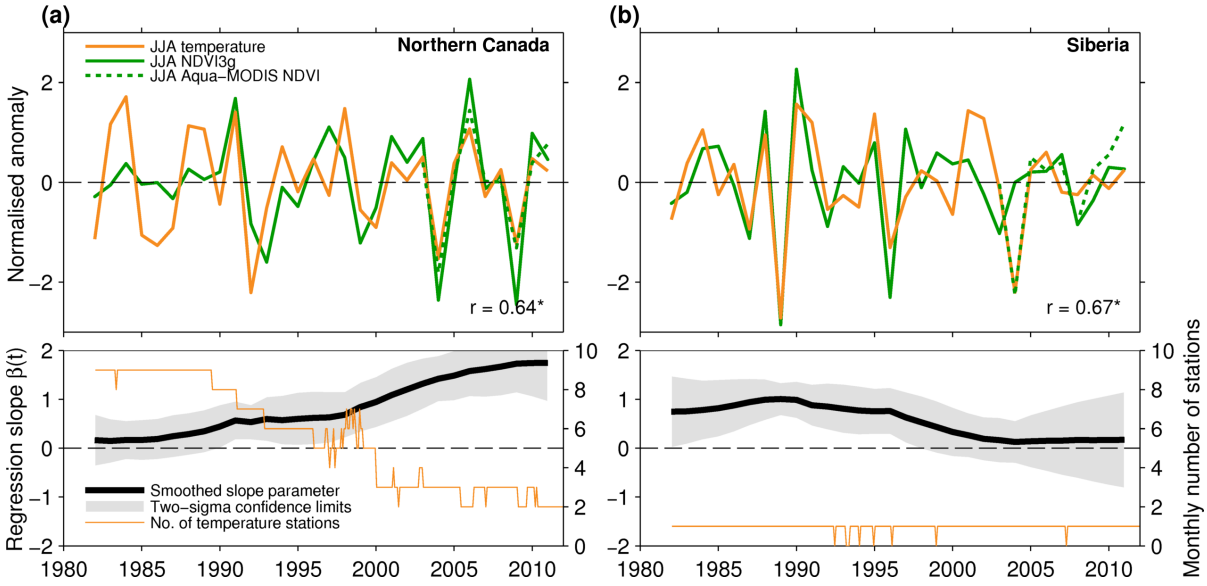

Figure 5.7: Illustration of the time-dependent association between interannual variability in summer NDVI and summer temperature in the regions indicated by the rectangles in Figure 5.6a. (a), Comparison of spatially averaged time series for the region in northern Canada (top) and the corresponding Kalman filter regression coefficients and pointwise confidence intervals over the period 1982–2011 (bottom). Where any of the confidence limits includes zero, the regression weights are not considered statistically significant at that point in time. The monthly number of station temperature records in the region included in the CRU TS 3.20 dataset is also shown (bottom). The Aqua-MODIS NDVI average for the same region is shown as a dotted line for comparison. The overall correlation between NDVI3g and temperature is displayed along with its significance (*: $p < 0.05$). (b) Same as in (a) but for a region in Siberia.

These regional-scale changes in empirical associations may be related to temporal changes in data quality in these remote regions rather than to real shifts in the temperature response of vegetation, but the exact causes are difficult to ascertain. The gridded temperature data

comprise very few station records in these regions and might contain large uncertainties, particularly during the past decade (Figure 5.7a–b). Changes in satellite sensors and data processing could also potentially affect the variability in NDVI3g and its association with temperature. In Siberia, Aqua-MODIS NDVI agrees better than NDVI3g with temperature anomalies during the 2000s (Figure 5.7b), suggesting that the apparent loss of temperature response in NDVI3g data over this region reflects a change in data quality rather than a real change in vegetation response.

5.3.2 Trends in NDVI and climate constraints

Significant spring and summer warming since the 1980s has alleviated cold constraints for temperature-limited vegetation, resulting in widespread summer greening trends over most of the circumpolar Arctic region and some parts of the Eurasian boreal forests in Scandinavia and eastern Siberia (Figure 5.8a,c). However, there are also strong greening trends in regions where climate has not warmed or interannual summer NDVI anomalies are not associated with temperature or moisture variability, suggesting a spatially consistent influence of some non-climatic factors on summer vegetation trends. Again, this includes the extensive areas of the Eurasian boreal forests and shrublands in most of northern Alaska and parts of north-western Canada where interannual climate variability does not appear to control summer NDVI anomalies (Figure 5.5d). The region experiencing strong greening in northern Alaska appears to be closely associated with continuous permafrost conditions (Figure 5.8c). Thus, extensive changes in permafrost dynamics that favour shrub growth could be driving this regional greening.

Strong drying and warming over most of the moisture-limited Eurasian steppes has not been associated with significant changes in summer greenness and only localised browning trends have occurred in the Mongolian steppes south of Lake Baikal (Figure 5.8c). Unlike the grasslands, most of the European and Canadian croplands have greened. This is generally consistent with coincident positive spring and summer moisture trends, although management practices might also play a strong role.

Most of the North American evergreen needleleaf boreal forests and adjacent open woodlands covering most of the discontinuous permafrost region up to the latitudinal treeline have experienced widespread browning trends whilst Arctic vegetation underlain by continuous permafrost has greened (Figure 5.8c). NDVI declines are widespread but spatially heterogeneous and occur in both temperature- and moisture-limited regions. Areas showing significant temperature or moisture trends are also scattered in space and are difficult to compare with NDVI trends, but most of the regions north of the boreal forest have warmed and drying trends are more common in the western half of the continent (Figure 5.8a–b). The only consistent environmental change across most of the northern part of the continent is a widespread decline in winter SWE (Figure 5.8b). Since interannual variability in winter snowpack is significantly associated with summer NDVI anomalies in large areas of the North American boreal forests (Figures 5.3b and 5.5a), declining snowpack is likely to be influencing the observed pattern in summer NDVI trends.

In order to quantitatively isolate any pattern of common temporal variability in winter snowpack and subsequent summer greenness in North America, Maximum Covariance Analysis (MCA) was applied to the NDVI and maximum SWE fields over the period 1982–2011. MCA identifies a coupled pattern of declining winter snowpack and summer NDVI since around 1991/2

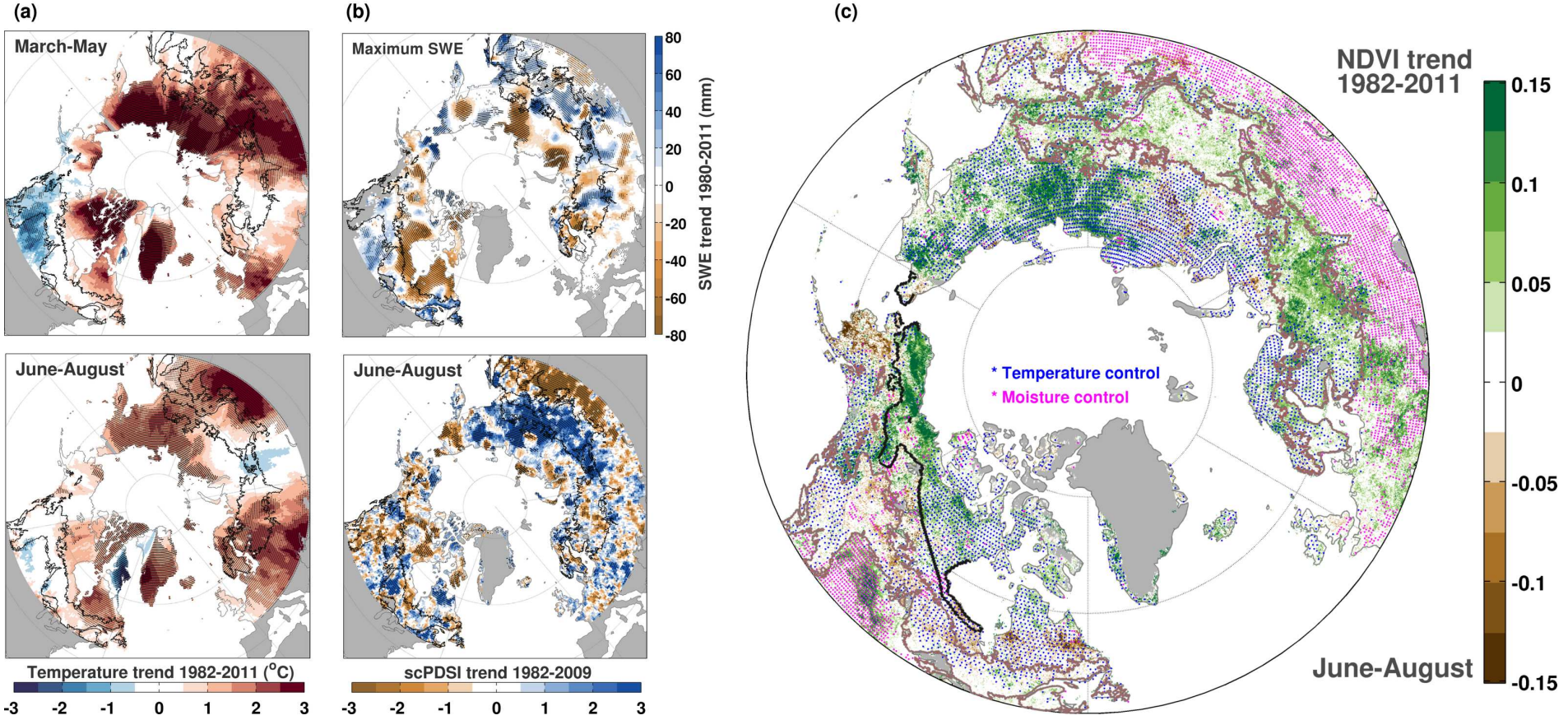

Figure 5.8: Linear trends in summer NDVI and dominant climate drivers since 1982. (a) Trends in spring and summer temperature between 1982 and 2011. (b) Trends in maximum SWE and summer scPDSI over the periods 1982–2011 and 1982–2009, respectively. (c) Statistically significant ($p < 0.1$) trends in summer NDVI between 1982 and 2011. Non significant trends are masked out as white. The coloured pattern indicates regions where spring-summer moisture (purple) and temperature (blue) variability significantly influence interannual summer NDVI anomalies as shown in Figure 5.5b–c. The black thick line in North America denotes the southern edge of the continuous permafrost region (Brown *et al.*, 1998). The stippling in (b) and (c) indicates statistically significant trends at the 90% confidence level.

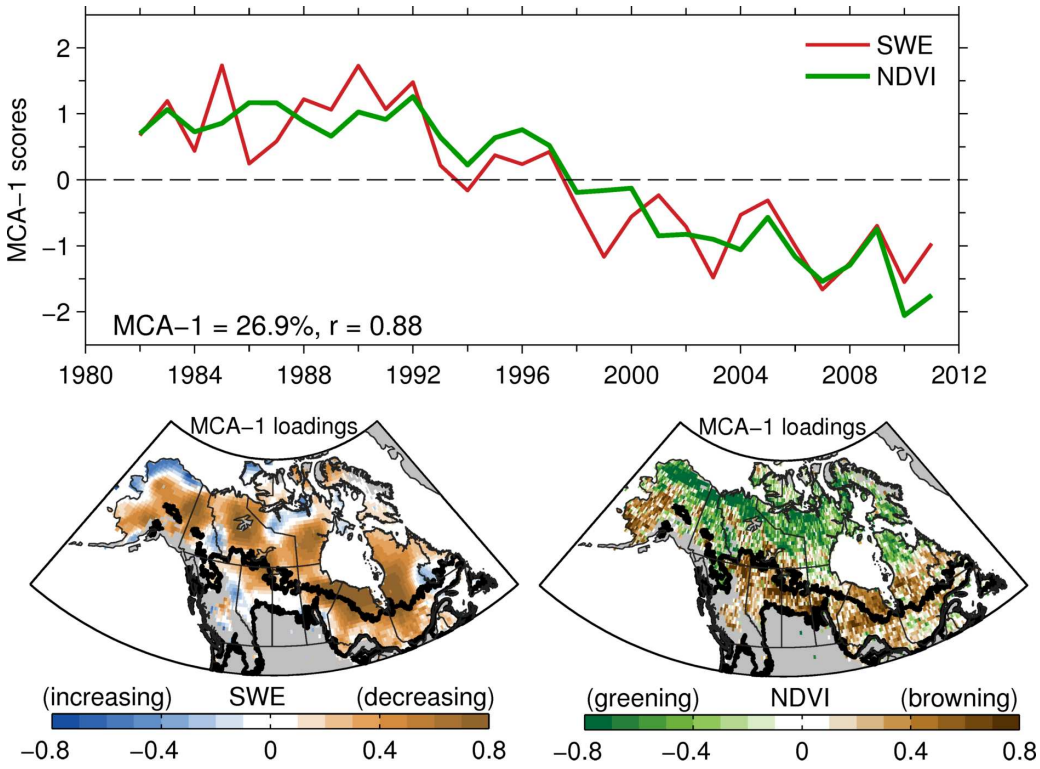

Figure 5.9: Temporal and spatial patterns of the leading Maximum Covariance Analysis (MCA) mode between maximum annual SWE and summer NDVI fields computed over the period 1982–2011. This mode explains 26.9% of the total cross-covariance and the correlation between the corresponding time expansion coefficients is 0.88.

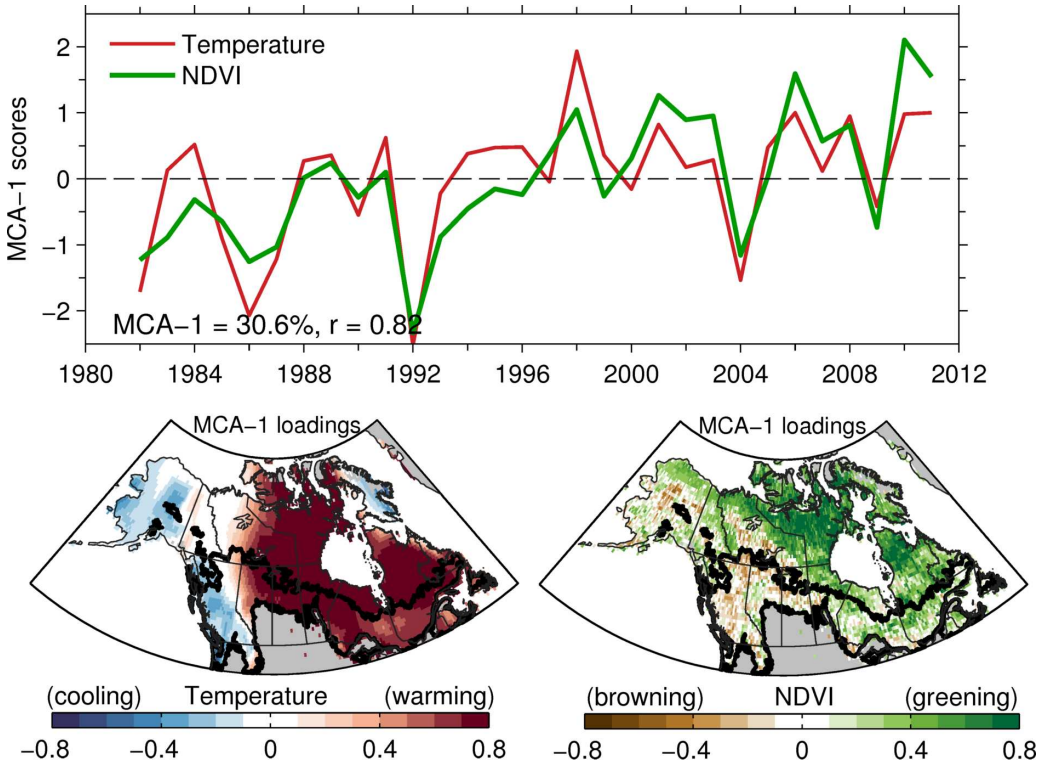

Figure 5.10: Temporal and spatial patterns of the leading MCA mode between summer temperature and summer NDVI fields computed over the period 1982–2011. This mode explains 30.6% of the total cross-covariance and the correlation between the corresponding time expansion coefficients is 0.82.

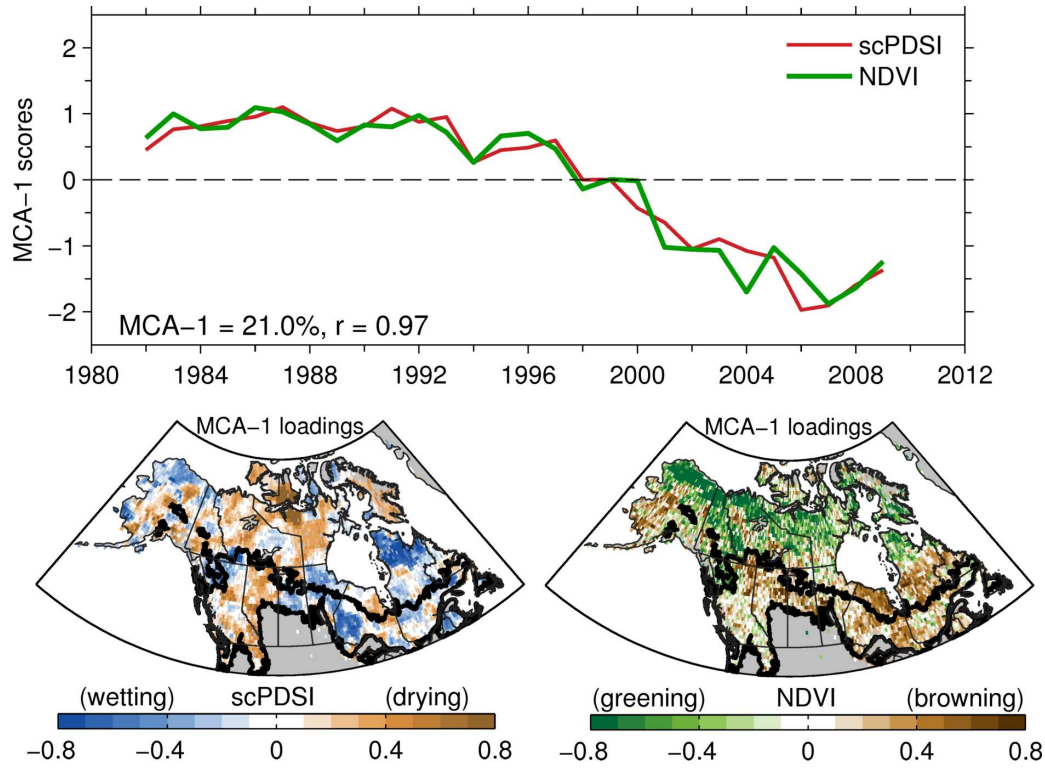

Figure 5.11: Temporal and spatial patterns of the leading MCA mode between March-August scPDSI and summer NDVI fields computed over the period 1982–2009. This mode explains 21% of the total cross-covariance and the correlation between the corresponding time expansion coefficients is 0.97.

as the leading mode of common variability (Figure 5.9). This mode explains 26.9% of the total cross-covariance. The corresponding spatial loadings are consistent with the spatial patterns of linear trends in maximum SWE and summer NDVI shown in Figure 5.8b–c, with contrasting browning trends in the boreal forests and greening trends in the Arctic shrublands and tundra in response to a common decline in snowpack accumulation.

A different pattern emerges when performing MCA using summer temperature and NDVI (Figure 5.10). In this case the resulting leading mode of coupled variability accounts for 30.6% of the total cross-covariance and shows an overall increasing trend with large interannual anomalies, among which is the short-term cooling in 1992 associated with the eruption of Mount Pinatubo. The corresponding spatial loadings indicate that this pattern represents a contrast between eastern and western North America. Coupled warming and greening trends occur across the temperature-limited regions in north-eastern Canada and cooling and browning trends in the western side of the continent, consistent with the spatial patterns of linear trends of the two variables (Figure 5.8a,c). The loadings also show that in the moisture-sensitive region along the western interior of Canada, warming trends coincide with weak or negative NDVI trends. Together with concurrent negative correlations at interannual scales (Figures 5.2a and 5.4a), this suggests a weak but consistent sensitivity of summer NDVI to increased evapotranspiration demand with summer warming in this region.

The MCA analysis was repeated using summer NDVI and spring-summer scPDSI over the period 1982–2009 in order to assess the NDVI response to the combined influence of changes in snow and temperature on soil water balance. The resulting coupled spatiotemporal pattern accounts for 21.0% of the total cross-covariance and is similar to that obtained with maximum

SWE, but with a slightly higher temporal correlation (Figure 5.11). Taken together, these coupled spatiotemporal patters consistently suggest that the observed trends in summer NDVI in North America can be largely explained by the combined effect of summer warming and a widespread decline in winter snowpack accumulation and summer moisture availability since around 1991. The browning trends in the boreal forests and greening trends in the cool Arctic region indicates contrasting vegetation responses to these interrelated environmental changes. On the one hand, declining snowpack together with summer warming reduces summer soil moisture availability and has an adverse impact on summer greenness in the dense and open (woodland) boreal forests. The similarity of the patterns shown in Figures 5.9 and 5.11 indicates that the decrease in summer moisture availability in the boreal region is primarily driven by reduced snow water supply whilst increased evapotranspiration demand with summer warming has a secondary effect that contributes to further drying. On the other hand, the same combination of reduced snow accumulation and warmer summers stimulates the greening of Arctic vegetation, likely due to the lengthening of the short growing seasons and changes in permafrost and nutrient availability.

5.4 Discussion

5.4.1 Spatially heterogeneous controls of interannual variability in summer greenness

The results show that spring and summer moisture availability exerts significant control on the interannual variability of summer greenness over about 29% (mean $r^2 = 0.29 \pm 0.16$) of the northern vegetated land, whilst temperatures during the same seasonal period exert a significant control over another 43% (mean $r^2 = 0.25 \pm 0.12$; Figures 5.2–5.5). However, the timing, magnitude and relative importance of these climate controls varied substantially between and within biomes, consistent with differences in climate responses between plant functional types observed in earlier studies (Goetz *et al.*, 2005; Welp *et al.*, 2007). Interannual correlations suggested that summer temperature is the dominant control of summer greenness anomalies in the cool boreal and Arctic regions, whereas spring and summer soil moisture availability is the main control of summer greenness across the continental interiors in the northern temperate grasslands and to a lesser extent in croplands (Figure 5.4). This is in good agreement with known patterns of climate constraints on vegetation productivity in northern biomes (Nemani *et al.*, 2003).

A new result of this study is that changes in cool-season snow accumulation exert a significant indirect influence on the variability of summer greenness in cool regions where it is often assumed that summer vegetation growth is dominantly temperature-limited, such as most of the boreal forests and Arctic shrublands along the dry western interior of Canada and Alaska, and open forests and shrublands in dry subarctic regions in eastern and south-central Siberia (Figure 5.4). Interannual anomalies in summer greenness in these areas are significantly and positively correlated with peak winter SWE, but correlations with summer rainfall and summer surface soil moisture anomalies based on the scPDSI and MW-SMO are weak (Figure 5.2). Positive correlations with the scPDSI become stronger and more consistent with vegetation responses to peak SWE anomalies when including the spring melting period in the seasonal average (Figure 5.3). This suggests that summer vegetation productivity in these relatively dry regions is sensitive to spring soil moisture recharge by snowmelt water at deeper layers of the rooting zone, a process that is not well captured by summer satellite retrievals and the shallow bucket used in the water balance model of the scPDSI.

At least a third of the yearly precipitation in these regions is stored in the winter snowpack (Supplementary Figure D1e). The melting of the snowpack in spring typically produces a large seasonal pulse in soil moisture recharge that can sustain vigorous vegetation growth and evapotranspiration well into the growing season until the start of a second period of moisture recharge by summer rainfalls (Yarie & Van Cleve, 2006; Kljun *et al.*, 2006; Yarie, 2008). However, summer rainfall may replenish moisture near the surface but may be less effective in recharging deeper soil layers because a large fraction is quickly lost to evaporation. As a result, for a given level of summer moisture demand, reductions in winter snowpack accumulation may induce greater drought stress than reductions in summer precipitation. This hypothesis is consistent with summer rainfall exclusion experiments in interior Alaska showing that tree growth in well-drained upland forests is maintained primarily by snowmelt water and is not affected by summer rainfall deficits (Yarie & Van Cleve, 2006; Yarie, 2008).

Positive influences of deeper winter snowpack on subsequent peak summer vegetation green-

ness and carbon uptake have been well documented in alpine forests in the western United States, where typically more than half of the annual precipitation falls as snow (Hu *et al.*, 2010; Trujillo *et al.*, 2012). These mountain forests rely heavily on snowmelt water even late into the growing season and variations in maximum snow accumulation can explain over 50% of the interannual variability in peak forest greenness (Trujillo *et al.*, 2012). Earlier growing seasons in these snow-dominated environments correlate with shallower snowpacks and result in reduced rather than increased growing season productivity because of insufficient spring soil moisture recharge to sustain summer growth (Hu *et al.*, 2010). In the northern latitudes, a positive association between summer NDVI and deeper snowpack has been previously documented in the taiga (subarctic woodland) and steppes of central Siberia (Grippa *et al.*, 2005), consistent with the results of this study in these regions (Figure 5.3b). This association has been interpreted as a positive vegetation response to increased water availability after snowmelt and also to enhanced thermal insulation of soils by thicker snowpacks during the cold Siberian winters.

Similar to the alpine forests in the western United States, a negative influence of earlier spring ground thaw on peak forest greenness has been recently documented across the drier western and central sections of the North American boreal forests (Buermann *et al.*, 2013). The results of this study show that maximum snow accumulation in these regions explains on average about 20% of the interannual summer NDVI variance (Figures 5.3b and 5.5a). Thus, this co-located negative response of summer greenness to earlier spring thaw is likely a reflection of soil moisture deficits resulting from both insufficient soil moisture recharge with shallow snowpacks and increased moisture depletion with an extended evaporative period. Taken together, these emerging results suggest that recent changes in snow regimes associated with rapid climatic warming (Brown & Robinson, 2011; Park *et al.*, 2012; Gan *et al.*, 2013) are likely to have played an important albeit unrecognised role in the observed spatiotemporal patterns of summer vegetation greenness across a large portion of the boreal region, particularly in North America.

Earlier studies have reported an apparent shift toward increased moisture limitation of vegetation productivity with continued warming since the early 1990s across much of the temperate and boreal ecosystems (Angert *et al.*, 2005; Goetz *et al.*, 2005; Zhang *et al.*, 2008). The results of this study, based on an objective dynamic regression analysis at the grid box level, indicate that the interannual association between climate (temperature, moisture and snow) and NDVI variability has not changed over time (Figure 5.6) and thus there is no evidence for consistent regional-scale temporal shifts from temperature to moisture limitation with recent warming on a year-to-year basis. A few instances of time-dependent association between temperature and NDVI were found in some remote northern regions and seem to indicate temporal changes in data quality rather than changing vegetation responses to climate (Figure 5.7). The temporal stability of the climate responses of summer NDVI at interannual time scales indicates that the apparent changes in climate response found in previous studies are linked to decadal time scales, where NDVI variability can be affected by a variety of other slowly-varying climatic and non-climatic factors (Piao *et al.*, 2006a; Alcaraz-Segura *et al.*, 2010). Also, previous studies have typically used continental or circumpolar averages for assessing the responses of NDVI. Large-scale averages are likely to include biomes or regions with contrasting climatic controls or little climate control (Figure 5.4) and thus may give a biased picture of vegetation responses to climate.

The results of this study highlighted extensive regions where interannual summer NDVI variance is not significantly associated with spring or summer climate variability, such as the boreal forests in central Eurasia, shrublands in the far east of Siberia and northern Alaska, European croplands and mixed forests in eastern North America (Figures 5.5d). Collectively, these regions represent 28% of the northern vegetated land. Land management practices (e.g., herding, irrigation, harvest, etc.) can easily override climate influences on NDVI in the croplands and some intensively managed grasslands, but it is less clear which factors are driving interannual NDVI anomalies in un-disturbed forests and remote high-latitude shrublands.

Correlations at short lags (1–2 years) did not show significant lagged climate responses in these regions (results not shown here). Uncertainties in the climate datasets and in the NDVI might account in part for the apparent lack of climate response. Extremely sparse coverage in the network of meteorological stations underlying the gridded temperature and particularly the precipitation fields could be reducing the correlations in the remote Arctic shrublands. The few data available might not represent coastal or mountainous areas well, where local climate conditions driving NDVI variability may differ substantially from conditions averaged over more continental regions. Moreover, permafrost and snow dynamics could also be modulating interannual climate-vegetation interactions in these cold and dry regions. Regional studies and comparisons with independent vegetation indices (Liu *et al.*, 2011; Joiner *et al.*, 2013) are needed to determine the causes for this apparent lack of climate control of NDVI3g in these extensive regions.

5.4.2 Drivers of greening and browning trends

Warming has stimulated productivity rates of northern vegetation by lifting low temperature limitations on vegetation metabolism (Nemani *et al.*, 2003; Zhang *et al.*, 2008). Consistent with this mechanism, practically all temperature-limited Arctic and boreal regions have greened since 1982 apparently in response to concurrent warming trends (Figure 5.8a,c). Moreover, a slight regional cooling in western Canada is consistent with co-located browning trends, as documented in earlier regional studies (Wang *et al.*, 2011). This is an indication that temperature-limited vegetation growth across the circumpolar region (43% of the northern vegetated land) has responded to temperature variability in a consistent manner at interannual and longer time scales, with no apparent decoupling between warming and greening trends during summer.

Another interesting result of the grid box-scale comparisons is that warming is not the only driving force of the widespread greening in the cool northern biomes. Most regions where NDVI is not correlated with climate on a year-to-year basis (∼28% of the northern vegetated land) have also greened (Figure 5.8c). This suggests the influence of other climatic or non-climatic factors not accounted for in this study operating at longer time scales and across different vegetation types. A number of possible factors could be at work but quantifying their relative contribution to these greening trends would require further analysis and is beyond the scope of this study. In part, these greening trends could indicate the effect of changes in diffuse radiation, and CO_2 and nitrogen fertilisation on northern vegetation. Modelling studies have estimated that CO_2 fertilisation alone explains at least about 40% of the observed global and Northern Hemisphere greening trends since the early 1980s, whilst other factors such as downwelling solar radiation, nitrogen deposition and satellite-related artifacts account for only a small fraction

of the trends (Piao *et al.*, 2006b; Los, 2013). Other mechanistic studies based on ecosystem models have identified a significant enhancement of canopy photosynthesis and the land carbon sink by long-term variations in diffuse radiation over the 'global dimming' period since the 1960s (Mercado *et al.*, 2009). Changes in permafrost seem to be a factor stimulating greening trends in some subarctic regions. For instance, extensive shrublands underlain by continuous permafrost in northern Alaska show a consistent greening trend despite a lack of interannual correlations with climate (Figure 5.8c). Shrub encroachment has been identified as an important driver of this regional greening (Tape *et al.*, 2006) and it is likely that this reflects gradual, warming-driven changes in permafrost dynamics and snow cover that favour shrub establishment. Significant declines in sea ice along the Arctic coast might have also contributed to the widespread greening of coastal tundra vegetation (Bhatt *et al.*, 2013).

The combined influence of warming and the positive effect of non-climatic factors has led to stronger and more widespread greening trends in Eurasia than in North America. Most of the Eurasian boreal forests and the Arctic region have greened, whereas in North America only the Arctic region underlain by continuous permafrost north of the treeline has greened and most of the boreal forests have undergone browning trends. Although these contrasting continental and biome trends have been well documented in earlier analyses of the GIMMS NDVI record (Goetz *et al.*, 2005; Bunn & Goetz, 2006; Beck & Goetz, 2011; Piao *et al.*, 2011; Barichivich *et al.*, 2013; Xu *et al.*, 2013), the empirical results of this study highlight the significant role of factors other than temperature and moisture on these vegetation patterns. A similar regional heterogeneity in the drivers of the greening trends in northern ecosystems has been found in attribution studies based on ecosystem models (Piao *et al.*, 2006b). Further regional studies are needed to understand the influence of non-climatic factors on the ongoing greening of northern landscapes and to explore the potential for future changes and their controls.

The contrast between greening trends in the subarctic tundra and browning trends in the boreal forests of North America has stimulated extensive research over the past decade and the possible causes of forest browning are still being debated (Verbyla, 2011). Forest browning across most of Canada and Alaska since the early 1990s has led to speculation that after an initial alleviation of cold constraints during the 1980s, subsequent warming has no longer promoted northern vegetation growth because of increased temperature-induced drought stress (Angert *et al.*, 2005; Goetz *et al.*, 2005; Bunn & Goetz, 2006; Beck *et al.*, 2011). This hypothesis has emphasised the role of increasing evaporative demand on surface water budget, whilst the potential influence of changes in moisture supply (snow and rainfall) and connections with concurrent changes in snow regimes have not been considered. The results of the Maximum Covariance Analysis confirm that NDVI declines across the North American boreal forests since around 1991/2 are consistent with a long-term decrease in summer soil moisture availability, as measured by spring-summer scPDSI (Figure 5.11). However, a new finding of this study is that the decrease in moisture availability has occurred primarily in response to declining snowpack water content and subsequent reductions in recharge from spring snowmelt. The effect of increasing evaporative demand, driven by summer warming, appears to be a secondary factor contributing to further drying and browning in some locations (Figure 5.10). Thus, the results of this study do not fully support the hypothesis of temperature-induced drought stress, which

overemphasises the role of temperature on the soil water budget and overlooks the influence of snow in the boreal region.

Using Maximum Covariance Analysis to isolate the coupled trends in winter snowpack (maximum SWE), soil moisture availability (scPDSI) and summer NDVI has shown that the temporal pattern of shared trends is strongly consistent with the temporal trajectory of regional-scale declines in NDVI, tree-ring growth, forest biomass and modelled productivity previously documented in the boreal region (e.g., Goetz *et al.*, 2005; Hogg & Wein, 2005; Beck *et al.*, 2011; Ma *et al.*, 2012; Buermann *et al.*, 2013). Furthermore, the spatial patterns of the coupled trends suggest contrasting vegetation responses to declining snowpack accumulation in the Arctic shrublands and boreal forests since the early 1990s. Thus, together with seasonal warming, declining snow cover appears to be playing an important role in driving the well-documented contrast between forest browning and tundra greening trends in North America (Goetz *et al.*, 2005; Bunn & Goetz, 2006; Beck *et al.*, 2011). Reduced peak snow accumulation can extend the short northern growing seasons and stimulate earlier and faster vegetation greening in some cool Arctic regions (Grippa *et al.*, 2005; Bhatt *et al.*, 2013), but it may have an adverse impact in the boreal forests due to reduced water availability during summer (Yarie, 2008) and soil insulation during the cold season (Schaberg *et al.*, 2008; Brooks *et al.*, 2011; Jarvis *et al.*, 2013).

Recent studies based on satellite and in-situ observations have shown that since around 1991 rapid winter/spring warming and changes in interdecadal climate modes have led to a significant decline in snowpack accumulation and snow cover duration across most of Alaska and Canada despite increasing winter precipitation (Biancamaria *et al.*, 2011; Callaghan *et al.*, 2011; Brown & Robinson, 2011; Park *et al.*, 2012; Gan *et al.*, 2013). In some regions of the North American Cordillera the recent loss of snowpack is unprecedented over the past millennium (Pederson *et al.*, 2011). Estimates based on satellite retrievals for the period 1979–2007 indicate a reduction in December-April SWE of about 0.4 to 0.5 mm yr^{-1} over North America, which corresponds to an overall reduction of snow depth of about 5-8 cm in 29 years, depending on snow density (Gan *et al.*, 2013). Without increases in summer precipitation, this reduction in snowpack is sufficient to result in soil moisture deficits later in the growing season over extensive boreal regions relying on spring snowmelt for water supply (Figure 5.3).

Soil moisture deficits and drought stress during the growing season might have been further exacerbated by the concurrent increase in evaporative demand with recent summer warming (Figures 2.1 and 2.2). However, during the past three decades this extra drying effect appears to have occurred mainly in the Arctic region of Canada and Alaska and not much in the Canadian boreal region as a whole (Figure 2.2). Summer temperature anomalies tend to correlate negatively with interannual summer NDVI anomalies over the moisture-sensitive areas in the continental interior of Canada and Alaska (Figure 5.4a), consistent with tree-ring studies showing an inverse relationship between annual tree growth and summer temperatures in these regions (Szeicz & MacDonald, 1996; Barber *et al.*, 2000; Wilmking & Juday, 2005; Yarie, 2008; McGuire *et al.*, 2010; Juday & Alix, 2012; Lloyd *et al.*, 2013). Nevertheless, the negative NDVI responses to temperature are weak and thus the drying effect of increased evaporation with higher temperatures does not drive a large fraction of the NDVI variance.

The significant sensitivity of the North American boreal forests to changes in snow hydrology has not been fully appreciated until now and could help explaining the apparent changes in

climate sensitivity of tree growth in the region (D'Arrigo *et al.*, 2008). It also raises concerns regarding forest responses to continued warming and possible impacts on the carbon cycle. The result of the lagged coupling between vegetation and seasonal snow dynamics is consistent with the hypothesis that spring productivity gains from earlier thaw and extension of the growing season could potentially be offset by drought-induced productivity losses later in the season (Angert *et al.*, 2005; Bunn & Goetz, 2006; Zhang *et al.*, 2008; Buermann *et al.*, 2013).

Climate models participating in the Coupled Model Intercomparison Project Phase 5 (CMIP5) project a shift towards low spring snow accumulation in the Northern Hemisphere despite a concurrent increase in winter precipitation, with parts of the North American boreal zone showing the strongest snow reductions during the near term decades when global mean surface temperatures rise to 2^{o}C above the pre-industrial baseline (Diffenbaugh *et al.*, 2012). Combined with projections of parallel increases in evapotranspiration demand (Dai, 2012), this will likely result in further lengthening and intensification of the period of summer drought stress and thus increase productivity losses across moisture-sensitive regions with snow-dominated hydrology.

5.5 Conclusions

The main conclusions of this Chapter are summarised as follows:

- The climatic control of summer NDVI across northern biomes is significant but highly heterogeneous in space. Unlike previous studies, the results of the present study show a strong regional influence of snow dynamics and possibly non-climatic factors (e.g., permafrost, changes in diffuse light and CO_2 and nitrogen fertilisation) on the interannual variability and trends in summer NDVI over vast areas of the boreal and Arctic regions, where temperature is often assumed to be the dominant environmental control of vegetation productivity. Further empirical studies are needed to quantify the influence of various non-climatic factors on the remaining unexplained variance of summer NDVI variability.

- Predominantly temperature-limited and moisture-limited vegetation growth has responded consistently to climate variability at interannual and longer time scales, with no apparent decoupling between climate and NDVI trends. Thus, in contrast to earlier regional-scale studies this study does not show evidence for temporal shifts in the type or magnitude of climate limitation at the grid box scale.

- Widespread NDVI declines across the North American boreal forests since around 1991/2 are consistent with a long-term increase in summer drought stress. However, the increase in drought stress appears to have occurred primarily in response to declining snowpack accumulation and insufficient soil moisture recharge from spring snowmelt rather than to temperature-induced increases in evaporative demand as hypothesised in earlier studies. Although summer warming has contributed to surface drying and NDVI declines through increased evaporative demand, the relative role of temperature on the soil water budget may have been overemphasised in previous remote sensing studies.

- Further increase in evapotranspiration demand and reduction in snowpack accumulation with any continued warming during the coming decades could intensify summer drought severity but highly heterogeneous vegetation responses should be expected across the circumpolar region.

Chapter 6

Re-assessing moisture limitation on tree-ring growth in the boreal forest: a case study in northwestern North America

Abstract

Several studies have reported recent tree growth 'declines' or an absence of growth increases in boreal trees at the same time as climate warming has occurred in several locations in Alaska and northwestern Canada. Such observations are at odds with expected vegetation responses in temperature-limited environments. These changes in tree growth have been primarily attributed to increasing moisture stress and non-linear growth responses to temperature. In this chapter, a tree-ring chronology network of 115 sites across northwestern North America is analysed to reassess the roles of soil moisture and non-linear responses on the observed growth patterns of white spruce, the dominant tree species in the region. A combined approach involving simple correlation analysis and process-based modelling with the Vaganov-Shashkin (VS) model of tree-ring formation calibrated with a Bayesian algorithm is used to infer climate controls on tree growth. Consistent with earlier studies, the results show a dominant moisture control of white spruce growth throughout the region but no clear evidence for a widespread increase in moisture limitation during recent decades. This moisture control of tree growth is also consistent with regional patterns of moisture limitation inferred from satellite observations of vegetation greenness and vegetation productivity simulated by ecosystem models. The calibrated VS model indicates that tree growth at high-elevation sites increases with temperatures above 6^{o}C but starts to decline when daily temperatures exceed a threshold of about 17^{o}C, without accounting for differences in elevation between the tree-ring sites and the temperature records. An increasing frequency of days exceeding this threshold over the past few decades seems to be relatively consistent with anomalous recent growth declines or 'tree-ring divergence' in some treeline sites across the region. These results highlight the significant influence of moisture limitation on boreal vegetation in this region and suggest the existence of non-linear growth responses of white spruce growth to recent warming at high elevations as reported in some earlier dendrochronological studies.

6.1 Introduction

Rapid warming over northern latitudes and changes in the chemistry of the global atmosphere are driving complex changes in the ecology of the boreal forests (Soja *et al.*, 2007). Since the growth of boreal trees is closely associated with temperatures (Jarvis & Linder, 2000; Evans *et al.*, 2006; Vaganov *et al.*, 2006; Rossi *et al.*, 2011; Briffa *et al.*, 2013), tree rings have been routinely used for evaluating both the unusual nature of recent warming and how the boreal forests are responding to this warming (Mann *et al.*, 1999; Briffa, 2000; Esper *et al.*, 2002; Briffa *et al.*, 2004; D'Arrigo *et al.*, 2006; Mann *et al.*, 2008). Tree rings record annual increments in stem wood over the whole lifespan of a tree. Thus, radial growth rates estimated from measurements of ring widths represent historical changes in above-ground tree productivity due to the influence of multiple environmental and internal age-related factors (Cook *et al.*, 1990; Vaganov *et al.*, 2011).

The analysis of networks of tree-ring chronologies of standardised ring-width measurements in the boreal region shows a general increase in tree growth with rising temperatures during the second half of the twentieth century (e.g., D'Arrigo *et al.*, 2006), consistent with increasing ecosystem carbon uptake (Keeling *et al.*, 1996) and satellite-observed greening trends (Myneni *et al.*, 1997). However, there are cases where the growth of boreal trees in some cool and relatively moist northern locations has shown positive responses to summer warming in the early part of the 20th century, but some chronologies do not track rising temperature trends since around the 1960s (Jacoby & D'Arrigo, 1995; Briffa *et al.*, 1998; D'Arrigo *et al.*, 2004, 2008). In these locations, the decadal-scale trends in ring widths (or density) indices and summer temperatures have diverged during recent decades as tree growth has apparently progressively declined relative to measured temperatures. Such a "divergence" phenomenon (Briffa *et al.*, 1998; D'Arrigo *et al.*, 2008) is at odds with the expected vegetation response in a temperature-limited environment and predictions of increased forest productivity throughout the twentieth century based on the current generation of ecosystem models (Piao *et al.*, 2013; Sitch *et al.*, 2013).

The divergence was first described in northern Alaska by Jacoby & D'Arrigo (1995) in tree-ring width and particularly maximum latewood density data from elevational and latitudinal treeline site chronologies of white spruce (*Picea glauca*). A similar pattern of divergence was noted later in a range of species in extensive regions of northern Canada, northern Europe and Russia (Briffa *et al.*, 1998). A number of causal factors related to environmental change and tree-ring methodologies have been proposed to explain these observations (D'Arrigo *et al.*, 2008) and these are still being debated. On the one hand, the at least partly common divergent behaviour of recent trends in tree-ring parameters found in these and subsequent studies could represent 'end-effects' in standardised tree-ring chronologies, which might result from the curve-fitting procedures used to remove the age-related trends of tree-ring measurements (Melvin, 2004; Melvin & Briffa, 2008; Briffa & Melvin, 2011). The earlier work in Alaska suggested that the cause of the observed relative growth decline and weakening of the tree-growth/temperature relationship since the 1960s was a shift in the forcing of tree growth from a direct dominant temperature control to a progressively increasing warmth-induced drought stress to the point where the temperature influence on tree growth eventually becomes negative (Jacoby & D'Arrigo, 1995; D'Arrigo *et al.*, 2004). This physiological turning point was estimated to occur when

the average July-August temperature exceeds 11^{o}C for a treeline site in northwestern Canada (D'Arrigo *et al.*, 2004). Subsequent studies in the region appear to support the hypothesis that current tree growth may no longer be responding positively and linearly to continued warming and that moisture stress is becoming increasingly limiting in extensive areas of the North American boreal forest (e.g., Lloyd & Fastie, 2002; Davi *et al.*, 2003; Wilmking *et al.*, 2004; Driscoll *et al.*, 2005; Pisaric *et al.*, 2007; Ohse *et al.*, 2012). However, the lack of moisture observations has hampered a robust assessment of the possible influence of reductions in soil moisture availability on forest growth with rising temperatures in this boreal region.

The results presented in the previous chapter of this thesis (see also Barichivich *et al.*, 2014) highlighted a significant snow-mediated moisture limitation of satellite-observed summer vegetation greenness along the drier and more continental regions of the North American boreal forest. Unlike earlier suggestions of warming-induced drought stress (Barber *et al.*, 2000; Bunn & Goetz, 2006), these new results indicate that changes in snowpack accumulation appear to be more important than increased evaporative demand in controlling changes in summer soil moisture availability and vegetation greenness across this region. In particular, regional declines in forest greenness (Angert *et al.*, 2005; Goetz *et al.*, 2005; Bunn & Goetz, 2006; Beck & Goetz, 2011) are consistent with reduced winter snowpack during recent decades. This suggests that tree growth declines in moisture-limited (Barber *et al.*, 2000; Hogg & Wein, 2005) as well as in some temperature-limited boreal locations (e.g., Jacoby & D'Arrigo, 1995; D'Arrigo *et al.*, 2004) could be consistent with reductions in forest greenness and changes in snowpack dynamics. However, the direct links between variations in ring-width and satellite vegetation indices have been difficult to demonstrate (Berner *et al.*, 2011; Beck *et al.*, 2013), except in some drier parts of interior Alaska, where declining trends in tree growth coincide with canopy browning trends (Beck *et al.*, 2011). Furthermore, tree-ring studies in boreal North America have not evaluated the potential influence of long-term changes in snowpack on tree growth patterns despite the evidence for this reported for northern Siberia and Finland (Vaganov *et al.*, 1999; Kirdyanov *et al.*, 2003; Helama *et al.*, 2013). Establishing the links between changes in tree-ring growth and changes in both satellite vegetation indices and snow-mediated moisture availability is necessary to understand how the boreal forest in this region are responding to climatic warming.

The aim of this final chapter is to re-assess the climate response of tree growth in northwestern North America during the second half of the 20th century and determine whether these responses are consistent with the climate controls of satellite-observed vegetation greenness and vegetation productivity simulated by Dynamic Global Vegetation Models (DGVMs). To achieve this, ring-width data from a network of 115 chronologies of white spruce are analysed to quantify empirically the responses of tree growth to temperature and moisture availability using the suite of vegetation and moisture datasets described in previous chapters. Empirical 'response functions' calculated using monthly climate data are compared with seasonal growth limitation simulated by the semi-empirical Vaganov-Shashkin-Lite (VSL) forward model of tree-ring width (Tolwinski-Ward *et al.*, 2011), which is able to model non-linear relationships between tree-rings and monthly temperature, soil moisture and light.

A more detailed investigation of divergent tree growth trends is conducted at three well-known treeline locations using the full process-based Vaganov-Shashkin (VS) model that simu-

lates daily tree-ring growth at the cell level as a non-linear function of temperature, moisture and light limitations (Vaganov *et al.*, 2006, 2011). The application of this model to tree-ring divergence settings has been in part limited in the past due to the lack of observational constraint of some key driving parameters for the North American boreal region. To overcome this limitation, a modern Bayesian calibration framework (Van Oijen *et al.*, 2005) is applied for the first time to calibrate the model, enabling process-based inferences on the nature of recent tree growth responses at these locations. The results of this study provide an improved perspective on the ongoing responses of the North American boreal forest to climate change based on multiple empirical and modelling lines of evidence.

6.2 Data and methods

6.2.1 Tree-ring data and chronology development

The case study area spans the region of the Alaskan and Canadian boreal forests west of 100^{o}W and north of 55° (Figure 6.1). The tree-ring data for this region were obtained primarily from the International Tree-ring Data Bank (ITRDB; `http://www.ncdc.noaa.gov/paleo/treering.html`) and also from the Tree-ring Laboratory of the University of Regina, Canada (D. Sauchyn, pers. comm.) and data representing some recent collections provided to the Climatic Research Unit by various collaborating researchers working in North America (Martin Wilmking, Trevor Porter, Michael Pisaric and Rossane D'Arrigo). After screening the available data for length, quality and sample size, ring width measurements for 115 sites of white spruce (*Picea glauca*) covering the entire period 1950–2000 were retained for analysis. The resulting tree-ring network is more representative of low to mid-elevation white spruce stands in Alaska (Figure 6.1), but also contains several high elevation and treeline sites collected specifically to study changing growth responses to temperature variability (e.g., D'Arrigo *et al.*, 2004; Wilmking *et al.*, 2004; D'Arrigo *et al.*, 2009; Pisaric *et al.*, 2007; Porter & Pisaric, 2011; Porter *et al.*, 2013). The location and descriptive statistics of each tree-ring site are shown in the Supplementary Table E1.

The series of tree-ring width measurements at each site were processed using a data-adaptive signal-free standardisation approach (Melvin, 2004; Melvin & Briffa, 2008) in order to estimate and remove their individual age-related trends without the influence of changes in their common climate-related growth forcing. The signal-free method iteratively removes the common growth signal at a given site before fitting an age-related growth model to the individual signal-free series. This procedure mitigates the impact of statistical artefacts in curve-fitting detrending methods that can lead to a severe misrepresentation of recent growth patterns in the resulting mean tree-ring chronologies. When not taken into consideration, these biases could produce an artificial divergence between recent warming trends and relative growth rates of temperature-sensitive boreal trees inferred from standardised tree-ring chronologies (Melvin & Briffa, 2008; Briffa & Melvin, 2011).

Two different standardisation methods were used to produce average tree-ring width chronologies for each site, preserving common growth variations at high and mid-frequency time scales. The first method (SPL10) involves detrending measured ring-width series by removing the variance represented by a (signal-free) 10-year fixed-length cubic smoothing spline: in effect

generating "high-pass filtered chronologies" containing little variability at time scales longer than 10 years. The second method (NEGEX) is based on a hierarchical detrending method, commonly applied in tree-ring studies, that uses either a modified negative exponential curve or a simple negative straight line to detrend the individual signal-free series, or a horizontal line through the mean if the curve fitting fails (Cook *et al.*, 1990). The resulting mean chronologies preserve high to medium-frequency common growth signals up to a time scale approaching the mean age of the trees, but with an arbitrary overall slope generally close to zero. An important caveat of this mixed approach is that ring-width series for which the best-fitting sloping straight line has a positive slope will still be fitted with a horizontal line through the mean and in such cases the resulting indices will have a positive trend, whilst the other fitting options are constrained to produce indices with near zero overall slope. The resulting chronology will then be created by averaging varying proportions of series of tree-ring indices with positive slope or without slope, affecting the overall slope of the chronology. This issue needs to be kept in mind when interpreting growth rates based on average NEGEX chronologies. The standardisation and chronology development were performed using the CRUST (*C*limatic *R*esearch Unit *S*tandardisation of *T*ree-ring data) software package (Melvin & Briffa, 2013, available at `http://www.cru.uea.ac.uk/cru/software/crust/`).

The resulting NEGEX tree-ring chronologies are shown in the upper panel of Figure 6.1 together with a regional mean series of growing season temperatures. About 80% of the sites in the network display increasing growth rates during recent decades of warming, though not all these increases are significant. Most of these sites are located in permafrost areas of Alaska, whilst sites showing recent growth declines tend to occur in the Canadian boreal forest.

6.2.2 Meteorological data and climatic forcing of tree growth

To identify the climatic forcing of year-to-year tree growth anomalies across the network, the SPL10 tree-ring chronologies were compared against co-located 10-year high-pass filtered series of monthly gridded mean temperature and estimates of surface soil moisture over the period 1950–2000. Mean air temperature data were obtained from the gridded CRUTS 3.20 dataset at a spatial resolution of 0.5° × 0.5° (Harris *et al.*, 2014). The GPCC-scPDSI dataset and surface soil moisture (0–10 cm) estimates of the GLDAS-2 Noah land surface model described in Chapter 4 were used to evaluate growth responses to moisture variability.

Each SPL10 tree-ring chronology was correlated with co-located gridded series of monthly mean climate variables for each month from April of the previous growing season to September of the current growing season using the *seascorr* Matlab routine (Meko *et al.*, 2011) with 1000 Monte Carlo simulations for significance testing. The use of such an extended temporal window allows the identification of lagged climate responses typically found in the growth of white spruce (Jacoby & D'Arrigo, 1995). The 36 monthly correlations between each tree-ring chronology and temperature and scPDSI were then analysed in a k-means cluster analysis (Seber, 2009) to identify groups of chronologies based on their climate response. The optimal number of clusters was estimated using the gap statistic (Tibshirani *et al.*, 2001). Finally, the time dependence of the association between each SPL10 tree-ring chronology and 10-year high-pass filtered monthly temperature and moisture variability was assessed using time-varying regression with the Kalman Filter (Visser & Molenaar, 1988).

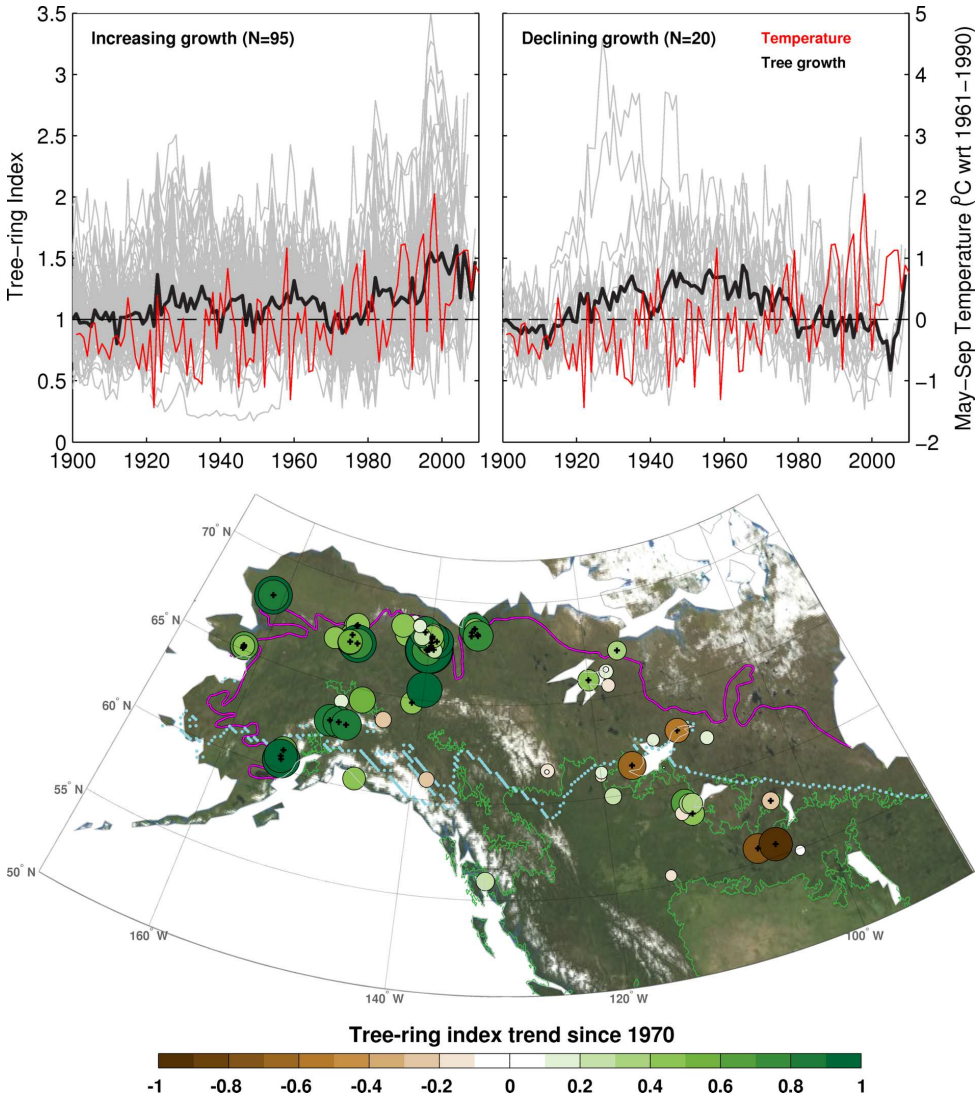

Figure 6.1: Location and recent linear trends of the 115 standardised (NEGEX) tree-ring chronologies used for analysis. The size and color of the symbols in the map indicate the magnitude and sign of the trends over the period 1970–2000. The black crosses indicate sites with significant ($p < 0.05$) trends. The boreal forest is outlined in green and the pink and cyan lines denote the location of the treeline and the southern edge of the discontinuous permafrost region, respectively. The top panel shows the averages of tree-ring sites with increasing and decreasing trends during 1970–2000 (black) together with the mean growing season temperature averaged across the 115 co-located grid boxes (red).

To evaluate the influence of the winter snowpack on subsequent tree growth, the SPL10 tree-ring chronologies were correlated with maximum monthly winter/spring Snow Water Equivalent (SWE) simulated by the scPDSI snow model over the period 1950-2000. Since the simple snow model underlying the scPDSI was calibrated against satellite observations (van der Schrier *et al.*, 2013), the variability of the resulting estimates of peak SWE is well correlated with the estimates based on the version 1.3 of the GlobSnow dataset (Takala *et al.*, 2011) over the common period 1979–2009 (results not shown).

Changes in the ground thermal regime and consequently in the dynamics of the seasonally active layer have a large impact on soil hydrology and ecosystem functioning in the northern latitudes, with direct consequences for plant growth (Bonan, 1989; Danby & Hik, 2007; Wirth *et al.*, 2008; Natali *et al.*, 2011). Therefore, to investigate the response of tree growth to year-to-year

variations in soil thaw dynamics, the SPL10 chronologies were compared with gridded estimates of maximum annual thaw depth obtained from the National Snow and Ice Data Center (NSIDC) at a spatial resolution of 25 km and for the period 1901–2001 (Zhang *et al.*, 2005b). These estimates are based on a variant of the Stefan solution of the heat diffusion equation driven by a spatially varying edaphic factor and a monthly thaw index derived from the CRUTS temperature dataset (Zhang *et al.*, 2005a; Frauenfeld *et al.*, 2007). Correlations between the chronologies and thaw estimates at the co-located grid boxes were computed over the period 1950–2000 using 10-year high-pass filtered thaw series.

6.2.3 Modelling tree-ring growth as a function of climate

Process-based tree growth models are useful tools to test hypotheses relating physical or biological mechanisms to changes in the response of tree growth to climate detected by empirical statistical methods (Evans *et al.*, 2013). Identification of differences between model simulations and actual tree-ring chronologies allows further exploration of the influences of tree-ring standardisation, changes in atmospheric composition and additional non-climatic factors. However, there are only a few models of tree-ring growth currently available, with varying degrees of complexity and approaches (Vaganov *et al.*, 2011; Wang *et al.*, 2012b).

In the upper range of model complexity, fully ecophysiological process-based models such as TREERING2000 (Fritts *et al.*, 1999) and MAIDEN (Misson, 2004) link photosynthesis and carbohydrate allocation (source) with stem growth (sink), either as a function of carbon accumulation or climate-driven cambial dynamics, to simulate tree-ring growth at a daily time scale. These models have been developed and tested in data-rich mid-latitude settings and contain a large number of parameters, many of which are unknown or difficult to constrain in remote regions such as those in the northern latitudes. The Vaganov-Shashkin (VS) model, representing a relatively lower level of complexity, is the most widely used process-based model of tree-ring formation in the tree-ring community. This model assumes that tree-ring growth is carbon sink-limited rather than a carbon source-limited process (Vaganov *et al.*, 2011) and thus simulates daily cambial dynamics and xylem growth of conifer tree rings only as a function of daily temperature, daily soil moisture estimates and day length. It does not consider photosynthesis and carbon allocation to stem growth. Despite this major simplification, the model is still able to simulate tree-ring width chronologies successfully in a variety of conditions from boreal to temperate and semi-arid environments with small changes in parameterisation (Vaganov *et al.*, 2006; Evans *et al.*, 2006; Anchukaitis *et al.*, 2006; Touchan *et al.*, 2012). Unlike TREERING2000 and MAIDEN, the VS model was specifically developed for the temperature-limited boreal region (Vaganov *et al.*, 2006, 2011). Because of its good ability to simulate tree-ring chronologies, the VS model has been taken as the cambial growth module in TREERING2000.

The paucity of daily meteorological data is usually an obstacle for the wide application of the VS model. To overcome this limitation, a simplified version of the model, termed Vaganov–Shashkin–Lite (VS–Lite), has been recently developed (Tolwinski-Ward *et al.*, 2011). VS–Lite requires only day length and monthly precipitation and temperature data as input to simulate tree-ring chronologies as a function of the most limiting factor, but lacks the cell-level processes of the full version as well as snow and thaw dynamics.

A combination of the two VS models was used here to study the nature of climate limitation

of tree growth across the tree-ring network and to validate the empirical results based on simple correlation analysis. The key structural features of the models and their parameterisation are described below.

6.2.3.1 The Vaganov-Shashkin model

The VS model simulates the growth of annual rings as a function of cell growth, based on the simplifying assumption that cell development in the cambium tissue is driven exclusively by the physical environment. The dynamics of cell growth, division and maturation are simulated in a specialised cambial module, which is driven by an environmental growth module. This growth module implements the principle of limiting factors (Fritts, 1976) and computes tree-ring growth rates during the course of the growing season, taking as input day length and daily temperature and precipitation data typically recorded at meteorological stations. The daily values of the growth rate are modelled as:

$$G(t) = g_E(t) \times min[g_T(t), g_W(t)] \tag{6.1}$$

where $g_E(t)$, $g_T(t)$ and $g_W(t)$ are the respective partial daily growth rates due to solar radiation, surface air temperature and soil water balance, respectively. All these growth rates are normalised quantities ranging from 0 to 1. $g_E(t)$ is a simple annual sinusoid dependent on latitude that mimics growth limitation by solar irradiation and day length. $g_T(t)$ and $g_W(t)$ are based on separate 3-segment piecewise linear growth response functions to temperature and moisture that mimic critical biological thresholds for growth. In the first segment, growth rates increase linearly with increasing temperature and moisture up to an optimal value. In the second segment, growth rates remain constant within an optimal range of temperature and moisture and then linearly decrease in the third segment as temperature and moisture levels move beyond this optimal range. These two response functions result in eight parameters: minimum temperature and minimum moisture for growth (T_{min} and W_{min}), the lower bound of the ranges of optimal temperature and of moisture (T_{opt1} and W_{opt1}), the upper bound of these optimal ranges (T_{opt2} and W_{opt2}), and the maximum values of temperature and moisture for growth (T_{max} and W_{max}).

The largest source of uncertainty in computing $G(t)$ is the estimation of the seasonal dynamics of volumetric soil water content (W) from daily precipitation and temperature data alone. W is computed using a simple water balance equation (Thornthwaite & Mather, 1955):

$$dW = f(P) - E - Q \tag{6.2}$$

where dW is the daily change in water content in the (thawed) soil profile of a given thickness, $f(P)$ is the daily precipitation effectively entering the soil after accounting for canopy interception, snowmelt and accumulation dynamics and soil saturation, E is the daily water loss from the soil by transpiration, and Q is daily runoff for saturated soil. The transpiration of soil water by the foliage E is assumed to vary exponentially with leaf temperature (T; Monteith & Unsworth, 1990) and linearly with the overall growth rate G. The influence of T on E in the model is strongly controlled by G, g_T and g_W (Evans *et al.*, 2006). A temperature increase in the range $T_{opt1} - T_{opt2}$ will increase g_T, but a concurrent temperature-driven increase in E will reduce soil moisture (W). If the moisture level falls outside the optimal range for growth $W_{opt1} - W_{opt2}$, E

will be limited by g_W through G.

The water balance in the model also considers soil freeze/thaw dynamics and the associated interannual transfer of soil moisture, which is an important hydrological feature in permafrost regions (Ohta *et al.*, 2008). The rate of thawing, S_{thaw}, is modelled as a function of temperature and decreases exponentially with increasing thickness of the thawing layer as:

$$S_{thaw}(t+1) = S_{thaw}(t) + a_1 T(t) e^{a_2 S_{thaw}(t)} \tag{6.3}$$

where a_1 and a_2 are empirical coefficients. The seasonally varying thaw depth decreases the partial growth rate due to moisture $g_W(t)$ as $g_W(t) * S_{thaw}(t)/S_r$, where S_r is the maximum rooting depth. For regions where there are no thaw dynamics S_{thaw} is constant and equal to S_r throughout the year. The parameterisations for thaw dynamics and the other components of soil water balance can have a large impact on the resulting simulations when soil moisture is a significant driver of tree growth. Although the model has been calibrated and extensively tested at high northern latitudes, the realism of moisture and thaw simulations should be evaluated against observations if possible (Vaganov *et al.*, 2006).

The output of the growth module, $G(t)$, is then used to compute the absolute rate ($V_i(t)$) at which each cambial cell grows and divides given its size and position i in the radial tracheid file as,

$$V_i(t) = V_{0,i} G(t) \tag{6.4}$$

where $V_{0,i}$ is the linear dependence of growth rate on position. A detailed description of the simulation of cell growth and xylogenesis in this module is given by Vaganov *et al.* (2006) and Vaganov *et al.* (2011). In short, annual xylem cell production is related to the number of cells in the cambial zone. Cambial cells move through the different phases of the cell cycle as they reach critical thresholds in size and daily growth rate. When daily cell growth rates fall below a minimum threshold, the cambium enters dormancy and the growing season ends. The cells forming the cambium at this point are the first to grow and divide at the beginning of the following growing season. This can be seen as a carry-over effect in simulated ring growth. The cambial activity, and consequently the model growing season, is initiated when the sum of daily temperatures over a given time period reaches a critical level T_{beg}. The simulated annual tree-ring width (TRW) corresponds to the normalised number of non-cambial cells N formed during the growing season of that year through the processes of cell growth, division and differentiation. The standardised ring width for a given year τ is computed as the ratio between the annual number of cells for that year N_τ and the mean annual number of cells $\hat{N}$ computed over the simulation period,

$$TRW_\tau = \frac{N_\tau}{\hat{N}}. \tag{6.5}$$

The model has about 30 primary parameters based on empirical and experimental data (Table 6.1), mainly from Siberia (Vaganov *et al.*, 2006). The main output consists of standardised annual tree-ring width chronologies, simulated daily growth rates (G, g_E, g_T and g_W) and annual number of cambial cells. The simulated chronologies represent the idealised climate signal in

tree growth at a given location and should be comparable with mean climate-sensitive tree-ring chronologies derived from appropriately detrended ring-width measurements, routinely produced by dendrochronologists. Differences between the simulated and real-world chronologies may be related to deficiencies in model structure, uncertainties in the meteorological forcings and to the influence of process not explicitly modelled, such as CO_2 fertilisation, nutrient dynamics, interseasonal carbon remobilisation, carbon allocation, tree competition and stand disturbance. In addition, errors and methodological biases in the site chronologies such as those described in the previous section will also lead to differences with simulated chronologies, particularly at decadal and longer time-scales and near the ends of the series.

The VS-Lite model is a simple parameterisation of the complex process of cambial dynamics underlying tree-ring growth that relies on a simplified version of the principle of limiting factors used in the environmental growth module of the full VS model (Tolwinski-Ward *et al.*, 2011). It was created as a compact mechanistic representation of tree growth as a function of climate, which can be efficiently inverted for regional paleoclimate reconstruction via computationally-demanding Bayesian methods. As a result, the model has 12 parameters and requires only latitude and more readily available mean monthly temperature and precipitation data as inputs. Monthly soil moisture is simulated using empirical equations from the one-layer 'Leaky Bucket' model (Huang *et al.*, 1996). Unlike in the full VS model, the VS-Lite moisture estimate does not account for snow and thaw dynamics.

The growth response functions for temperature and moisture in VS-Lite have no upper bound for the optimal range and thus involve only two parameters instead of four. The first parameter represents the temperature (T_1) or moisture (M_1) threshold below which growth will not occur, while the the second is the lower bound for the optimal range of temperature (T_2) or moisture (M_2). This simplification is justified because the upper bounds of the original response function are seldom reached in practice and thus the model is insensitive to these thresholds (Tolwinski-Ward *et al.*, 2011). The overall and partial growth rates due to moisture, temperature and light are computed in a similar way to that in the full model but at a monthly rather than daily resolution. As a result of the simplifications, the timing of the start and end of the growing season can not be explicitly determined in VS-Lite. The simulated annual tree-ring chronology is obtained by normalising the integral of the overall growth response function (G) computed over an arbitrary number of months spanning the actual growing season.

6.2.3.2 Simulation setup and model calibration

The VS model was used to explore the extent to which shifts in limiting factors and non-linear growth responses can explain the empirical evidence for changing relationships between climate and white spruce growth over recent decades in three locations in Northwestern North America (D'Arrigo *et al.*, 2008): (1) *Arrigetch* (1586–1975, 716 m asl), a treeline site in the Brooks Range of Alaska studied by Jacoby & D'Arrigo (1995), (2) *Twisted Tree-Heartrot Hill* (TTHH; 1459–1999, 915 m asl), an elevational tree line site in the Yukon Territory, Canada studied by D'Arrigo *et al.* (2004), and (3) *Thelon River Sanctuary* (1288–2004, 160 m asl), a site located in the latitudinal treeline in Nunavut in the northern interior of Canada studied by D'Arrigo *et al.* (2009). These three tree-ring sites were chosen because their change in climate response has been well documented in the literature using traditional correlation analysis but no modelling work

Table 6.1: Parameters of the VS and VS-Lite models. Parameter values are the defaults used by Vaganov *et al.* (2006) and Evans *et al.* (2006) for the VS model and by Tolwinski-Ward *et al.* (2011) for VS-Lite. Where appropriate, ranges for parameter values are indicated in brackets.

Parameter	Description	Value
Full VS model		
Temperature response function		
T_{min}	Minimum temperature for growth (°C)	5
T_{opt1}	Lower optimal temperature for growth (°C)	18
T_{op2}	Upper optimal temperature for growth (°C)	24
T_{max}	Maximum temperature for growth (°C)	31
Moisture response function		
W_{min}	Minimum soil moisture for growth (wilting moisture;v/v)	0.04
W_{opt1}	Lower optimal soil moisture for growth (v/v)	0.2
W_{opt2}	Upper optimal soil moisture for growth (v/v)	0.8
W_{max}	Maximum soil moisture for growth (v/v)	0.9
Water balance		
k_1	Fraction of precipitation reaching the soil (dimensionless)	0.72
k_2	First coefficient for transpiration (mm/day)	0.12
k_3	Second coefficient for transpiration (1/degrees)	0.175
P_{max}	Maximum daily precipitation infiltrating in the soil (mm)	20
S_r	Rooting depth (mm)	1000
T_{melt}	Sum of temperature for starting soil thawing (^{o}C)	60
t_{melt}	Period for summing temperatures for soil thawing (days)	10
a_1	First coefficient for soil thaw (mm/^{o}C)	10
a_2	Second coefficient for soil thaw (1/day)	0.006
SN_r	Rate of snow melting (mm/^{o}C/day)	1
SN_{mt}	Minimum temperature for snow melting (^{o}C)	0
Λ	Rate of soil water drainage (dimensionless)	0.001
Cambial module		
T_{beg}	Temperature sum to starting growth (^{o}C)	60
t_{beg}	Period for temperature sum (days)	10
V_{cr}	Critical rate of cell transition to resting (μm/days)	0.04
b_1	Coefficients of growth rate function from position j (μ m/days)	0.42
b_2	$V_o(j) = b_1 + b_2 j$ (μ m/days)	0.25
b_3	Coefficients of minimum growth rate fucntion (μ m/days)	-1.62
b_4	$V_m in = b_3 + b_4 j$ (μ m/days)	0.54
v_0	Growth rate in phase S, G_2 and M (μ m/days)	1
Y_{G1}	Maximum cell size in phase G_1 (μ m)	8
Y_S	Maximum cell size in phase S (μ m)	9
Y_{G2}	Maximum cell size in phase G_2 (μ m)	9.5
Y_M	Maximum cell size in phase M (μ m)	10
d_t	Tangential tracheid size (μ m)	40
VS-Lite model		
Temperature response function		
T_1	Minimum temperature for growth (∘C)	[0 8.5]
T_2	Optimal temperature for growth (°C)	[9 20]
Moisture response function		
M_1	Minimum moisture for growth (v/v)	[0.01 0.03]
M_2	Optimal moisture for growth (v/v)	[0.1 0.5]
Water balance		
α	First coefficient for runoff (1/month)	0.093
μ	Second coefficient for runoff (dimensionless)	5.8
m	Third coefficient for runoff (dimensionless)	4.886
W_{max}	Maximum moisture held by soil (field capacity; v/v)	0.76
W_{min}	Minimum moisture held by soil (wilting point; v/v)	0.01
d_r	Rooting depth (mm)	1000
Integration period for growth		
I_0	Relative month for integration start	-4
I_f	Relative month for integration end	12

exploring the mechanisms has been published. Moreover, these sites are central to the issue of changing climate sensitivity of tree growth in recent decades (D'Arrigo *et al.*, 2008). The

data were obtained from the ITRDB. Note that these chronologies were not used in correlation analysis and are not included included in the network of 115 sites described in Supplementary Table E1 because not all sites spanned the complete common period 1950–2000.

For each site, daily precipitation and temperature data from the nearest meteorological station having the longest and more continuous records were used to drive the model: (1) *University Experimental Station* for Arrigetch – 400 km south and ∼850 m lower than the sampling site, (2) *Baker Lake* for Thelon – 378 km west and ∼140 m lower than the sampling site, and (3) *Dawson* for TTHH – 152 km south and ∼906 m lower than the trees. Data were obtained from the Global Historical Climatology Network (GHCND, `ftp://ftp.ncdc.noaa.gov/pub/data/ghcn/daily/`; Klein Tank *et al.*, 2002) and the Adjusted Historical Canadian Climate Data (AHCCD, `http://www.cccma.ec.gc.ca/hccd/`) developed by the Meteorological Service of Canada (Vincent *et al.*, 2002; Mekis & Vincent, 2011). No seasonal soil freeze/thaw dynamics was used in the simulations because the simulated thaw dynamics appeared unrealistic and had a large impact on volumetric soil moisture. Therefore, a constant soil depth of 50 cm was used.

Difficulties in constraining model parameters have hampered modelling studies in these remote settings. In this study for the first time, a generic Bayesian approach as outlined by Van Oijen *et al.* (2005) was used to conduct a probabilistic calibration of the VS model and provide uncertainty estimates in simulated tree growth at each site. In this framework, the uncertainty in model parameterisation is represented as a probability distribution over the parameters, which expresses our initial knowledge about these uncertain quantities. This initial probability distribution, and hence our knowledge about the parameters, is then updated conditional on new information from experimental or field observations (e.g., standardised tree-ring chronologies), expressed in terms of the likelihood of the model output being equal to the available data. In a statistical sense, given a model parameter vector θ and data $\mathbf{D}$, the Bayesian calibration of a dynamical model $\mathbf{M}$ involves computing the posterior distribution $p(\theta|\mathbf{D})$ according to Bayes's Theorem:

$$p(\theta|\mathbf{D}) = cp(\mathbf{D}|\theta)p(\theta) \tag{6.6}$$

where $c = p(\mathbf{D})^{-1}$. c is a normalisation constant and does not need to be computed explicitly. $p(\mathbf{D}|\theta)$ is known as the likelihood function of θ, and $p(\theta)$ as the prior distribution for θ.

A subset of 10 critical model parameters was selected for calibration (Table 6.2). This includes the 8 parameters of the response functions for moisture and temperature, the rate of drainage, and the critical temperature sum for starting growth. Therefore, $\theta = (T_{min}, T_{opt1}, T_{opt2}, T_{max}, W_{min}, W_{opt1}, W_{opt2}, W_{max}, \Lambda, T_{beg})$. Each parameter was given a flat (uniform) prior distribution $[\theta_i^{min}, \theta_i^{max}]$ with physically plausible minimum and upper bounds based on the literature (Vaganov *et al.*, 2006; Evans *et al.*, 2006; Anchukaitis *et al.*, 2006) and previous experimentation with the model (Table 6.2). If the strength of the climate signal in the sampled tree-ring chronologies is sufficiently strong, the uncertainty (spread) of the posterior distribution of the parameters should decrease, otherwise the posteriors will not differ much from their flat priors.

Model calibration was then performed by maximizing the negative logarithm of a likelihood function (Van Oijen *et al.*, 2005; Schoups & Vrugt, 2010), which quantifies the probability that

the observed tree-ring chronology at a given site was generated by a particular parameter set, accounting for measurement error. For simplicity, the measurement error was set to 10% of the mean value and assumed to be uncorrelated and normally distributed with zero mean. An efficient Markov-Chain Monte Carlo (MCMC) scheme based on the differential evolution adaptive Metropolis algorithm (DREAM) was used to sample the joint posterior parameter distribution (Vrugt *et al.*, 2009; Laloy & Vrugt, 2012). DREAM runs multiple Markov chains (one for each parameter) in parallel and uses a discrete proposal distribution to efficiently evolve the sampler toward the posterior distribution. The first 10% of the iterations were discarded as unrepresentative 'burn-in' period where the chains are more related to their initial starting points (Gelman *et al.*, 2013). Convergence to the stationary posterior distribution is reached when the variance between chains no longer exceeds the variance within each individual chain. This was evaluated using the $\hat{R}$ statistic (Gelman & Rubin, 1992).

The last 20% of the iterations were considered as a representative sample of the posterior and then were thus used to compute statistics of expectation and spread of the distribution of each parameter and characterise model predictive uncertainty. The maximum a *posteriori* (MAP) estimation of θ, i.e., the iteration that maximises the likelihood, was used as the calibrated parameter set to run the model. The calibration was performed independently for the SPL10 and NEGEX chronologies at each site using the initial 20 years of the corresponding meteorological record. However, only the results for the SPL10 chronologies are shown here. The ability of the calibrated model to simulate tree growth was verified by comparing the site chronologies with the simulations over the remaining common period, which includes the most recent decades when the apparent changes in climate sensitivity of tree growth have occurred.

The VS–Lite model was used to characterise the general patterns of climate limitation on tree growth across the entire chronology network using the same gridded temperature and precipitation data utilised for empirical correlation analysis. The model was calibrated over the period 1950–1970 using an inbuilt Bayesian approach described in detail by Tolwinski-Ward *et al.* (2013). The lack of snow dynamics on simulated soil moisture is the main caveat of the application of this model in the boreal region.

6.2.4 Relationship between tree growth and variations in growing season and DGVM-based productivity

The response of tree growth to variations in the growing season was evaluated by comparing the SPL10 tree-ring chronologies with the suite of gridded parameters describing the timing and magnitude of the thermal (STS, ETS, LTS, PEAK-TEM and TI-TEM; see Table 3.1), and photosynthetic (SOS, EOS, LOS, PEAK-NDVI and TI-NDVI) growing seasons developed in Part I of this thesis. Correlations were computed using mutually 10-year high-pass filtered data over the period 1950–2000 for the thermal growing season (2.5° × 3.75°) and over the period 1982–2000 for the photosynthetic growing season (8 × 8 km).

Finally, the consistency between variations in tree growth inferred from tree-rings and Gross Primary Productivity (GPP) derived from an ensemble of 10 DGVMs was evaluated (Sitch *et al.*, 2013). Each SPL10 chronology was correlated against 10-year high-pass filtered summer GPP from the co-located grid box.

6.3 Results

6.3.1 Correlations between tree rings and climate

Figure 6.2 summarises the correlations between the 115 SPL10 tree-ring chronologies and monthly 10-year high-pass filtered moisture and temperature variability over the period 1950–2000. Correlation patterns suggest that despite the northerly location, annual tree growth anomalies through most of the region are strongly associated with moisture variability during the current spring and the previous summer as indicated by highly significant negative correlations with temperature and positive correlations with surface soil moisture estimates based on GLDAS-2 Noah. The patterns of correlation with monthly scPDSI are less significant and differ substantially from those of simulated soil moisture, except for sites south of 65°N. A simple comparison between the annual cycles of soil moisture simulated by Noah and Snow Water Equivalent (SWE) from Globsnow shows that the seasonality of simulated moisture is highly consistent with snowpack dynamics at the grid boxes corresponding to the tree-ring sites (Supplementary Figure E1). This suggests that the difference in the correlation patterns between the two products and interannual tree growth might be related to limitations in the ability of the scPDSI water balance model to correctly represent soil moisture dynamics at the northernmost sites, most of which are strongly clustered along the latitudinal treeline (Figure 6.1).

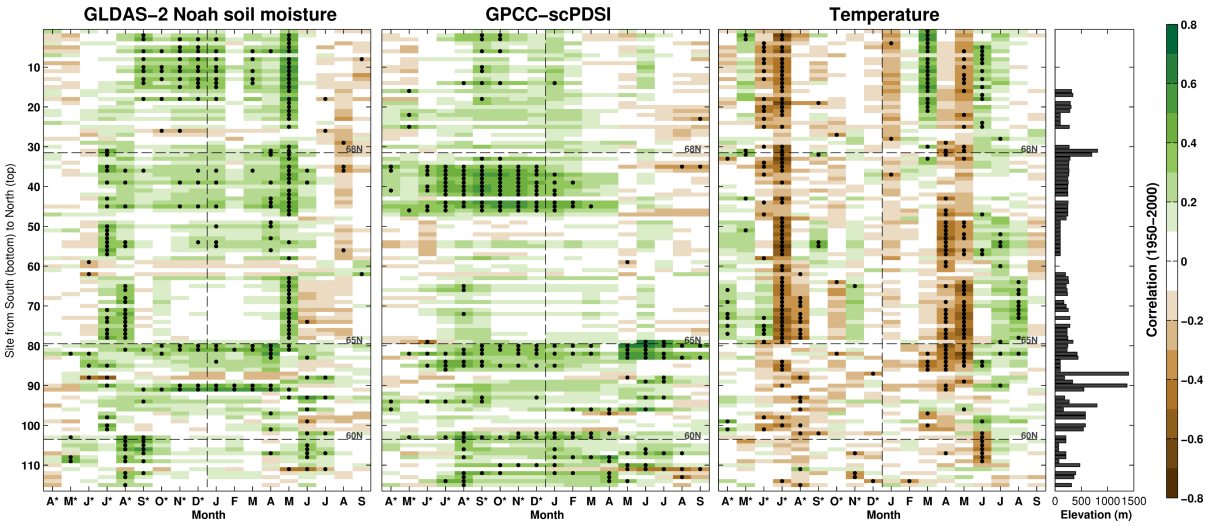

Figure 6.2: Correlation between each SPL10 tree-ring chronology in the network (rows) and monthly surface soil moisture (0-10 cm), scPDSI and mean air temperature (columns) between 1950 and 2000. Correlations are given for an 18-month window from April of the previous growing season (*) to September of the current growing season. The stippling indicates months with significant correlations ($p < 0.05$). The elevation of the chronologies is shown in the right panel.

Dynamic regression with the Kalman filter indicates that the spring and summer moisture responses of tree growth revealed by the correlations with temperature and simulated soil moisture are generally stable through time on a year-to-year basis (Figure 6.3). However, some sites do display a moderated degree of time-dependence in their responses to current May and previous July temperatures and moisture.

The regional clustering of tree-ring sites with similar climate responses based on correla-

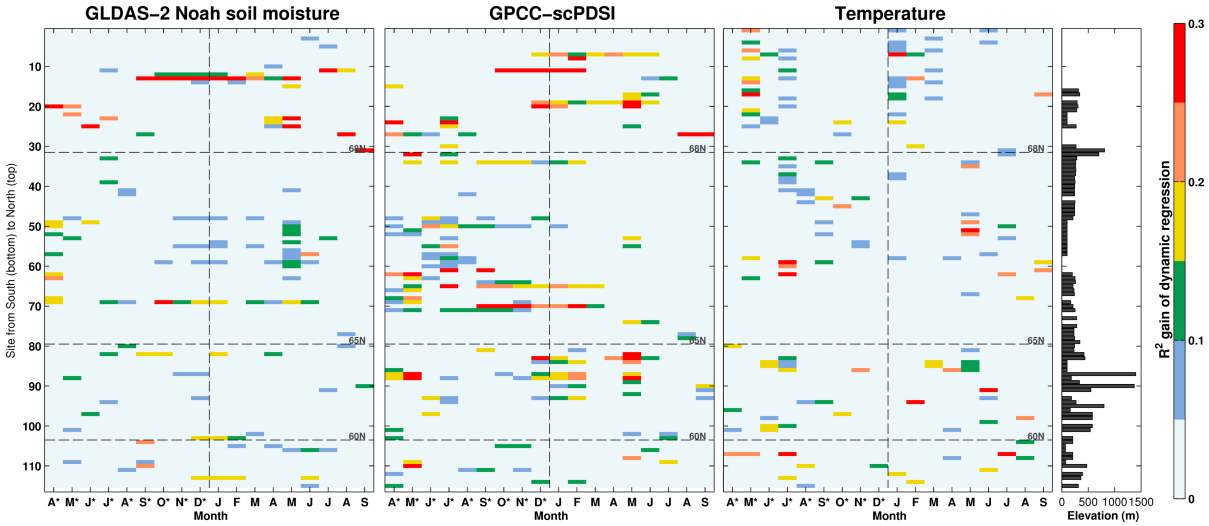

Figure 6.3: Additional variance (R^2) explained by the dynamic Kalman filter regression model between the SPL10 chronologies and monthly air temperature and soil moisture compared with a standard time-invariant linear regression model. R^2 values are shown for months when the dynamic regression model was selected over the standard model based on the minimum Akaike Information Criteria (AIC). Higher R^2 indicates stronger time-dependence in the associations.

tions with temperature and the scPDSI is shown in Figure 6.4a–b. The first cluster includes sites located at relatively high elevations and along the latitudinal treeline. Trees at these sites show a pattern of growth response to moisture over a short period during the previous summer and current spring (i.e., concurrent negative correlations with temperature and positive correlations with the scPDSI), followed by a positive response to temperature during the current summer (Figure 6.4b). The second cluster, representing most of the tree-ring sites (N=75), shows a stronger and more sustained growth response to moisture conditions between the previous summer and the current spring. Similar temporal patterns of short versus extended period of moisture response are obtained when using Noah soil moisture instead of the scPDSI for cluster analysis (Supplementary Figure E2). However, the growth response to spring moisture availability is more clearly represented and the spatial clustering of sites changes in the southern part of the network in Canada.

Negative growth responses to July temperatures during the previous season and the current spring are more common and significant in Alaska and northwestern Canada (Figure 6.4c–d), whilst significant positive responses to current summer temperature tend to occur in colder locations at high elevations and along the latitudinal treeline (Figure 6.4e). The negative growth response to previous July temperature across most of Alaska is consistent with even stronger negative correlations with maximum thaw depth (Figure 6.5). Similarly, growth at some high-elevation sites on the west coast that respond positively to current summer temperatures show comparatively stronger positive correlations with maximum thaw depth during the current growing season. The apparently stronger association with thaw depth than with simple air temperatures suggests that soil thermal regime has an important influence on modulating tree physiology and growth, particularly in the discontinuous permafrost region.

Positive responses to soil moisture availability during the previous summer and current spring inferred from both Noah and the scPDSI are widespread along the western interior of Canada and interior Alaska (Figure 6.4f, Supplementary Figure E2). The positive response of tree growth to

spring soil moisture availability in this region suggests an influence of winter snowpack, however tree growth is poorly correlated with estimates of maximum SWE based on either the snow model of the scPDSI (Figure 6.4g) or Globsnow data (not shown).

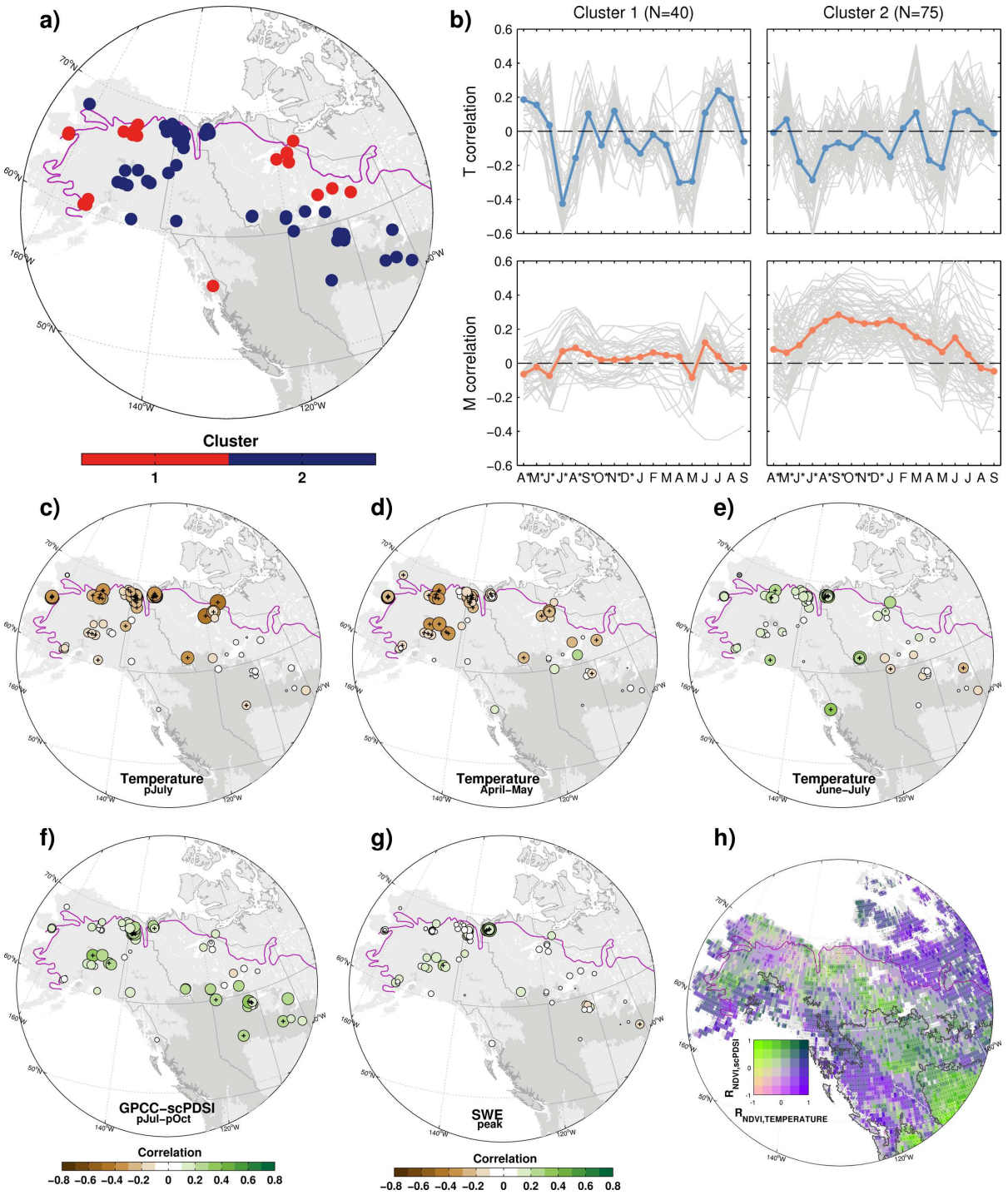

Figure 6.4: Clustering of tree-ring sites based on their patterns of monthly correlations with temperature and the scPDSI. (a) Map of dominant k-means clusters of sites with similar climate response. (b) Individual and cluster-averaged monthly correlations with temperature (T) and the scPDSI (M). (d–g) Spatial distribution of the strongest correlations between tree growth (SPL10) and temperature, scPDSI, and maximum SWE estimated by the snow model of the scPDSI. (h) Map of moisture and temperature constraints of summer NDVI as explained in Figure 5.5. The dark gray shading in the maps denotes the boreal forests. The purple and cyan lines indicate the location of the treeline and the southern edge of the discontinuous permafrost, respectively.

Overall, linear correlations between the SPL10 tree-ring chronologies and monthly temperature and estimated moisture availability suggest a dominant moisture limitation of white spruce growth across the study domain, predominantly reflecting conditions during both previous and current growing seasons. This pattern of response is broadly consistent with the dominant moisture limitation of peak summer vegetation greenness in the same regions that were shown in Chapter 5 for correlations between summer NDVI and summer temperature and scPDSI (Figure 6.4h).

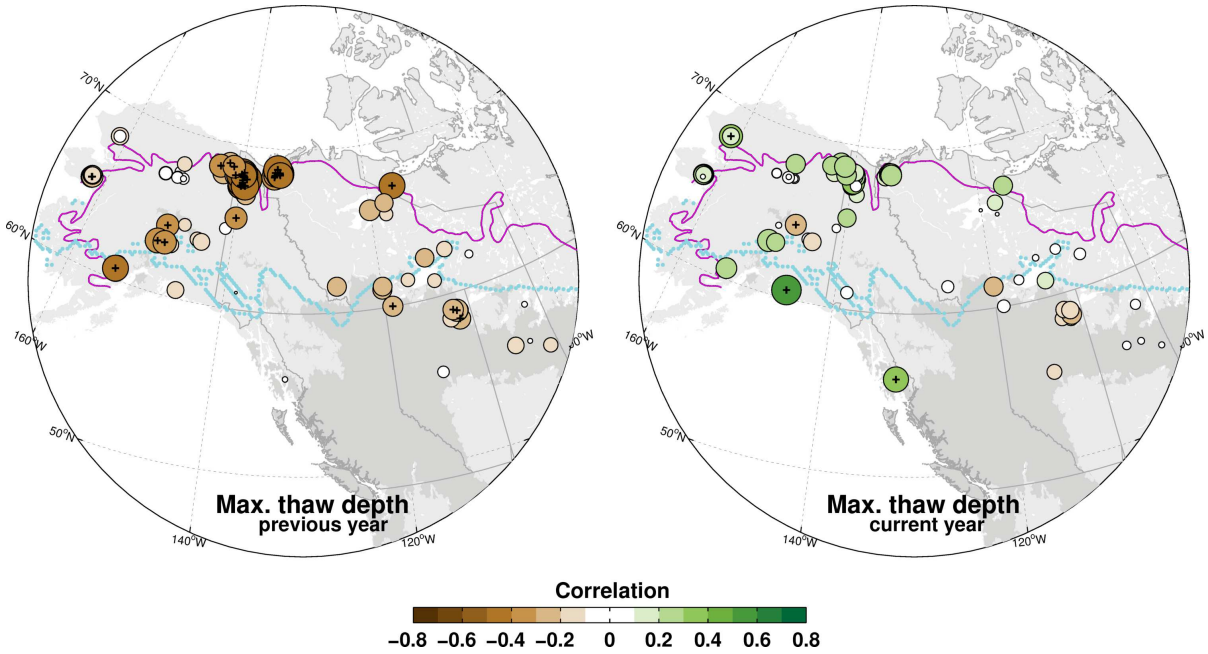

Figure 6.5: Correlations between year-to-year variations in tree growth (SPL10) and maximum thaw depth during the previous and current growing seasons. The small black crosses indicate significant ($p < 0.05$) correlations.

6.3.2 Relationships between tree-ring width and growing season parameters

Tree-ring width over most of the discontinuous permafrost region is positively correlated with the start of the current thermal growing season (Figure 6.6), suggesting that warmer and earlier growing seasons tend to have an adverse effect on annual tree growth in these predominantly moisture-sensitive boreal forests. This is consistent with the ubiquitous negative growth response to April-May monthly temperature and the simultaneous positive response to moisture availability shown above in Figure 6.2. The timing of the termination of the thermal growing season is poorly correlated with interannual variations in tree growth, whilst negative correlations between the duration of the thermal season and tree growth at some sites reflect the negative influence of earlier timing of the start.

Unlike the timing of the start, the magnitude of peak temperatures during the thermal growing season is positively correlated with concurrent tree growth (Figure 6.6). Again, this is consistent with the positive growth response to current summer temperature shown in Figure 6.2. Similarly, negative growth responses to previous summer temperature in the Northwestern Territories and southern Alaska are consistent with negative correlations between tree growth

and peak thermal growing season temperature. Time-integrated temperatures over the entire thermal growing season have a generally adverse effect on tree growth during the following year, as indicated by significant negative correlations at several sites near the latitudinal treeline.

Simple correlations between tree-ring width and parameters of the photosynthetic growing season over the short period 1982–2000, are generally consistent with those described above for the thermal growing seasons (Figure 6.7), but are strongly influenced by good agreements between a few extreme anomalies such as the cooling associated with Pinatubo Eruption. An interesting feature is that tree growth at some sites near the latitudinal treeline in northeastern Alaska shows concurrent significant correlations with the start, end and peak of the photosynthetic growing season as well as with time-integrated NDVI over the previous growing season. This suggests some degree of agreement between tree-ring width and canopy photosynthesis at these locations.

6.3.3 Simulated climate controls of regional tree growth based on VS-Lite

Based on significant correlations between the simulated and observed chronologies during the recent period 1971–2000, the locally-calibrated VS-Lite model was able to successfully simulate 37% of the 115 NEGEX tree-ring chronologies (Figure 6.8). A simple cluster analysis of the monthly growth rates due to moisture and temperature identifies three distinct patterns of climate limitation during the growing season (Figure 6.8b,d). These patterns range from a dominant temperature limitation in sites with very short growing seasons in western Alaska to a mixed temperature and moisture limitation in the northern Yukon and a dominant moisture limitation in sites with longer growing seasons in interior Alaska and the Canadian boreal forest in northern Alberta.

Despite its simplicity and lack of snow dynamics, the model is still able to capture most of the decadal to multidecadal variability of the chronologies during the 20th century, including the increase in tree growth since the 1970s in more temperature-limited sites (Figure 6.8c). An examination of the most limiting factor of monthly growth rates during the growing season at sites with mixed climate response shows that the model does not simulate any widespread temporal change toward increasing moisture limitation (Figure 6.9).

Similar patterns of climate limitation are obtained when simulating SPL10 chronologies, but fewer (21%) chronologies are successfully simulated (Supplementary Figure E3). Despite the caveats of this simple application of the VS-Lite model, these results are in general broad agreement with the regional pattern of moisture limitation of tree growth revealed by simple linear correlations.

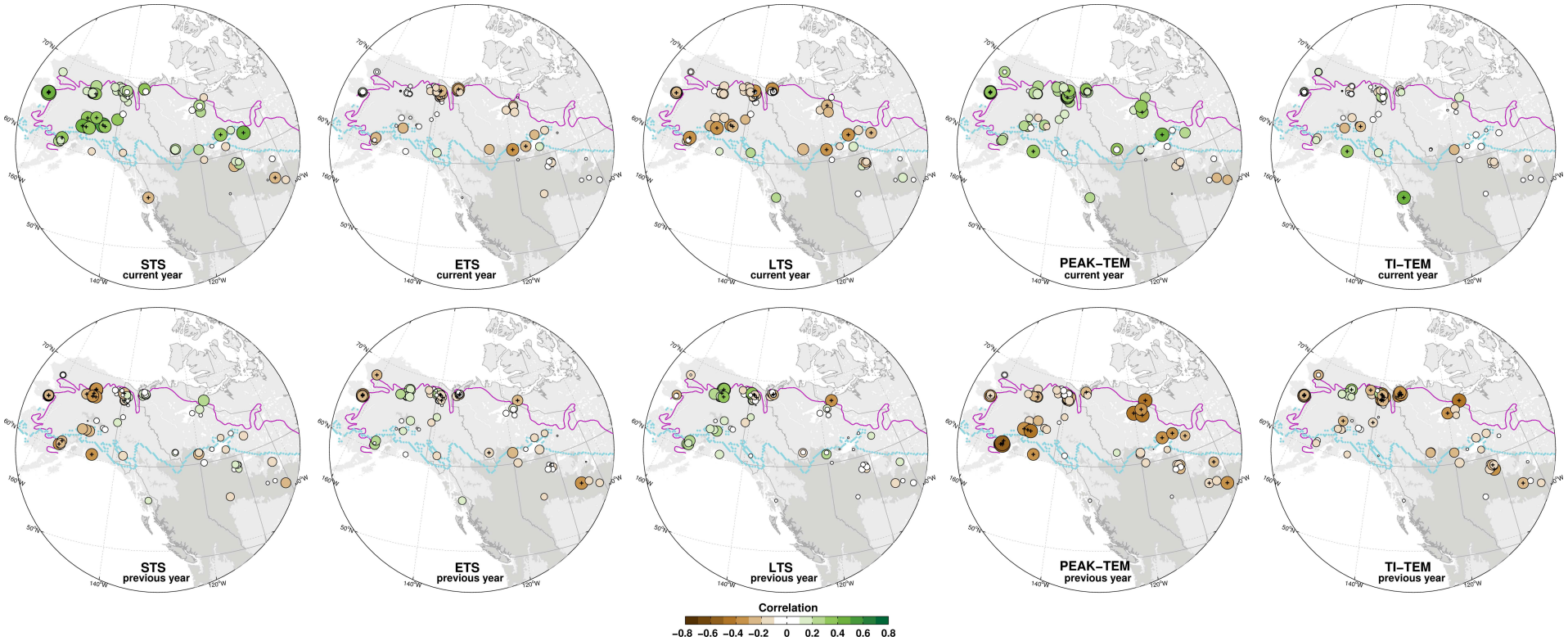

Figure 6.6: Correlations between year-to-year variation in tree growth and variation in timing (STS and ETS), length (LTS), peak and time integrated temperatures (TI-TEM) of the previous and current thermal growing seasons. The small black crosses denote significant ($p < 0.05$) correlations.

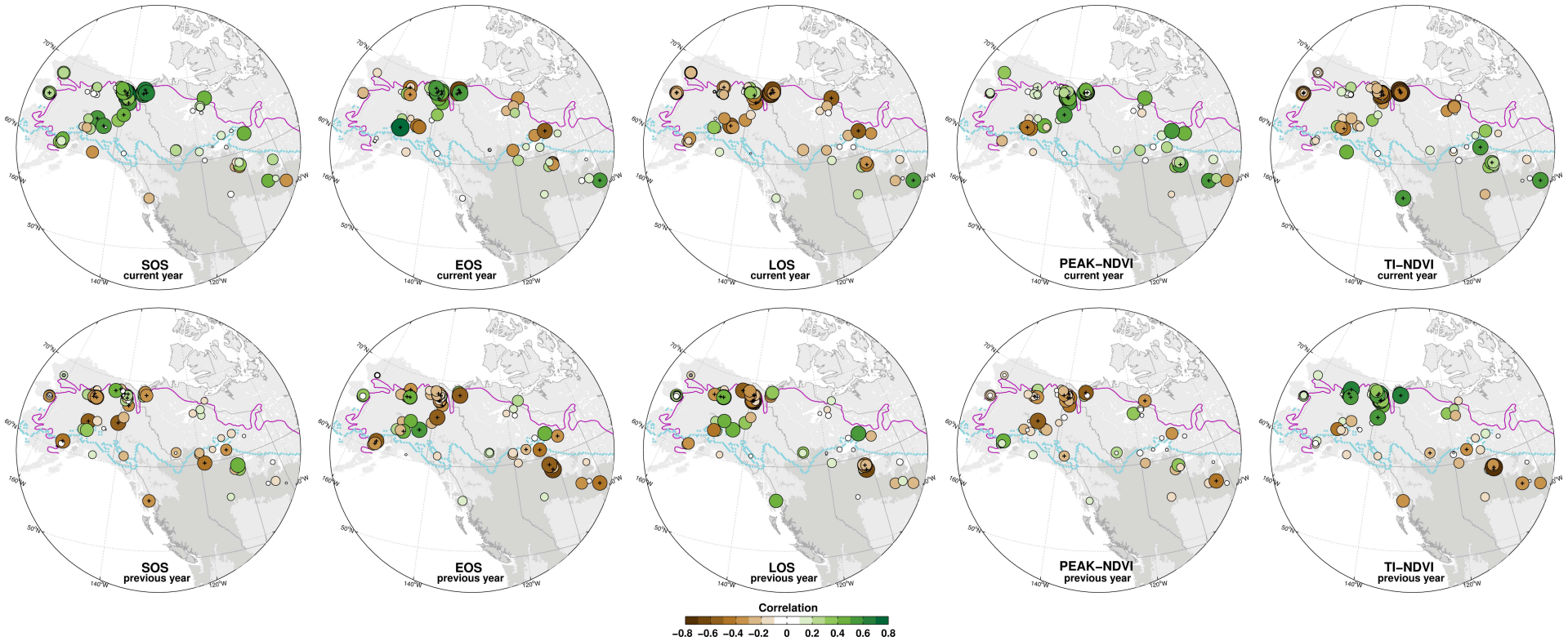

Figure 6.7: Correlations between year-to-year variation in tree growth and variations in timing (SOS and EOS), length (LOS), peak and magnitude (TI-NDVI) of the previous and current photosynthetic growing seasons. The small black crosses denote significant ($p < 0.05$) correlations.

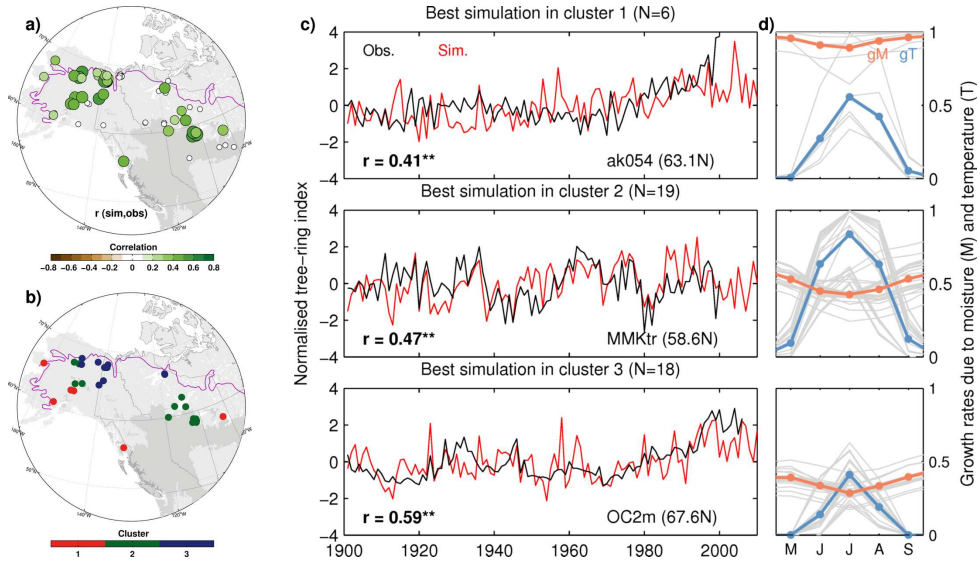

Figure 6.8: Distinct regional patterns of simulated climate limitation of tree growth. (a) Spatial distribution of significant correlations between simulated and observed NEGEX tree-ring chronologies during the verification period 1971–2000. White circles in the map represent chronologies that were not successfully simulated. (b) Regional clusters of simulated climate limitation based on growth rates due to moisture (g_M, orange) and temperature (g_T, blue). (c) Best simulated tree-ring chronology in each cluster. (d) Mean and individual growth rates due to moisture and temperature in each cluster.

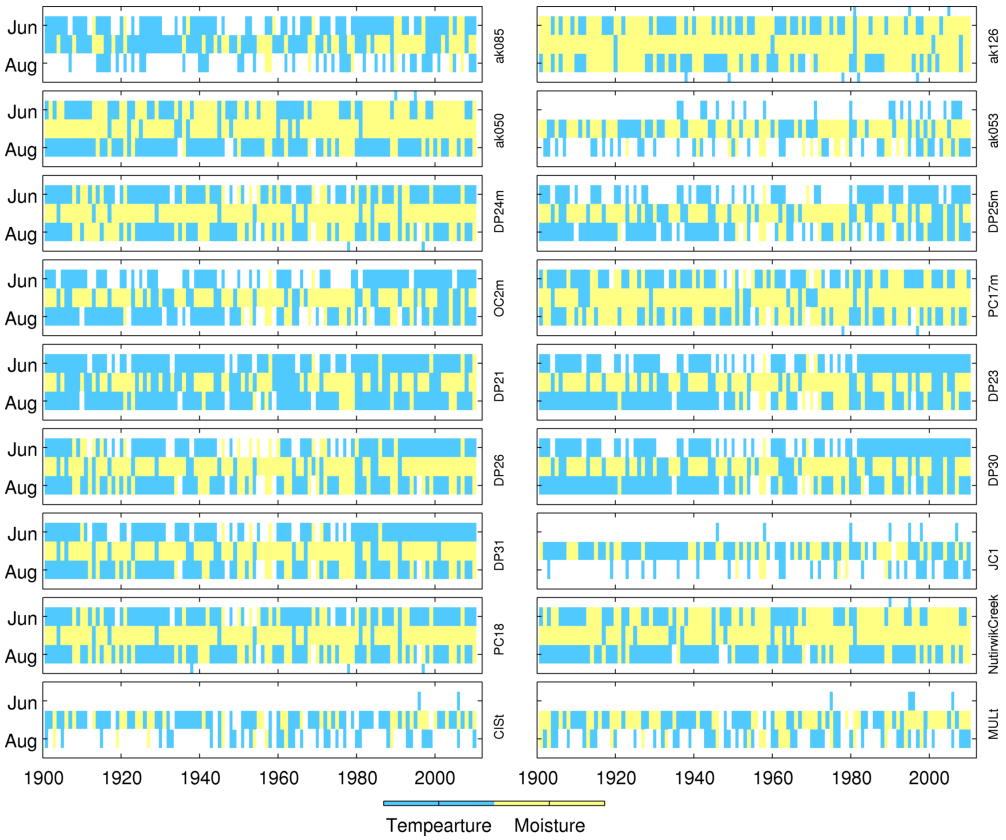

Figure 6.9: Temporal evolution of dominant climatic limitation of simulated tree-ring chronologies at sites with mixed temperature-moisture limitation (cluster 3). Blue indicates that temperature (g_T) is the most limiting factor for the overall monthly growth rate (G), whilst yellow indicates that moisture (g_M) is the most limiting factor.

6.3.4 Simulated climate controls of tree growth in 'divergence' case studies

Figure 6.10 summarises the results of the Bayesian calibration of the VS model in the three selected case studies characterised by tree-ring divergence at decadal and longer time scales. To investigate climate controls on year-to-year growth variability at these sites, the calibration was performed using SPL10 tree-ring chronologies over the first 20 years of available climate data, which in all cases corresponds to periods before the 1970s (1918–1937 for Arrigetch, 1903–1920 for TTHH and 1951–1970 for Thelon). The calibrated parameter values are summarised in Table 6.2.

Table 6.2: Calibrated VS model parameters for the three case studies of 'tree-ring divergence'. The prior range and posterior mean ($\bar{\theta}$), coefficient of variation (CV) and maximum *a posteriori* (θ_{MAP}) statistics are indicated for each parameter. The calibration was performed using SPL10 tree-ring chronologies over the first 20 years of overlap with the available meteorological records at each site, without accounting for differences in elevation between the tree-ring sites and the meteorological stations. The calibration periods were 1918–1937 for Arrigetch (ARRI), 1903–1920 for TTHH and 1951–1970 for Thelon (THEL).

Parameter	Prior	Posterior distribution								
		$\bar{\theta}_i$			CV_i			θ_{MAP}		
	range	ARRI	TTHH	THEL	ARRI	TTHH	THEL	ARRI	TTHH	THEL
T_{min}	4.0-7.0	6.34	5.76	6.74	7.2	11.7	0.61	6.37	6.00	6.73
T_{opt1}	7.1-12.0	11.89	9.05	7.13	11.7	12.9	2.5	11.63	8.48	7.16
T_{op2}	12.1-18.0	17.87	17.80	13.81	2.7	4.3	11.3	17.44	17.00	17.76
T_{max}	18.1-24.0	22.81	20.17	23.16	2.1	6.6	7.1	23.07	20.79	23.78
W_{min}	0.04-0.15	0.06	0.05	0.05	37.7	35.1	35.8	0.07	0.12	0.05
W_{opt1}	0.16-0.30	0.17	0.17	0.17	14.9	14.6	18.4	0.17	0.19	0.22
W_{op2}	0.31-0.70	0.53	0.33	0.42	19.2	23.8	21.4	0.57	0.31	0.41
W_{max}	0.71-0.90	0.74	0.75	0.73	7.2	6.7	7.2	0.80	0.74	0.84
Λ	0.0001-0.02	0.0002	0.0003	0.0007	101.1	76.5	64.3	0.0003	0.0007	0.002
T_g	10-60	28.4	30.45	47.43	38.2	40.4	40.1	45.16	15.81	47.15

The uncertainty in the parameters of the temperature and moisture response functions was substantially reduced after calibration, which produces narrower unimodal parameter distributions in most cases. This indicates that the SPL10 chronologies contain a substantial amount of climate signal over the periods used for calibration. The parameters related to soil water drainage and temperature sum for starting growth were not well constrained during the calibration, suggesting that they have limited effect on simulated growth at these sites.

The calibrated temperature response functions for Arrigetch and TTHH strongly suggest a non-linear growth response to mean temperatures because the upper temperature limits for growth limitation were well constrained by the data. Without accounting for differences in absolute temperature between the stations and the tree-ring sites, the calibrated parameters indicate that tree growth at these relatively high-elevation sites increases with temperatures above 6^{o}C but starts to decline when daily temperatures exceed a threshold of about 17^{o}C. The two lower critical moisture thresholds for growth were also well constrained by the data at these sites. Unlike these two sites, the calibrated temperature response function for Thelon does not suggest a growth limitation by high temperatures but the two lower moisture parameters were similarly well constrained despite the fact that this site is located in a relatively cooler environment, at the latitudinal treeline.

Consistent with the reduction of parameter uncertainty in the posterior distributions, the simulated chronologies based on maximum *a posteriori* parameter sets are all significantly corre-

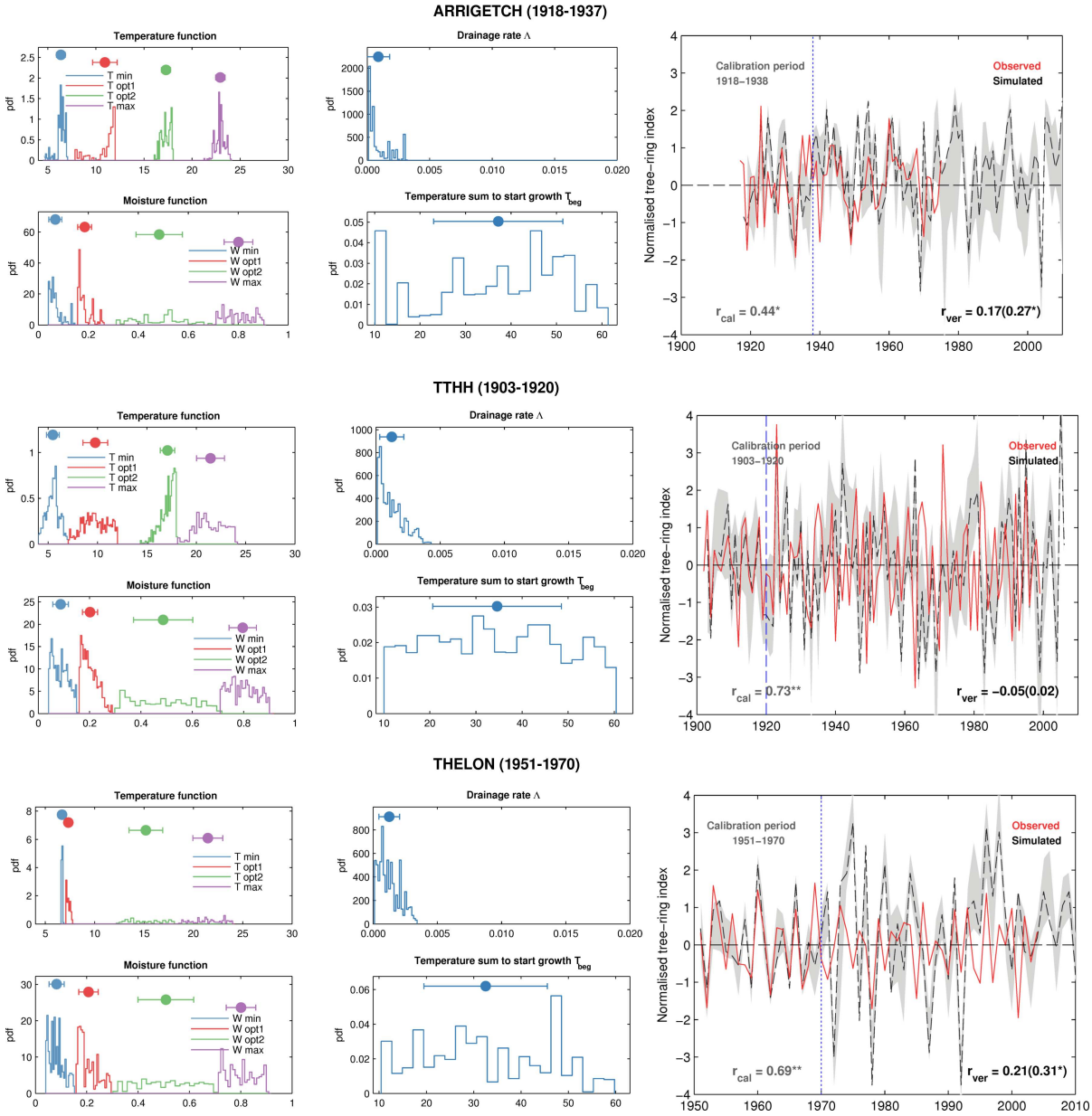

Figure 6.10: Posterior distributions of calibrated parameters of the VS model and simulated tree-ring chronologies at Arrigetch (top), TTHH (middle) and Thelon (bottom). The posterior mean and associated error bars (±1 SD) are shown for each parameter next to the distributions (see also Table 6.2). The right panels show a comparison between the simulated (black) and the observed SPL10 chronology at each site. Correlations are given for the calibration (r_{cal}) and verification (r_{ver}) periods, and the overall correlation is indicated in brackets. The gray shading denotes the 95% confidence intervals of the simulations based on 1000 random samples from the posterior.

lated with the SPL10 tree-ring chronologies during the calibration period (r = 0.44 to 0.73, $p < 0.05$). However, the calibrated model is unable to consistently simulate the observed year-to-year tree-ring width variability during the verification period (Figure 6.10). Expanding the calibration period to the longest possible period in order to capture the full range of variability does not improve the interannual correlations between the simulated and observed SPL10 chronologies but the extra information further constrains the posterior distributions of the response function parameters (Supplementary Figure E4). Although the overall correlation between the simulated

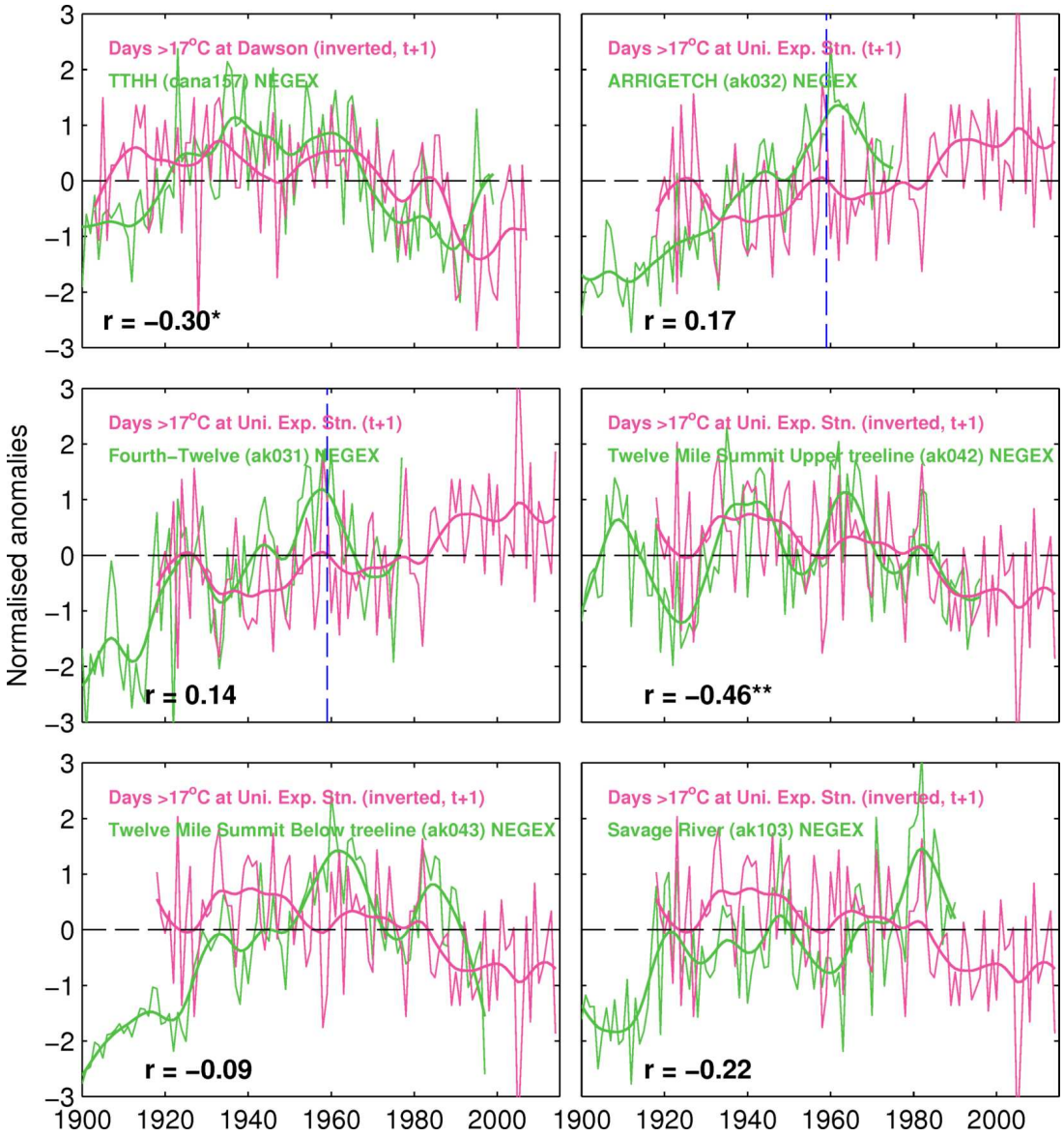

Figure 6.11: Comparison between annual frequency of days exceeding 17°C (purple) and a number of 'divergent' NEGEX tree-ring chronologies (green) in Alaska (ak031, ak032, ak042, ak043 and ak103) and in the Yukon Territory (TTHH – cana157) collected originally by Jacoby & D'Arrigo (1995) and D'Arrigo *et al.* (2004). The bold smoothed lines correspond to a low-pass filter with a period of 15 years to enhance decadal variability. Note that relative ring width declines since around the 1960s are highly consistent with an increasing frequency of days exceeding the 17°C threshold (shown as inverted anomalies) identified in the calibrated response function of the VS model. Also note that the negative effect of high temperatures on tree growth tends to occur during the following growing season. Two sites (ak031 and ak032) display a positive response to high temperatures before the 1960s but thereafter the response turned negative.

and the SPL10 tree-ring chronologies is low, the model correctly simulates growth anomalies in several years but produces out-of-phase anomalies in other years when growth responses in the real chronologies lag climate anomalies. Consequently, the model seems to simulate the climate limitation of tree-ring growth reasonably well but fails to mimic the strong biological persistence apparent in the real chronologies, likely linked to interseasonal carbon remobilisation.

The most significant result of the application of the VS model in these sites is the indication of a non-linear growth response to temperature at some high-elevation forests. This aspect was

further explored by examining temporal changes in the exceedance of the critical threshold of 17^{o}C suggested by the calibrated parameters, above which tree growth starts to decline with increasing temperatures. A simple analysis of daily mean temperature data in the region indicates that the annual number of days with temperatures above this threshold has almost doubled since the 1980s, with a very similar pattern at Dawson and University Experiment Station in Fairbanks (Supplementary Figure E5). The similarity between the two stations suggests that the increase in 'hot days' is unlikely to be related to inhomogeneities in the station records. Although with a smaller magnitude, the increased frequency in hot days is also evident at Baker Lake station, near Thelon.

To evaluate the impact of the increased frequency of extremely high daily temperatures on tree growth, the annual count of days exceeding 17^{o}C derived from Dawson and University Experiment Station records was compared with the NEGEX chronology for TTHH and with a group of other 5 sites near Arrigetch (Figure 6.11). The increase in days exceeding this threshold during recent decades is consistent with declining growth trends in these sites. This negative relationship occurs with one year lag on an interannual basis and is particularly important in TTHH (r = -0.30 for 1902–1999, $p < 0.05$) and in other treeline site called Twelve Mile summit in northern Alaska (r = -0.46 for 1918–1996, $p < 0.01$), described a decade ago by Jacoby & D'Arrigo (1995). Moreover, tree growth at two of the six sites showed a positive correlation with the frequency of hot days before the 1960s but after that time the relationship appears negative. These results do not change when comparing the SPL10 version of the tree-ring chronologies and 10-year high-pass filtered series of hot days (Supplementary Figure E6). Taken together, these modelling and empirical results suggest that the pattern of tree-ring divergence described for these elevational treeline sites in earlier studies appears to be consistent with a non-linear growth response to temperature and the existence of a common physiological threshold above which the effect of temperature is no longer positive.

6.3.5 Climate controls of interannual vegetation productivity simulated by DGVMs and consistency with tree-ring widths and remote sensing observations

The empirical and modelling analyses of tree-ring growth presented above confirm the significant moisture limitation of boreal vegetation productivity along the western interior of North America revealed by the interannual correlations between NDVI and summer climate presented in Chapter 5 (Figure 5.5). Such extensive moisture control of vegetation growth inferred from these complementary ground and satellite-based observational records is unusual in the boreal region and would be expected to be represented in ecosystem models. Interannual correlations between summer DGVM-simulated GPP and summer temperature and scPDSI over the period 1982–2009 indicate that such models are able to reproduce much of this observed regional pattern of moisture limitation, in close agreement with the NDVI climate response (Figure 6.12). This indicates that the dominant plant functional types in the region are reasonably well parameterised in current DGVMs.

Interannual correlations between the SPL10 chronologies and annual GPP during the current and previous year are generally poor and in a few northern sites reflect the negative response of tree growth to temperatures during previous growing season (Figure 6.12). The relationship

between tree-ring width (wood formation or above-ground biomass increment) and productivity (GPP or NPP) is not straightforward due to the important influence of allocation and carbon remobilisation processes on stem growth, which typically result in considerable biological persistence in tree-ring width. This usually results in out of phase interannual anomalies, reducing the correlations.

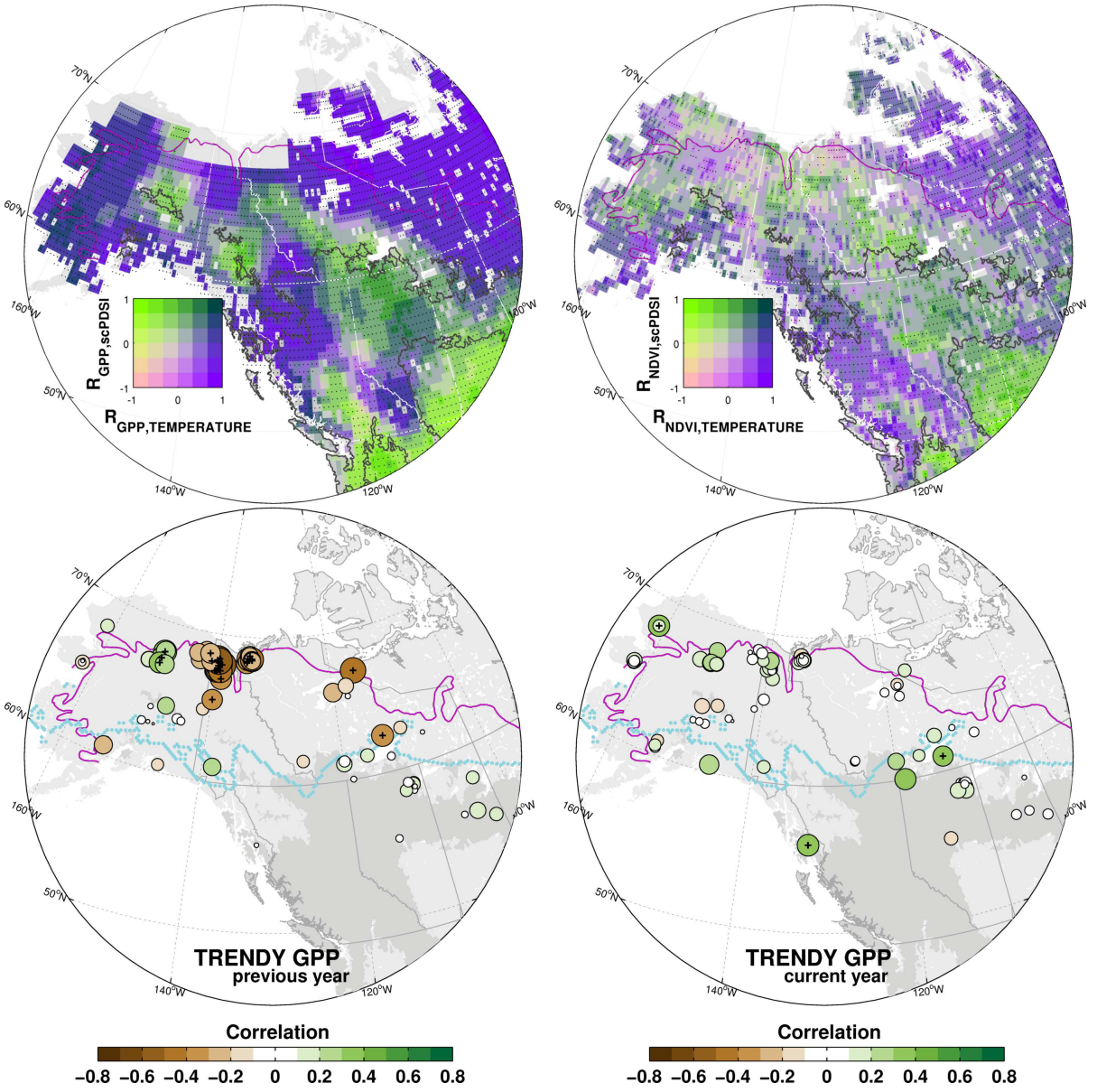

Figure 6.12: Geography of moisture and temperature controls on summer (June–August) NDVI and simulated GPP in northwestern North America during the period 1982–2009. Light greens indicate a strong moisture limitation (i.e., strong positive correlation with moisture and negative correlation with temperature), whilst purple shades indicate a dominant temperature limitation (i.e., strong positive correlation with summer temperature and weak correlation with moisture). The stippling indicates grid boxes where correlations with temperature or with the scPDSI are statistically significant at the 90% confidence level. The lower two panels show the correlations between year-to-year variations in annual tree growth (SPL10) and annual GPP during the previous and current years over the period 1950–2000.

6.4 Discussion

The growth of temperature-limited boreal trees is expected to have increased with warming during recent decades. However, the analysis of standardised tree-ring chronologies of white spruce from some treeline locations of Alaska and northwestern Canada has revealed anomalous tree growth 'declines' or a lack of growth increases with recent warming (D'Arrigo *et al.*, 2008). These observations are at odds with the expected vegetation responses in these environments and raise concerns on boreal forest responses to continued warming. A warming-induced increase in moisture stress (Jacoby & D'Arrigo, 1995; Wilmking & Juday, 2005; D'Arrigo *et al.*, 2009; Griesbauer & Green, 2012) and non-linear growth responses to temperature (D'Arrigo *et al.*, 2004) have been invoked as the most likely causes for these observations, although several other environmental and methodological factors have been proposed (D'Arrigo *et al.*, 2008).

The analysis of a tree-ring chronology network of 115 sites covering a range of environments across northwestern North America shows a significant moisture control of interannual white spruce growth throughout the region (Figure 6.2). This year-to-year moisture control of tree growth is also consistent with regional patterns of moisture limitation inferred from satellite observations of vegetation greenness (Figure 6.4) and vegetation productivity simulated by ecosystem models (Figure 6.12). Correlation analysis indicates that tree growth anomalies across the network are particularly sensitive to moisture availability during the current spring and the previous summer, and thus growth tends to be anticorrelated with temperatures at these times of the year as noticed in earlier studies (Barber *et al.*, 2000; Lloyd & Bunn, 2007; McGuire *et al.*, 2010; Juday & Alix, 2012; Lloyd *et al.*, 2013). As a result, earlier start of the growing season and consequently snowmelt has an adverse effect on tree growth (Figures 6.6–6.7). This implies that further advance of the growing season in spring expected with continued warming (Christidis *et al.*, 2007) will have a negative rather than a positive impact on the growth of moisture-sensitive white spruce forests.

Despite the consistent growth response to moisture during the spring melting period detected using Noah soil moisture estimates, there are no significant correlations between the interannual variability of tree growth and estimates of maximum SWE. The analysis of the NDVI climate responses presented in Chapter 5 and experimental rainfall exclusion studies in the region (Yarie & Van Cleve, 2006; Yarie, 2008) suggest that snowmelt water is important for maintaining tree growth during the subsequent summer. The lack of correlations with SWE could be related to uncertainties in the snow data or could simply indicate that at the location of the tree-ring sites peak SWE is not a good indicator of the actual amount of water effectively staying in the soil after spring melting since most of it can be loss to runoff when the soil saturates. This aspect should be studied in more detail using snow measurements from long-term meteorological stations.

Contrary to earlier suggestions (Jacoby & D'Arrigo, 1995; Wilmking & Juday, 2005; D'Arrigo *et al.*, 2008), there is no clear evidence for a widespread increase in moisture limitation during recent decades, at least on an interannual time scale (Figure 6.3). The interannual correlations between white spruce growth and monthly temperature and moisture seem to be relatively stable over time in most of the tree-ring sites during the period 1950–2000 (Figure 6.3). Furthermore, the monthly growth responses simulated by the VS-Lite forward model, calibrated

locally over the period 1950–1970, do not suggest any apparent shift toward increased moisture limitation over time in the correctly simulated sites (Figure 6.9). Earlier empirical studies based on some of the data analysed here have reported changing growth responses to both temperature and moisture (Wilmking & Juday, 2005; Pisaric *et al.*, 2007; Griesbauer & Green, 2012). However, these earlier analyses have used higher quality station data and longer periods including the early part 20th century, capturing contrasting multidecadal climate regimes (Ohse *et al.*, 2012; Chavardès *et al.*, 2013). Furthermore, the gridded data used for correlations in this study are uncertain due to the lack of stations at the remote northern locations where the sampled trees are located. This could lead to poor correlations with the chronologies and thus no changes in signal could be detected.

The Bayesian calibration of the full VS model enabled the skilful simulation of the three SPL10 tree-ring chronologies at the selected divergence study sites over the calibration period (Figure 6.10). However, the calibrated model was unable to simulate these chronologies over the most recent verification period when the chronologies have been shown to diverge from temperature trends in earlier studies (Jacoby & D'Arrigo, 1995; D'Arrigo *et al.*, 2004, 2008). The most important result of the application of the VS model is that the calibrated parameters suggest a non-linear temperature response of white spruce growth at two of these three sites during the earlier part of the 20th century (Figure 6.10), before the occurrence of divergence. This type of response is consistent with earlier findings of D'Arrigo *et al.* (2004). Using a simple statistical analysis based on monthly data, they suggested that high-elevation temperatures in central Yukon may have exceeded a plant physiological threshold in recent decades and now adversely affect tree growth, possibly as a result of temperature-driven soil moisture deficits. Based on temperature data from Dawson Airport, they estimated that average July-August temperatures exceeding 11.3^{o}C reduce white spruce growth at the TTHH treeline site.

For TTHH, the calibrated VS model suggested an equivalent physiological threshold of around 17^{o}C based on daily data from Dawson and an updated chronology (Table 6.2 and Figure 6.10). A similar threshold value was obtained with the calibrated VS model for the Arrigetch treeline site in northern Alaska using daily meteorological data from Fairbanks. This suggests that this upper limit for optimal growth of white spruce is not restricted to the particular location of the TTHH site. Indeed, the model suggests similar climate response functions for these two distant treeline sites over slightly different calibration periods and even when using different station data. However, the actual absolute threshold at the location of the trees might be lower than the one estimated using these low-elevation and distant meteorological stations. A recent analysis based on regression between ring-width data across Alaska and mean June-July temperatures Williams *et al.* (2011) showed that temperature thresholds for which white spruce growth starts to decline vary between about 9.5^{o}C and 13^{o}C, depending on mean climate conditions of the sites.

An increasing frequency of days exceeding a threshold of 17^{o}C during recent decades appears to be consistent with declining tree growth trends in TTHH, Arrigetch and some other divergent treeline sites in the region (Figure 6.11). The anticorrelation is also consistent at interannual time scales but with a lag of one year in the response of tree growth. Although this finding agrees with the hypothesis of D'Arrigo *et al.* (2004), the VS model does not suggest a clear increase in moisture limitation at these sites during recent decades when this threshold has been

increasingly exceeded. Therefore, this response may be more complicated than simply a decrease in soil moisture as initially hypothesised by D'Arrigo *et al.* (2004).

The Bayesian calibration of the full VS model enabled the skilful simulation of the three SPL10 tree-ring chronologies at the selected divergence study sites over the calibration period (Figure 6.10). However, the calibrated model was unable to simulate these chronologies over the most recent verification period when the chronologies have been shown to diverge from temperature trends in earlier studies (Jacoby & D'Arrigo, 1995; D'Arrigo *et al.*, 2004, 2008). The most important result of the application of the VS model is that the calibrated parameters suggest a non-linear temperature response of white spruce growth at two of these three sites during the earlier part of the 20th century (Figure 6.10), before the occurrence of divergence. This type of response is consistent with earlier findings of D'Arrigo *et al.* (2004). Using a simple statistical analysis based on monthly data, they suggested that high-elevation temperatures in central Yukon may have exceeded a plant physiological threshold in recent decades and now adversely affect tree growth, possibly as a result of temperature-driven soil moisture deficits. Based on temperature data from Dawson Airport, they estimated that average July-August temperatures exceeding 11.3^{o}C reduce white spruce growth at the TTHH treeline site.

An increasing frequency of days exceeding a threshold of 17^{o}C during recent decades appears to be consistent with declining tree growth trends in TTHH, Arrigetch and some other divergent treeline sites in the region (Figure 6.11). The anticorrelation is also consistent at interannual time scales but with a lag of one year in the response of tree growth. Although this finding agrees with the temperature threshold hypothesis of D'Arrigo *et al.* (2004), the lack of skill of the VS model during the verification period in recent decades hampers a robust assessment of the drought mechanism proposed in this early study. Therefore, testing the hypothesis of warming-induced drought stress as the mechanism for this non-linear spruce growth response remains a challenge.

More detailed work with the VS model is needed in these sites to better understand this apparent non-linear climate response and the general lack of model skill during the divergence period. In particular, simulations using improved soil thaw and moisture dynamics should be attempted. The current implementation of soil thaw in the model tends to produce unrealistic seasonal thaw dynamics at the study sites, which have a disproportionally large effect on estimates of volumetric soil water content. Because of this model behaviour it was decided to turn the thaw module off in all simulations analysed here and assume a constant soil depth instead. Furthermore, intensive ecophysiological measurements and monitoring of xylogenesis (e.g., Rossi *et al.*, 2008) are urgently needed in these treeline environments to identify the mechanisms underlying this apparent non-linear growth response of white spruce. Some of these mechanisms should be included in ecosystem models used to evaluate contemporary and projected responses of terrestrial ecosystems and the carbon cycle with continued warming (Piao *et al.*, 2013; Sitch *et al.*, 2013). Therefore, site-level modelling experiments with such models could be used to test the influence of well-known physiological mechanisms on the apparent threshold-like non-linear growth response of white spruce.

6.5 Conclusions

The main conclusions of this Chapter are summarised as follows:

- Positive correlations with soil moisture and negative correlations with temperatures during the current spring and the previous summer indicate that moisture is the predominant limiting factor of interannual white spruce growth in most of the tree ring sites of the chronology network.
- The tree-ring based moisture response of white spruce is consistent with regional patterns of moisture limitation inferred from satellite observations of NDVI and vegetation productivity simulated by ecosystem models across the dry and cold western interior of Canada and Alaska. This regional moisture limitation is unusual in the boreal biome and should be considered when discussing climate responses of boreal vegetation.
- Correlation analysis and simulations with the VS-Lite forward model do not show evidence for a widespread increase in moisture limitation of tree growth during recent decades on a year-to-year basis. This result is in contrast with earlier reports of apparent increases in moisture limitation of white spruce growth with recent warming.
- The calibrated VS model is able to simulate the SPL10 tree-ring chronologies at the selected divergence study sites during the calibration period but not during the verification period, when the chronologies have been shown to diverge from temperature trends.
- The calibrated parameters of the VS model suggest a non-linear temperature response of white spruce growth at two of the three study sites during the calibration periods, before the start of local divergence. Simulated tree growth at these treeline sites increases with temperatures above 6^{o}C but starts to decline when daily temperatures exceed a threshold of about 17^{o}C. An increasing annual frequency of days exceeding 17^{o}C during recent decades appears to be consistent with declining tree-ring chronology trends in some of the divergent study sites.
- The apparent non-linear response of tree growth indicated by the VS model is consistent with earlier findings of D'Arrigo *et al.* (2004) in one of the study sites. However, the lack of skill of the model to simulate tree growth during recent decades of tree-ring chronology divergence precluded a robust analysis of possible increases in moisture limitation with warming as postulated in the study by D'Arrigo *et al.* (2004). Testing this hypothesis remains a challenge at these treeline sites and requires further modelling work and in-situ growth monitoring.

Chapter 7

Conclusions and further research

The aim of this thesis was to explore how the growth of boreal vegetation has varied as a result of recent changes in climate, specifically in growing season temperatures and drought severity during the latter half of the 20th and the first decade of the 21st centuries. This final chapter presents a brief summary of the main findings and points to the implications for the understanding of current and future boreal vegetation growth in response to climate change. The chapter concludes with some general suggestions for future work.

7.1 Main research findings

7.1.1 Contrasting ecosystem responses to the extension of the growing season in spring and autumn

Until recently, only ecosystem responses to spring changes have been studied because of their significant influence on the local and global carbon cycle. Autumn responses had received less attention, mostly because no much warming had occurred in this transitional season compared with spring. The common expectation was that both spring and autumn warming could enhance carbon sequestration and extend the period of net carbon uptake in the future (Churkina *et al.*, 2005). Using atmospheric carbon dioxide concentration data, Piao *et al.* (2008) showed for the first time that, contrary to earlier expectations, large-scale autumn warming stimulated net ecosystem carbon losses rather than gains. They estimated that autumn carbon losses could offset up to about 90% of spring carbon gains due to earlier growing seasons. Subsequently, similar ecosystem responses have been found at local scales in eddy-covariance sites (Vesala *et al.*, 2010) but positive responses have also been observed at these scales (Richardson *et al.*, 2010; Dragoni *et al.*, 2011). Piao *et al.* (2008) also found a general trend toward earlier autumn-to-winter carbon dioxide build-up that led to a shorter net carbon uptake period.

The main contributions of this thesis to the understanding of current responses of northern ecosystems to changes in growing season are the following:

- The results presented in Chapters 2 and 3 confirm the contrasting ecosystem responses to spring and autumn warming. However, these results also suggest that ecosystem responses in autumn are generally more complex than in spring. This seems to be related to a higher sensitivity of vegetation photosynthesis to temperature in spring and to a more significant

influence of factors other than temperature during autumn, including leaf aging processes, day length and soil moisture.

- Unlike the results of Piao *et al.* (2008), no shortening trends in carbon uptake period were observed at high latitudes over the analysis period 1987–2009. Moreover, the inverse relationship between the timing of autumn zero-crossing and the termination of the thermal growing season appears to have decoupled during the second half of the 2000s when a period of unprecedented autumn warming started. This recent change in ecosystem response warrants further investigation because it could indicate some emerging interaction in ecosystem processes with increased autumn warming not captured in the analyses of previous decades.

- Another important finding of this research is the observation that the NDVI-based photosynthetic growing season has closely tracked the pace of warming and extension of the potential growing season in spring, but not in autumn. This is an indication that the photosynthetic period does not further extend with autumn warming, consistent with earlier suggestions of a respiration-dominated ecosystem response. This result also implies that it is likely that continued autumn warming will offset spring carbon gains.

7.1.2 Warming, increased evapotranspiration demand and summer drought

The evaluation and intercomparison of multiple estimates of soil moisture dynamics (in-situ, satellite, land-surface models and scPDSI) at high latitudes is an important contribution of this thesis and serves as a basis for the improvement and better application of these datasets for studying vegetation responses to moisture variability. Such an analysis was lacking in the literature and was possible here because of the timely release of new datasets.

Several vegetation remote sensing studies have speculated that warming has increased drought severity at high latitudes but there has been no quantitative regional assessment of such an effect (but see Sheffield & Wood, 2007). The contributions of this thesis to the debate of drought changes with recent warming at high northern latitudes are summarised as follows:

- The scPDSI dataset validated in this thesis suggests that increased evapotranspiration demand, driven mainly by surface warming, has significantly influenced the severity of regional droughts over most of the northern latitudes since the late 1980s. However, for the high latitudes as a whole, the estimated enhancement of atmospheric moisture demand during this recent period has been balanced by the increase in precipitation and has not imposed an increasing trend in dry area. This finding is consistent with ongoing amplification of the hydrological cycle (Rawlins *et al.*, 2010; Miralles *et al.*, 2013) and with early model projections of summer drying at northern latitudes in response to anthropogenic warming (Manabe & Wetherald, 1987).

- The scPDSI also suggests that the impact of increased evapotranspiration demand on the summer moisture balance has been stronger and more widespread in Eurasia than in North America. Large continental areas in central Asia that are moisture-limited and observed to be warming fast, are especially vulnerable to this type of drying. Boreal and northern

temperate North America have not been affected by increased evapotranspiration demand but if summer temperatures rise this region will also experience more drying.

- Contrary to earlier suggestions in the literature, the results presented in Chapters 4 and 5 indicated that despite the widespread increase in moisture demand, snow has demonstrably greater effect on early summer soil moisture availability. The influence of summer evaporative losses has been overestimated in the literature and the dramatic changes in snowpack with winter and spring warming are likely to play a dominant role in influencing the soil water balance in these regions with snow-domninated hydrology. Current trends toward earlier growing seasons and snowmelt may be an extra factor enhancing summer drying by extending and accelerating moisture depletion by evapotranspiration during the earlier part of the growing season (Zhang *et al.*, 2011; Buermann *et al.*, 2013).

In reaching these conclusions, it is necessary to bear in mind that the scPDSI is a simple index and that uncertainties in the meteorological drivers at high northern latitudes are still high. Furthermore, permafrost dynamics in these cold regions may result in very different patterns of moisture variability to those estimated by the scPDSI. The moisture water balance of the bucket model of the scPDSI gives realistic estimates in most regions but there are some localised areas were the bucket is nearly always saturated. This affects the scPDSI variability in these locations. The problem is not widespread but this aspect of the soil water model should be further explored in the next version of the product.

7.1.3 Moisture controls of northern vegetation and non-linear tree growth responses

The NDVI and tree-ring analyses presented in last two chapters of this thesis (Chapters 5 and 6) revealed a consistent pattern of moisture limitation along the relatively dry western interior of Canada and Alaska. Earlier tree-ring analyses have usually indicated a moisture sensitivity of white spruce growth in the region but this has not been shown before for satellite-derived NDVI. The satellite data suggested that this control was largely related to snowmelt water but tree rings do not suggest a clear correlation with snowpack. Nevertheless, there is a clear linkage between tree growth and spring moisture availability as indicated by negative correlations with temperature and positive correlations with Noah soil moisture estimates.

The most important contributions of this thesis to the ongoing discussion on moisture responses of northern vegetation are the following:

- NDVI declines ('browning' trends) in the boreal forest of North America are more consistent with reduced snowpack than with temperature-induced increases in evaporative demand than previously thought (Chapter 5). This strongly suggests that changes in snowpack dynamics are likely more important than increased evaporative demand in controlling changes in summer soil moisture availability in this extensive moisture-sensitive boreal region. Interestingly, the analysis of DGVM-simulated GPP from the TRENDY compendium shows that this moisture control is well captured by the model average. Further work is needed to evaluate the performance of the ten individual models included in the compendium.

- The Vaganov-Shashkin (VS) forward model of tree-ring growth provided evidence for an apparent non-linear growth response of white spruce at some high elevation sites showing tree-ring divergence during recent decades (Chapter 6). The calibrated VS model indicated that in these treeline sites, white spruce tree growth increases with daily temperatures above 6^oC and starts to decline when temperatures exceed a threshold of about 17^oC. This overall result is consistent with earlier findings by D'Arrigo *et al.* (2004) in one of the study sites. They hypothesised that this type of response represented a shift to moisture limitation at temperatures above their 11.3^oC threshold of July-August temperatures. However, the lack of skill of the VS model to simulate growth during recent decades within the period of tree-ring divergence precluded a robust evaluation of this hypothesis. Testing this hypothesis remains a challenge at these treeline sites and would require further modelling work and in-situ monitoring of xylogenesis and photosynthetic dynamics.

7.2 Further research

This thesis has demonstrated that ecosystem responses to the lengthening of the growing season in autumn are not as simple as in spring. The relationships between climate and vegetation indicators of the growing season are consistent in spring but breakdown in autumn. The complexities of the autumn response should be evaluated in ecosystem models to test their behaviour and obtain insights into processes. This is needed because net carbon losses in autumn could potentially offset net carbon uptake in spring, reducing the strength of the carbon sink.

The significant snow-mediated moisture controls on northern vegetation revealed by this research have been overlooked in earlier studies, which have overemphasised the influence of potential evapotranspiration on the soil water budget. This finding, published in Barichivich *et al.* (2014), will likely trigger research into the links between vegetation, snow and moisture dynamics. Although the DGVMs are able to reproduce the regional moisture control of vegetation productivity in northwestern North America, it is not clear whether the models can simulate the influence of snow on summer moisture availability and productivity. Therefore, this is an aspect that warrants further research.

The main focus of this thesis was on climate drivers of vegetation growth at decadal and shorter time scales, where the influence of climate on vegetation is generally stronger. Little analysis was conducted to disentangle the influence of non-climatic factors, such as CO_2 and nitrogen fertilisation, 'diffuse-light' fertilisation and permafrost changes on vegetation growth at interannual to multi-decadal time scales. The analysis of NDVI data presented in Chapter 5 showed that the fraction of variance of summer NDVI variability not explained by climate (temperature and moisture) at the grid cell level can be considerably high across large regions. The statistical modelling presented here could be taken one step further to investigate the non-climatic drivers of this unaccounted variance in order to provide observational constraints on these large unknowns on the future of the land carbon sink.

The apparent non-linear growth response of white spruce at some marginal treeline sites described in Chapter 6 has important implications for our expectations on how boreal trees might respond to continued warming. Research of this issue is needed to identify the physiological causes and whether it is a species specific response restricted to the treeline or is widespread at

lower elevations. More modelling work with the VS model together with in-situ monitoring of tree growth will allow an improved testing of hypotheses of tree-ring divergence. The approach used here to apply the VS model in divergence case studies should be used to reassess other known instances of divergence in the latitudinal treeline (e.g., Pisaric *et al.*, 2007) in northern Canada. The analysis could also be extended to the circumpolar tree-ring network to determine if this type of non-linear response is common in other regions. The results of the later would be relevant for the carbon cycle. However,

Appendix A

Supplementary material for Chapter 2

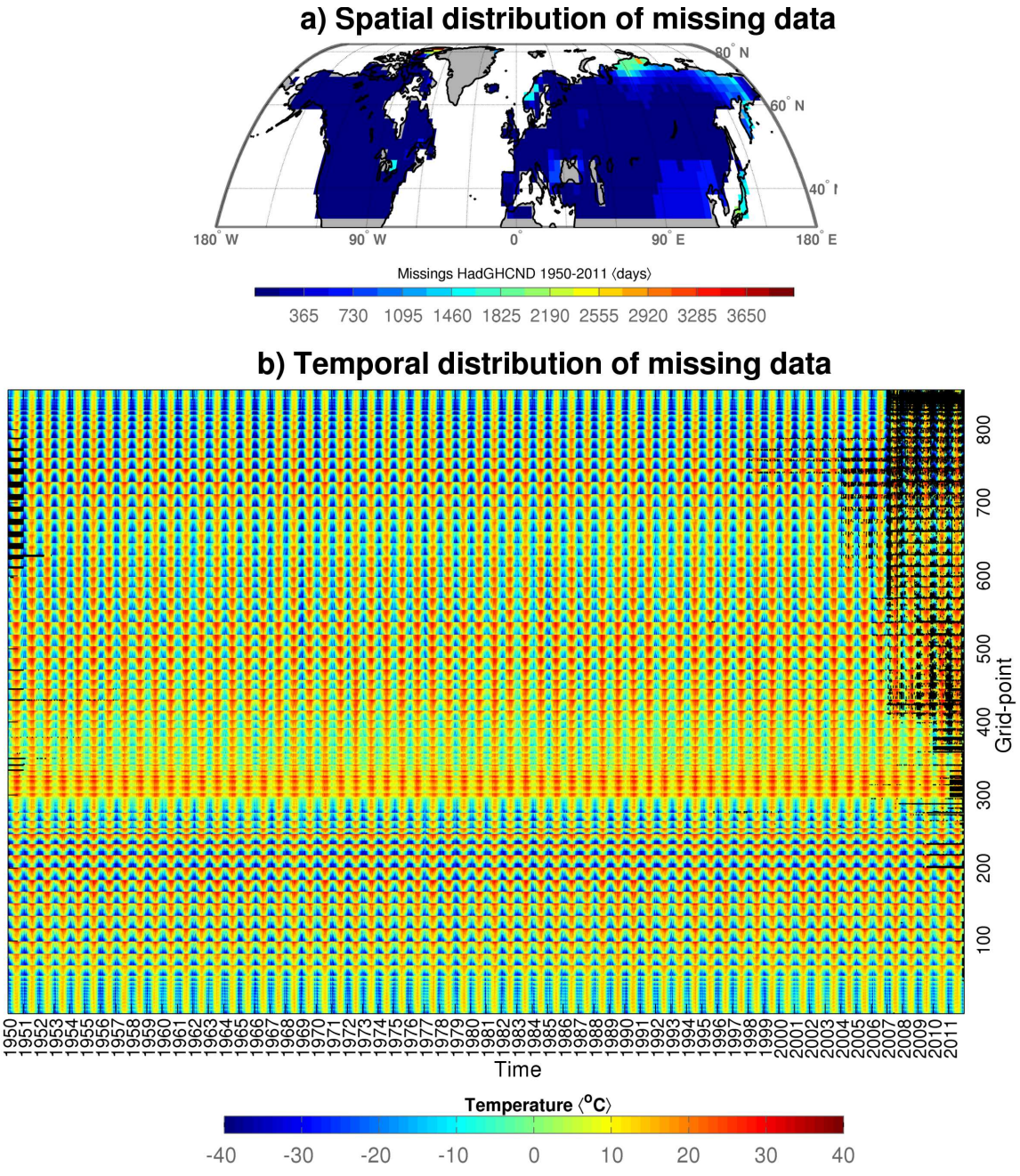

Supplementary Figure A1: Spatial (a) and temporal (b) distribution of missing data. Black color in (b) indicates missing values in the mean daily temperature data matrix (22630 days x 854 grids) after discarding grid boxes with more than three years of missing data.

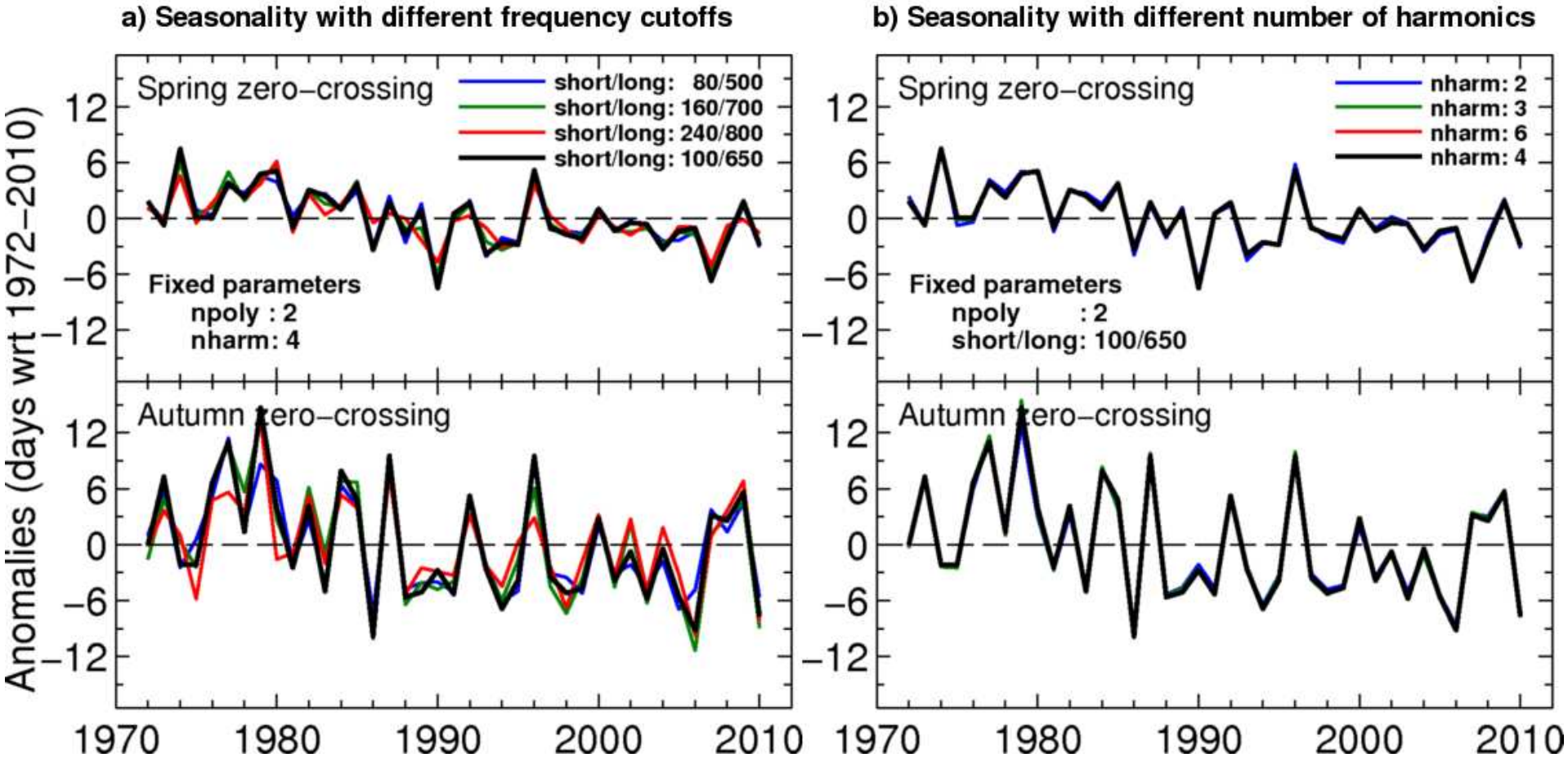

Supplementary Figure A2: Sensitivity of zero-crossing time anomalies to different frequency cutoffs in the low-pass filtering (a) and number of annual harmonics used to extract the annual cycle from monthly CO_2 observations at Point Barrow. The black line represents the parameters selected for analysis (see Section 2.2 in the article). The degree of the polynomial used to fit the long-term trend was held constant at 2.

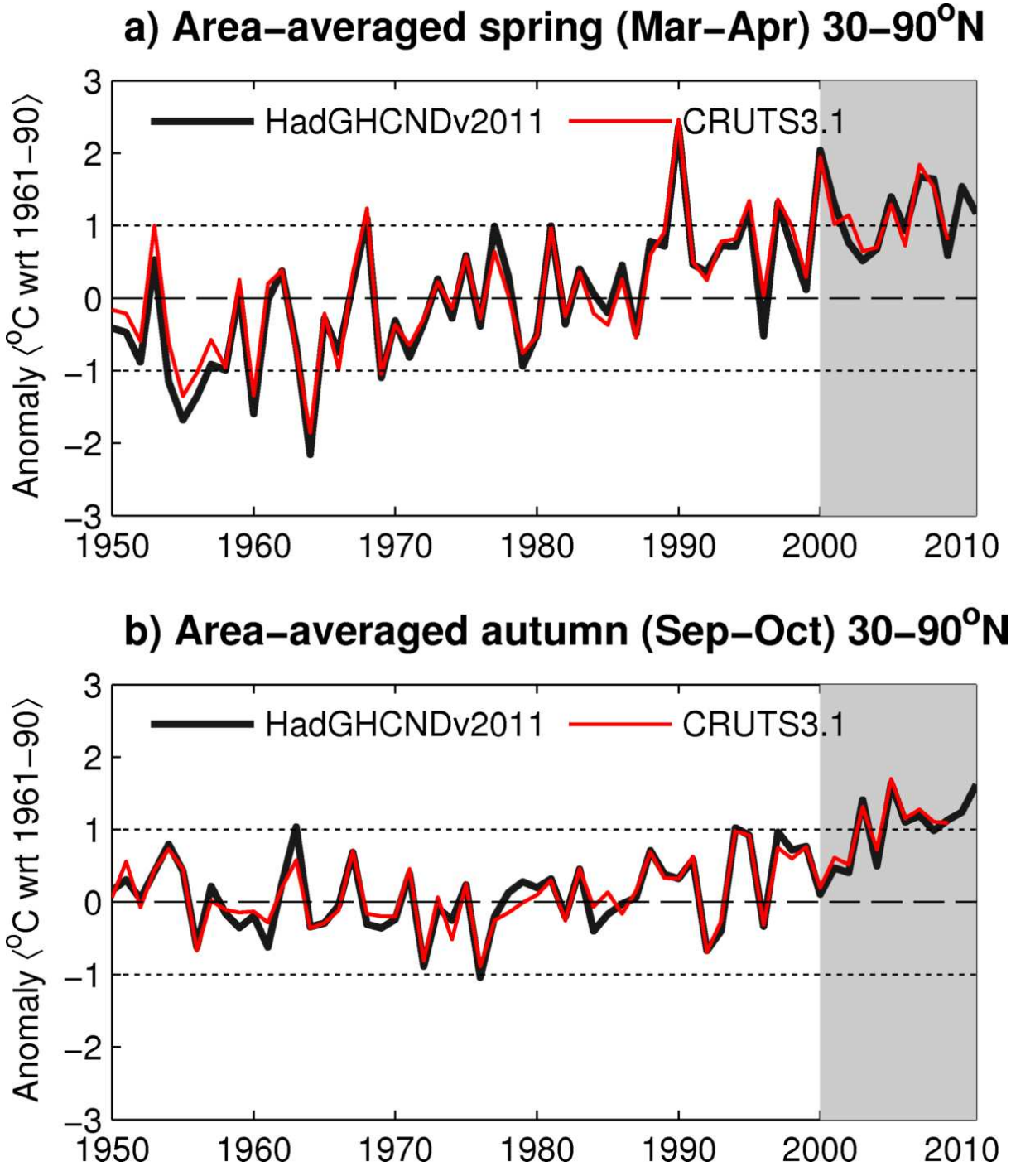

Supplementary Figure A3: Comparison of time series of spring (a) and autumn (b) mean surface air temperatures from the HadGHCND and CRUTS3.1 datasets averaged over land regions north of 30°N. Gray shading highlights the period 2000-2011.

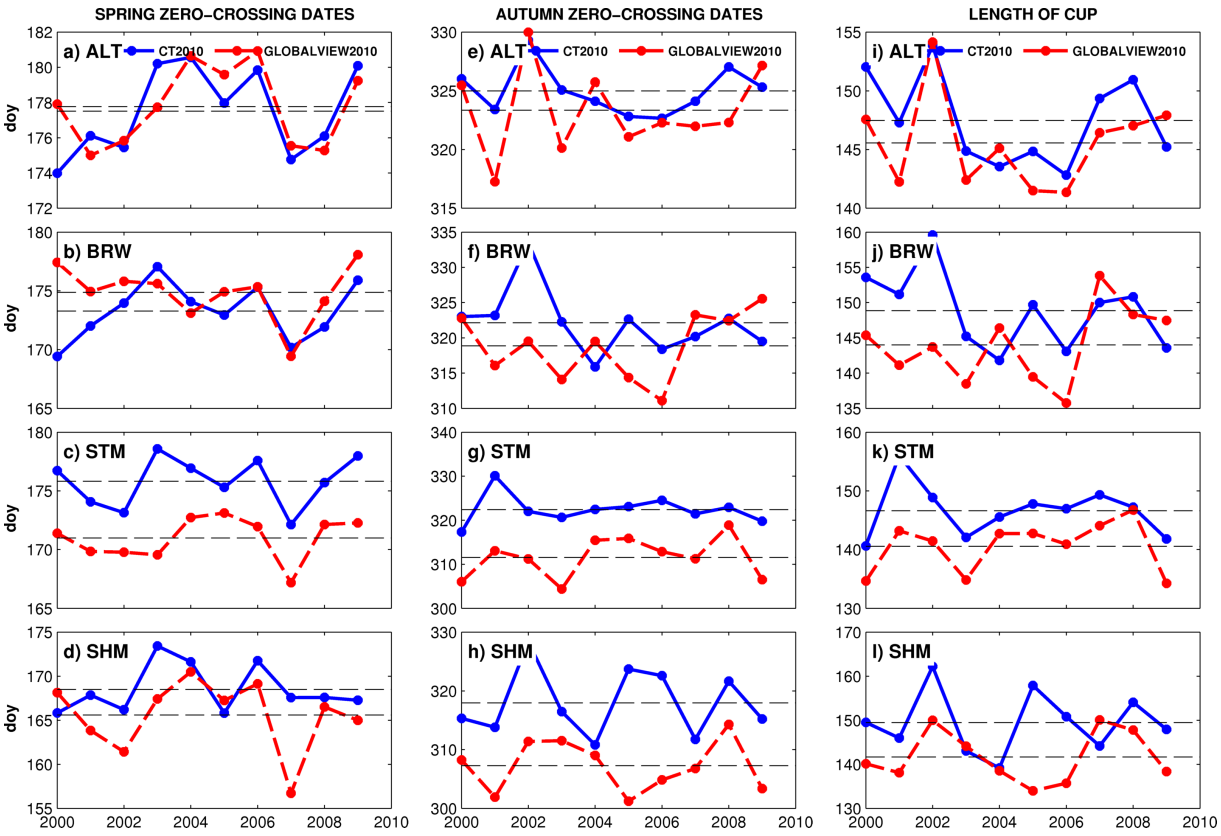

Supplementary Figure A4: Comparison between observed (GLOBALVIEW2010) and CarbonTracker-based (CT2010) time series of SZC (left), AZC (middle), and CUP (right) at each of our CO_2 observing stations. For each station, the co-located grid box (3^ox2^o) of column-averaged CO_2 mole fraction in the free-troposphere from CT2010 is used for comparison. The correlation between the series is indicated in each plot and significant correlations ($p < 0.05$) are indicated by an asterisk.

Appendix B

Supplementary material for Chapter 3

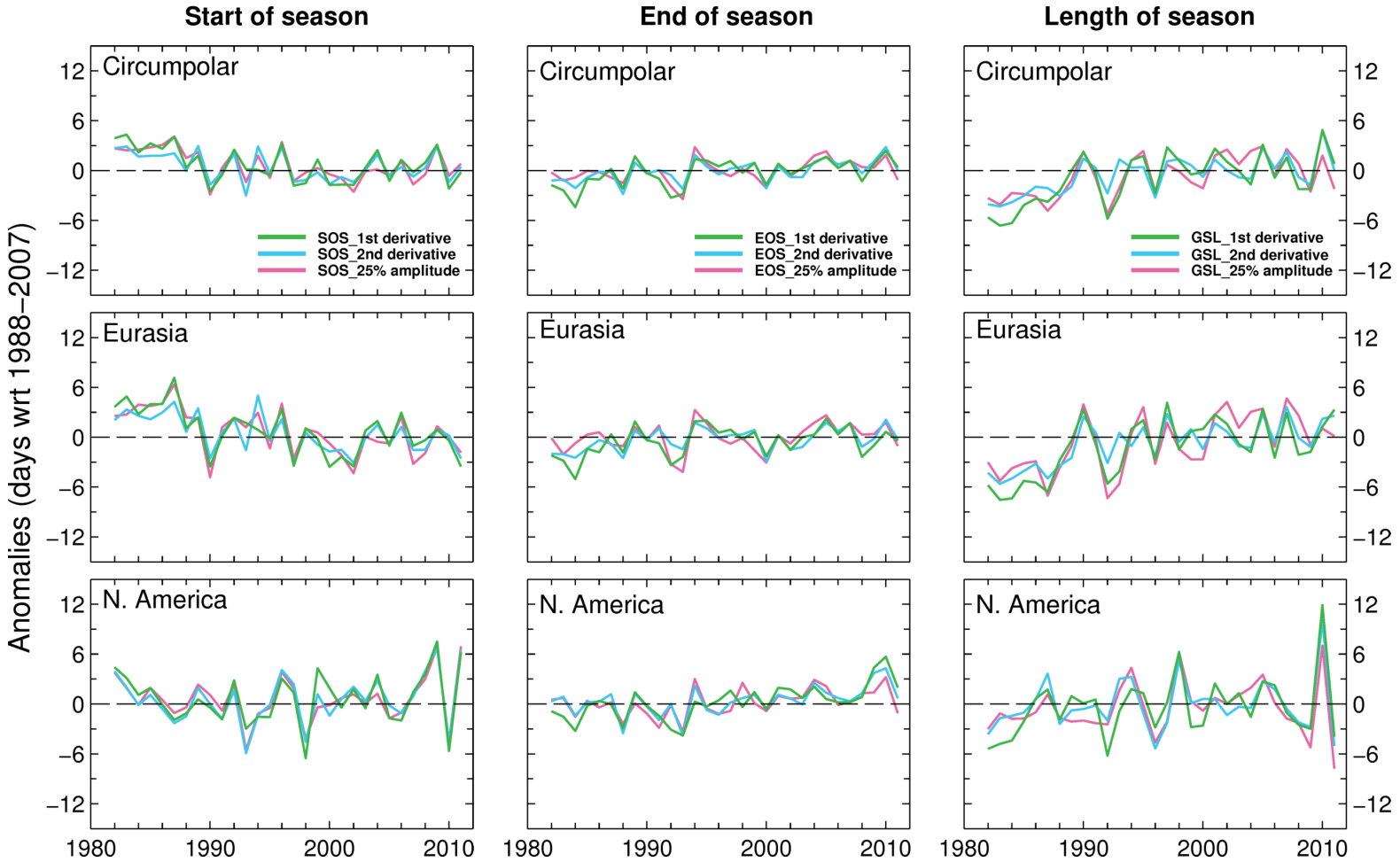

Supplementary Figure B1: Comparison of large-scale variations in the timing and length of the photosynthetic growing season showing that the results are not sensitive to differences in the methods used to extract phenology (see *Methods section*). In this context, for a given 8-km grid box and year, the start of the photosynthetic growing season (SOS) corresponds to the time of the year when the NDVI rises above a threshold value in spring, while the end (EOS) occurs when the NDVI falls below a threshold value in autumn. In the first approach (*25% amplitude – pink*), an arbitrary threshold of 25% of the amplitude of the annual cycle of NDVI is used in spring and in autumn each year. In the second approach (*1st derivative – green*), the spring and autumn NDVI thresholds used across all years in a given grid box correspond to the NDVI levels at which the inflection points for green-up and senescence occur in the first derivative of the 30-year NDVI climatology of that grid box. This is the method used to compute the phenological parameters presented in the chapter. The third approach (*2nd derivative – cyan*) uses the NDVI levels for the inflection points for green-up and senescence in the second derivative of the 30-year NDVI climatology. Areas designated as water bodies, croplands, urban and barren or sparsely vegetated regions were masked out from analysis.

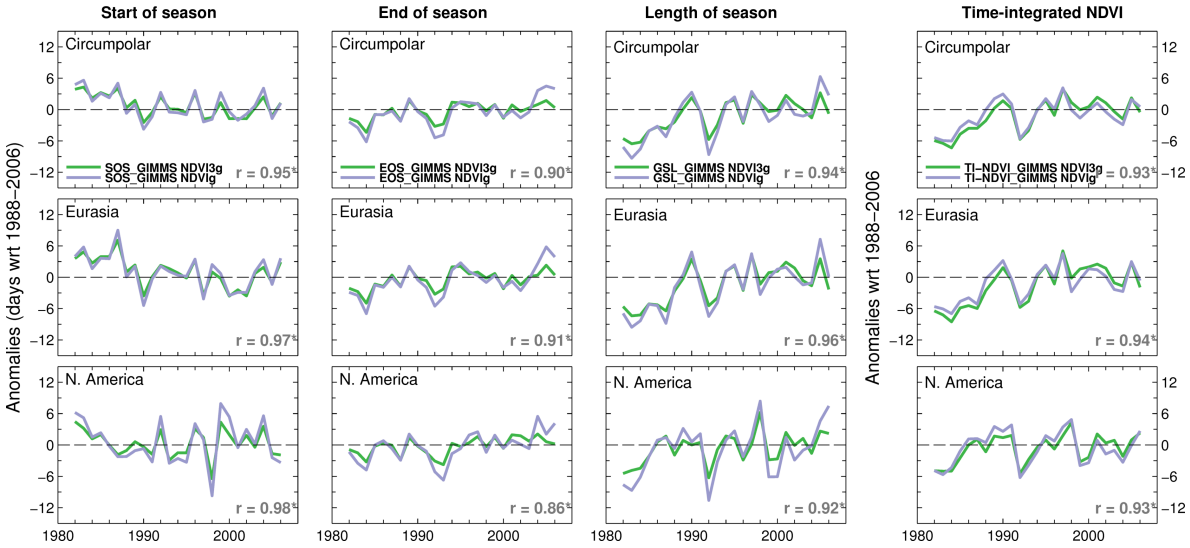

Supplementary Figure B2: Comparison of variations in timing, length and intensity of the photosynthetic growing seasons between 1982 and 2006 based on the latest version of biweekly AVHRR GIMMS NDVI data (*GIMMS NDVI3g – green*) and the earlier version of the dataset (*GIMMS NDVIg – gray*). Inland water bodies, croplands, urban and barren or sparsely vegetated regions were excluded from the analysis.

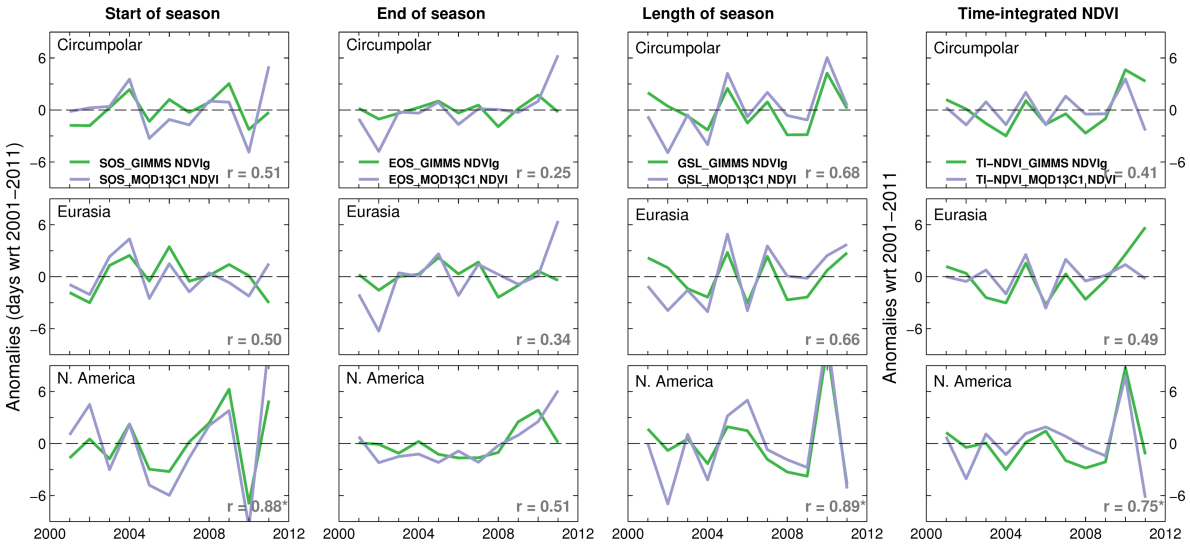

Supplementary Figure B3: Changes in spring (a) and autumn (b) number of non-frozen days based on satellite microwave (SSM/I) and gridded surface air temperature observations (HadGHCND) north of 45^{o}N. Correlations between the series for the period 1988-2007 and trends (β) for the HadGHCND series over the period 1950-2011 are given in each panel. An asterisk denotes significance at the $p < 0.05$ level.

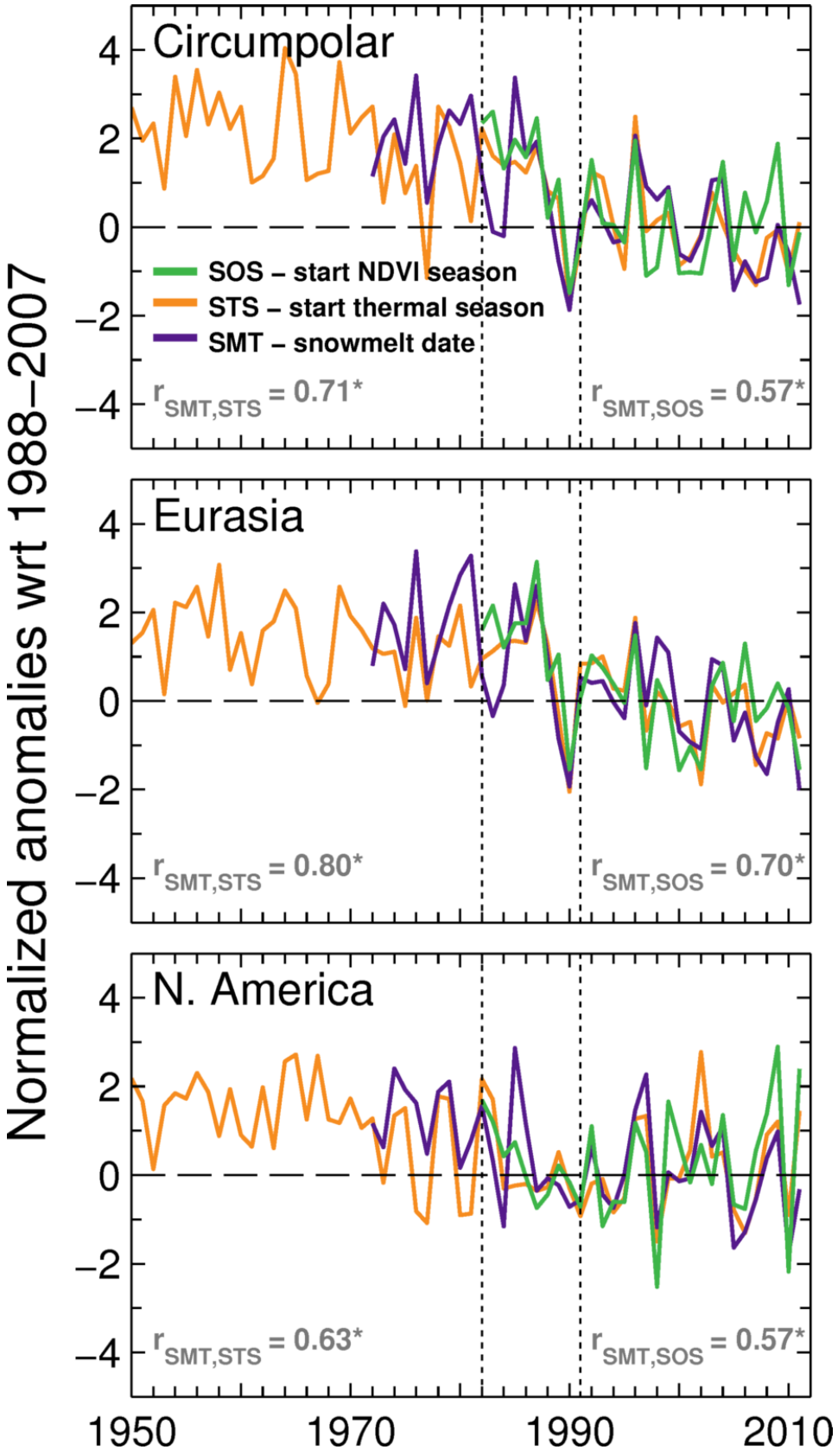

Supplementary Figure B4: Comparison of variations in the timing of spring snowmelt based on NOAA weekly snow cover (*SMT – purple*) with the timing of start of the thermal growing season (*STS – orange*) and the start of the photosynthetic growing season (*SOS – green*) at latitudes north of 45°N. The correlations of SMT with STS and SOS over the common period 1982–2011 are shown in the lower-left and lower-right corner of each plot, respectively. An asterisk denotes significance at the $p < 0.05$ level. The vertical dotted lines indicate the dates of the eruptions of El Chichón in 1982 and Mount Pinatubo in 1991.

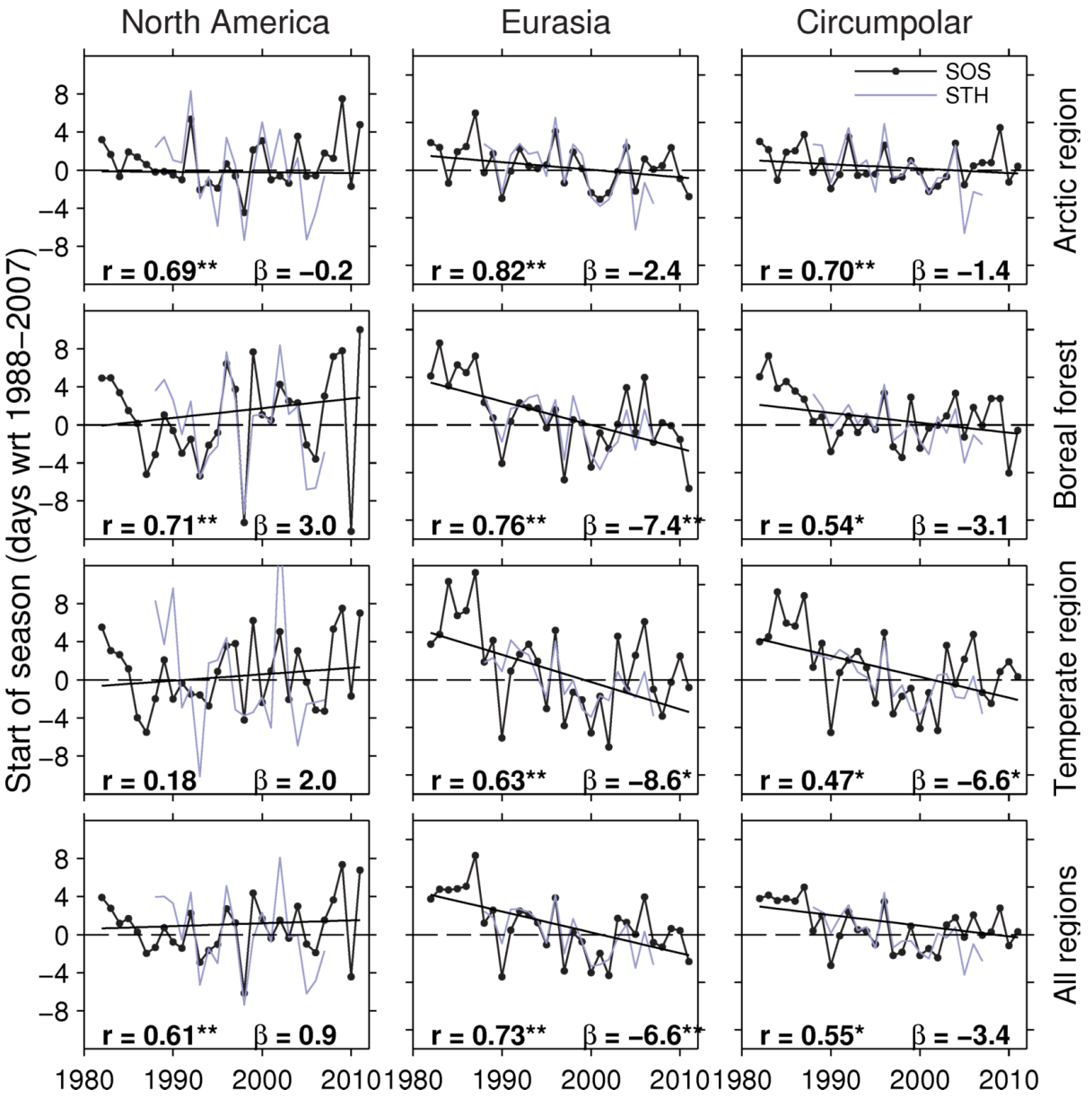

Supplementary Figure B5: Comparison of continental and circumpolar time series of the timing of the start of the photosynthetic growing season (*SOS – black*) and spring thaw (*STH – gray*) for each biome. Correlations between the series for the period 1988-2007 and trends (β) for SOS over the period 1982–2011 are shown in each panel. A single asterisk denotes significance at the $p < 0.05$ level and a double asterisk indicates further significance at the $p < 0.01$ level.

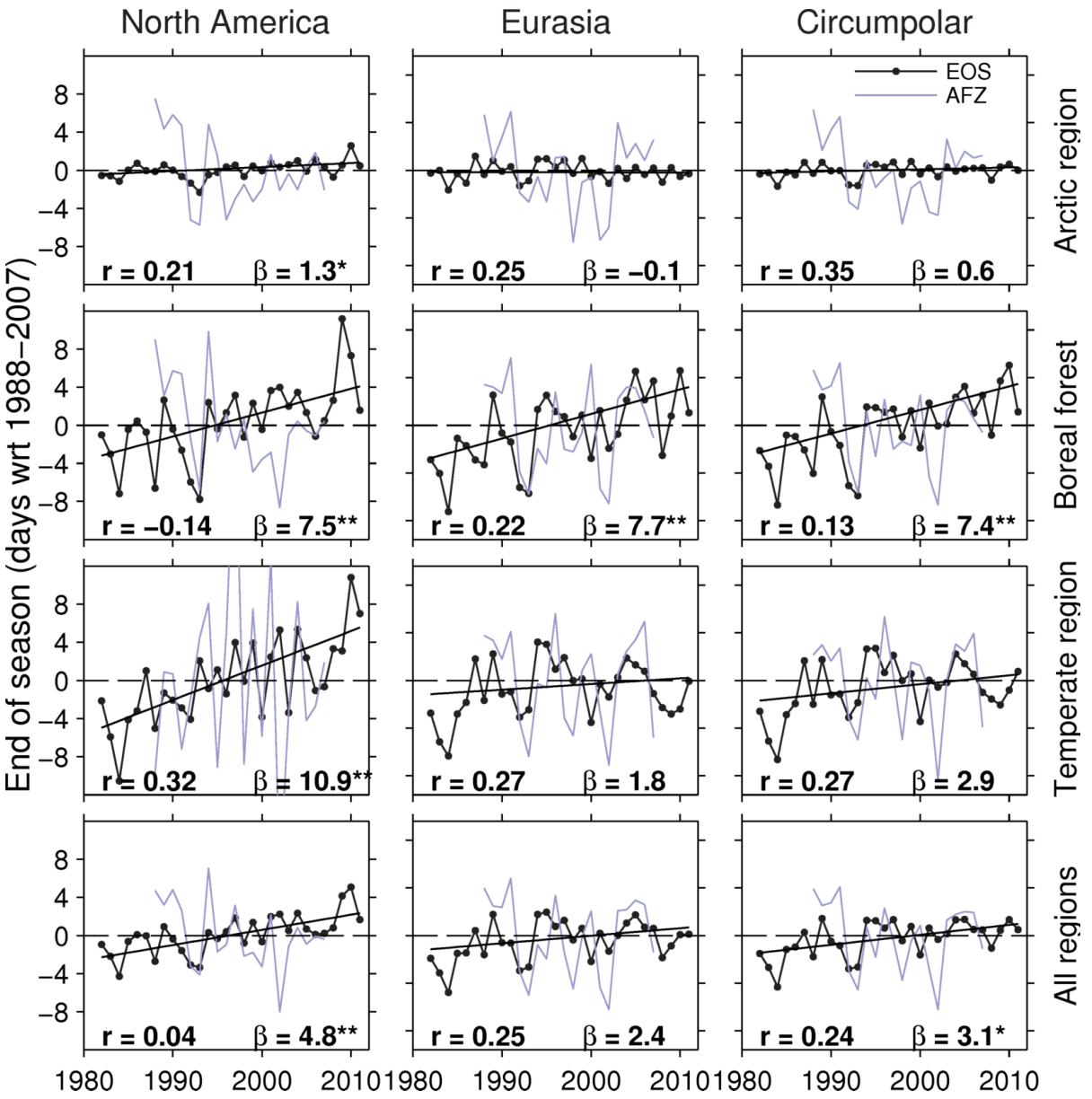

Supplementary Figure B6: Comparison of continental and circumpolar time series of the timing of the termination of the photosynthetic growing season (*EOS – black*) and autumn freeze (*AFZ – gray*) for each biome. Correlations between the series for the period 1988-2007 and trends (β) for EOS over the period 1982–2011 are shown in each panel. A single asterisk denotes significance at the $p < 0.05$ level and a double asterisk indicates significance at the $p < 0.01$ level.

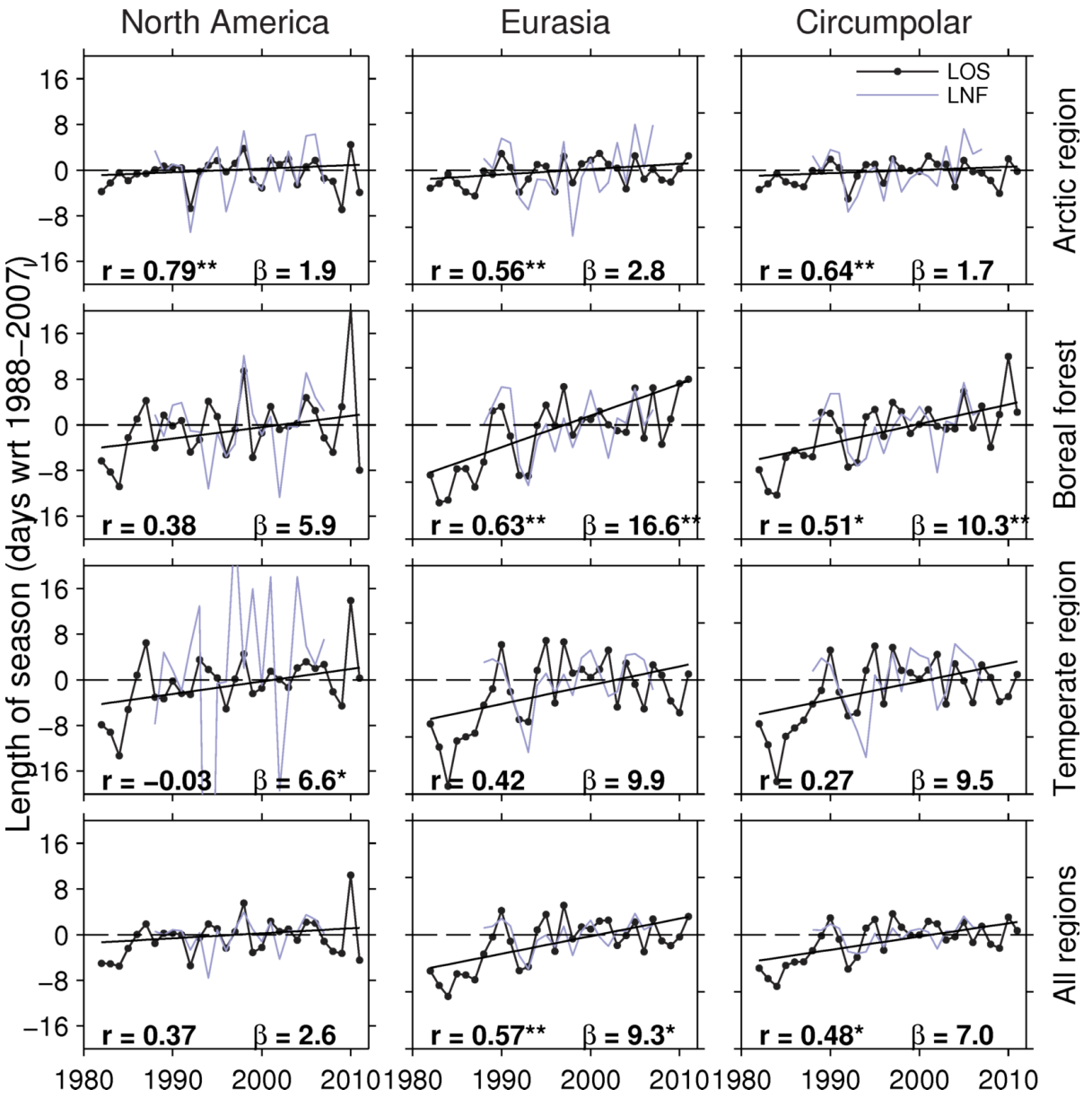

Supplementary Figure B7: Comparison of continental and circumpolar time series of length of the photosynthetic growing season (*GSL – black*) and non-frozen season (*LNF – gray*) for each biome. Correlations between the series for the period 1988-2007 and trends (β) for GSL over the period 1982–2011 are shown in each panel. A single asterisk denotes significance at the $p < 0.05$ level and a double asterisk indicates significance at the $p < 0.01$ level.

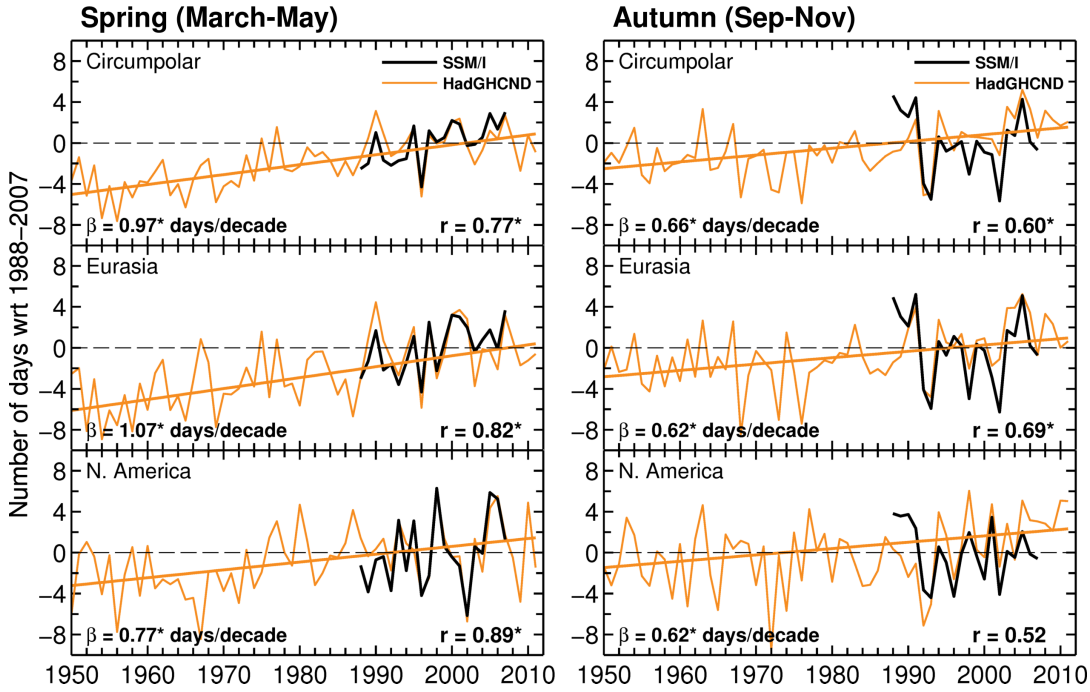

Supplementary Figure B8: Changes in the number of spring and autumn non-frozen days based on satellite microwave (*SSM/I – black*) and gridded surface air temperature observations (*HadGHCND – orange*) north of 45°N. Correlations between the series for the period 1988-2007 and linear trends (β) for the HadGHCND series over the period 1950-2011 are given in each panel. An asterisk denotes significance at the $p < 0.05$ level.

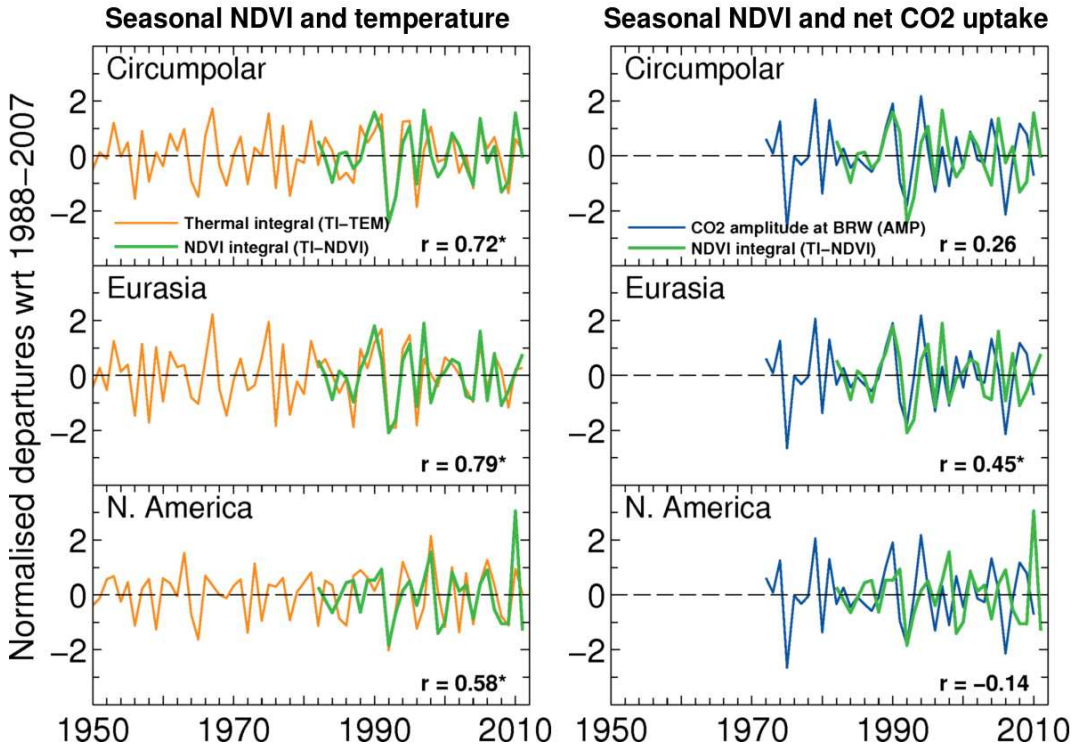

Supplementary Figure B9: Comparison of 10-year high-pass filtered variations in seasonally integrated NDVI (*green*) with seasonally integrated temperature (*orange*), and peak-to-trough amplitude of the annual cycle of atmospheric CO_2 at Point Barrow (*blue*). The correlation between the series over their common period is shown in each panel. An asterisk denotes significance at the $p < 0.05$ level.

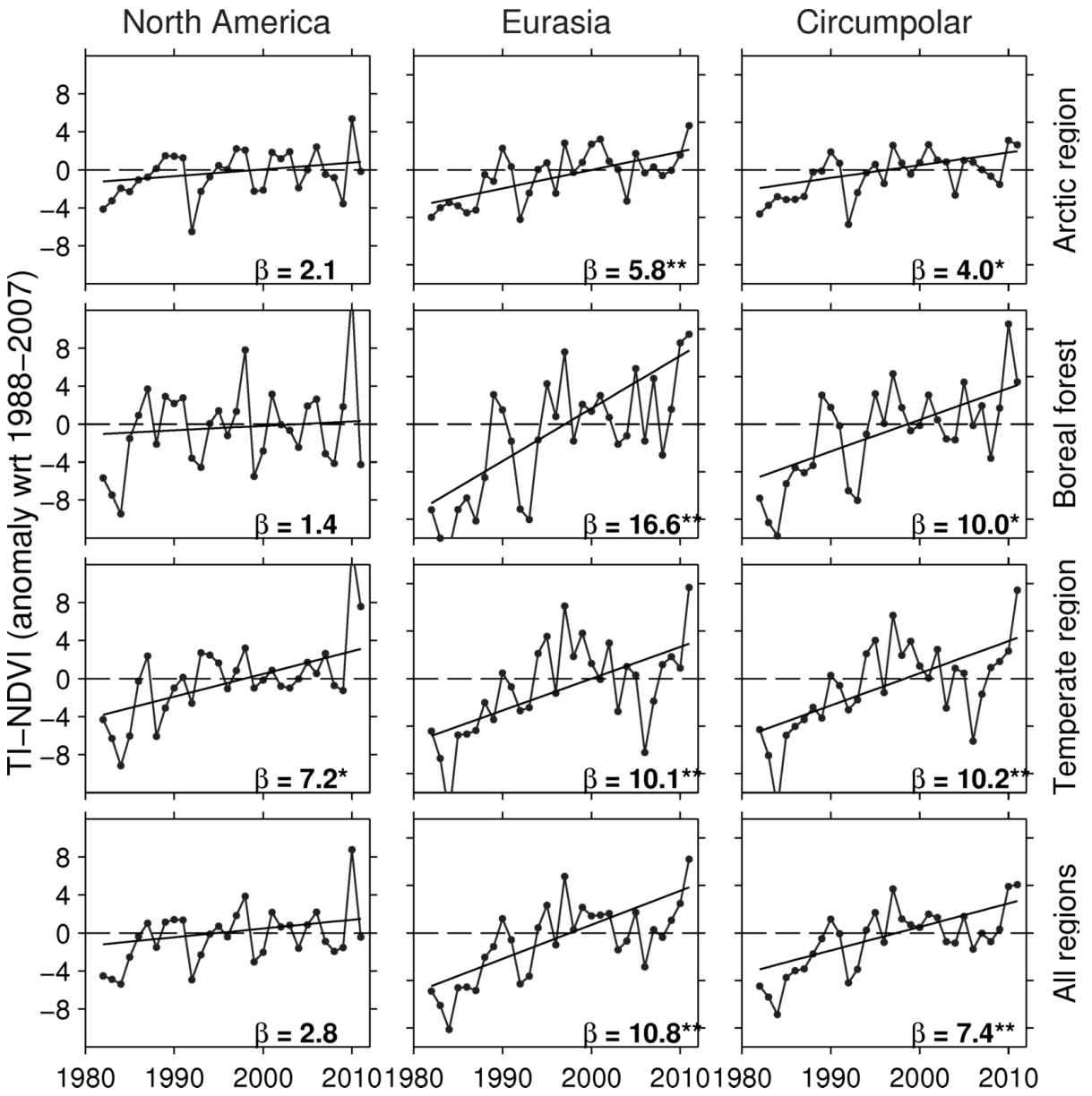

Supplementary Figure B10: Continental and circumpolar time series of seasonally integrated NDVI (TI-NDVI) for each biome. Trends (β) over the period 1982–2011 are shown in each panel. A single asterisk denotes significance at the $p < 0.05$ level and a double asterisk indicates significance at the $p < 0.01$ level.

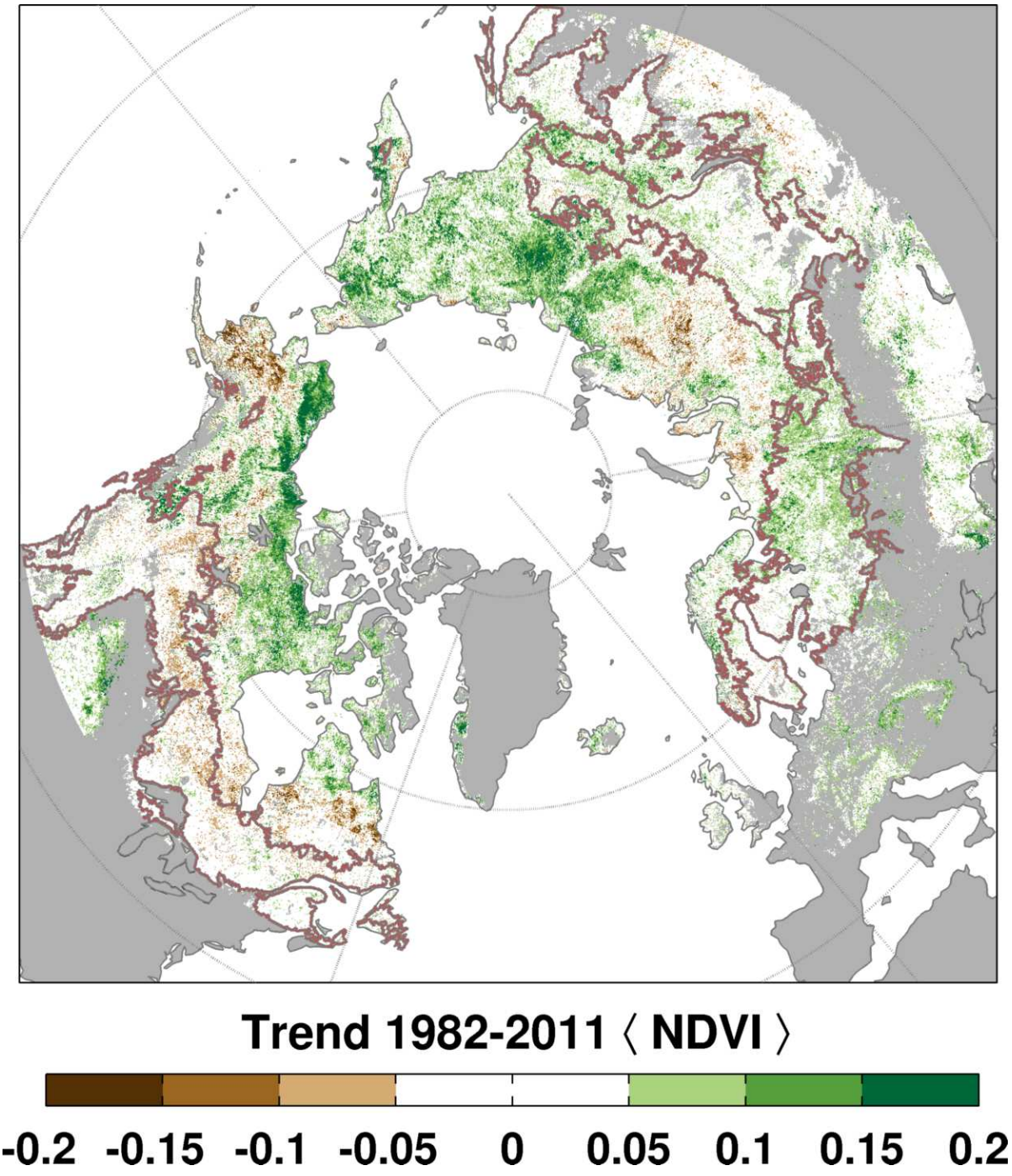

Supplementary Figure B11: Spatial distribution of linear trends in peak summer greenness between 1982 and 2011. This parameter corresponds to the maximum annual value of smoothed NDVI data from TIMESAT. Non significant trends ($p > 0.1$) are masked out as white. The brown polygons indicate the extent of the boreal forests. The gray background denotes land areas excluded from analysis.

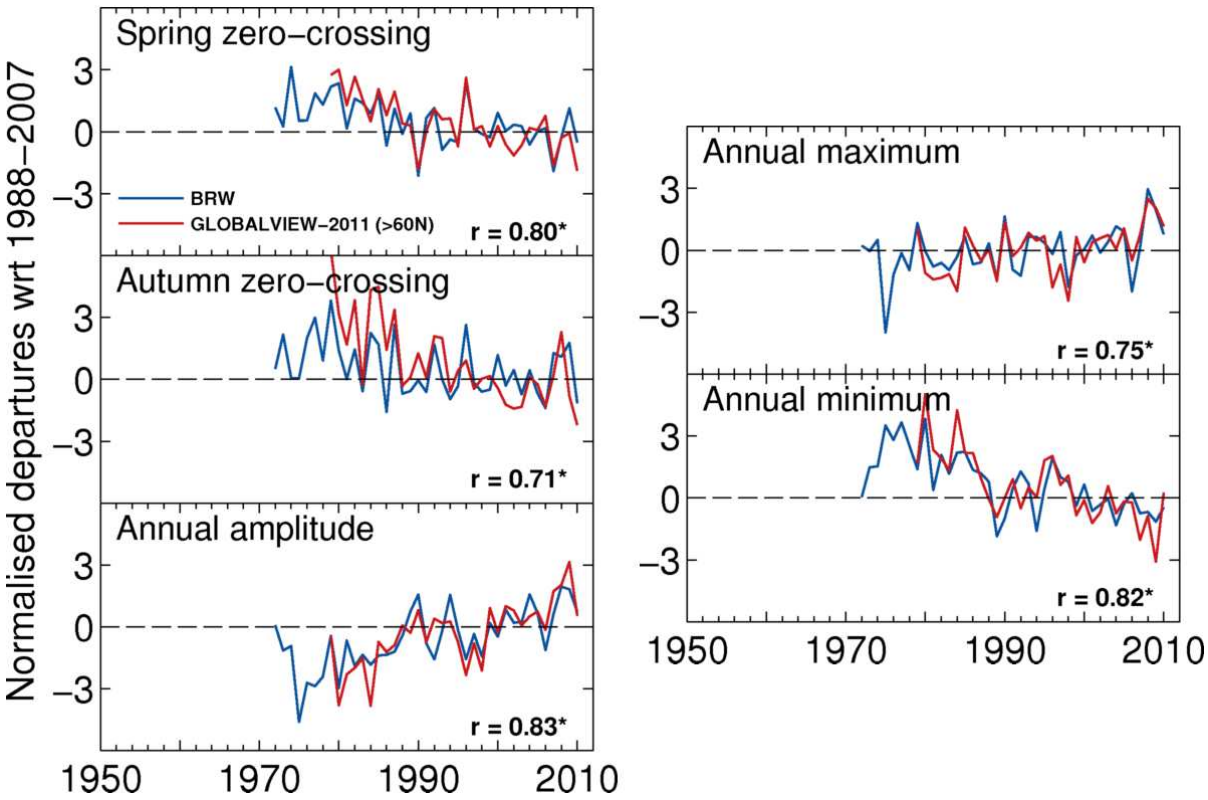

Supplementary Figure B12: Comparison of changes in the amplitude and phase of the annual cycle of atmospheric CO_2 at northern latitudes based on observations at Point Barrow (71^oN – *blue*) and on estimates from the marine boundary layer matrix of GLOBALVIEW–2011 averaged north of 60°N (*red*). The correlation between the series over the period 1979–2010 is shown in each panel. An asterisk denotes significance at the $p < 0.05$ level.

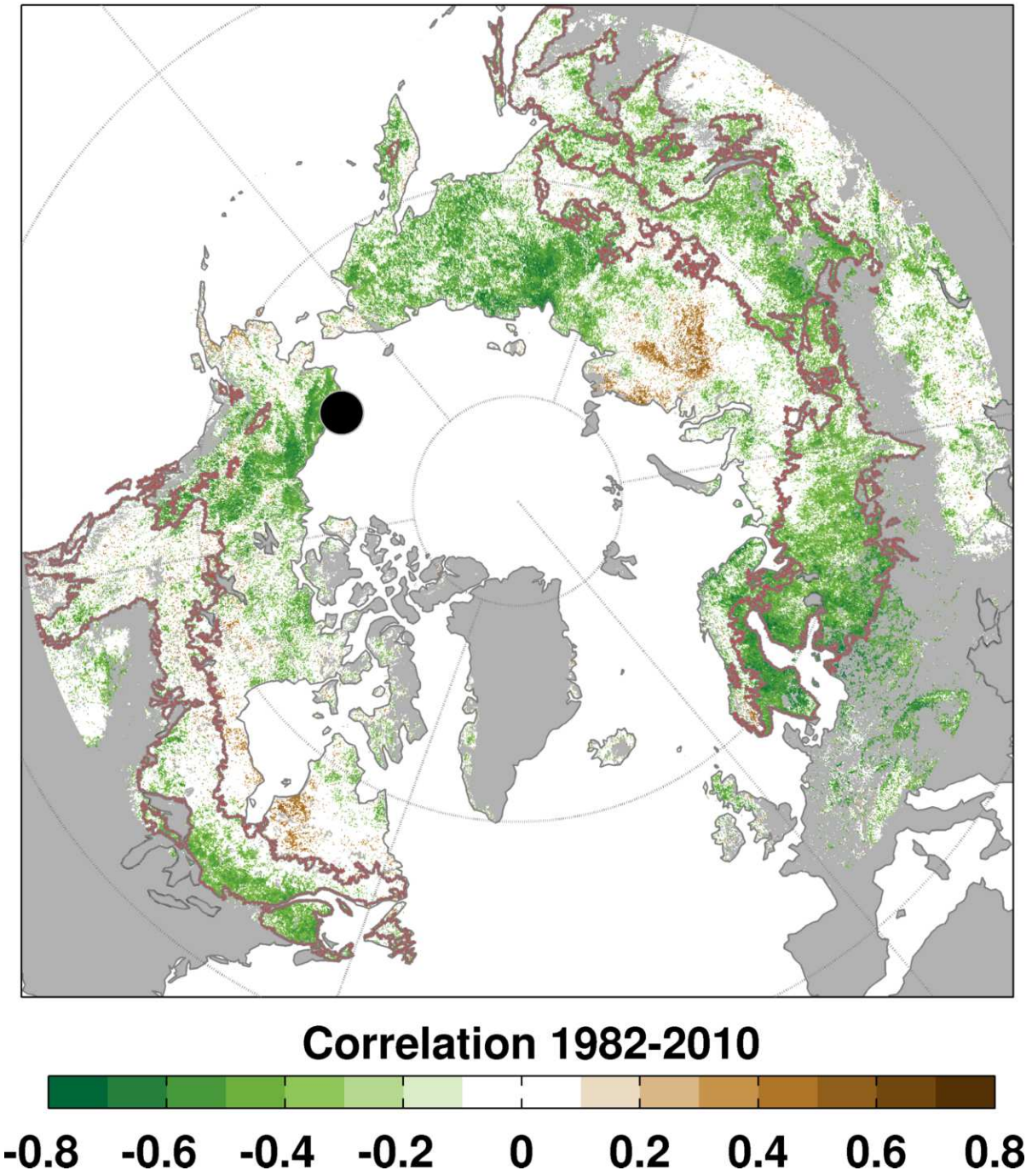

Supplementary Figure B13: Correlation between growing season integrated GIMMS NDVI3g (TI–NDVI) and peak-to-trough amplitude of the annual cycle of atmospheric CO_2 at Point Barrow (*black dot*) from 1982 to 2010. Data were detrended prior to correlation analysis and non significant correlations ($p > 0.1$) are masked out as white. The brown polygon indicates the extent of the boreal forests. The gray background denotes land areas excluded from analysis.

Appendix C

Supplementary material for Chapter 4

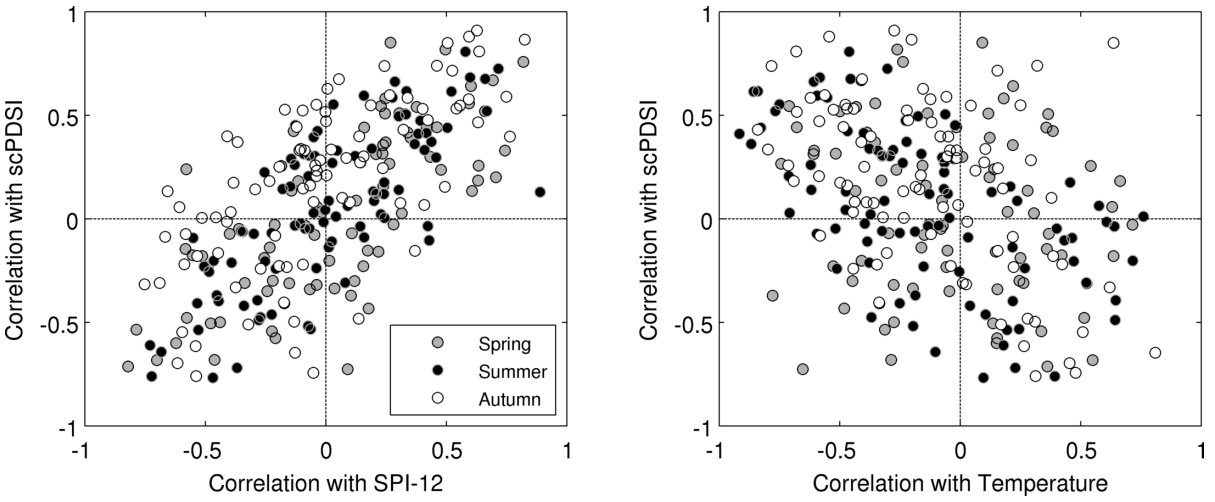

Supplementary Figure C1: Scatterplot of correlation coefficients between in-situ measurements of surface soil moisture and scPDSI, SPI-12mo and temperature by season.

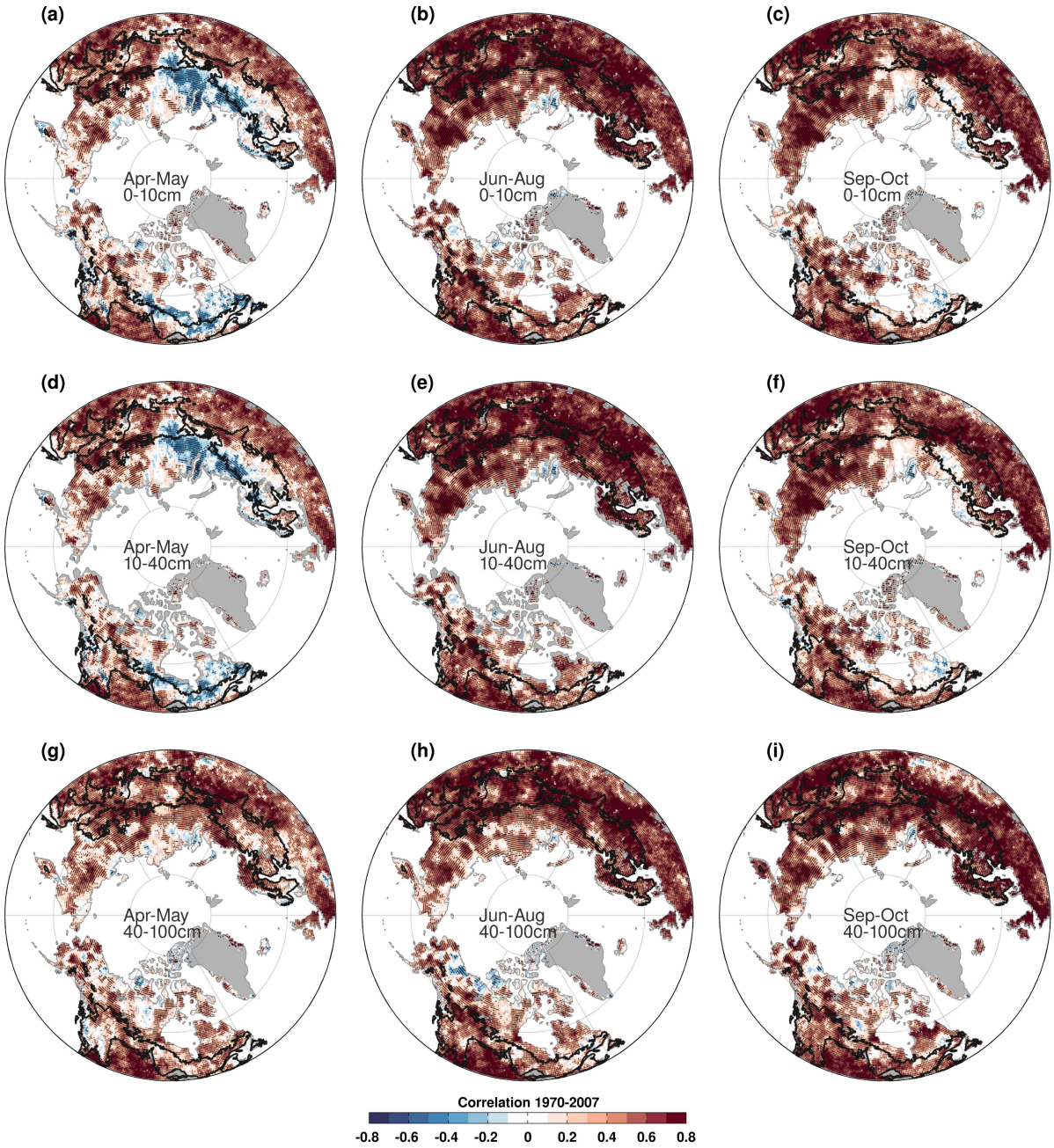

Supplementary Figure C2: Correlation between the scPDSI and soil moisture simulated by the GLDAS-2 Noah land surface model at different depths during spring, summer and autumn. The stippling denotes significant ($p < 0.1$) correlations.

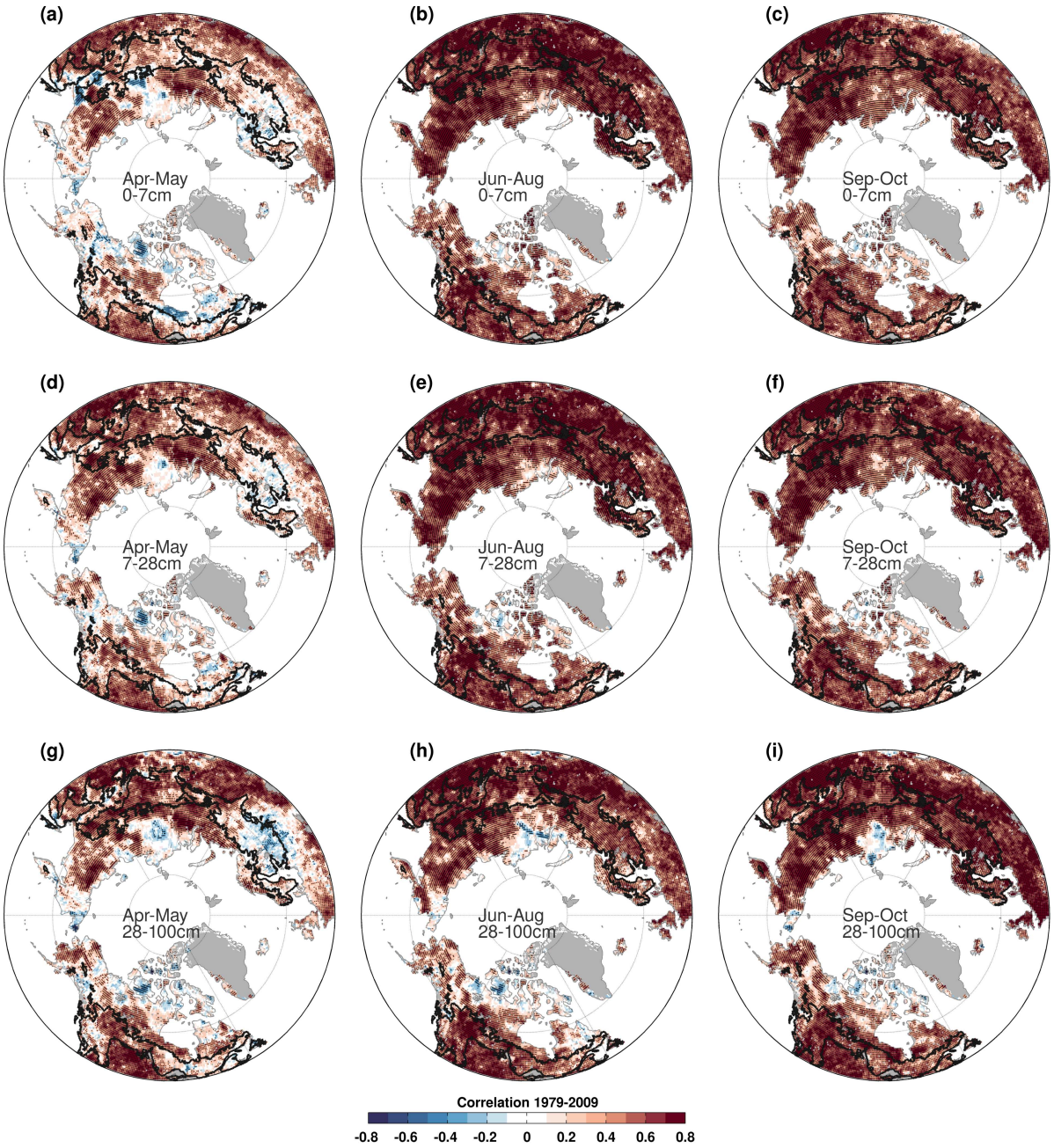

Supplementary Figure C3: Correlation between the scPDSI and simulated soil moisture from ERA-Land at different depths during spring, summer and autumn. The stippling denotes significant ($p < 0.1$) correlations.

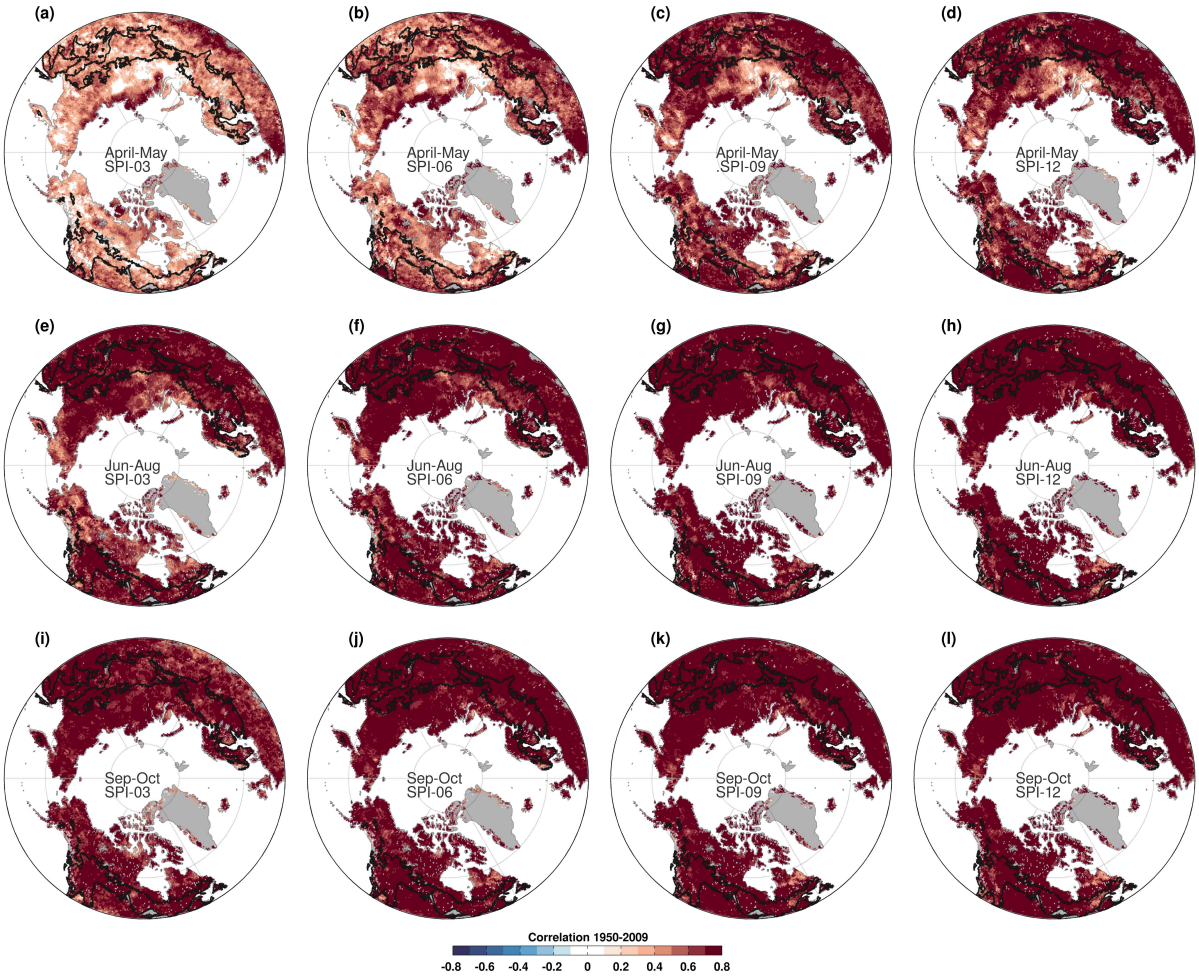

Supplementary Figure C4: Correlation between the scPDSI and the SPI at time scales of 3, 6, 9 and 12 months during spring, summer and autumn. The stippling denotes significant ($p < 0.1$) correlations.

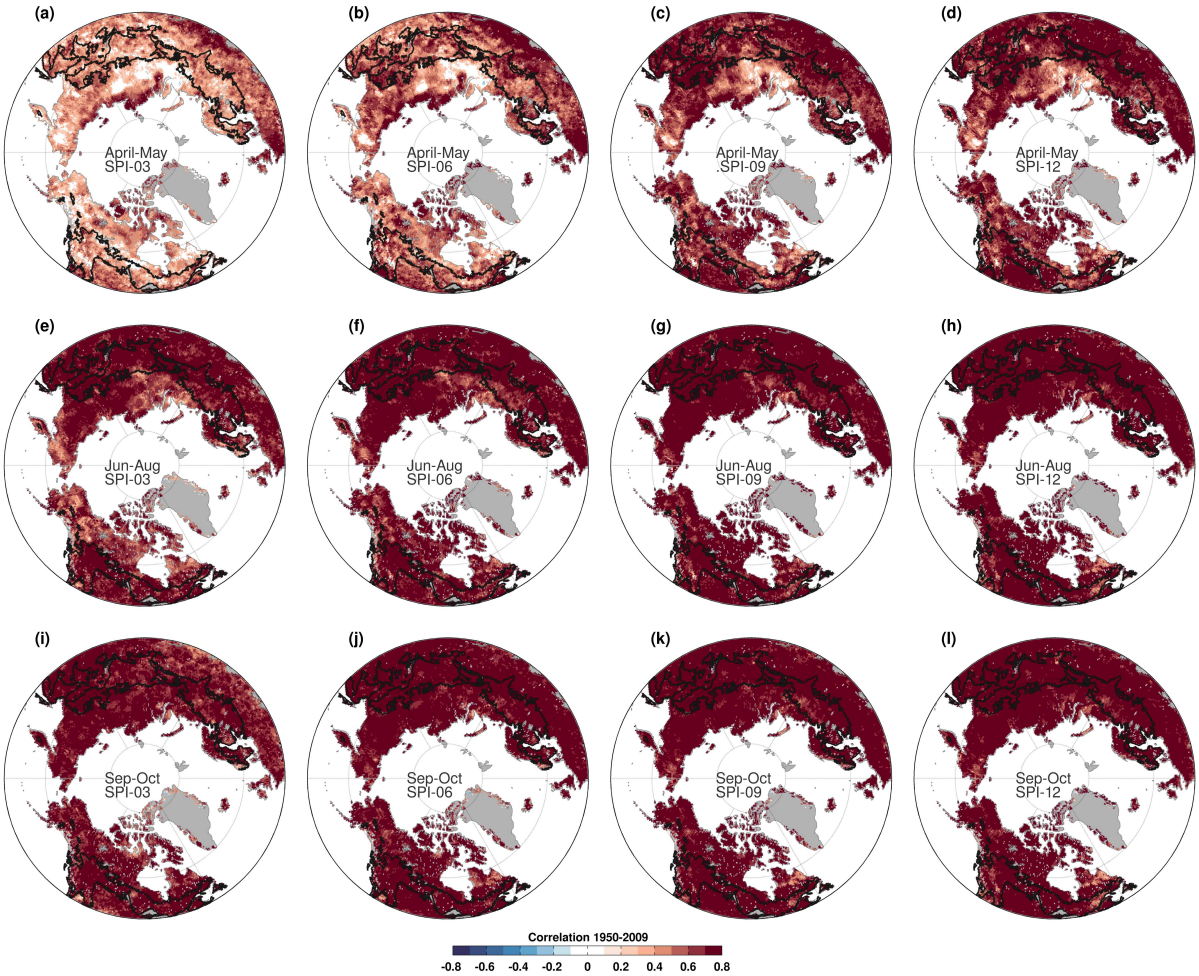

Supplementary Figure C5: Correlation between the scPDSI and the SPEI at time scales of 3, 6, 9 and 12 months during spring, summer and autumn. The stippling denotes significant ($p < 0.1$) correlations.

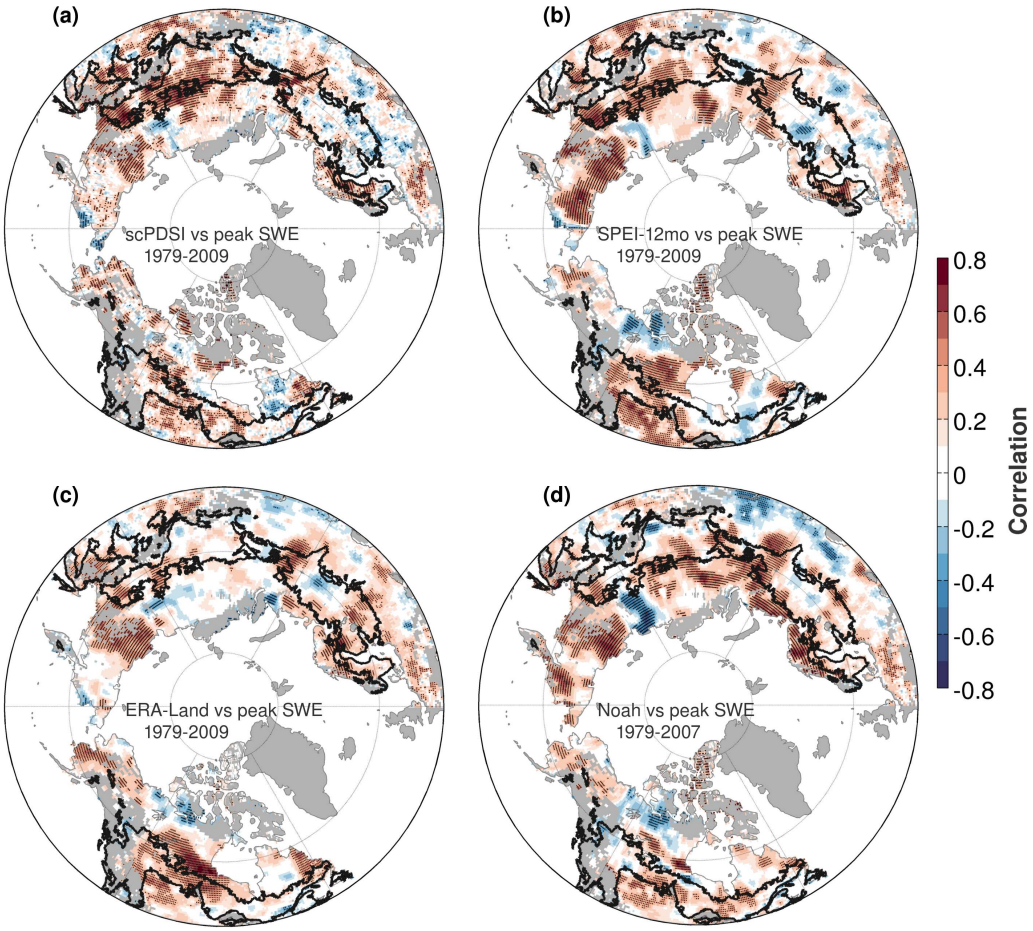

Supplementary Figure C6: Correlations between variations in peak SWE and early-summer (May-June) moisture anomalies produced by drought indices and land surface models. (a) scPDSI. (b) SPEI-12mo. (c) Soil moisture simulated by ERA-Land. (d) Soil moisture simulated by Noah. Correlations are shown only for non-mountainous areas without snow cover during June (SWE < 10 mm).

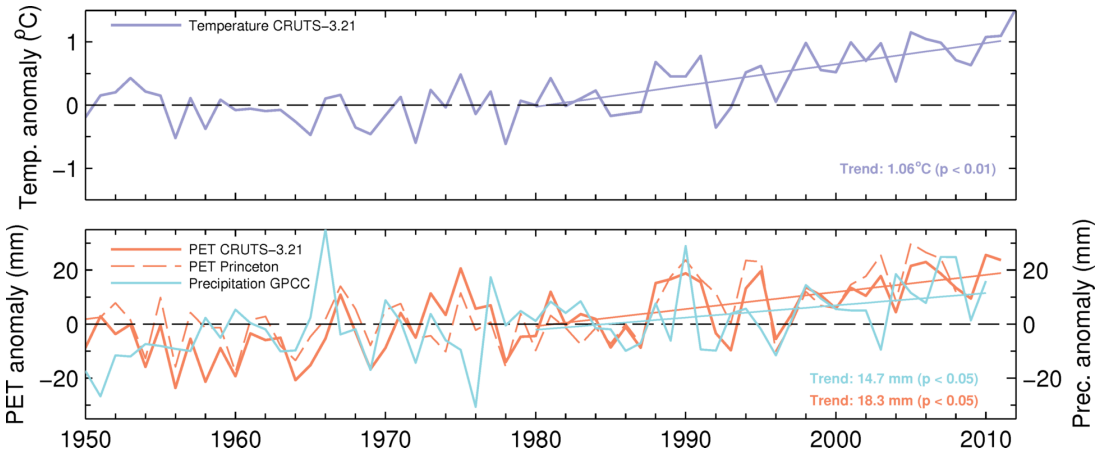

Supplementary Figure C7: Recent warming over the warm season (May–September) and increasing trends in annual (Jan–Dec) precipitation (cyan) and potential evapotranspiration (orange) in the northern latitudes. The dashed orange line corresponds to potential evapotranspiration derived from the Princeton forcing dataset using empirical estimates for net radiation (Sheffield *et al.*, 2012). Trend values over the period 1980–2009 are shown for each variable.

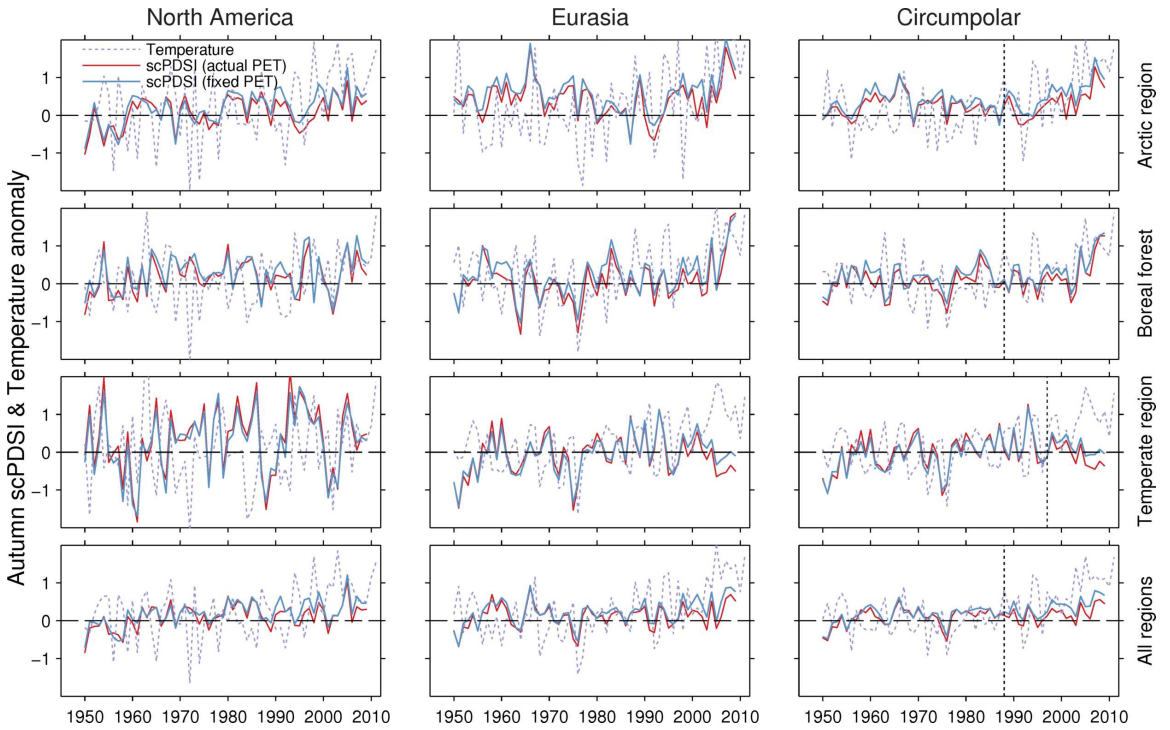

Supplementary Figure C8: Comparisons of autumn (September–October) scPDSI averages with (red) and without (blue) changes in potential evapotranspiration and snowmelt by region and continent. Mean September–October temperature anomalies relative to the period 1961–1990 (dotted line) are shown for each region. The vertical dotted lines denote the years 1988 or 1997.

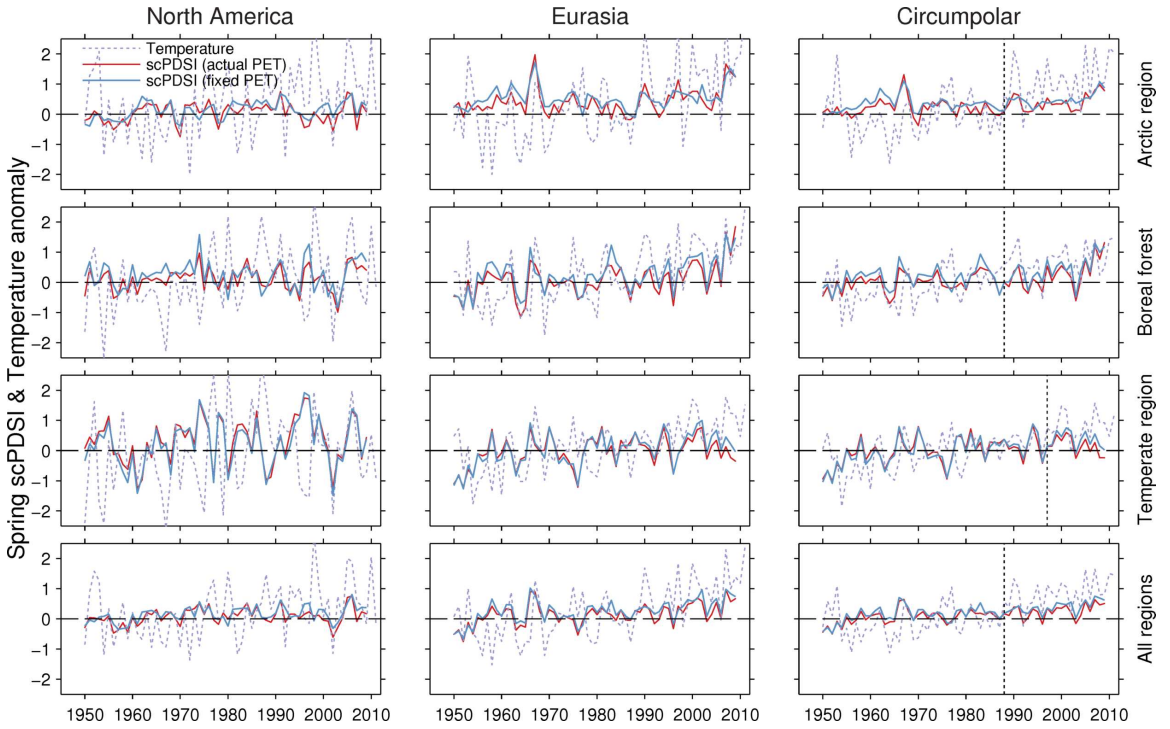

Supplementary Figure C9: Comparisons of spring (April–May) scPDSI averages with (red) and without (blue) changes in potential evapotranspiration and snowmelt by region and continent. Mean April-May temperature anomalies relative to the period 1961–1990 (dotted line) are shown for each region. The vertical dotted lines denote the years 1988 or 1997.

Appendix D

Supplementary material for Chapter 5

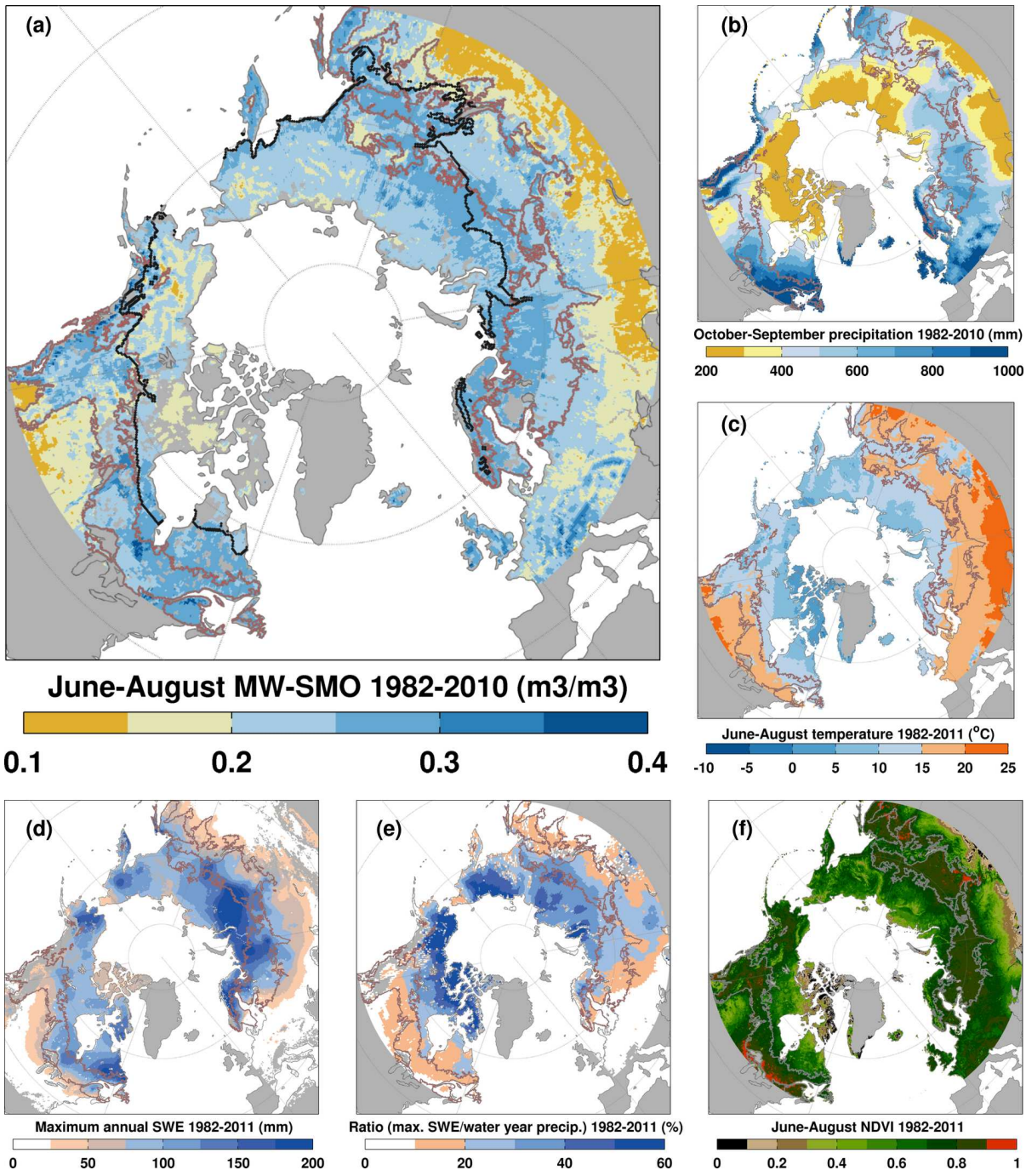

Supplementary Figure D1: Extent of the boreal forest biome and climatologies of soil moisture, NDVI and primary climate variables since 1982. (a) Summer satellite microwave soil moisture (MW-SMO) with an overlay of the southern edge of the continuous permafrost (black line). (b) Water year (October–September) precipitation from the GPCC dataset v6. (c) Summer mean air temperature from the CRUTS 3.2 dataset. (d) Maximum annual Snow Water Equivalent from the GlobSnow product version 1.3. (e) Ratio between maximum annual Snow Water Equivalent and water year precipitation. (f) Mean summer NDVI. The areas north and south of the boreal forest correspond to the Arctic, and northern temperate regions, respectively. Note that the climatology of the MW-SMO is based on the GLDAS NOAH land surface model and is therefore only illustrative of the spatial patterns rather than the absolute values.

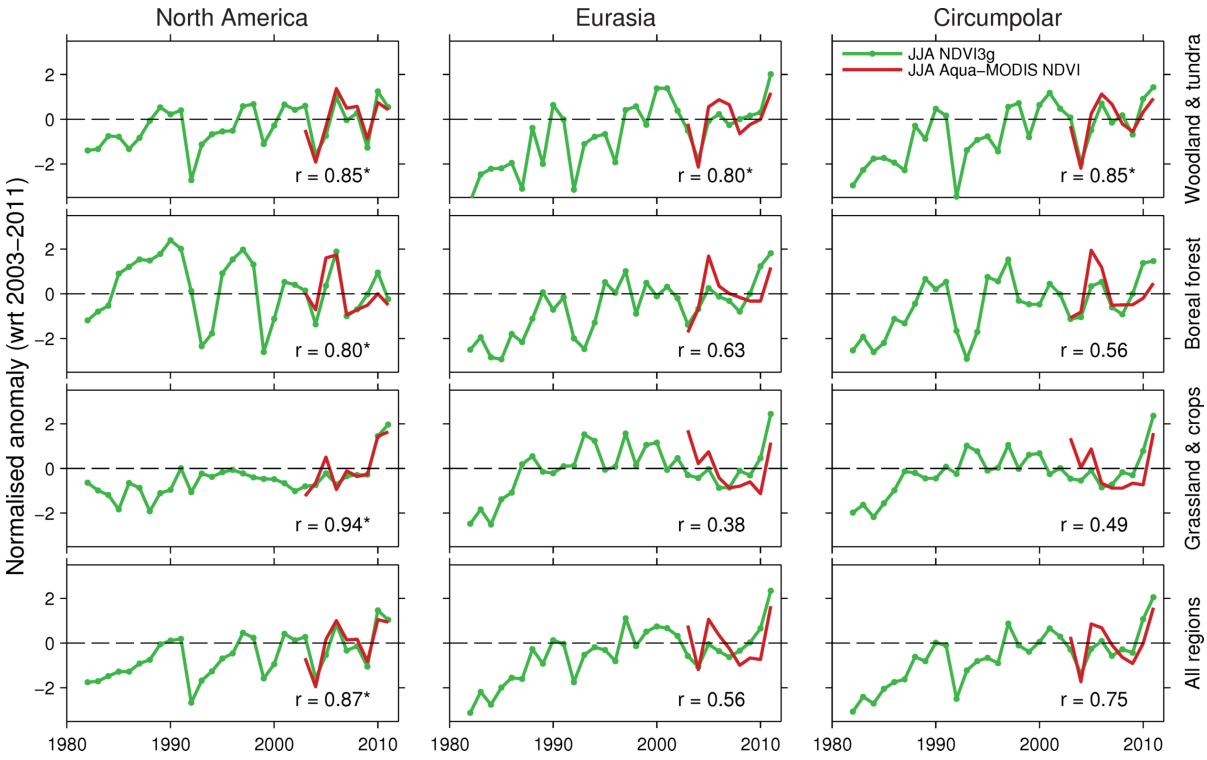

Supplementary Figure D2: Comparison between summer averages of NDVI3g (green) and Aqua-MODIS NDVI (red) by region and continent during the period 2003–2011.

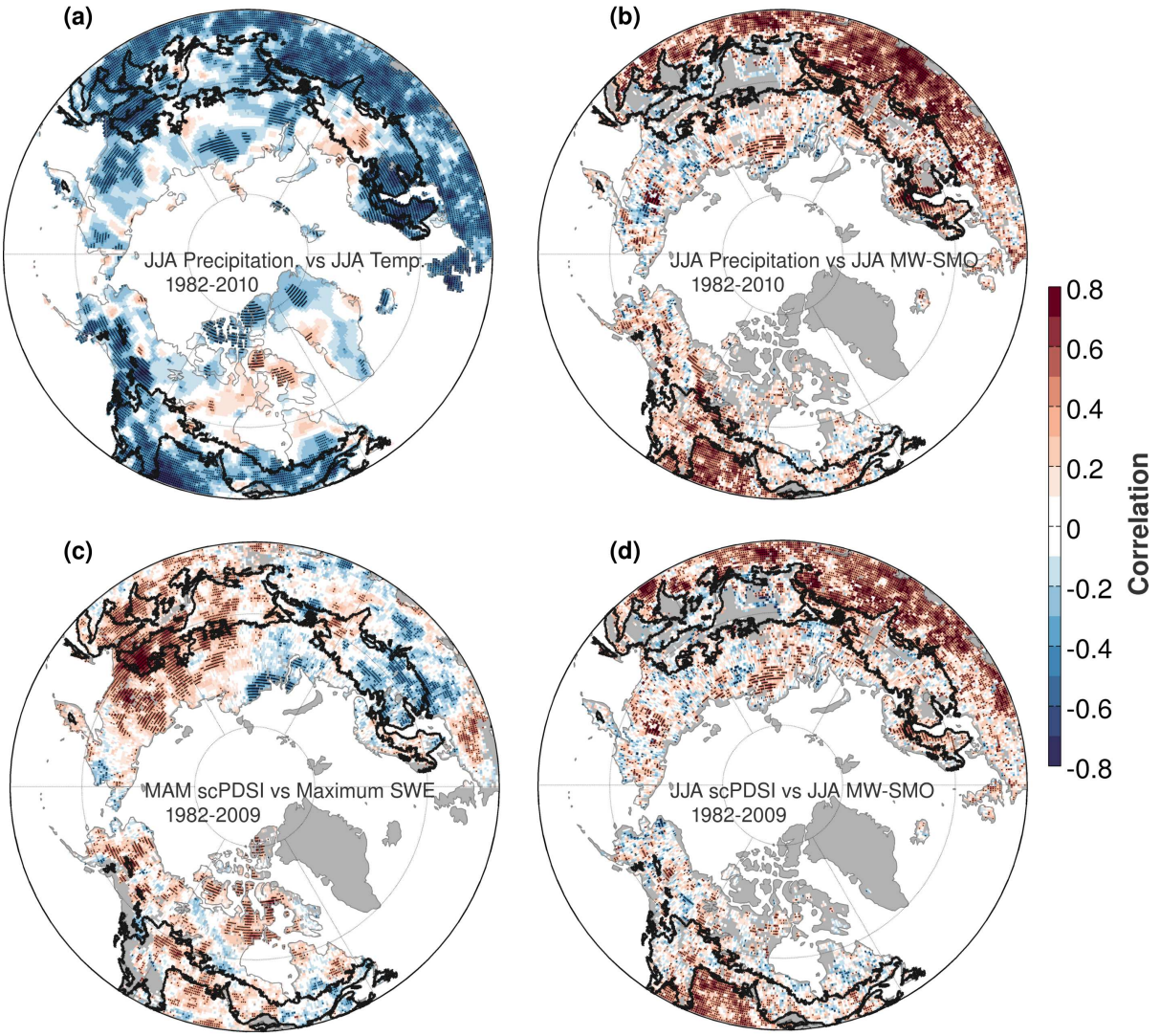

Supplementary Figure D3: Correlation between linearly detrended climate fields. (a) Correlation of summer precipitation with summer temperature. (b) Correlation of summer precipitation with summer MW-SMO. (c) Correlation between spring scPDSI and maximum SWE. (d) Correlation between summer scPDSI and summer MW-SMO. The stippling indicates statistically significant ($p < 0.1$) correlations.

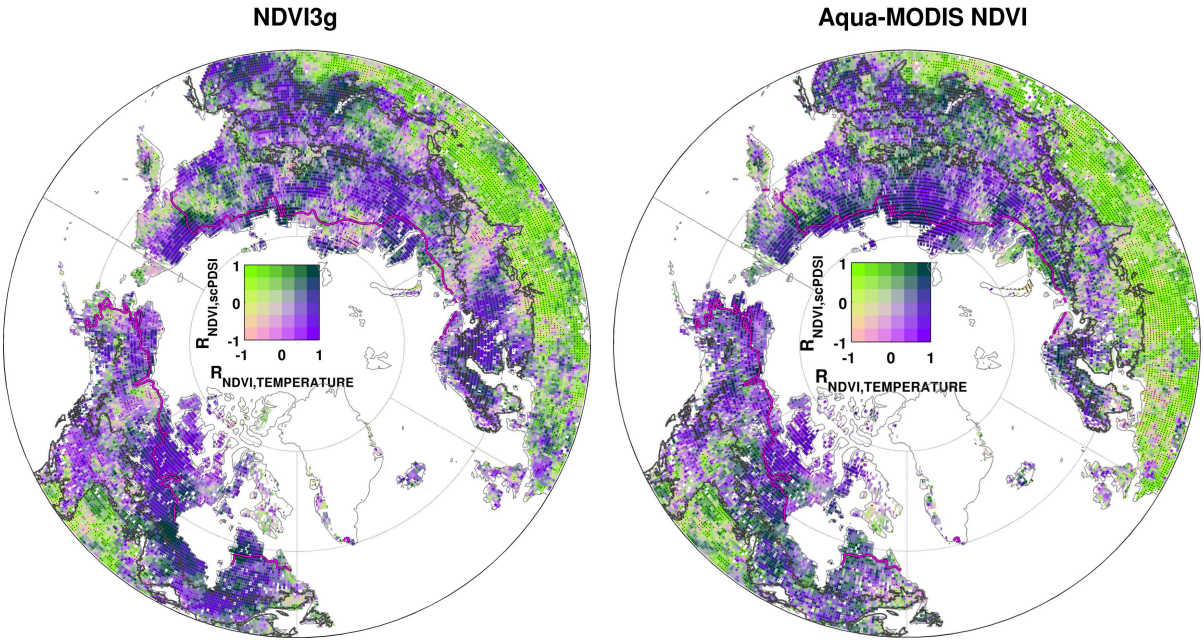

Supplementary Figure D4: Comparison between maps of climate limitation based on NDVI3g and Aqua-MODIS NDVI during the common period 2002–2009. Each map combines correlations of detrended summer NDVI with detrended summer temperature and scPDSI averaged over spring-summer (March–August). Light greens indicate strong moisture limitation (i.e., strong positive correlation with precipitation and negative correlation with temperature), whilst purple shades indicate a dominant temperature limitation (i.e., strong positive correlation with temperature and weak correlation with precipitation). The stippling indicates grid boxes where either correlations with temperature or scPDSI are statistically significant ($p < 0.1$). Although the significance of these relationships over this very short period is difficult to establish, the spatial patterns are still informative for a comparative purpose. The gray polygons in the maps denote the extent of the boreal forests.

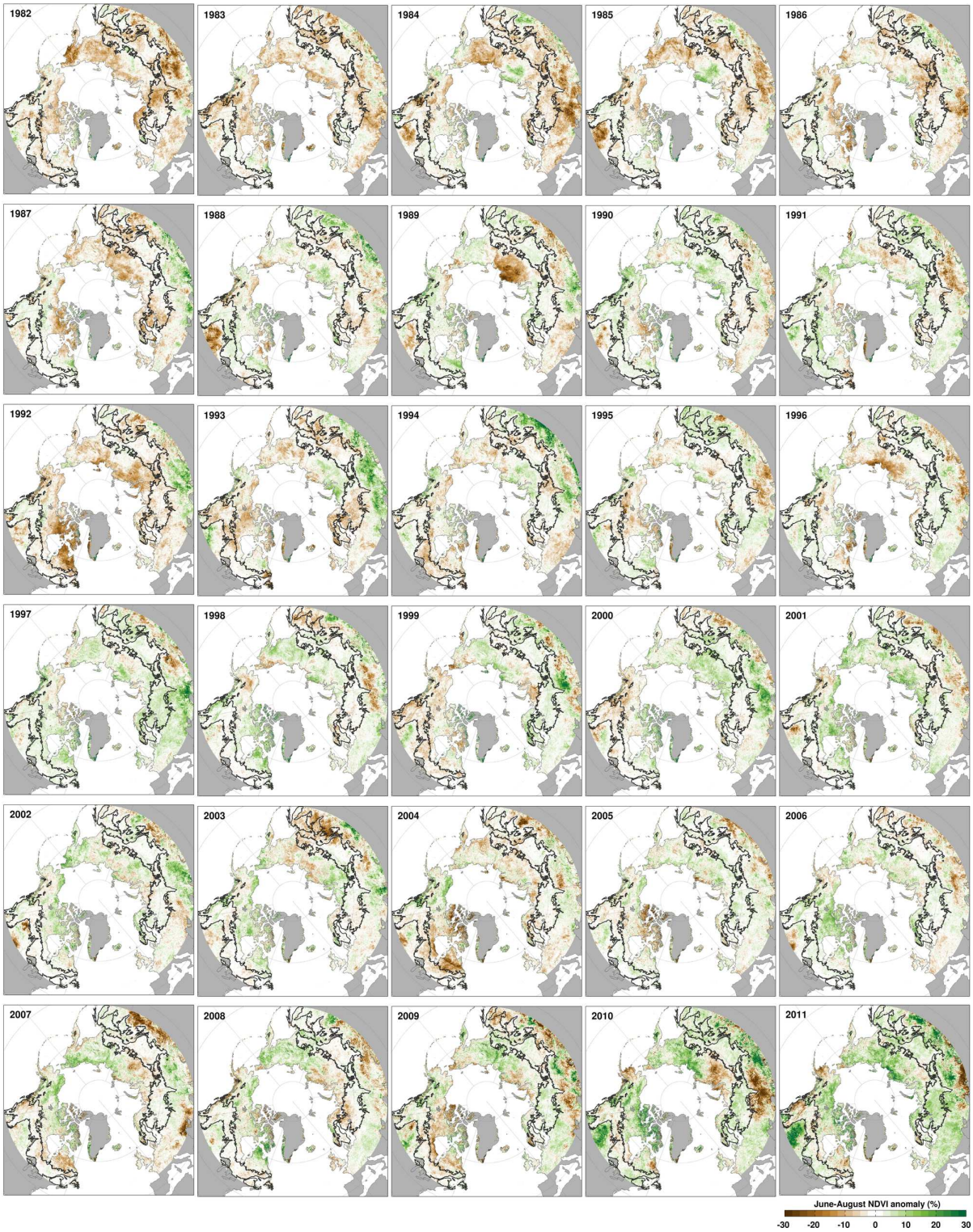

Supplementary Figure D5: Annual maps of summer NDVI anomalies as percentage relative to the mean over the period 1982–2011. Gray shading denotes areas without data or regions outside the study domain.

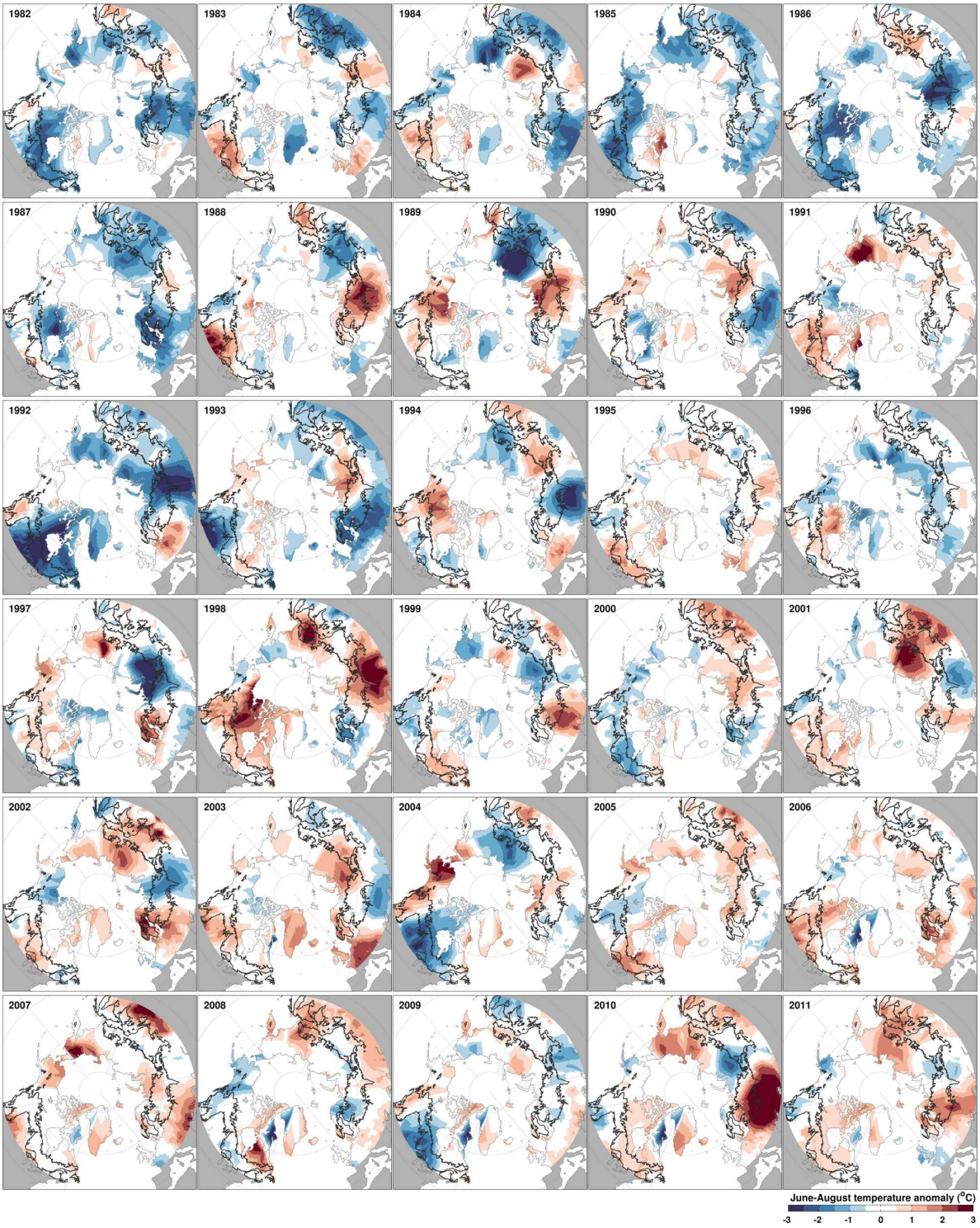

Supplementary Figure D6: Annual maps of summer mean air temperature anomalies relative to the mean of the period 1982–2011.

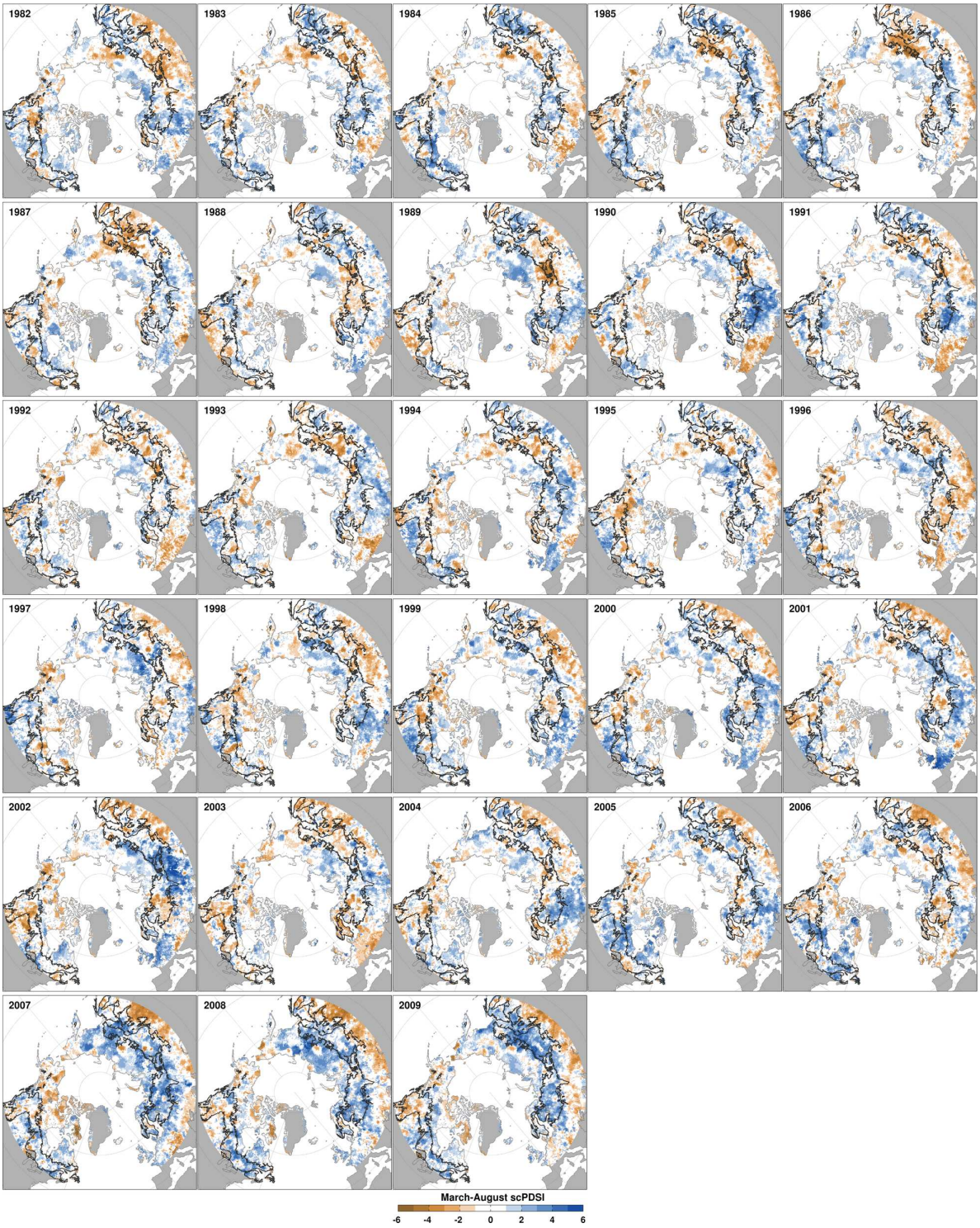

Supplementary Figure D7: Annual maps of spring-summer (March–August) scPDSI since 1982.

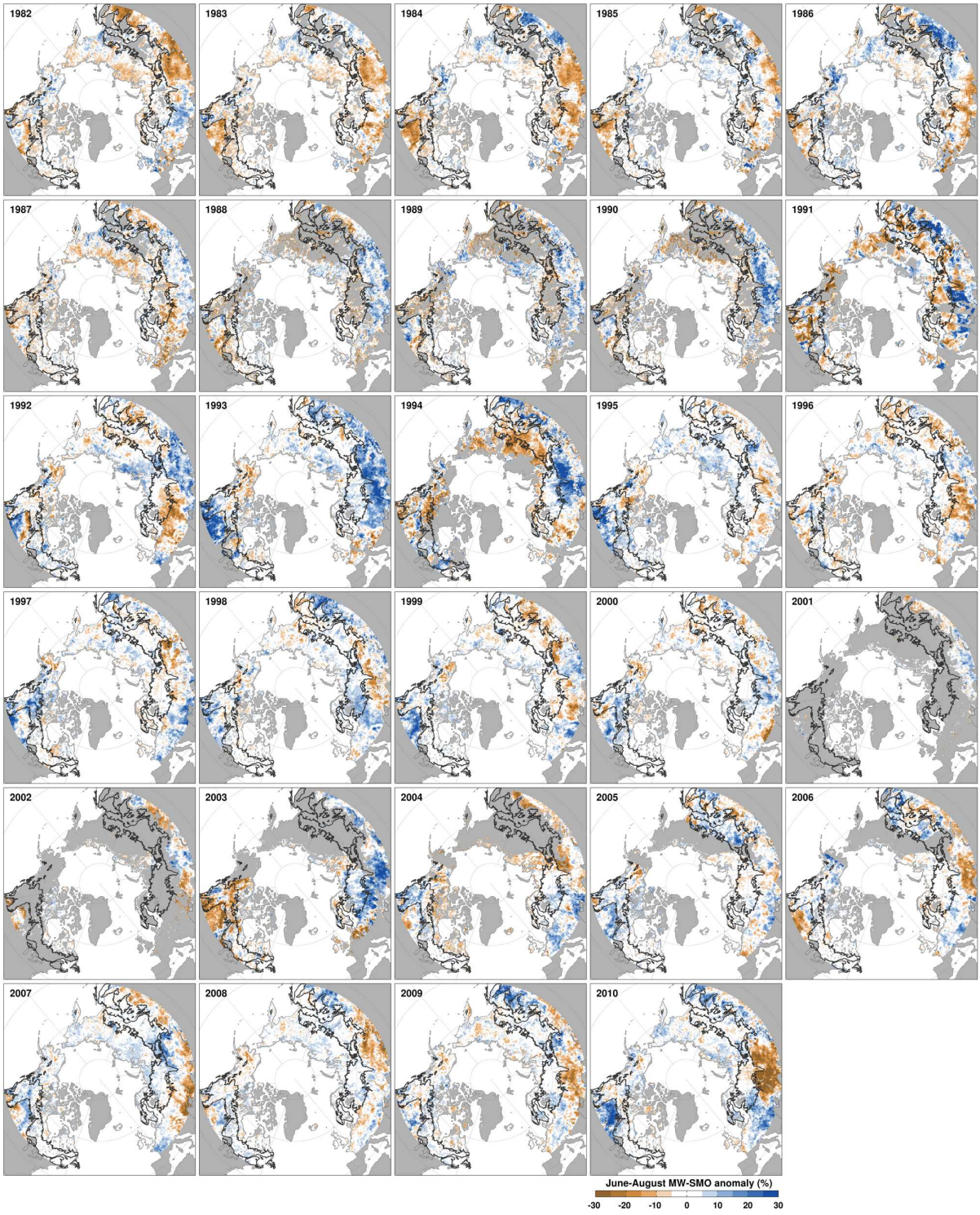

Supplementary Figure D8: Annual maps of summer MW–SMO anomalies as percentage relative to the mean of the period 1982–2010.

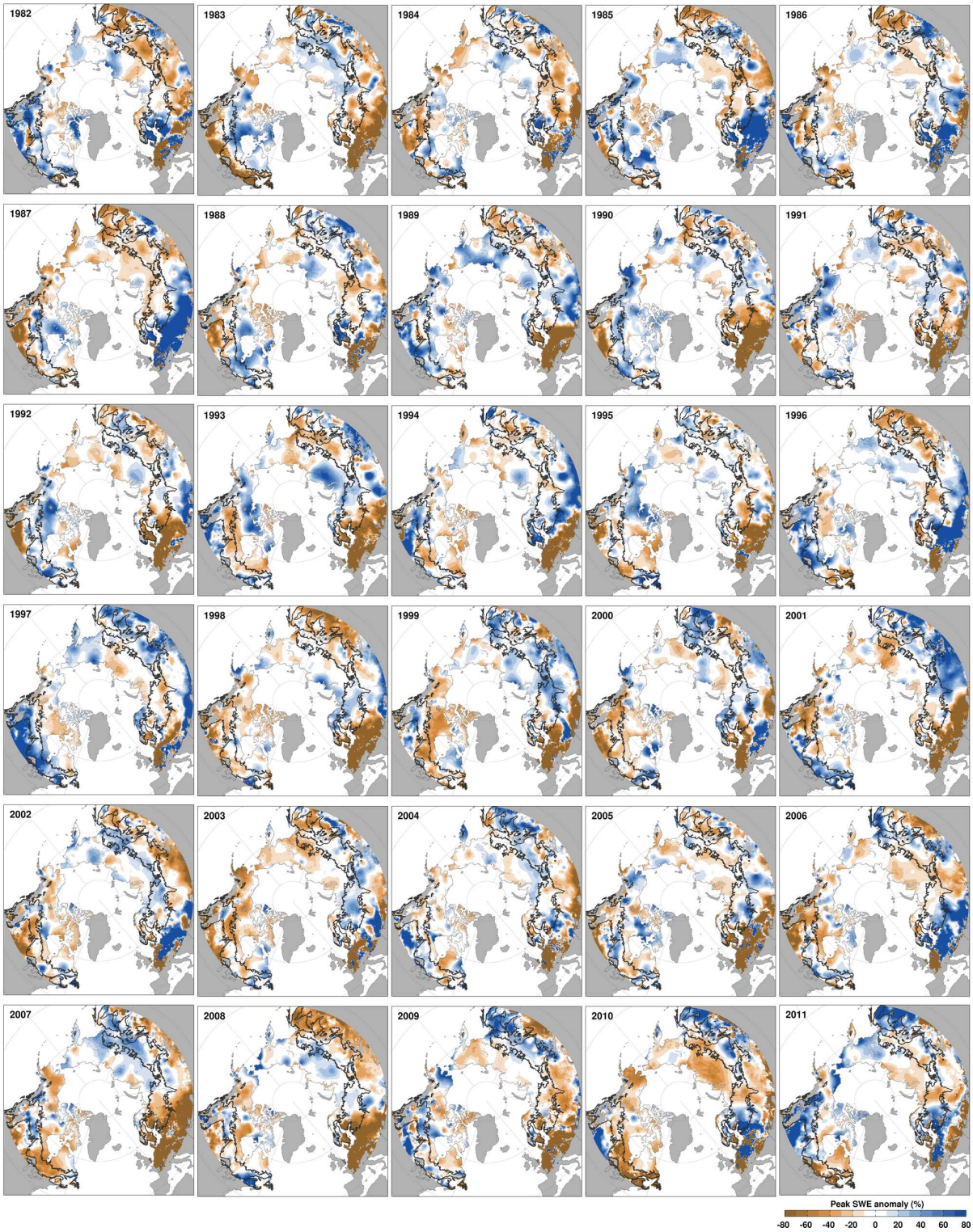

Supplementary Figure D9: Annual maps of maximum annual SWE anomalies as percentage relative to the mean of the period 1982–2010.

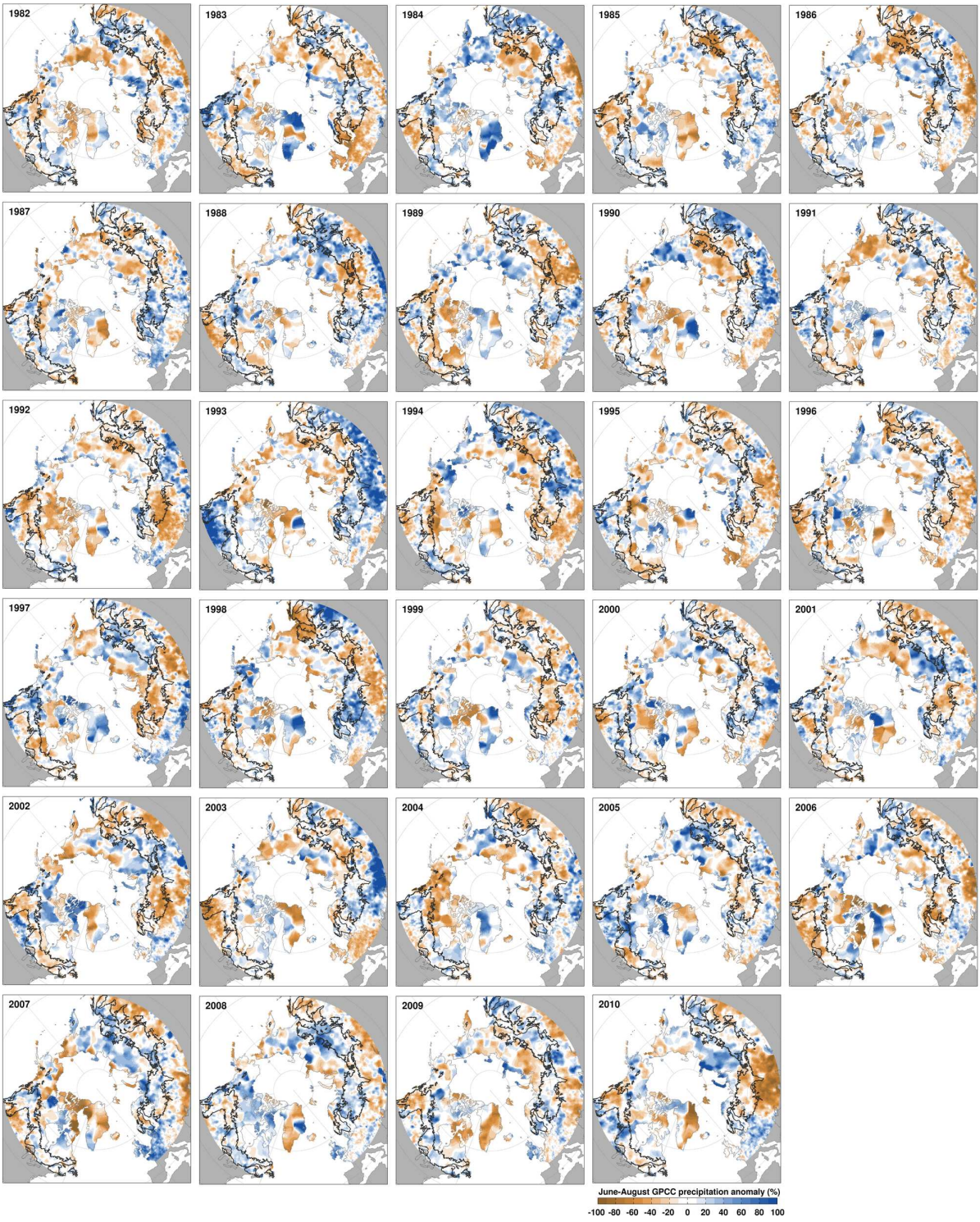

Supplementary Figure D10: Annual maps of summer precipitation anomalies as percentage relative to the mean of the period 1982–2010.

Appendix E

Supplementary material for Chapter 6

Supplementary Table E1: Location and summary of descriptive statistics of the tree-ring chronologies used in this study. Cluster memberships and significant ($p < 0.05$) correlations with thaw depth and thermal and NDVI parameters are indicated for each site. The subscript p in phenological parameters denote previous year.

ID	Name	Elev. (m)	Lat	Lon	First year	Last year	N years	Cores	R.Fun. Clus.[a]	VSL Clus.[b]	AR Order[c]	AR1[d]	Kal.Fil. AR1 Clus.	THAWp	STS	PEAK TEM	PEAK TEMp	TI TEMp	SOS	EOS	PEAK NDVI	TI NDVI	TI NDVIp
1	cana315	-	68.8	-142.4	1067	2002	936	76	2	-	5	0.24	6	-0.27	-	-	-	-	-	-	-	-	-
2	hlm	-	68.7	-134.3	1563	2003	441	27	2	-	2	0.40	4	-0.45	-	-	-0.27	-0.30	-	-0.66	-	-0.61	-
3	msm	-	68.7	-134.3	1611	2003	393	40	2	-	2	0.33	2	-0.49	-	-	-	-0.33	0.60	-0.67	-	-0.66	-
4	mwlc	-	68.6	-141.6	1067	2002	936	159	2	-	2	0.21	3	-0.31	-	-	-	-	-	0.54	-	-	-
5	PC1m	1	68.5	-134.6	1648	2006	359	26	2	-	3	0.19	5	-0.39	-	-	-	-0.31	-	-	-	-	-
5	ftm	-	68.5	-133.9	1332	2003	672	32	2	-	3	0.09	5	-0.47	-	-	-	-0.38	-	-	-	-0.65	-
7	brsj	-	68.5	-143.8	1715	2007	293	153	2	-	1	0.84	4	-0.32	-	-	-	-0.24	-	-	-	-	-
8	mm	-	68.5	-133.9	1398	2003	606	25	2	-	3	0.25	5	-0.31	-	-	-	-	-	0.57	-	-0.69	-
9	cmm	-	68.5	-133.9	1751	2003	253	13	1	-	3	0.36	5	-0.40	-	-	-	-0.31	-	-	-	-0.79	-
10	dwm	-	68.5	-133.9	1483	2003	521	37	2	-	3	0.36	5	-0.37	-	-	-	-0.26	-	-	-	-0.66	-
11	ecm	-	68.5	-133.9	1581	2003	423	19	2	-	3	0.15	5	-0.47	-	-	-	-0.35	-	-	-	-0.54	-
12	mpm	-	68.5	-133.9	1545	2003	459	54	2	-	1	0.46	5	-	-	-	-	-	-	-	-	-0.52	-
13	bbm	-	68.4	-133.8	1501	2006	506	63	2	-	1	0.07	5	-0.35	-	-	-	-0.26	-	-	0.52	-0.65	-
14	tmm	-	68.4	-133.8	1529	2003	475	34	2	-	2	0.53	4	-0.40	-	-	-	-0.26	0.61	0.57	-	-0.42	0.60
15	SC1m	1	68.4	-134.7	1616	2006	391	32	2	-	3	0.19	5	-0.30	-	-	-	-	-	-	0.54	-	-
16	TM1	315	68.3	-139.7	1631	2007	377	94	2	-	1	0.34	1	-0.33	-	0.32	-	-	-	0.56	-	-0.38	-
17	TH1	339	68.3	-140.8	1650	2007	358	89	2	-	4	0.41	1	-	-	-	-	-	0.65	0.53	-	-	0.64
18	AK1m	1	68.3	-134.7	1631	2006	376	34	2	-	5	0.18	5	-0.39	-	-	-	-0.31	0.68	-0.45	-	-	-
29	OC54	292	68.2	-140.1	1615	2007	393	30	2	-	1	0.44	2	-0.59	-	-	-	-0.44	-	-	-	-0.45	-
20	TM2	305	68.2	-139.8	1522	2007	486	60	2	-	2	0.47	6	-0.41	-	-	-	-0.25	-	-	-	-	-
21	OC50	282	68.1	-139.9	1668	2007	340	45	2	-	5	0.47	-	-0.35	-	-	-	-	0.63	-	-	-	-
22	ak047	100	68.1	-141.1	1676	2002	327	16	2	-	1	0.20	3	-0.26	-	-	-	-	-	0.62	-	-	0.59
23	FirthRiver	100	68.1	-141.1	1696	2002	307	90	2	-	1	0.20	-	-0.28	-	-	-	-	-	0.53	-	-	0.53
24	ak053	100	68.1	-143.1	1715	2000	286	153	2	3	2	1.10	-	-	-	-	-	-	-	-	-	-	-
25	OC51	272	68.1	-139.8	1680	2007	328	79	2	-	4	0.46	1	-0.31	-	-	-	-	-	-	-	-	-
26	kgf1	-	68.1	-161.4	1773	2004	232	55	2	-	2	0.39	4	-	-	-	-	-	-	-	-	-	-
27	kgf2	-	68.1	-161.4	1783	2004	222	48	2	-	2	0.32	-	-	-	-	-	-	-	-	-	-	-
28	kgwl1	-	68.1	-161.4	1921	2004	84	13	1	-	3	0.59	-	-	-	-	-	-	-	-	-	-	-
39	kgwl2	-	68.1	-161.4	1886	2004	119	12	2	-	5	0.47	-	-	-	-	-	-	-	-	-	-	-
30	OC52	269	68.1	-139.6	1749	2007	259	53	2	-	5	0.40	1	-0.42	-	-	-	-0.19	-	-0.52	-	-	-
31	ak085	810	68.0	-149.7	1806	2005	200	22	1	3	1	0.39	1	-	-	-	-	-	-	-	-	-	0.61
32	ak104	701	68.0	-149.8	1303	2000	698	100	1	-	1	0.63	-	-	-	-	-	0.32	-	-0.45	-	-	-
33	JC1	286	68.0	-139.1	1744	2007	264	73	2	3	4	0.55	4	-0.53	-	-	-	-0.39	-	-	-	-0.61	-
34	OC53	265	67.9	-139.8	1648	2007	360	75	2	-	4	0.55	-	-0.39	-	-	-	-	0.74	-	-	-0.61	-
35	OC10m	262	67.7	-139.8	1800	2006	207	27	2	-	3	0.48	6	-0.37	-	-	-	-0.26	-	-	0.71	-	-
36	OC9	267	67.7	-139.8	1874	2007	134	50	2	-	3	0.33	-	-0.50	-	-	-	-0.36	-	-	0.60	-	-
37	OC2m	261	67.6	-139.8	1691	2006	316	22	2	3	2	0.64	1	-0.32	-	-	-	-0.15	-	-	0.50	-	0.52
38	PC17m	244	67.5	-139.4	1803	2006	204	47	2	3	1	0.95	-	-0.28	-	-	-	-	-	-	0.47	-	-
39	PC18	251	67.5	-139.3	1686	2006	321	60	2	3	1	0.70	-	-0.47	-	-	-	-0.26	-	-	-	-	-
40	DP26	243	67.5	-140.0	1728	2006	279	35	2	3	1	0.91	1	-0.26	-	-	-	-	-	-	-	-	0.57
41	DP25m	241	67.5	-140.0	1759	2006	248	22	2	3	1	0.92	4	-0.42	-	-	-	-0.26	-	-	-	-	-
42	DP24m	242	67.5	-140.0	1735	2006	272	21	2	3	1	0.87	1	-0.32	-	0.39	-	-	-	-	-	-	0.59
43	ak113	-	67.5	-150.0	952	2000	1049	248	1	-	1	0.53	-	-	-	-	-	-	-	-	-	-	0.57
44	DP23	249	67.5	-140.0	1711	2007	297	44	2	3	1	1.01	1	-0.40	-	-	-	-	-	-	-	-	0.54
45	DP27	243	67.5	-140.1	1608	2007	400	55	2	-	2	0.47	2	-	-	-	-	-	-	-	-	-	-
46	DP30	244	67.5	-140.3	1552	2007	456	61	2	3	5	0.59	-	-	-	-	-	-	-	-	-	-	-
47	DP31	245	67.5	-140.3	1617	2007	391	70	2	3	5	0.45	6	-	-	-	-	-	-	0.47	-	-	-
48	cana314	213	67.2	-115.9	1046	2003	958	311	1	-	1	0.15	6	-0.41	-	-	-0.43	-0.43	-	-	-	-	-
49	ak049	100	67.2	-150.1	1715	2001	287	99	1	2	1	0.66	1	-	-	-	-	-	-	-	-	-	-
50	ak050	100	67.2	-149.1	1731	2000	270	161	1	3	1	0.69	-	-	-	-	-	-	-	-0.35	-	-	-
51	ak051	100	67.2	-149.1	1828	2001	174	39	1	-	1	0.92	1	-	0.31	-	-0.27	-	-	-0.37	-	-	-
52	NorthFork	100	67.2	-150.1	1659	2000	342	40	1	2	1	0.47	-	-	-	-	-	-	-	-	-	-	-
53	NutirwikCreek	100	67.2	-149.1	1632	2002	371	131	1	3	1	0.63	1	-	-	-	-	-	-	-0.37	-	-	0.51
54	ak052	100	67.1	-152.1	1730	2002	273	200	1	2	2	0.56	6	-	-	-	-	-	-	-	-	-	-
55	HuntFork	100	67.1	-152.1	1730	2002	273	97	1	2	2	0.53	6	-	-	-	-	-	-	-	-	-	-
56	ak048	100	67.1	-150.1	1725	2001	277	77	1	2	2	0.44	-	-	-	-	-	-	-	-	-	-	-
57	ChimneyLake	100	67.1	-150.1	1725	2000	276	86	1	2	2	0.53	-	-	-	-	-	-	-	-	-	-	-
58	cana326	-	67.0	-139.0	1067	2002	936	131	2	-	1	0.32	6	-	-	-	-	-	0.57	-	-	-	-
59	CIS	-	66.4	-117.7	1579	2003	425	19	1	3	2	-0.16	5	-	-	-	-	-	-	-	-	-	-
60	MUL	-	66.3	-117.7	1614	2003	390	19	1	3	1	-0.28	5	-	-	-	-0.35	-	-	-	-	-	-
61	cana322	-	66.0	-120.0	1046	2003	958	449	1	-	4	0.12	6	-	-	-	-0.46	-0.32	-	-	-	-	-
62	CLL	200	65.6	-117.7	1615	2001	387	52	1	-	2	0.07	2	-	-	0.33	-0.43	-	-	-	-	-	-
63	DP21	251	65.5	-139.9	1657	2007	351	67	2	3	2	0.71	-	-0.30	-	-	-	-	0.43	-	0.58	-	0.57
64	ak060	259	65.2	-162.3	1621	2002	382	24	1	-	2	0.50	6	-	0.32	0.35	-	-	-	-	-	-	-

[a] Cluster for monthly correlation function with temp. and scPDSI; [b] Cluster for monthly G_T and G_W response functions of VLS; [c] Autoregressive order; [d] Autocorrelation of order 1.

Supplementary Table E1: Continued.

ID	Name	Elev. (m)	Lat	Lon	First year	Last year	N years	Cores	R.Fun. Clus.	VSL Clus.	AR Order	AR1	Kal.Fil. AR1 Clus.	THAWp	STS	PEAK TEM	PEAK TEMp	TI TEMp	SOS	EOS	PEAK NDVI	TI NDVI	TI NDVIp
65	ak066	213	65.2	-162.2	1533	2002	470	50	1	-	2	0.44	3	-	0.39	-	-	-0.22	-	-	-	-0.33	-
66	ak067	229	65.2	-162.2	1383	2002	620	67	1	-	2	0.37	1	-	0.40	-	-	-0.21	-	-	-	-	-
67	ak062	239	65.2	-162.3	1358	2002	645	49	1	-	2	0.21	3	-	0.35	-	-	-0.30	-	-	-	-	-
68	ak065	-	65.2	-162.2	1400	2002	603	20	1	-	1	0.80	6	-	-	-	-	-0.29	-	-	-	-	-
79	ak057	168	65.2	-162.2	1607	2002	396	37	2	1	2	0.38	6	-	-	-	-	-0.31	-	-	-	-	-
70	ak058	213	65.2	-162.2	1406	2002	597	59	1	-	2	0.60	6	-	0.38	-	-	-0.31	-	-	-	-	-
71	ak070	251	65.2	-162.2	1556	2002	447	48	1	-	2	0.34	6	-	0.42	0.31	-	-0.24	-	-	-	-	-
72	ak115	-	65.2	-162.3	1389	2001	613	46	1	-	2	0.31	6	-	0.43	-	-	-0.20	0.43	-	-	-	-
73	ak059	282	65.1	-162.2	1542	2002	461	94	1	-	2	0.20	2	-	0.49	-	-	-0.19	-	-	-	-	-
74	ak063	-	65.1	-162.2	1590	2002	413	36	1	-	2	0.22	3	-0.27	0.49	0.39	-0.35	-0.40	-	-	-	-	-
75	ak061	282	65.1	-162.2	1575	2002	428	34	1	-	2	0.39	1	-	0.38	0.36	-	-	-	-	-	-0.53	-
76	ak064	229	65.1	-162.2	1611	2002	392	47	1	-	2	0.37	3	-	0.50	-	-	-0.28	-	-	-	-	-
77	ak068	229	65.1	-162.2	1550	2002	453	53	1	-	2	0.34	3	-	0.49	-	-	-0.27	-	-	-	-	-
78	ak069	244	65.1	-162.2	1718	2002	285	34	1	-	2	0.42	2	-0.28	0.40	-	-	-0.28	-	-	-	-	-
79	ak126	341	64.8	-141.2	1854	2009	156	30	2	3	5	0.20	-	-	-	-	-	-0.19	-	-	-	-	-
80	ak125	245	64.5	-147.0	1890	2009	120	20	2	2	1	0.53	-	-	0.33	-	-	-	0.56	-	-	-	-
81	ak124	229	64.2	-149.3	1827	2009	183	29	2	2	1	0.58	2	-0.31	0.39	-	-	-0.22	-	-	-	-	-
82	ak122	420	63.8	-144.8	1835	2009	175	29	2	-	3	0.90	-	-	0.51	-	-	-	0.56	-	-	-	-
83	ak123	437	63.7	-144.2	1851	2009	159	20	2	-	3	0.27	-	-	0.34	-	-	-	-	-	-	-	-
84	ak056	100	63.1	-149.0	1735	2000	266	107	2	1	5	0.05	-	-0.34	0.41	-	-0.39	-	-	0.73	-0.48	-	-
85	ak054	100	63.1	-150.0	1735	2000	266	107	2	1	5	0.05	-	-0.38	0.41	-	-0.39	-	-	-	-	-	-
86	ak055	100	63.1	-148.1	1788	2002	215	92	2	-	3	0.60	1	-	-	-	-0.42	-	-	-	-	-0.42	-
87	PPN	1400	62.7	-111.0	1827	2001	175	24	1	-	1	0.15	-	-	-	-	-0.30	-	-	-0.55	-	-	-
88	CHB	181	62.5	-113.8	1646	2002	357	25	1	2	3	-0.27	2	-	0.38	0.43	-0.34	-	-	-	-	-	-
89	GRLPg	335	61.9	-108.1	1770	2001	232	33	1	-	3	0.10	3	-	0.43	-	-0.22	-	-	-	-	-	-
90	SBM	1370	61.7	-125.6	1699	2001	303	20	2	-	3	0.14	2	-	-	-	-	-	-	-	-	-	-
91	VIF	550	61.6	-125.7	1665	2001	337	13	2	-	3	0.33	-	-	-	-	-	-	-	-	-	-	-0.25
92	cana295	-	61.4	-116.6	1933	2008	76	18	2	2	3	1.14	-	-	-	-	-	-	-	-	-	-	-0.33
93	TRPg	183	61.3	-119.9	1757	2001	245	35	2	-	3	0.50	2	-	-	-	-	-	-	-	-	-	-
94	cana296	270	61.1	-120.0	1819	2008	190	16	2	-	3	0.78	-	-	-	-	-	-	-	-	-	-	-
95	cana354	800	61.0	-138.5	913	2001	1089	86	2	-	5	0.23	1	-	-	-	-	-	-	-	-	-	-
96	NCH	160	61.0	-113.3	1870	2001	132	15	2	2	1	0.46	-	-	-	-	-	-	-	-	-	0.56	-
97	ak088	580	61.0	-153.9	1769	2004	236	20	1	-	2	0.29	4	-	0.35	-	-0.23	-	-	-	-	-	-
98	ak089	580	60.7	-154.0	1600	2003	404	34	2	1	2	0.52	-	-0.41	-	-	-0.52	-	-	-	-	-	-
99	ak112	-	60.5	-146.0	1247	2002	756	284	2	-	1	0.59	4	-	-	0.38	-0.32	-	-	-	-	-	-
100	ak087	580	60.5	-153.9	1672	2003	332	51	1	-	1	0.87	-	-	-	-	-0.56	-	-	-	-	-	-
101	ak086	540	60.5	-154.3	1627	2003	377	41	1	-	2	0.36	-	-	-	-	-0.43	-	-	-	-	-	-
102	cana298	-	60.0	-119.0	1903	2008	106	41	2	2	4	0.49	-	-0.25	-	-	-	-	-	-	-	-	-
103	PPR	209	59.0	-112.0	1698	2000	303	22	2	2	2	1.00	-	-0.25	-	-	-	-	-	-	-	-	-
104	HSS	209	58.9	-111.6	1801	2000	200	12	2	2	1	0.79	-	-0.30	-	-	-	-0.25	-	-	-	0.46	-
105	RCO	70	58.9	-111.3	1742	2000	259	29	2	2	1	0.81	-	-	-	-	-	-	-	-	-	-	-
106	CQF	70	58.8	-111.5	1712	2000	289	29	2	2	1	0.80	-	-	-	-	-	-	-	-	-	-	-
107	MMK	209	58.6	-111.3	1859	2000	142	11	2	2	2	0.19	-	-	-	-	-	-	-	-	0.56	-	-0.70
108	BCR	209	58.5	-112.5	1757	2000	244	14	2	2	4	0.87	-	-	-	-	-	-	-	-	-	-	-
109	ATR	75	58.4	-111.5	1708	2000	293	19	2	2	1	0.81	-	-0.27	-	-	-	-0.35	-	-	-	-	-0.36
110	WLPg	474	57.8	-103.8	1852	2002	151	14	2	1	1	0.31	-	-	-	-	-0.23	-	-	-	-	-	-
111	ak114	-	56.0	-132.0	1343	2000	658	138	1	1	5	0.50	-	-	-0.29	-	-	-	-	-	-	0.57	-
112	KIL	390	55.7	-106.4	1840	2001	162	27	2	-	1	0.60	-	-	-	-	-0.20	-0.28	-	-	0.51	-	-0.39
113	ORP	360	55.6	-104.7	1879	2002	124	21	2	-	4	0.57	-	-	-0.29	-	-	-	-	-	-	-	-
114	MTM	-	55.5	-114.8	1817	2004	188	6	2	-	1	0.76	-	-	-	-	-	-	-	-	-	-	-
115	DBY	315	54.9	-102.8	1839	2001	163	24	2	-	3	0.46	-	-	-	-	-0.38	-	-	0.51	-	0.57	-

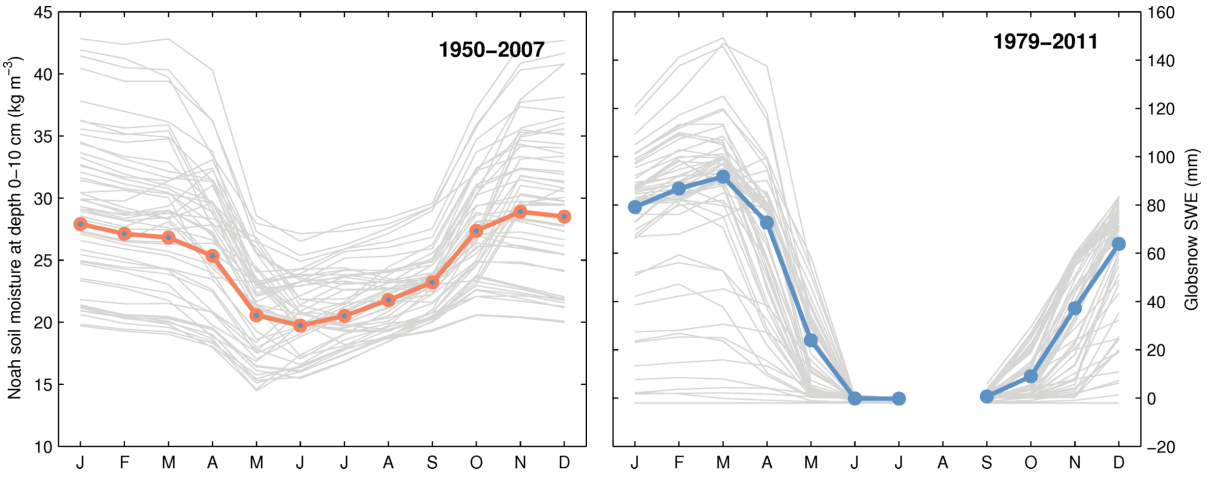

Supplementary Figure E1: Mean monthly climatologies of Noah surface soil moisture (0–10 cm) and Globsnow Snow Water Equivalent averaged across the grid boxes co-located with the tree-ring sites.

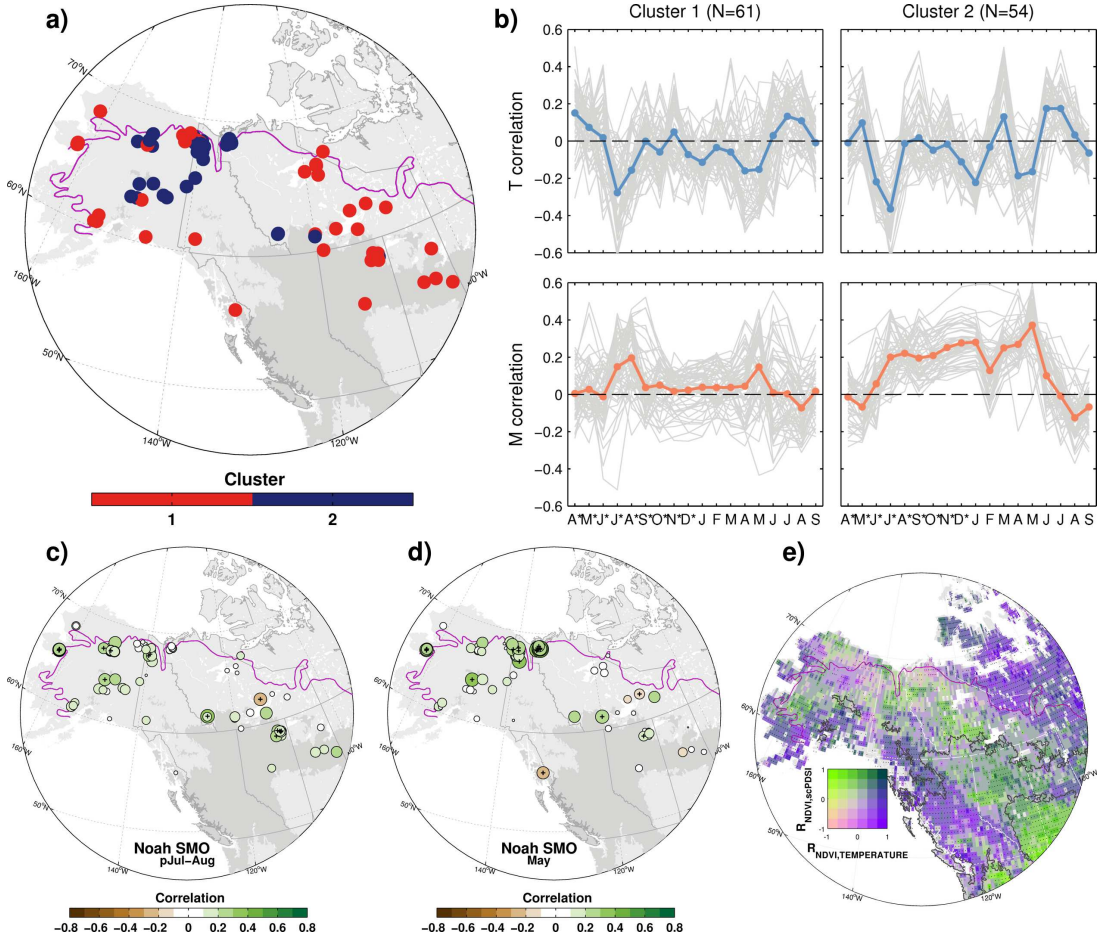

Supplementary Figure E2: (a) Clustering of tree-ring sites based on their patterns of monthly correlations with temperature (T) and Noah surface soil moisture (M). (b) Individual and cluster-averaged monthly correlations. (c–d) Spatial distribution of correlations between tree growth (SPL10 tree-ring chronologies) and previous summer and current spring soil moisture availability. (e) Map of moisture and temperature constraints of summer NDVI as explained in Figure 5.5. The dark gray shading in the maps denotes the the boreal forests. The purple and cyan lines indicate the location of the treeline and the southern edge of the discontinuous permafrost, respectively.

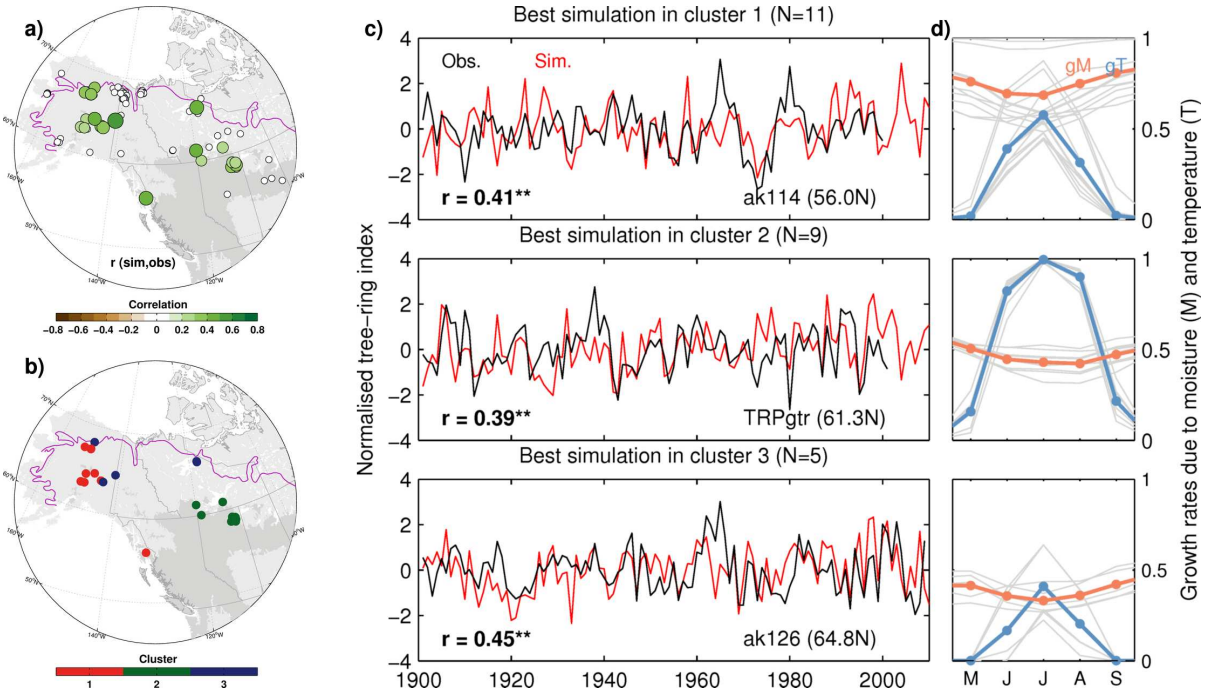

Supplementary Figure E3: Distinct regional patterns of simulated climate limitation of tree growth. (a) Spatial distribution of significant correlations between simulated and observed SPL10 tree-ring chronologies during the verification period 1971–2000. White circles in the map represent chronologies that were not successfully simulated. (b) Regional clusters of simulated climate limitation based on growth rates due to moisture (g_M, orange) and temperature (g_T, blue). (c) Best simulated tree-ring chronology in each cluster. (d) Mean and individual growth rates due to moisture and temperature in each cluster.

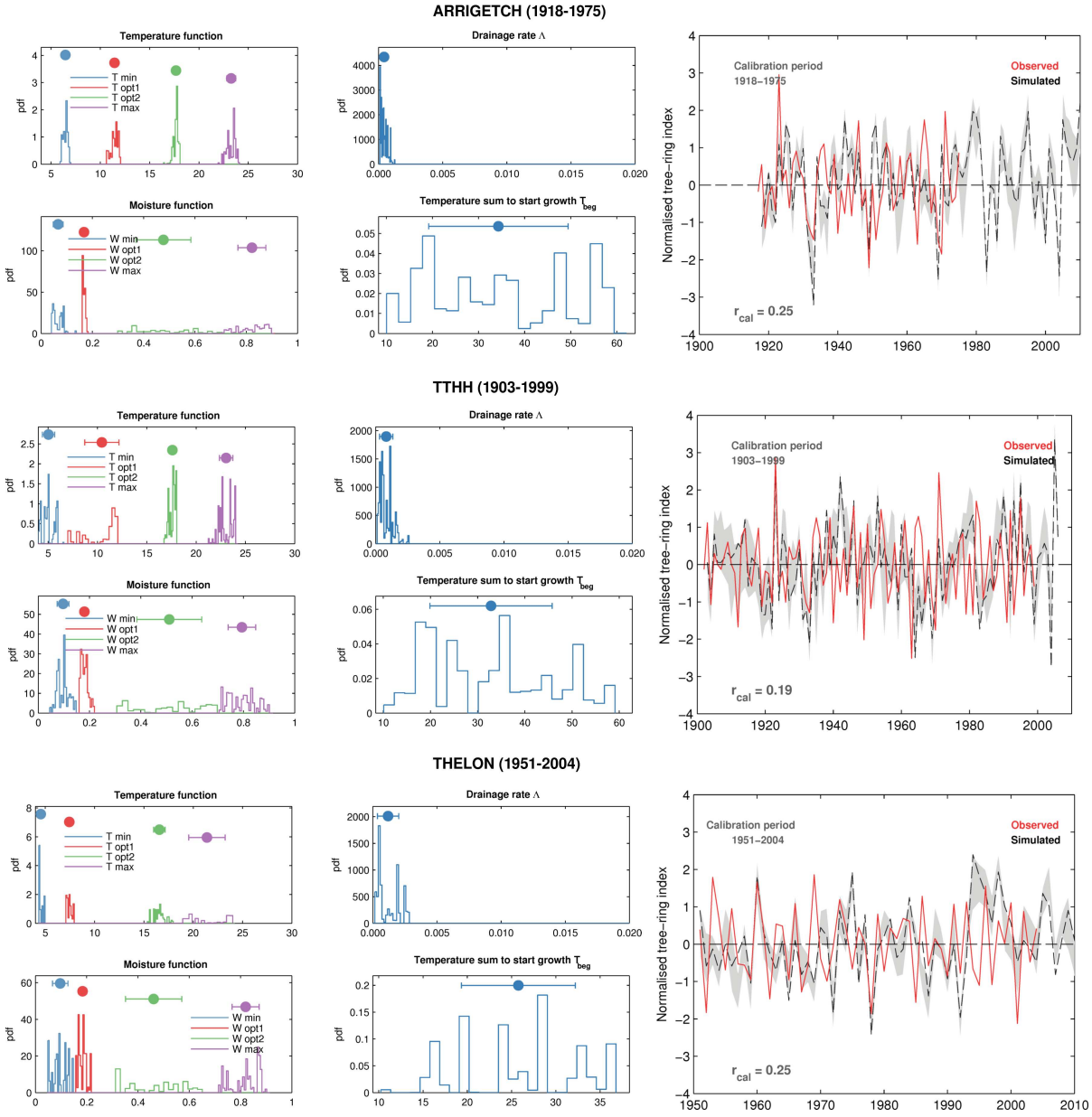

Supplementary Figure E4: Posterior distributions of calibrated parameters of the VS model and simulated tree-ring chronologies at Arrigetch, TTHH and Thelon using the full period of available data for calibration.

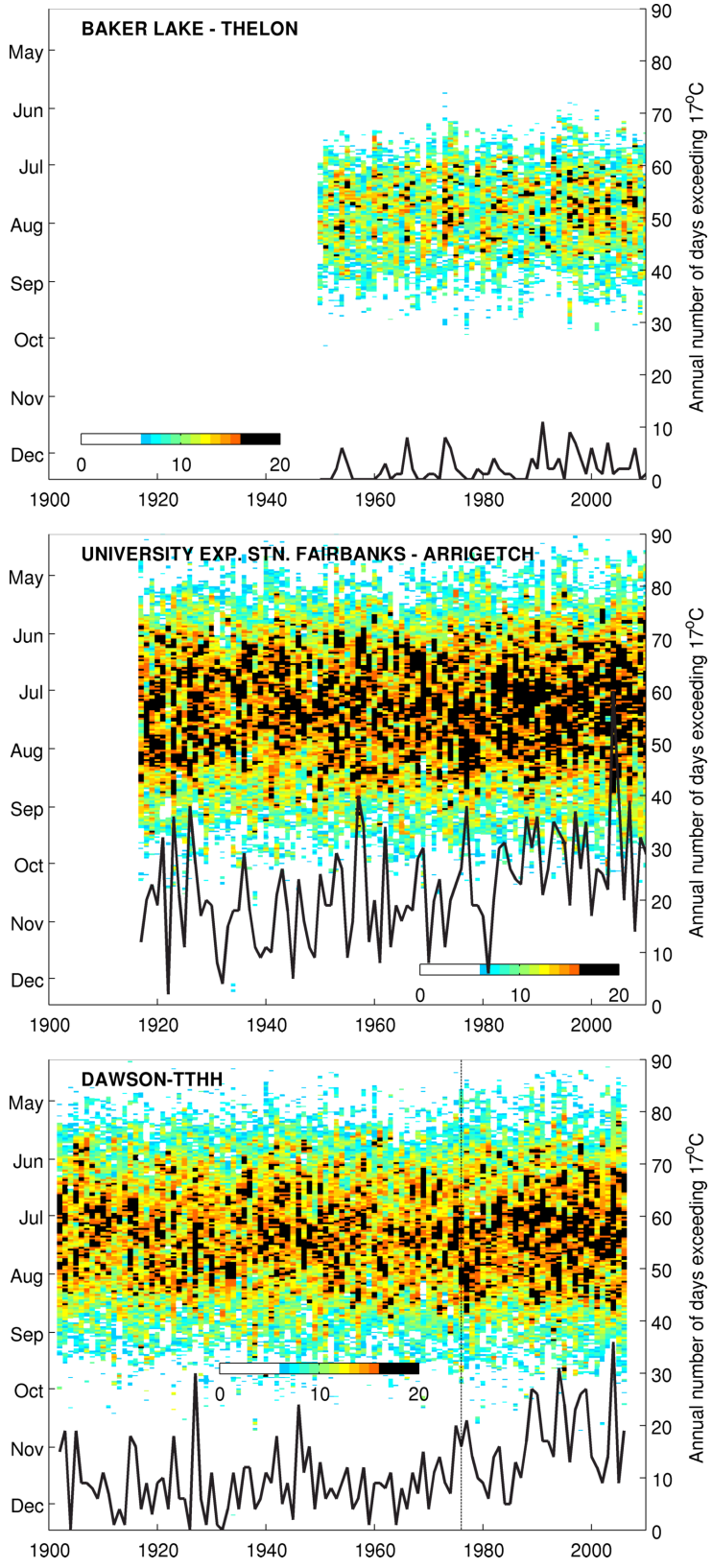

Supplementary Figure E5: Frequency of exceedance of the 17°C threshold at the stations used for modelling tree growth. Daily mean temperatures above the threshold are shown in black, whilst temperatures lower than 5°C are masked out as white.

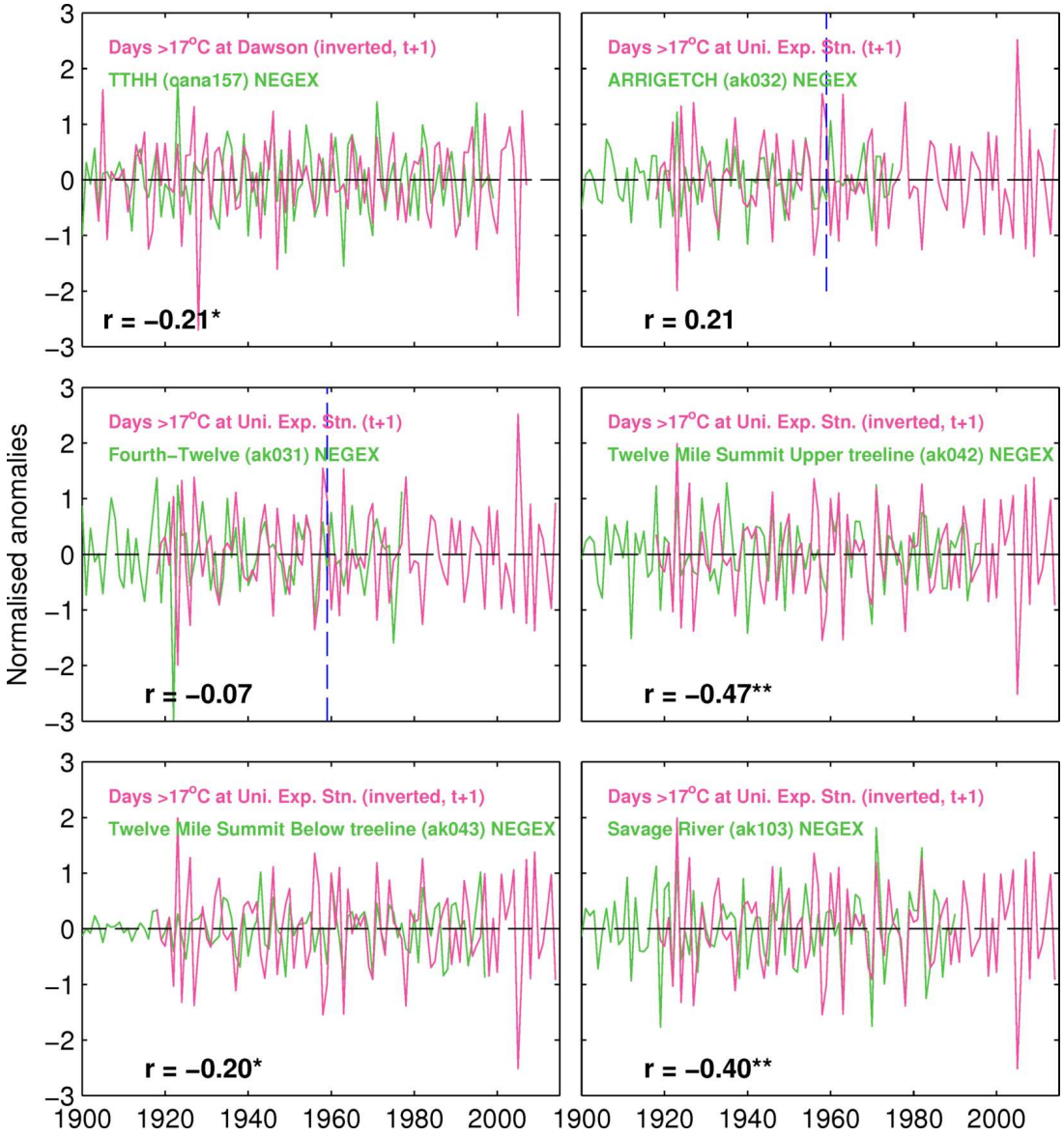

Supplementary Figure E6: Comparison between 10-year high-pass filtered series of annual frequency of days exceeding 17°C (purple) and a number of 'divergent' SPL10 tree-ring chronologies (green) in Alaska (ak031, ak032, ak042, ak043 and ak103) and in the Yukon Territory (TTHH – cana157) collected originally by Jacoby & D'Arrigo (1995) and D'Arrigo *et al.* (2004). Note that relative ring width declines since around the 1960s are highly consistent with an increasing frequency of days exceeding the 17°C threshold (shown as inverted anomalies) identified in the calibrated response function of the VS model. Also note that the negative effect of high temperatures on tree growth tends to occur during the following growing season. Two sites (ak031 and ak032) display a positive response to high temperatures before the 1960s but thereafter the response turned negative.

References

Albergel, C., Rüdiger, C., Pellarin, T., Calvet, J.C., Fritz, N., Froissard, F., Suquia, D., Petitpa, A., Piguet, B., Martin, E. *et al.* (2008). From near-surface to root-zone soil moisture using an exponential filter: an assessment of the method based on in-situ observations and model simulations. *Hydrology and Earth System Sciences Discussions*, **12**, 1323–1337.

Albergel, C., De Rosnay, P., Balsamo, G., Isaksen, L. & Muñoz-Sabater, J. (2012). Soil moisture analyses at ECMWF: evaluation using global ground-based in situ observations. *Journal of Hydrometeorology*, **13**, 1442–1460.

Albergel, C., Dorigo, W., Reichle, R., Balsamo, G., de Rosnay, P., Muñoz-Sabater, J., Isaksen, L., de Jeu, R. & Wagner, W. (2013a). Skill and global trend analysis of soil moisture from reanalyses and microwave remote sensing. *Journal of Hydrometeorology*, **14**, 1259–1277.

Albergel, C., Dorigo, W., Balsamo, G., Muñoz-Sabater, J., de Rosnay, P., Isaksen, L., Brocca, L., de Jeu, R. & Wagner, W. (2013b). Monitoring multi-decadal satellite earth observation of soil moisture products through land surface reanalyses. *Remote Sensing of Environment*, **138**, 77–89.

Alcaraz-Segura, D., Chuvieco, E., Epstein, H.E., Kasischke, E.S. & Trishchenko, A. (2010). Debating the greening vs. browning of the North American boreal forest: differences between satellite datasets. *Global Change Biology*, **16**, 760–770.

Allen, M.R. & Ingram, W.J. (2002). Constraints on future changes in climate and the hydrologic cycle. *Nature*, **419**, 224–232.

Anchukaitis, K., Evans, M., Kaplan, A., Vaganov, E., Hughes, M., Grissino-Mayer, H. & Cane, M. (2006). Forward modeling of regional scale tree-ring patterns in the southeastern United States and the recent influence of summer drought. *Geophysical Research Letters*, **33**.

Angert, A., Biraud, S., Bonfils, C., Henning, C., Buermann, W., Pinzon, J., Tucker, C. & Fung, I. (2005). Drier summers cancel out the CO2 uptake enhancement induced by warmer springs. *Proceedings of the National Academy of Sciences of the United States of America*, **102**, 10823.

Archibold, O.W. (1995). *Ecology of World Vegetation*. Chapman and Hall, Toronto.

Baldocchi, D. & Wilson, K. (2001). Modeling CO_2 and water vapor exchange of a temperate broadleaved forest across hourly to decadal time scales. *Ecological Modelling*, **142**, 155–184.

Balsamo, G., Albergel, C., Beljaars, A., Boussetta, S., Cloke, H., Dee, D., Dutra, E., Muñoz-Sabater, J., Pappenberger, F., de Rosnay, P. *et al.* (2013). ERA-Interim/Land: a global land water resources dataset. *Hydrology and Earth System Sciences Discussions*, **10**, 14705–14745.

Barber, V.A., Juday, G.P. & Finney, B.P. (2000). Reduced growth of Alaskan white spruce in the twentieth century from temperature-induced drought stress. *Nature*, **405**, 668–673.

Barichivich, J., Briffa, K.R., Osborn, T.J., Melvin, T.M. & Caesar, J. (2012). Thermal growing season and timing of biospheric carbon uptake across the Northern Hemisphere. *Global Biogeochemical Cycles*, **26**, 4015.

Barichivich, J., Briffa, K.R., Myneni, R., Osborn, T.J., Melvin, T.M., Ciais, P., Piao, S.L. & Tucker, C. (2013). Large-scale variations in the vegetation growing season and annual cycle of atmospheric CO_2 at high northern latitudes from 1950 to 2011. *Global Change Biology*, **19**, 3167–3183.

Barichivich, J., Briffa, K.R., Myneni, R., Schrier, G.v.d., Dorigo, W., Tucker, C.J., Osborn, T.J. & Melvin, T.M. (2014). Temperature and Snow-Mediated Moisture Controls of Summer Photosynthetic Activity in Northern Terrestrial Ecosystems between 1982 and 2011. *Remote Sensing*, **6**, 1390–1431.

Barnett, T.P., Adam, J.C. & Lettenmaier, D.P. (2005). Potential impacts of a warming climate on water availability in snow-dominated regions. *Nature*, **438**, 303–309.

Barr, A., Black, T.A. & McCaughey, H. (2009). Climatic and phenological controls of the carbon and energy balances of three contrasting boreal forest ecosystems in Western Canada. In A. Noormets, ed., *Phenology of ecosystem processes*, Springer, New York.

Bauerle, W., Oren, R., Way, D., Qian, S., Stoy, P., Thornton, P., Bowden, J., Hoffman, F. & Reynolds, R. (2012). Photoperiodic regulation of the seasonal pattern of photosynthetic capacity and the implications for carbon cycling. *Proceedings of the National Academy of Sciences*, **109**, 8612–8617.

Beaulieu, C., Sarmiento, J.L., Fletcher, S.E.M., Chen, J. & Medvigy, D. (2012). Identification and characterization of abrupt changes in the land uptake of carbon. *Global Biogeochemical Cycles*, **26**, GB1007.

Beck, P. & Goetz, S. (2011). Satellite observations of high northern latitude vegetation productivity changes between 1982 and 2008: ecological variability and regional differences. *Environmental Research Letters*, **6**, 045501.

Beck, P., Atzberger, C., Høgda, K., Johansen, B. & Skidmore, A. (2006). Improved monitoring of vegetation dynamics at very high latitudes: A new method using MODIS NDVI. *Remote Sensing of Environment*, **100**, 321–334.

Beck, P.S., Juday, G.P., Alix, C., Barber, V.A., Winslow, S.E., Sousa, E.E., Heiser, P., Herriges, J.D. & Goetz, S.J. (2011). Changes in forest productivity across Alaska consistent with biome shift. *Ecology Letters*, **14**, 373–379.

Beck, P.S., Andreu-Hayles, L., D'Arrigo, R., Anchukaitis, K.J., Tucker, C.J., Pinzón, J.E. & Goetz, S.J. (2013). A large-scale coherent signal of canopy status in maximum latewood density of tree rings at arctic treeline in North America. *Global and Planetary Change*, **100**, 109–118.

Berner, L.T., Beck, P.S., Bunn, A.G., Lloyd, A.H. & Goetz, S.J. (2011). High-latitude tree growth and satellite vegetation indices: Correlations and trends in Russia and Canada (1982–2008). *Journal of Geophysical Research: Biogeosciences (2005–2012)*, **116**.

Bhatt, U., Walker, D., Raynolds, M., Comiso, J., Epstein, H., Jia, G., Gens, R., Pinzon, J., Tucker, C., Tweedie, C. *et al.* (2010). Circumpolar Arctic tundra vegetation change is linked to sea ice decline. *Earth Interactions*, **14**, 1–20.

Bhatt, U.S., Walker, D.A., Raynolds, M.K., Bieniek, P.A., Epstein, H.E., Comiso, J.C., Pinzon, J.E., Tucker, C.J. & Polyakov, I.V. (2013). Recent Declines in Warming and Vegetation Greening Trends over Pan-Arctic Tundra. *Remote Sensing*, **5**, 4229–4254.

Biancamaria, S., Cazenave, A., Mognard, N.M., Llovel, W. & Frappart, F. (2011). Satellite-based high latitude snow volume trend, variability and contribution to sea level over 1989/2006. *Global and Planetary Change*, **75**, 99–107.

Bonan, G.B. (1989). Environmental factors and ecological processes controlling vegetation patterns in boreal forests. *Landscape Ecology*, **3**, 111–130.

Bonan, G.B. (2002). *Ecological climatology: concepts and applications*. Cambridge University Press.

Bonan, G.B., Chapin III, F.S. & Thompson, S.L. (1995). Boreal forest and tundra ecosystems as components of the climate system. *Climatic Change*, **29**, 145–167.

Bonsal, B. & Regier, M. (2007). Historical comparison of the 2001/2002 drought in the Canadian Prairies. *Climate Research*, **33**, 229.

Bretherton, C.S., Smith, C. & Wallace, J.M. (1992). An intercomparison of methods for finding coupled patterns in climate data. *Journal of Climate*, **5**, 541–560.

Briffa, K.R. (2000). Annual climate variability in the Holocene: interpreting the message of ancient trees. *Quaternary Science Reviews*, **19**, 87–105.

Briffa, K.R. & Melvin, T.M. (2011). *Dendroclimatology: Progress and Prospects*, chap. A closer look at regional curve standardization of tree-ring records: justification of the need, a warning of some pitfalls, and suggested improvements in its application, 113–145. Springer Verlag, New York City.

Briffa, K.R., Schweingruber, F., Jones, P., Osborn, T., Shiyatov, S. & Vaganov, E. (1998). Reduced sensitivity of recent tree-growth to temperature at high northern latitudes. *Nature*, **391**, 678–682.

Briffa, K.R., Osborn, T.J. & Schweingruber, F.H. (2004). Large-scale temperature inferences from tree rings: a review. *Global and Planetary Change*, **40**, 11–26.

Briffa, K.R., Melvin, T.M., Osborn, T.J., Hantemirov, R.M., Kirdyanov, A.V., Mazepa, V.S., Shiyatov, S.G. & Esper, J. (2013). Reassessing the evidence for tree-growth and inferred temperature change during the Common Era in Yamalia, northwest Siberia. *Quaternary Science Reviews*, **72**, 83–107.

Bronaugh, D. (2009). zyp: Zhang + Yue-Pilon trends package. R package version 2.1. Available at: http://CRAN.R-project.org/package=zyp.

Brooks, P.D., Grogan, P., Templer, P.H., Groffman, P., Öquist, M.G. & Schimel, J. (2011). Carbon and Nitrogen Cycling in Snow-Covered Environments. *Geography Compass*, **5**, 682–699.

Brown, J., Ferrians Jr., J., Heginbottom, J. & Melnikov, E. (1998). Revised February 2001. Circum-Arctic map of permafrost and ground-ice conditions. Boulder, CO: National Snow and Ice Data Center/World Data Center for Glaciology. Digital Media.

Brown, R. & Robinson, D. (2011). Northern Hemisphere spring snow cover variability and change over 1922–2010 including an assessment of uncertainty. *The Cryosphere*, **5**, 219–229.

Buermann, W., Anderson, B., Tucker, C.J., Dickinson, R.E., Lucht, W., Potter, C.S. & Myneni, R.B. (2003). Interannual covariability in Northern Hemisphere air temperatures and greenness associated with El Niño-Southern Oscillation and the Arctic Oscillation. *Journal of Geophysical Research: Atmospheres (1984–2012)*, **108**.

Buermann, W., Lintner, B., Koven, C., Angert, A., Pinzon, J., Tucker, C. & Fung, I. (2007). The changing carbon cycle at Mauna Loa Observatory. *Proceedings of the National Academy of Sciences*, **104**, 4249.

Buermann, W., Bikash, P.R., Jung, M., Burn, D.H. & Reichstein, M. (2013). Earlier springs decrease peak summer productivity in North American boreal forests. *Environmental Research Letters*, **8**, 024027.

Bunn, A. & Goetz, S. (2006). Trends in satellite-observed circumpolar photosynthetic activity from 1982 to 2003: the influence of seasonality, cover type, and vegetation density. *Earth Interactions*, **10**, 1–19.

Bunn, A.G., Goetz, S.J. & Fiske, G.J. (2005). Observed and predicted responses of plant growth to climate across Canada. *Geophysical Research Letters*, **32**, L16710.

Bunn, A.G., Goetz, S.J., Kimball, J.S. & Zhang, K. (2007). Northern high-latitude ecosystems respond to climate change. *Eos*, **88**, 333–335.

Burrows, M., Schoeman, D., Buckley, L., Moore, P., Poloczanska, E., Brander, K., Brown, C., Bruno, J., Duarte, C., Halpern, B. *et al.* (2011). The pace of shifting climate in marine and terrestrial ecosystems. *Science*, **334**, 652–655.

Caesar, J., Alexander, L. & Vose, R. (2006). Large-scale changes in observed daily maximum and minimum temperatures: Creation and analysis of a new gridded data set. *Journal of Geophysical Research*, **111**, D05101.

Callaghan, T., Johansson, M., Brown, R., Groisman, P., Labba, N., Radionov, V., Barry, R., Bulygina, O., Essery, R., Frolov, D. *et al.* (2011). The changing face of Arctic snow cover: A synthesis of observed and projected changes. *AMBIO: A Journal of the Human Environment*, **40**, 17–31.

Chapin, F., McGuire, A., Randerson, J., Pielke, R., Baldocchi, D., Hobbie, S., Roulet, N., Eugster, W., Kasischke, E., Rastetter, E. *et al.* (2000). Arctic and boreal ecosystems of western North America as components of the climate system. *Global Change Biology*, **6**, 211–223.

Chavardès, R.D., Daniels, L.D., Waeber, P.O., Innes, J.L. & Nitschke, C.R. (2013). Unstable climate- growth relations for white spruce in southwest Yukon, Canada. *Climatic Change*, **116**, 593–611.

Chou, C. & Lan, C.W. (2012). Changes in the annual range of precipitation under global warming. *Journal of Climate*, **25**, 222–235.

Christidis, N., Stott, P., Brown, S., Karoly, D. & Caesar, J. (2007). Human Contribution to the Lengthening of the Growing Season during 1950-99. *Journal of Climate*, **20**, 5441–5454.

Churkina, G., Schimel, D., Braswell, B. & Xiao, X. (2005). Spatial analysis of growing season length control over net ecosystem exchange. *Global Change Biology*, **11**, 1777–1787.

Cleland, E., Chuine, I., Menzel, A., Mooney, H. & Schwartz, M. (2007). Shifting plant phenology in response to global change. *Trends in Ecology & Evolution*, **22**, 357–365.

Cohen, J., Furtado, J., Barlow, M., Alexeev, V. & Cherry, J. (2012). Asymmetric seasonal temperature trends. *Geophysical Research Letters*, **39**, L04705.

Cook, E.R., Briffa, K., Shiyatov, S. & Mazepa, V. (1990). *Tree-ring standardization and growth-trend estimation*, 102–123. Kluwer, Dordrecht.

Curtis, C.J. & Simpson, G.L. (2014). Trends in bulk deposition of acidity in the UK, 1988–2007, assessed using additive models. *Ecological Indicators*, **37**, 274–286.

Dai, A. (2011a). Characteristics and trends in various forms of the Palmer Drought Severity Index during 1900–2008. *Journal of Geophysical Research*, **116**, D12115.

Dai, A. (2011b). Drought under global warming: a review. *Wiley Interdisciplinary Reviews: Climate Change*, **2**, 45–65.

Dai, A. (2012). Increasing drought under global warming in observations and models. *Nature Climate Change*, **3**, 52–58.

Dai, A., Trenberth, K.E. & Qian, T. (2004). A global dataset of Palmer Drought Severity Index for 1870-2002: Relationship with soil moisture and effects of surface warming. *Journal of Hydrometeorology*, **5**, 1117–1130.

Danby, R. & Hik, D. (2007). Responses of white spruce (Picea glauca) to experimental warming at a subarctic alpine treeline. *Global Change Biology*, **13**, 437–451.

D'Arrigo, R., Wilson, R. & Jacoby, G. (2006). On the long-term context for late twentieth century warming. *Journal of Geophysical Research*, **111**, D03103.

D'Arrigo, R., Wilson, R., Liepert, B. & Cherubini, P. (2008). On the divergence problemin northern forests: a review of the tree-ring evidence and possible causes. *Global and Planetary Change*, **60**, 289–305.

D'Arrigo, R., Jacoby, G., Buckley, B., Sakulich, J., Frank, D., Wilson, R., Curtis, A. & Anchukaitis, K. (2009). Tree growth and inferred temperature variability at the North American Arctic treeline. *Global and Planetary Change*, **65**, 71–82.

D'Arrigo, R.D., Kaufmann, R.K., Davi, N., Jacoby, G.C., Laskowski, C., Myneni, R.B. & Cherubini, P. (2004). Thresholds for warming-induced growth decline at elevational tree line in the Yukon Territory, Canada. *Global Biogeochemical Cycles*, **18**.

Davi, N.K., Jacoby, G.C. & Wiles, G.C. (2003). Boreal temperature variability inferred from maximum latewood density and tree-ring width data, Wrangell Mountain region, Alaska. *Quaternary Research*, **60**, 252–262.

de Beurs, K.M. & Henebry, G.M. (2008). Northern annular mode effects on the land surface phenologies of Northern Eurasia. *Journal of Climate*, **21**, 4257–4279.

Delbart, N., Le Toan, T., Kergoat, L. & Fedotova, V. (2006). Remote sensing of spring phenology in boreal regions: A free of snow-effect method using NOAA-AVHRR and SPOT-VGT data (1982–2004). *Remote Sensing of Environment*, **101**, 52–62.

Denman, K., Brasseur, G., Chidthaisong, A., Ciais, P., Cox, P., Dickinson, E., Hauglustaine, D., Heinze, C., Holland, E., Jacob, D., Lohmann, U., Ramachandran, S., Leite da Silva Dias, P., Wofsy, S., Zhang, X. *et al.* (2007). *Climate Change 2007: The Physical Science Basis*, chap. Couplings Between Changes in the Climate System and Biogeochemistry, 499–588. Cambridge University Press, Cambridge, UK, and New York.

Diffenbaugh, N.S., Scherer, M. & Ashfaq, M. (2012). Response of snow-dependent hydrologic extremes to continued global warming. *Nature Climate Change*, **3**, 379–384.

Dorigo, W., Wagner, W., Hohensinn, R., Hahn, S., Paulik, C., Xaver, A., Gruber, A., Drusch, M., Mecklenburg, S., Oevelen, P.v. *et al.* (2011). The International Soil Moisture Network: a data hosting facility for global in situ soil moisture measurements. *Hydrology and Earth System Sciences*, **15**, 1675–1698.

Dorigo, W., Jeu, R., Chung, D., Parinussa, R., Liu, Y., Wagner, W. & Fernández-Prieto, D. (2012). Evaluating global trends (1988–2010) in harmonized multi-satellite surface soil moisture. *Geophysical Research Letters*, **39**.

Dorigo, W., Xaver, A., Vreugdenhil, M., Gruber, A., Hegyiová, A., Sanchis-Dufau, A., Zamojski, D., Cordes, C., Wagner, W. & Drusch, M. (2013a). Global Automated Quality Control of In Situ Soil Moisture Data from the International Soil Moisture Network. *Vadose Zone Journal*, doi:10.2136/vzj2012.0097.

Dorigo, W., Gruber, A., De Jeu, R., Wagner, W., Stacke, T., Loew, A., Albergel, C., Brocca, L., Chung, D., Parinussa, R. & Kidd, R. (2013b). Evaluation of the ESA CCI soil moisture product using ground-based observations. *Remote Sensing of Environment*, in press.

Dragoni, D. & Rahman, A.F. (2012). Trends in fall phenology across the deciduous forests of the Eastern USA. *Agricultural and Forest Meteorology*, **157**, 96 – 105.

Dragoni, D., Schmid, H., Wayson, C., Potter, H., Grimmond, C. & Randolph, J. (2011). Evidence of increased net ecosystem productivity associated with a longer vegetated season in a deciduous forest in south-central Indiana, USA. *Global Change Biology*, **17**, 886–897.

Driscoll, W.W., Wiles, G.C., D'Arrigo, R.D. & Wilmking, M. (2005). Divergent tree growth response to recent climatic warming, Lake Clark National Park and Preserve, Alaska. *Geophysical Research Letters*, **32**.

Dye, D. & Tucker, C. (2003). Seasonality and trends of snow-cover, vegetation index, and temperature in northern Eurasia. *Geophysical Research Letters*, **30**, 1405.

Ebisuzaki, W. (1997). A Method to Estimate the Statistical Significance of a Correlation When the Data Are Serially Correlated. *Journal of Climate*, **10**, 2147–2153.

Elmendorf, S.C., Henry, G.H., Hollister, R.D., Björk, R.G., Boulanger-Lapointe, N., Cooper, E.J., Cornelissen, J.H., Day, T.A., Dorrepaal, E., Elumeeva, T.G. *et al.* (2012). Plot-scale evidence of tundra vegetation change and links to recent summer warming. *Nature Climate Change*, **2**, 453–457.

Epstein, H., Raynolds, M., Walker, D., Bhatt, U., Tucker, C. & Pinzon, J. (2012). Dynamics of aboveground phytomass of the circumpolar Arctic tundra during the past three decades. *Environmental Research Letters*, **7**, 015506.

Esper, J., Cook, E.R. & Schweingruber, F.H. (2002). Low-frequency signals in long tree-ring chronologies for reconstructing past temperature variability. *Science*, **295**, 2250–2253.

Estrella, N. & Menzel, A. (2006). Responses of leaf colouring in four deciduous tree species to climate and weather in Germany. *Climate Research*, **32**, 253.

Euskirchen, E., McGuire, A., Kicklighter, D., Zhuang, Q., Clein, J., Dargaville, R., Dye, D., Kimball, J., McDonald, K., Melillo, J. *et al.* (2006). Importance of recent shifts in soil thermal dynamics on growing season length, productivity, and carbon sequestration in terrestrial high-latitude ecosystems. *Global Change Biology*, **12**, 731–750.

Evans, M., Reichert, B., Kaplan, A., Anchukaitis, K., Vaganov, E., Hughes, M. & Cane, M. (2006). A forward modeling approach to paleoclimatic interpretation of tree-ring data. *Journal of Geophysical Research: Biogeosciences (2005–2012)*, **111**.

Evans, M.N., Tolwinski-Ward, S., Thompson, D. & Anchukaitis, K.J. (2013). Applications of proxy system modeling in high resolution paleoclimatology. *Quaternary Science Reviews*, **76**, 16–28.

Fensholt, R. & Proud, S.R. (2012). Evaluation of Earth Observation based global long term vegetation trendsComparing GIMMS and MODIS global NDVI time series. *Remote Sensing of Environment*, **119**, 131–147.

Forkel, M., Thonicke, K., Beer, C., Cramer, W., Bartalev, S. & Schmullius, C. (2012). Extreme fire events are related to previous-year surface moisture conditions in permafrost-underlain larch forests of Siberia. *Environmental Research Letters*, **7**, 044021.

Frauenfeld, O.W., Zhang, T. & Mccreight, J.L. (2007). Northern hemisphere freezing/thawing index variations over the twentieth century. *International Journal of Climatology*, **27**, 47–63.

Frich, P., Alexander, L., Della-Marta, P., Gleason, B., Haylock, M., Klein Tank, A. & Peterson, T. (2002). Observed coherent changes in climatic extremes during the second half of the twentieth century. *Climate Research*, **19**, 193–212.

Friedl, M., Sulla-Menashe, D., Tan, B., Schneider, A., Ramankutty, N., Sibley, A. & Huang, X. (2010). MODIS Collection 5 global land cover: Algorithm refinements and characterization of new datasets. *Remote Sensing of Environment*, **114**, 168–182.

Fritts, H. (1976). *Tree rings and climate*. Academic Press, London.

Fritts, H.C., Shashkin, A., Downes, G.M., Wimmer, R., Vetter, R. *et al.* (1999). A simulation model of conifer ring growth and cell structure. *Tree-ring analysis: biological, methodological and environmental aspects.*, 3–32.

Gan, T.Y., Barry, R.G., Gizaw, M., Gobena, A. & Rajagopalan, B. (2013). Changes in North American Snow packs for 1979-2007 Detected from the Snow Water Equivalent data of SMMR and SSM/I Passive Microwave and related Climatic Factors. *Journal of Geophysical Research: Atmospheres*.

Gao, F., Morisette, J., Wolfe, R., Ederer, G., Pedelty, J., Masuoka, E., Myneni, R., Tan, B. & Nightingale, J. (2008). An algorithm to produce temporally and spatially continuous MODIS-LAI time series. *Geoscience and Remote Sensing Letters, IEEE*, **5**, 60–64.

Gedney, N., Cox, P., Betts, R., Boucher, O., Huntingford, C. & Stott, P. (2006). Detection of a direct carbon dioxide effect in continental river runoff records. *Nature*, **439**, 835–838.

Gelman, A. & Rubin, D.B. (1992). Inference from iterative simulation using multiple sequences. *Statistical Science*, 457–472.

Gelman, A., Carlin, J.B., Stern, H.S., Dunson, D.B., Vehtari, A. & Rubin, D.B. (2013). *Bayesian data analysis*. CRC press, 3rd edn.

GLOBALVIEW-CO_2 (2011). Cooperative Atmospheric Data Integration Project – Carbon Dioxide. ftp://ftp.cmdl.noaa.gov/ccg/co2/GLOBALVIEW.

Goetz, S., Bunn, A., Fiske, G. & Houghton, R. (2005). Satellite-observed photosynthetic trends across boreal North America associated with climate and fire disturbance. *Proceedings of the National Academy of Sciences of the United States of America*, **102**, 13521.

Goulden, M., Wofsy, S., Harden, J., Trumbore, S., Crill, P., Gower, S., Fries, T., Daube, B., Fan, S., Sutton, D. *et al.* (1998). Sensitivity of boreal forest carbon balance to soil thaw. *Science*, **279**, 214.

Griesbauer, H.P. & Green, D.S. (2012). Geographic and temporal patterns in white spruce climate–growth relationships in Yukon, Canada. *Forest Ecology and Management*, **267**, 215–227.

Grippa, M., Kergoat, L., Le Toan, T., Mognard, N., Delbart, N., L'Hermitte, J. & Vicente-Serrano, S. (2005). The impact of snow depth and snowmelt on the vegetation variability over central Siberia. *Geophysical Research Letters*, **32**, L21412.

Hamilton, E., Eade, R., Graham, R., Scaife, A., Smith, D., Maidens, A. & MacLachlan, C. (2012). Forecasting the number of extreme daily events on seasonal timescales. *Journal of Geophysical Research*, **117**, D03114.

Hancock, S., Baxter, R., Evans, J. & Huntley, B. (2013). Evaluating global snow water equivalent products for testing land surface models. *Remote Sensing of Environment*, **128**, 107–117.

Hänninen, H. & Tanino, K. (2011). Tree seasonality in a warming climate. *Trends in Plant Science*, **16**, 412–416.

Harris, I., Jones, P.D., Osborn, T.J. & Lister, D.H. (2014). Updated high-resolution grids of monthly climatic observations–the CRU TS3. 10 Dataset. *International Journal of Climatology*, **34**, 623–642, dOI:10.1002/joc.3711.

Heimann, M., Esser, G., Haxeltine, A., Kaduk, J., Kicklighter, D., Knorr, W., Kohlmaier, G., McGuire, A., Melillo, J., Moore III, B. *et al.* (1998). Evaluation of terrestrial carbon cycle models through simulations of the seasonal cycle of atmospheric CO_2: First results of a model intercomparison study. *Global Biogeochemical Cycles*, **12**, 1–24.

Helama, S., Mielikäinen, K., Timonen, M., Herva, H., Tuomenvirta, H. & Venäläinen, A. (2013). Regional climatic signals in Scots pine growth with insights into snow and soil associations. *Dendrobiology*, **70**.

Held, I.M. & Soden, B.J. (2006). Robust responses of the hydrological cycle to global warming. *Journal of Climate*, **19**, 5686–5699.

Hogg, E. & Wein, R.W. (2005). Impacts of drought on forest growth and regeneration following fire in southwestern Yukon, Canada. *Canadian Journal of Forest Research*, **35**, 2141–2150.

Hogg, E., Brandt, J. & Michaelian, M. (2008). Impacts of a regional drought on the productivity, dieback, and biomass of western Canadian aspen forests. *Canadian Journal of Forest Research*, **38**, 1373–1384.

Hollingsworth, J. (2005). Bonanza Creek Experimental Forest: Hourly Soil Moisture at varying depths from 1988 to Present, Bonanza Creek LTER - University of Alaska Fairbanks. BNZ:5, http://www.lter.uaf.edu/data_detail.cfm?datafile_pkey=5.

Houghton, R. (1987). Terrestrial Metabolism and Atmospheric CO 2 Concentrations. *BioScience*, **37**, 672–678.

Hu, J., Moore, D., Burns, S. & Monson, R. (2010). Longer growing seasons lead to less carbon sequestration by a subalpine forest. *Global Change Biology*, **16**, 771–783.

Huang, J., van den Dool, H.M. & Georgarakos, K.P. (1996). Analysis of model-calculated soil moisture over the United States (1931-1993) and applications to long-range temperature forecasts. *Journal of Climate*, **9**, 1350–1362.

Huete, A., Didan, K., Miura, T., Rodriguez, E.P., Gao, X. & Ferreira, L.G. (2002). Overview of the radiometric and biophysical performance of the MODIS vegetation indices. *Remote Sensing of Environment*, **83**, 195–213.

Hufkens, K., Friedl, M., Keenan, T., Sonnentag, O., Bailey, A., O'Keefe, J. & Richardson, A. (2012). Ecological impacts of a widespread frost event following early spring leaf-out. *Global Change Biology*, **18**, 2365–2377.

Huntington, T.G. (2006). Evidence for intensification of the global water cycle: review and synthesis. *Journal of Hydrology*, **319**, 83–95.

Jacoby, G.C. & D'Arrigo, R.D. (1995). Tree ring width and density evidence of climatic and potential forest change in Alaska. *Global Biogeochemical Cycles*, **9**, 227–234.

Jacoby, G.C., Lovelius, N.V., Shumilov, O.I., Raspopov, O.M., Karbainov, J.M. & Frank, D.C. (2000). Long-term temperature trends and tree growth in the Taymir region of northern Siberia. *Quaternary Research*, **53**, 312–318.

James, M. & Kalluri, S.N. (1994). The Pathfinder AVHRR land data set: an improved coarse resolution data set for terrestrial monitoring. *International Journal of Remote Sensing*, **15**, 3347–3363.

Jarvis, P. & Linder, S. (2000). Constraints to growth of boreal forests. *Nature*, **405**, 904–905.

Jarvis, S.K., Wiles, G.C., Appleton, S.N., D'Arrigo, R.D. & Lawson, D.E. (2013). A Warming-Induced Biome Shift Detected in Tree Growth of Mountain Hemlock [Tsuga mertensiana (Bong.) Carrière] Along the Gulf of Alaska. *Arctic, Antarctic, and Alpine Research*, **45**, 211–218.

Jeong, S., Ho, C., Gim, H. & Brown, M. (2011). Phenology shifts at start vs. end of growing season in temperate vegetation over the Northern Hemisphere for the period 1982-2008. *Global Change Biology*, **17**, 2385–2399.

Jiang, F., Hu, R., Zhang, Y., Li, X. & Tong, L. (2011). Variations and trends of onset, cessation and length of climatic growing season over Xinjiang, NW China. *Theoretical and Applied Climatology*, 1–10.

Joiner, J., Guanter, L., Lindstrot, R., Voigt, M., Vasilkov, A., Middleton, E., Huemmrich, K., Yoshida, Y. & Frankenberg, C. (2013). Global monitoring of terrestrial chlorophyll fluorescence from moderate spectral resolution near-infrared satellite measurements: methodology, simulations, and application to GOME-2. *Atmospheric Measurement Techniques Discussions*, **6**, 3883–3930.

Jones, M., Jones, L., Kimball, J. & McDonald, K. (2011). Satellite passive microwave remote sensing for monitoring global land surface phenology. *Remote Sensing of Environment*, **115**, 1102–1114.

Jones, P.D. & Briffa, K.R. (1995). Growing season temperatures over the former Soviet Union. *International Journal of Climatology*, **15**, 943–959.

Jönsson, P. & Eklundh, L. (2004). TIMESAT–a program for analyzing time-series of satellite sensor data. *Computers & Geosciences*, **30**, 833–845.

Jorgenson, M.T., Romanovsky, V., Harden, J., Shur, Y., O'Donnell, J., Schuur, E.A., Kanevskiy, M. & Marchenko, S. (2010). Resilience and vulnerability of permafrost to climate change. *Canadian Journal of Forest Research*, **40**, 1219–1236.

Juday, G.P. & Alix, C. (2012). Consistent negative temperature sensitivity and positive influence of precipitation on growth of floodplain *Picea glauca* in Interior Alaska. *Canadian Journal of Forest Research*, **42**, 561–573.

Julien, Y. & Sobrino, J. (2009). Global land surface phenology trends from GIMMS database. *International Journal of Remote Sensing*, **30**, 3495–3513.

Kaminski, T., Giering, R. & Heimann, M. (1996). Sensitivity of the seasonal cycle of CO2 at remote monitoring stations with respect to seasonal surface exchange fluxes determined with the adjoint of an atmospheric transport model. *Physics and Chemistry of the Earth*, **21**, 457–462.

Kasischke, E.S. & Turetsky, M.R. (2006). Recent changes in the fire regime across the North American boreal regionSpatial and temporal patterns of burning across Canada and Alaska. *Geophysical Research Letters*, **33**.

Kaufmann, R., Kauppi, H., Mann, M. & Stock, J. (2011). Reconciling anthropogenic climate change with observed temperature 1998–2008. *Proceedings of the National Academy of Sciences*, **108**, 11790.

Keeling, C., Chin, J. & Whorf, T. (1996). Increased activity of northern vegetation inferred from atmospheric CO_2 measurements. *Nature*, **382**, 146–149.

Kim, Y., Kimball, J., McDonald, K. & Glassy, J. (2011). Developing a Global Data Record of Daily Landscape Freeze/Thaw Status Using Satellite Passive Microwave Remote Sensing. *Geoscience and Remote Sensing, IEEE Transactions on*, **49**, 949–960.

Kim, Y., Kimball, J., Zhang, K. & McDonald, K. (2012). Satellite detection of increasing Northern Hemisphere non-frozen seasons from 1979 to 2008: Implications for regional vegetation growth. *Remote Sensing of Environment*, **121**, 472–487.

Kimball, J., McDonald, K., Running, S. & Frolking, S. (2004). Satellite radar remote sensing of seasonal growing seasons for boreal and subalpine evergreen forests. *Remote Sensing of Environment*, **90**, 243 – 258.

Kirdyanov, A., Hughes, M., Vaganov, E., Schweingruber, F. & Silkin, P. (2003). The importance of early summer temperature and date of snow melt for tree growth in the Siberian Subarctic. *Trees*, **17**, 61–69.

Klein Tank, A., Wijngaard, J., Können, G., Böhm, R., Demarée, G., Gocheva, A., Mileta, M., Pashiardis, S., Hejkrlik, L., Kern-Hansen, C. *et al.* (2002). Daily dataset of 20th-century surface air temperature and precipitation series for the European Climate Assessment. *International Journal of Climatology*, **22**, 1441–1453.

Kljun, N., Black, T., Griffis, T., Barr, A., Gaumont-Guay, D., Morgenstern, K., McCaughey, J. & Nesic, Z. (2006). Response of net ecosystem productivity of three boreal forest stands to drought. *Ecosystems*, **9**, 1128–1144.

Kogan, F., Adamenko, T. & Guo, W. (2013). Global and regional drought dynamics in the climate warming era. *Remote Sensing Letters*, **4**, 364–372.

Kozlowski, T.T. & Pallardy, S.G. (1997). *Physiology of Woody Plants*. Academic Press, NY.

Krol, M., Houweling, S., Bregman, B., Van den Broek, M., Segers, A., Van Velthoven, P., Peters, W., Dentener, F., Bergamaschi, P. *et al.* (2005). The two-way nested global chemistry-transport zoom model TM5: algorithm and applications. *Atmospheric Chemistry and Physics*, **5**, 417–432.

Kurz, W.A., Dymond, C., Stinson, G., Rampley, G., Neilson, E., Carroll, A., Ebata, T. & Safranyik, L. (2008). Mountain pine beetle and forest carbon feedback to climate change. *Nature*, **452**, 987–990.

Laloy, E. & Vrugt, J.A. (2012). High-dimensional posterior exploration of hydrologic models using multiple-try DREAM (ZS) and high-performance computing. *Water Resources Research*, **48**.

Legendre, P. (2010). *Encyclopedia of Research Design*, chap. Coefficient of concordance, 164–169. SAGE Publications, Inc., Los Angeles.

Linderholm, H. (2006). Growing season changes in the last century. *Agricultural and Forest Meteorology*, **137**, 1–14.

Liu, Y., Dorigo, W., Parinussa, R., De Jeu, R., Wagner, W., McCabe, M., Evans, J. & Van Dijk, A. (2012). Trend-preserving blending of passive and active microwave soil moisture retrievals. *Remote Sensing of Environment*, **123**, 280–297.

Liu, Y.Y., de Jeu, R.A., McCabe, M.F., Evans, J.P. & van Dijk, A.I. (2011). Global long-term passive microwave satellite-based retrievals of vegetation optical depth. *Geophysical Research Letters*, **38**, L18402.

Lloyd, A.H. & Bunn, A.G. (2007). Responses of the circumpolar boreal forest to 20th century climate variability. *Environmental Research Letters*, **2**, 045013.

Lloyd, A.H. & Fastie, C.L. (2002). Spatial and temporal variability in the growth and climate response of treeline trees in Alaska. *Climatic Change*, **52**, 481–509.

Lloyd, A.H., Duffy, P. & Mann, D.H. (2013). Nonlinear responses of white spruce growth to climate variability in interior Alaska. *Canadian Journal of Forest Research*.

Loew, A., Stacke, T., Dorigo, W., de Jeu, R. & Hagemann, S. (2013). Potential and limitations of multidecadal satellite soil moisture observations for climate model evaluation studies. *Hydrology and Earth System Sciences Discussions*, **10**, 3541–3594.

Los, S. (2013). Analysis of trends in fused AVHRR and MODIS NDVI data for 1982–2006: Indication for a CO2 fertilization effect in global vegetation. *Global Biogeochemical Cycles*.

Los, S.O., Justice, C. & Tucker, C. (1994). A global 1 by 1 NDVI data set for climate studies derived from the GIMMS continental NDVI data. *International Journal of Remote Sensing*, **15**, 3493–3518.

Lotsch, A., Friedl, M., Anderson, B. & Tucker, C. (2005). Response of terrestrial ecosystems to recent Northern Hemispheric drought. *Geophysical Research Letters*, **32**, L06705.

Lucht, W., Prentice, I., Myneni, R., Sitch, S., Friedlingstein, P., Cramer, W., Bousquet, P., Buermann, W. & Smith, B. (2002). Climatic control of the high-latitude vegetation greening trend and Pinatubo effect. *Science*, **296**, 1687.

Ma, Z., Peng, C., Zhu, Q., Chen, H., Yu, G., Li, W., Zhou, X., Wang, W. & Zhang, W. (2012). Regional drought-induced reduction in the biomass carbon sink of Canada's boreal forests. *Proceedings of the National Academy of Sciences*, **109**, 2423–2427.

Manabe, S. & Wetherald, R. (1987). Large-scale changes of soil wetness induced by an increase in atmospheric carbon dioxide. *Journal of the Atmospheric Sciences*, **44**, 1211–1236.

Mann, D.H., Rupp, T.S., Olson, M.A. & Duffy, P.A. (2012). Is Alaska's Boreal Forest Now Crossing a Major Ecological Threshold? *Arctic, Antarctic, and Alpine Research*, **44**, 319–331.

Mann, M., Bradley, R.S. & Hughes, M.K. (1999). Northern hemisphere temperatures during the past millennium: inferences, uncertainties, and limitations. *Geophysical Research Letters*, **26**, 759–762.

Mann, M.E., Zhang, Z., Hughes, M.K., Bradley, R.S., Miller, S.K., Rutherford, S. & Ni, F. (2008). Proxy-based reconstructions of hemispheric and global surface temperature variations over the past two millennia. *Proceedings of the National Academy of Sciences*, **105**, 13252–13257.

McDonald, K., Kimball, J., Njoku, E., Zimmermann, R. & Zhao, M. (2004). Variability in springtime thaw in the terrestrial high latitudes: monitoring a major control on the biospheric assimilation of atmospheric CO_2 with spaceborne microwave remote sensing. *Earth Interactions*, **8**, 1–23.

McGuire, A.D., Melillo, J.M., Kicklighter, D.W. & Joyce, L.A. (1995). Equilibrium responses of soil carbon to climate change: Empirical and process-based estimates. *Journal of Biogeography*, 785–796.

McGuire, A.D., Ruess, R.W., Lloyd, A., Yarie, J., Clein, J.S. & Juday, G.P. (2010). Vulnerability of white spruce tree growth in interior Alaska in response to climate variability: dendrochronological, demographic, and experimental perspectives. *Canadian Journal of Forest Research*, **40**, 1197–1209.

McKee, T.B., Doeskin, N.J. & Kleist, J. (1993). The relationship of drought frequency and duration to time scales. In *8th Conf. on Applied Climatology*, 179–184, Am. Meteorol. Soc.

Meehl, G., Stocker, T., Collins, W., Friedlingstein, P., Gaye, A., Gregory, J., Kitoh, A., Knutti, R., Murphy, J., Noda, A. *et al.* (2007). *Climate Change 2007: The Physical Science Basis*, chap. Global climate projections, 747–845. Cambridge University Press, Cambridge, UK, and New York.

Mekis, É. & Vincent, L.A. (2011). An overview of the second generation adjusted daily precipitation dataset for trend analysis in Canada. *Atmosphere-Ocean*, **49**, 163–177.

Meko, D., Touchan, R. & Anchukaitis, K. (2011). Seascorr: A MATLAB program for identifying the seasonal climate signal in an annual tree-ring time series. *Computers & Geosciences*, **37**, 1234–1241.

Melvin, T.M. (2004). *Historical growth rates and changing climatic sensitivity of boreal conifers*. Ph.D. thesis, University of East Anglia.

Melvin, T.M. & Briffa, K.R. (2008). A signal-free approach to dendroclimatic standardisation. *Dendrochronologia*, **26**, 71–86.

Melvin, T.M. & Briffa, K.R. (2013). CRUST: Software for the implementation of Regional Chronology Standardisation: Part 1. Signal-Free RCS. *Dendrochronologia*, **32**, 7–20.

Menzel, A. & Fabian, P. (1999). Growing season extended in Europe. *Nature*, **397**, 659–659.

Menzel, A., Jakobi, G., Ahas, R., Scheifinger, H. & Estrella, N. (2003). Variations of the climatological growing season (1951-2000) in Germany compared with other countries. *International Journal of Climatology*, **23**, 793–812.

Menzel, A., Sparks, T., Estrella, N., Koch, E., Aasa, A., Ahas, R., Alm-Kübler, K., Bissolli, P., Braslavska, O., Briede, A. *et al.* (2006). European phenological response to climate change matches the warming pattern. *Global Change Biology*, **12**, 1969–1976.

Mercado, L.M., Bellouin, N., Sitch, S., Boucher, O., Huntingford, C., Wild, M. & Cox, P.M. (2009). Impact of changes in diffuse radiation on the global land carbon sink. *Nature*, **458**, 1014–1017.

Miralles, D., Van den Berg, M., Gash, J., Parinussa, R., De Jeu, R., Beck, H., Holmes, D., Jimenez, C., Verhoest, N., Dorigo, W., Teuling, A. & Dolman, A. (2013). El Nio–La Nia cycle and recent trends in continental evaporation. *Nature Climate Change*, doi:10.1038/nclimate2068.

Misson, L. (2004). MAIDEN: a model for analyzing ecosystem processes in dendroecology. *Canadian Journal of Forest Research*, **34**, 874–887.

Mitchell, T. & Jones, P. (2005). An improved method of constructing a database of monthly climate observations and associated high-resolution grids. *International journal of climatology*, **25**, 693–712.

Mohammat, A., Wang, X., Xu, X., Peng, L., Yang, Y., Zhang, X., Myneni, R.B. & Piao, S. (2013). Drought and spring cooling induced recent decrease in vegetation growth in Inner Asia. *Agricultural and Forest Meteorology*, **178179**, 21 – 30.

Monteith, J. & Unsworth, M. (1990). *Principles of environmental physics*. Edward Arnold, London.

Myneni, R., Keeling, C., Tucker, C., Asrar, G. & Nemani, R. (1997). Increased plant growth in the northern high latitudes from 1981 to 1991. *Nature*, **386**, 698–702.

Myneni, R.B., Hall, F.G., Sellers, P.J. & Marshak, A.L. (1995). The interpretation of spectral vegetation indexes. *Geoscience and Remote Sensing, IEEE Transactions on*, **33**, 481–486.

Natali, S.M., Schuur, E.A., Trucco, C., HICKS PRIES, C.E., Crummer, K.G. & BARON LOPEZ, A.F. (2011). Effects of experimental warming of air, soil and permafrost on carbon balance in Alaskan tundra. *Global Change Biology*, **17**, 1394–1407.

Nemani, R., Keeling, C., Hashimoto, H., Jolly, W., Piper, S., Tucker, C., Myneni, R. & Running, S. (2003). Climate-driven increases in global terrestrial net primary production from 1982 to 1999. *Science*, **300**, 1560 – 1563.

Ohse, B., Jansen, F. & Wilmking, M. (2012). Do limiting factors at Alaskan treelines shift with climatic regimes? *Environmental Research Letters*, **7**, 015505.

Ohta, T., Maximov, T.C., Dolman, A.J., Nakai, T., van der Molen, M.K., Kononov, A.V., Maximov, A.P., Hiyama, T., Iijima, Y., Moors, E.J. *et al.* (2008). Interannual variation of water balance and summer evapotranspiration in an eastern Siberian larch forest over a 7-year period (1998–2006). *Agricultural and Forest Meteorology*, **148**, 1941–1953.

Oksanen, J., Blanchet, F., Kindt, R., Legendre, P., Minchin, P., OHara, R., Simpson, G., Oksanen, M. & Suggests, M. (2011). Vegan: community ecology package. R package version 1.13-1. Available at: http://vegan.r-forge.r-project.org.

Palmer, W.C. (1965). *Meteorological drought*. US Department of Commerce, Weather Bureau Washington, DC, USA.

Park, H., Yabuki, H. & Ohata, T. (2012). Analysis of satellite and model datasets for variability and trends in Arctic snow extent and depth, 1948–2006. *Polar Science*, **6**, 23–37.

Park, H., Walsh, J., Fedorov, A., Sherstiukov, A., Iijima, Y. & Ohata, T. (2013). The influence of climate and hydrological variables on opposite anomaly in active-layer thickness between Eurasian and North American watersheds. *The Cryosphere*, **7**, 631–645.

Parmesan, C. & Yohe, G. (2003). A globally coherent fingerprint of climate change impacts across natural systems. *Nature*, **421**, 37–42.

Pederson, G.T., Gray, S.T., Woodhouse, C.A., Betancourt, J.L., Fagre, D.B., Littell, J.S., Watson, E., Luckman, B.H. & Graumlich, L.J. (2011). The unusual nature of recent snowpack declines in the North American Cordillera. *Science*, **333**, 332–335.

Peng, S., Chen, A., Xu, L., Cao, C., Fang, J., Myneni, R., Pinzon, J., Tucker, C. & Piao, S. (2011). Recent change of vegetation growth trend in China. *Environmental Research Letters*, **6**, 044027.

Peñuelas, J., Rutishauser, T. & Filella, I. (2009). Phenology feedbacks on climate change. *Science*, **324**, 887–888.

Peters, W., Jacobson, A., Sweeney, C., Andrews, A., Conway, T., Masarie, K., Miller, J., Bruhwiler, L., Petron, G., Hirsch, A. *et al.* (2007). An atmospheric perspective on North American carbon dioxide exchange: CarbonTracker. *Proceedings of the National Academy of Sciences*, **104**, 18925.

Peters, W., Krol, M., Van der Werf, G., Houweling, S., Jones, C., Hughes, J., Schaefer, K., Masarie, K., Jacobson, A., Miller, J. *et al.* (2010). Seven years of recent European net terrestrial carbon dioxide exchange constrained by atmospheric observations. *Global Change Biology*, **16**, 1317–1337.

Piao, S., Fang, J., Zhou, L., Ciais, P. & Zhu, B. (2006a). Variations in satellite-derived phenology in China's temperate vegetation. *Global Change Biology*, **12**, 672–685.

Piao, S., Friedlingstein, P., Ciais, P., Zhou, L. & Chen, A. (2006b). Effect of climate and CO2 changes on the greening of the Northern Hemisphere over the past two decades. *Geophysical Research Letters*, **33**, L23402.

Piao, S., Friedlingstein, P., Ciais, P., Viovy, N. & Demarty, J. (2007). Growing season extension and its effects on terrestrial carbon flux over the last two decades. *Global Biogeochemical Cycles*, **21**, GB3018.

Piao, S., Ciais, P., Friedlingstein, P., Peylin, P., Reichstein, M., Luyssaert, S., Margolis, H., Fang, J., Barr, A., Chen, A. *et al.* (2008). Net carbon dioxide losses of northern ecosystems in response to autumn warming. *Nature*, **451**, 49–52.

Piao, S., Wang, X., Ciais, P., Zhu, B., Wang, T. & Liu, J. (2011). Changes in satellite-derived vegetation growth trend in temperate and boreal Eurasia from 1982 to 2006. *Global Change Biology*, **17**, 3228–3239.

Piao, S., Sitch, S., Ciais, P., Friedlingstein, P., Peylin, P., Wang, X., Ahlström, A., Anav, A., Canadell, J.G., Cong, N. *et al.* (2013). Evaluation of terrestrial carbon cycle models for their response to climate variability and to CO2 trends. *Global change biology*, **19**, 2117–2132.

Pinzon, J. & Tucker, C. (2013). Revisiting error, precision and uncertainty in NDVI AVHRR data: development of a consistent NDVI3g time series. *Remote Sensing*, in Review.

Pisaric, M.F., Carey, S.K., Kokelj, S.V. & Youngblut, D. (2007). Anomalous 20th century tree growth, Mackenzie Delta, Northwest Territories, Canada. *Geophysical Research Letters*, **34**.

Polson, D., Hegerl, G.C., Zhang, X. & Osborn, T.J. (2013). Causes of robust seasonal land precipitation changes. *Journal of Climate*, **26**, 6679–6697.

Porter, T.J. & Pisaric, M.F. (2011). Temperature-growth divergence in white spruce forests of Old Crow Flats, Yukon Territory, and adjacent regions of northwestern North America. *Global Change Biology*, **17**, 3418–3430.

Porter, T.J., Pisaric, M.F., Kokelj, S.V. & deMontigny, P. (2013). A ring-width-based reconstruction of June–July minimum temperatures since AD1245 from white spruce stands in the Mackenzie Delta region, northwestern Canada. *Quaternary Research*, **80**, 167–179.

Randerson, J., Thompson, M., Conway, T., Fung, I. & CB, F. (1997). The contribution of terrestrial sources and sinks to trends in the seasonal cycle of atmospheric carbon dioxide. *Global Biogeochemical Cycles*, **11**, 535–560.

Randerson, J., Field, C., Fung, I. & Tans, P. (1999). Increases in early season ecosystem uptake explain recent changes in the seasonal cycle of atmospheric CO_2 at high northern latitudes. *Geophysical Research Letters*, **26**, 2765–2768.

Rawlins, M.A., Steele, M., Holland, M.M., Adam, J.C., Cherry, J.E., Francis, J.A., Groisman, P.Y., Hinzman, L.D., Huntington, T.G., Kane, D.L. *et al.* (2010). Analysis of the Arctic system for freshwater cycle intensification: Observations and expectations. *Journal of Climate*, **23**, 5715–5737.

Raynolds, M.K., Walker, D.A., Epstein, H.E., Pinzon, J.E. & Tucker, C.J. (2012). A new estimate of tundra-biome phytomass from trans-Arctic field data and AVHRR NDVI. *Remote Sensing Letters*, **3**, 403–411.

Reed, B., Brown, J., VanderZee, D., Loveland, T., Merchant, J. & Ohlen, D. (1994). Measuring phenological variability from satellite imagery. *Journal of Vegetation Science*, **5**, 703–714.

Richardson, A., Andy Black, T., Ciais, P., Delbart, N., Friedl, M., Gobron, N., Hollinger, D., Kutsch, W., Longdoz, B., Luyssaert, S. *et al.* (2010). Influence of spring and autumn phenological transitions on forest ecosystem productivity. *Philosophical Transactions of the Royal Society B: Biological Sciences*, **365**, 3227.

Richardson, A.D., Keenan, T.F., Migliavacca, M., Ryu, Y., Sonnentag, O. & Toomey, M. (2013). Climate change, phenology, and phenological control of vegetation feedbacks to the climate system. *Agricultural and Forest Meteorology*, **169**, 156–173.

Robinson, D., Dewey, K. & Heim Jr, R. (1993). Global snow cover monitoring: An update. *Bulletin of the American Meteorological Society*, **74**, 1689–1696.

Robock, A., Vinnikov, K.Y., Schlosser, C.A., Speranskaya, N.A. & Xue, Y. (1995). Use of midlatitude soil moisture and meteorological observations to validate soil moisture simulations with biosphere and bucket models. *Journal of Climate*, **8**, 15–35.

Rosenthal, S.I. & Camm, E.L. (1997). Photosynthetic decline and pigment loss during autumn foliar senescence in western larch (Larix occidentalis). *Tree Physiology*, **17**, 767–775.

Rossi, S., Deslauriers, A., Griçar, J., Seo, J.W., Rathgeber, C.B., Anfodillo, T., Morin, H., Levanic, T., Oven, P. & Jalkanen, R. (2008). Critical temperatures for xylogenesis in conifers of cold climates. *Global Ecology and Biogeography*, **17**, 696–707.

Rossi, S., Morin, H., Deslauriers, A. & PLOURDE, P.Y. (2011). Predicting xylem phenology in black spruce under climate warming. *Global change biology*, **17**, 614–625.

Roy, J., Saugier, B. & Mooney, H. (2001). *Terrestrial global productivity*. Academic Press.

Rui, H. (2011). *README Document for Global Land Data Assimilation System Version 2 (GLDAS-2) Products*. NASA Goddard Earth Sci. Data and Inf. Serv. Cent, Greenbelt.

Ruosteenoja, K., Räisänen, J. & Pirinen, P. (2011). Projected changes in thermal seasons and the growing season in Finland. *International Journal of Climatology*, **31**, 1473–1487.

Sarmiento, J., Gloor, M., Gruber, N., Beaulieu, C., Jacobson, A., Fletcher, S., Pacala, S. & Rodgers, K. (2010). Trends and regional distributions of land and ocean carbon sinks. *Biogeosciences*, **7**, 2351–2367.

Schaberg, P.G., Hennon, P.E., D'amore, D.V. & Hawley, G.J. (2008). Influence of simulated snow cover on the cold tolerance and freezing injury of yellow-cedar seedlings. *Global Change Biology*, **14**, 1282–1293.

Schneider, T. (2001). Analysis of incomplete climate data: Estimation of mean values and covariance matrices and imputation of missing values. *Journal of Climate*, **14**, 853–871.

Schneider, U., Becker, A., Finger, P., Meyer-Christoffer, A., Ziese, M. & Rudolf, B. (2013). GPCC's new land surface precipitation climatology based on quality-controlled in situ data and its role in quantifying the global water cycle. *Theoretical and Applied Climatology*, 1–26.

Schoups, G. & Vrugt, J.A. (2010). A formal likelihood function for parameter and predictive inference of hydrologic models with correlated, heteroscedastic, and non-Gaussian errors. *Water Resources Research*, **46**.

Schwartz, M., Ahas, R. & Aasa, A. (2006). Onset of spring starting earlier across the Northern Hemisphere. *Global Change Biology*, **12**, 343–351.

Seager, R., Naik, N. & Vecchi, G.A. (2010). Thermodynamic and Dynamic Mechanisms for Large-Scale Changes in the Hydrological Cycle in Response to Global Warming*. *Journal of Climate*, **23**, 4651–4668.

Seber, G.A. (2009). *Multivariate observations*, vol. 252. John Wiley & Sons.

Seneviratne, S., Nicholls, N., Easterling, D., Goodess, C., Kanae, S., Kossin, J., Luo, Y., Marengo, J., McInnes, K., Rahimi, M., Reichstein, M., Sorteberg, A., Vera, C. & Zhang, X. (2012). *Changes in climate extremes and their impacts on the natural physical environment. In: Managing the Risks of Extreme Events and Disasters to Advance Climate Change Adaptation [Field, C.B., V. Barros, T.F. Stocker, D. Qin, D.J. Dokken, K.L. Ebi, M.D. Mastrandrea, K.J. Mach, G.-K. Plattner, S.K. Allen, M. Tignor, and P.M. Midgley (eds.)]. A Special Report of Working Groups I and II of the Intergovernmental Panel on Climate Change*. IPCC.

Serreze, M.C. & Barry, R.G. (2011). Processes and impacts of Arctic amplification: A research synthesis. *Global and Planetary Change*, **77**, 85–96.

Shabbar, A. & Skinner, W. (2004). Summer Drought Patterns in Canada and the Relationship to Global Sea Surface Temperatures. *Journal of Climate*, **17**, 2866–2880.

Sheffield, J. & Wood, E.F. (2007). Characteristics of global and regional drought, 1950–2000: Analysis of soil moisture data from off-line simulation of the terrestrial hydrologic cycle. *Journal of Geophysical Research: Atmospheres (1984–2012)*, **112**.

Sheffield, J. & Wood, E.F. (2008). Projected changes in drought occurrence under future global warming from multi-model, multi-scenario, IPCC AR4 simulations. *Climate Dynamics*, **31**, 79–105.

Sheffield, J., Goteti, G. & Wood, E.F. (2006). Development of a 50-year high-resolution global dataset of meteorological forcings for land surface modeling. *Journal of Climate*, **19**, 3088–3111.

Sheffield, J., Wood, E.F. & Roderick, M.L. (2012). Little change in global drought over the past 60 years. *Nature*, **491**, 435–438.

Sitch, S., Friedlingstein, P., Gruber, N., Jones, S., Murray-Tortarolo, G., Ahlström, A., Doney, S., Graven, H., Heinze, C., Huntingford, C. *et al.* (2013). Trends and drivers of regional sources and sinks of carbon dioxide over the past two decades. *Biogeosciences Discussions*, **10**, 20113–20177.

Smith, N., Saatchi, S. & Randerson, J. (2004). Trends in high northern latitude soil freeze and thaw cycles from 1988 to 2002. *J. Geophys. Res*, **109**, D12101.

Smol, J.P. & Douglas, M.S. (2007). Crossing the final ecological threshold in high Arctic ponds. *Proceedings of the National Academy of Sciences*, **104**, 12395–12397.

Soja, A.J., Tchebakova, N.M., French, N.H., Flannigan, M.D., Shugart, H.H., Stocks, B.J., Sukhinin, A.I., Parfenova, E., Chapin, F.S. & Stackhouse, P.W. (2007). Climate-induced boreal forest change: predictions versus current observations. *Global and Planetary Change*, **56**, 274–296.

Solomon, S., Qin, D., Manning, M., Chen, Z., Marquis, M., Averyt, K., Tignor, M. & Miller, H., eds. (2007). *Climate change 2007: The physical science basis. Contribution of Working Group I to the Fourth Assessment Report of the Intergovernmental Panel on Climate Change*. Cambridge University Press, Cambridge, UK.

Stockli, R. & Vidale, P. (2004). European plant phenology and climate as seen in a 20-year AVHRR land-surface parameter dataset. *Int. J. Remote Sensing*, **25**, 3303–3330.

Sugimoto, A., Yanagisawa, N., Naito, D., Fujita, N. & Maximov, T.C. (2002). Importance of permafrost as a source of water for plants in east Siberian taiga. *Ecological Research*, **17**, 493–503.

Suni, T., Berninger, F., Markkanen, T., Keronen, P., Rannik, Ü. & Vesala, T. (2003). Interannual variability and timing of growing-season CO_2 exchange in a boreal forest. *Journal of Geophysical Research*, **108**, 4265.

Szczypta, C., Calvet, J.C., Maignan, F., Dorigo, W., Baret, F. & Ciais, P. (2013). Suitability of modelled and remotely sensed essential climate variables for monitoring Euro-Mediterranean droughts. *Geoscientific Model Development Discussions*, **6**, 5553–5594.

Szeicz, J.M. & MacDonald, G.M. (1996). A 930-year ring-width chronology from moisture-sensitive white spruce (Picea glauca Moench) in northwestern Canada. *The Holocene*, **6**, 345–351.

Takala, M., Luojus, K., Pulliainen, J., Derksen, C., Lemmetyinen, J., Kärnä, J.P., Koskinen, J. & Bojkov, B. (2011). Estimating northern hemisphere snow water equivalent for climate research through assimilation of space-borne radiometer data and ground-based measurements. *Remote Sensing of Environment*, **115**, 3517–3529.

Tan, B., Morisette, J., Wolfe, R., Gao, F., Ederer, G., Nightingale, J. & Pedelty, J. (2011). An enhanced TIMESAT algorithm for estimating vegetation phenology metrics from MODIS data. *Selected Topics in Applied Earth Observations and Remote Sensing, IEEE Journal of*, **4**, 361–371.

Tape, K., Sturm, M. & Racine, C. (2006). The evidence for shrub expansion in northern Alaska and the Pan-Arctic. *Global Change Biology*, **12**, 686–702.

Tebaldi, C., Hayhoe, K., Arblaster, J. & Meehl, G. (2006). Going to the extremes: An intercomparison of model-simulated historical and future changes in extreme events. *Climatic Change*, **79**, 185–211.

Thompson, R. (2011). The relationship of the phase and amplitude of the annual cycle of CO2 to phenological events. *Plant Ecology & Diversity*, **4**, 213–226.

Thoning, K., Tans, P., Komhyr, W. *et al.* (1989). Atmospheric carbon dioxide at Mauna Loa Observatory: 2, Analysis of the NOAA GMCC data, 1974–1985. *J. Geophys. Res*, **94**, 8549–8565.

Thornthwaite, C. & Mather, J. (1955). The water balance. Centerton: Drexel Institute of Technology, 1955. 104 p. *Publications in climatology*, **8**.

Tibshirani, R., Walther, G. & Hastie, T. (2001). Estimating the number of clusters in a data set via the gap statistic. *Journal of the Royal Statistical Society: Series B (Statistical Methodology)*, **63**, 411–423.

Tolwinski-Ward, S., Anchukaitis, K.J. & Evans, M.N. (2013). Bayesian parameter estimation and interpretation for an intermediate model of tree-ring width. *Climate of the Past*, **9**.

Tolwinski-Ward, S.E., Evans, M.N., Hughes, M.K. & Anchukaitis, K.J. (2011). An efficient forward model of the climate controls on interannual variation in tree-ring width. *Climate Dynamics*, **36**, 2419–2439.

Touchan, R., Shishov, V., Meko, D., Nouiri, I., Grachev, A. & Carswell, F. (2012). Process based model sheds light on climate sensitivity of Mediterranean tree-ring width. *Biogeosciences*, **9**.

Townshend, J. (2011). User Guide for the MODIS Vegetation Continuous Fields product Collection 5 version 1. Available at:https://lpdaac.usgs.gov/sites/default/files/public/modis/docs/VCF_C5_UserGuide_Dec2011.pdf.

Trenberth, K.E., Jones, P.D., Ambenje, P., Bojariu, R., Easterling, D., Klein Tank, A., Parker, D., Rahimzadeh, F., Renwick, J.A., Rusticucci, M., Soden, B. & Zhai, P. (2007). Observations: Surface and Atmospheric Climate Change. In S. Solomon, D. Qin, M. Manning, Z. Chen, M. Marquis, K.B. Averyt, M. Tignor & H.L. Miller, eds., *Climate Change 2007: The Physical Science Basis. Contribution of Working Group I to the Fourth Assessment Report of the Intergovernmental Panel on Climate Change*, chap. 3, 235–336, Cambridge University Press, Cambridge, United Kingdom.

Trenberth, K.E., Dai, A., van der Schrier, G., Jones, P.D., Barichivich, J., Briffa, K.R. & Sheffield, J. (2014). Global warming and changes in drought. *Nature Climate Change*, **4**, doi:10.1038/nclimate2067.

Trujillo, E., Molotch, N.P., Goulden, M.L., Kelly, A.E. & Bales, R.C. (2012). Elevation-dependent influence of snow accumulation on forest greening. *Nature Geoscience*, **5**, 705–709.

Tucker, C. (1979). Red and photographic infrared linear combinations for monitoring vegetation. *Remote sensing of Environment*, **8**, 127–150.

Tucker, C., Slayback, D., Pinzon, J., Los, S., Myneni, R. & Taylor, M. (2001). Higher northern latitude normalized difference vegetation index and growing season trends from 1982 to 1999. *International Journal of Biometeorology*, **45**, 184–190.

Tucker, C., Pinzón, J., Brown, M., Slayback, D., Pak, E., Mahoney, R., Vermote, E. & El Saleous, N. (2005). An extended AVHRR 8-km NDVI dataset compatible with MODIS and SPOT vegetation NDVI data. *International Journal of Remote Sensing*, **26**, 4485–4498.

Vaganov, E., Hughes, M., Kirdyanov, A., Schweingruber, F. & Silkin, P. (1999). Influence of snowfall and melt timing on tree growth in subarctic Eurasia. *Nature*, **400**, 149–151.

Vaganov, E., Hughes, M. & Shashkin, A. (2006). *Growth Dynamics of Conifer Tree Rings: Images of Past and Future Environments*. Ecological Studies, Springer.

Vaganov, E.A., Anchukaitis, K.J. & Evans, M.N. (2011). *Dendroclimatology: Progress and Prospects*, chap. How well understood are the processes that create dendroclimatic records? A mechanistic model of the climatic control on conifer tree-ring growth dynamics, 37–75. Springer Verlag.

van der Schrier, G., Barichivich, J., Briffa, K.R. & Jones, P.D. (2013). A scPDSI-based global data set of dry and wet spells for 1901–2009. *Journal of Geophysical Research: Atmospheres*.

Van Oijen, M., Rougier, J. & Smith, R. (2005). Bayesian calibration of process-based forest models: bridging the gap between models and data. *Tree Physiology*, **25**, 915–927.

Verbyla, D. (2011). Browning boreal forests of western North America. *Environmental Research Letters*, **6**, 041003.

Vesala, T., Launiainen, S., Kolari, P., Pumpanen, J., Sevanto, S., Hari, P., Nikinmaa, E., Kaski, P., Mannila, H., Ukkonen, E. *et al.* (2010). Autumn temperature and carbon balance of a boreal Scots pine forest in Southern Finland. *Biogeosciences*, **7**, 163–176.

Vicente-Serrano, S.M., Beguería, S. & López-Moreno, J.I. (2010). A multiscalar drought index sensitive to global warming: the standardized precipitation evapotranspiration index. *Journal of Climate*, **23**, 1696–1718.

Vicente-Serrano, S.M., Beguería, S., Lorenzo-Lacruz, J., Camarero, J.J., López-Moreno, J.I., Azorin-Molina, C., Revuelto, J., Morán-Tejeda, E. & Sanchez-Lorenzo, A. (2012). Performance of drought indices for ecological, agricultural, and hydrological applications. *Earth Interactions*, **16**, 1–27.

Vicente-Serrano, S.M., Gouveia, C., Camarero, J.J., Beguería, S., Trigo, R., López-Moreno, J.I., Azorín-Molina, C., Pasho, E., Lorenzo-Lacruz, J., Revuelto, J. *et al.* (2013). Response of vegetation to drought time-scales across global land biomes. *Proceedings of the National Academy of Sciences*, **110**, 52–57.

Vincent, L.A., Zhang, X., Bonsal, B. & Hogg, W. (2002). Homogenization of daily temperatures over Canada. *Journal of Climate*, **15**.

Vinnikov, K.Y. & Yeserkepova, I. (1991). Soil moisture: Empirical data and model results. *Journal of Climate*, **4**, 66–79.

Visser, H. & Molenaar, J. (1988). Kalman filter analysis in dendroclimatology. *Biometrics*, 929–940.

Vitasse, Y., Porté, A.J., Kremer, A., Michalet, R. & Delzon, S. (2009). Responses of canopy duration to temperature changes in four temperate tree species: relative contributions of spring and autumn leaf phenology. *Oecologia*, **161**, 187–198.

Vrugt, J.A., Ter Braak, C., Diks, C., Robinson, B.A., Hyman, J.M. & Higdon, D. (2009). Accelerating Markov chain Monte Carlo simulation by differential evolution with self-adaptive randomized subspace sampling. *International Journal of Nonlinear Sciences and Numerical Simulation*, **10**, 273–290.

Wang, D., Morton, D., Masek, J., Wu, A., Nagol, J., Xiong, X., Levy, R., Vermote, E. & Wolfe, R. (2012a). Impact of sensor degradation on the MODIS NDVI time series. *Remote Sensing of Environment*, **119**, 55–61.

Wang, K. & Dickinson, R.E. (2012). A review of global terrestrial evapotranspiration: Observation, modeling, climatology, and climatic variability. *Reviews of Geophysics*, **50**.

Wang, X., Piao, S., Ciais, P., Li, J., Friedlingstein, P., Koven, C. & Chen, A. (2011). Spring temperature change and its implication in the change of vegetation growth in North America from 1982 to 2006. *Proceedings of the National Academy of Sciences*, **108**, 1240.

Wang, Z., Yang, B., Qin, C. & Shi, F. (2012b). Research progress in monitoring and simulating stem radius growth: an overview. *Sciences in Cold and Arid Regions*, **4**, 0175–0183.

Warren, J.M., Norby, R.J. & Wullschleger, S.D. (2011). Elevated CO2 enhances leaf senescence during extreme drought in a temperate forest. *Tree physiology*, **31**, 117–130.

Wells, N., Goddard, S. & Hayes, M.J. (2004). A self-calibrating Palmer drought severity index. *Journal of Climate*, **17**, 2335–2351.

Welp, L., Randerson, J. & Liu, H. (2007). The sensitivity of carbon fluxes to spring warming and summer drought depends on plant functional type in boreal forest ecosystems. *Agricultural and Forest Meteorology*, **147**, 172–185.

Wendler, G., Conner, J., Moore, B., Shulski, M. & Stuefer, M. (2011). Climatology of Alaskan wildfires with special emphasis on the extreme year of 2004. *Theoretical and Applied Climatology*, **104**, 459–472.

Westerling, A.L., Hidalgo, H.G., Cayan, D.R. & Swetnam, T.W. (2006). Warming and earlier spring increase western US forest wildfire activity. *Science*, **313**, 940–943.

White, M. & Nemani, R. (2003). Canopy duration has little influence on annual carbon storage in the deciduous broad leaf forest. *Global Change Biology*, **9**, 967–972.

White, M., de Beurs, K., Didan, K., Inouye, D., Richardson, A., Jensen, O., O'KEEFE, J., Zhang, G., Nemani, R., van Leeuwen, W. *et al.* (2009). Intercomparison, interpretation, and assessment of spring phenology in North America estimated from remote sensing for 1982–2006. *Global Change Biology*, **15**, 2335–2359.

Wilks, D. (2011). *Statistical Methods in the Atmospheric Sciences*, vol. 100 of *International Geophysics Series*. Academic Press, Third edn.

Williams, A.P., Xu, C. & McDowell, N.G. (2011). Who is the new sheriff in town regulating boreal forest growth? *Environmental Research Letters*, **6**, 041004.

Wilmking, M. & Juday, G.P. (2005). Longitudinal variation of radial growth at Alaska's northern treeline–Recent changes and possible scenarios for the 21st century. *Global and Planetary Change*, **47**, 282–300.

Wilmking, M., Juday, G.P., Barber, V.A. & Zald, H.S. (2004). Recent climate warming forces contrasting growth responses of white spruce at treeline in Alaska through temperature thresholds. *Global Change Biology*, **10**, 1724–1736.

Wirth, C., Lichstein, J., Dushoff, J., Chen, A. & Chapin, F. (2008). White spruce meets black spruce: dispersal, postfire establishment, and growth in a warming climate. *Ecological Monographs*, **78**, 489–505.

Wittenberg, U., Heimann, M., Esser, G., McGuire, A. & Sauf, W. (1998). On the influence of biomass burning on the seasonal CO2 signal as observed at monitoring stations. *Global biogeochemical cycles*, **12**, 531–544.

Wood, S. (2006). *Generalized Additive Models: An Introduction with R*. Chapman and Hall/CRC.

Wood, S.N. (2011). Fast stable restricted maximum likelihood and marginal likelihood estimation of semiparametric generalized linear models. *Journal of the Royal Statistical Society (B)*, **73**, 3–36.

Wu, C., Gonsamo, A., Chen, J.M., Kurz, W.A., Price, D.T., Lafleur, P.M., Jassal, R.S., Dragoni, D., Bohrer, G., Gough, C.M. *et al.* (2012). Interannual and spatial impacts of phenological transitions, growing season length, and spring and autumn temperatures on carbon sequestration: A North America flux data synthesis. *Global and Planetary Change*.

Xu, L., Myneni, R.B., Chapin, F.S., III, Callaghan, T.V., Pinzon, J.E., Tucker, C.J., Zhu, Z., Bi, J., Ciais, P., Tømmervik, H., Euskirchen, E.S., Forbes, B.C., Piao, S.L., Anderson, B.T., Ganguly, S., Nemani, R.R., Goetz, S.J., Beck, P.S.A., Bunn, A.G., Cao, C. & Stroeve, J.C. (2013). Temperature and vegetation seasonality diminishment over northern lands. *Nature Climate Change*, **3**, 581–586.

Yarie, J. (2008). Effects of moisture limitation on tree growth in upland and floodplain forest ecosystems in interior Alaska. *Forest Ecology and Management*, **256**, 1055–1063.

Yarie, J. & Van Cleve, K. (2006). *Alaska's changing boreal forest*, chap. Controls over forest production in interior Alaska. Oxford University Press, New York.

Yue, S., Pilon, P., Phinney, B. & Cavadias, G. (2002). The influence of autocorrelation on the ability to detect trend in hydrological series. *Hydrological Processes*, **16**, 1807–1829.

Zeng, H., Jia, G. & Epstein, H. (2011). Recent changes in phenology over the northern high latitudes detected from multi-satellite data. *Environmental Research Letters*, **6**, 045508.

Zhang, G., Zhang, Y., Dong, J. & Xiao, X. (2013). Green-up dates in the Tibetan Plateau have continuously advanced from 1982 to 2011. *Proceedings of the National Academy of Sciences*, **110**, 4309–4314.

Zhang, K., Kimball, J.S., McDonald, K.C., Cassano, J.J. & Running, S.W. (2007). Impacts of large-scale oscillations on pan-Arctic terrestrial net primary production. *Geophysical Research Letters*, **34**.

Zhang, K., Kimball, J., Hogg, E., Zhao, M., Oechel, W., Cassano, J. & Running, S. (2008). Satellite-based model detection of recent climate-driven changes in northern high-latitude vegetation productivity. *J. Geophys. Res*, **113**, G03–033.

Zhang, K., Kimball, J.S., Mu, Q., Jones, L.A., Goetz, S.J. & Running, S.W. (2009). Satellite based analysis of northern ET trends and associated changes in the regional water balance from 1983 to 2005. *Journal of Hydrology*, **379**, 92–110.

Zhang, K., Kimball, J., Kim, Y. & McDonald, K. (2011). Changing freeze-thaw seasons in northern high latitudes and associated influences on evapotranspiration. *Hydrological Processes*, **25**, 4142–4151.

Zhang, T., Frauenfeld, O.W., Serreze, M.C., Etringer, A., Oelke, C., McCreight, J., Barry, R.G., Gilichinsky, D., Yang, D., Ye, H. *et al.* (2005a). Spatial and temporal variability in active layer thickness over the Russian Arctic drainage basin. *Journal of Geophysical Research: Atmospheres (1984–2012)*, **110**.

Zhang, T., McCreight, J. & Barry, R. (2005b). Arctic EASE-Grid freeze and thaw depths, 1901 - 2002. Boulder, CO: National Snow and Ice Data Center. Digital media. Digital Media.

Zhao, M. & Running, S. (2010). Drought-induced reduction in global terrestrial net primary production from 2000 through 2009. *Science*, **329**, 940–943.

Zhou, L., Tucker, C., Kaufmann, R., Shabanov, N. & Myneni, R. (2001). Variations in northern vegetation activity inferred from satellite data of vegetation index during 1981 to 1999. *Journal of Geophysical Research*, **106**, 20–069.

Zhu, W., Tian, H., Xu, X., Pan, Y., Chen, G. & Lin, W. (2012). Extension of the growing season due to delayed autumn over mid and high latitudes in North America during 1982–2006. *Global Ecology and Biogeography*, **21**, 260–271.